RESPONSE OF CANADIAN ROCKIES GLACIER HYDROLOGY TO CHANGING CLIMATE

A Thesis Submitted to the
College of Graduate and Postdoctoral Studies
in Partial Fulfillment of the Requirements
for the Degree of Doctor of Philosophy
in the Department of Geography and Planning
(Centre for Hydrology)
University of Saskatchewan
Saskatoon

By

DHIRAJ PRADHANANGA

Permission to Use

In presenting this thesis in partial fulfilment of the requirements for a Postgraduate degree from the University of Saskatchewan, I agree that the Libraries of this University may make it freely available for inspection. I further agree that permission for copying of this thesis in any manner, in whole or in part, for scholarly purposes may be granted by the professor or professors who supervised my thesis work or, in their absence, by the Head of the Department or the Dean of the College in which my thesis work was done. It is understood that any copying or publication or use of this thesis or parts thereof for financial gain shall not be allowed without my written permission. It is also understood that due recognition shall be given to me and to the University of Saskatchewan in any scholarly use which may be made of any material in my thesis.

Requests for permission to copy or to make other use of material in this thesis in whole or part should be addressed to:

Head of the Department of Geography and Planning
117 Science Place
University of Saskatchewan
Saskatoon, Saskatchewan S7N 5C8
Canada

Or

Dean
College of Graduate and Postdoctoral Studies
University of Saskatchewan
116 Thorvaldson Building, 110 Science Place
Saskatoon, Saskatchewan S7N 5C9
Canada

Abstract

This thesis investigates the impact of snow and glaciers in mountain hydrology under changing climate conditions and glacier configurations in the Canadian Rockies, where a warming climate and glacier retreat cause concern about changes in mountain hydrology for water availability downstream. The general objectives of the study are (1) to model snow and glacier ablation and accumulation dynamics, (2) to determine how they influence high mountain hydrology, and (3) to improve hydrological modeling capacity in high mountain cold regions. The specific objectives are: (1) to develop a new model to estimate shortwave irradiance from temperature and humidity observations; (2) to include snow redistribution and the full energy and mass budget in a glacier hydrological modelling platform; (3) to apply the model to diagnose the individual and combined impacts of changes in climate and glacier mass on headwater hydrology. The thesis has four major parts. First, it describes the methodology used to produce meteorological data to force a hydrological model for the Peyto Glacier Research Basin (PGRB) in the Canadian Rockies. Second, it develops a new approach for estimating shortwave irradiance based on temperature and humidity observations that is suitable for snow and ice melt calculations for mountains and other cold regions around the world. Observations from thirty mostly mountain sites in South and North America, Europe and the Himalayas were used to evaluate existing algorithms and reanalysis products. The new algorithm, coupled to an existing extraterrestrial shortwave irradiance model, permitted more accurate estimation of shortwave irradiance from standard meteorological observations than was previously possible. The globally available reanalysis products also offer the potential for application to large-scale hydrological models. Third, the thesis develops a novel glacier hydrology model, developed within the Cold Regions Hydrological Model platform (CRHM), which is a physically based, integrated model capable of simulating the hydrology of both ice-covered and ice-free areas within a mountain basin. Fourth, the thesis focuses on diagnosing the impacts of climate change and changing glacier configuration on mountain headwater hydrology. The modelling results reveal that glacier retreat and ablation are due to the joint effect of a warming climate and an increase in ice exposure, which increase both seasonal melt and runoff. Increased streamflow is due to climate warming. However, the increases in melt and runoff are reduced somewhat by the reduction in glacial area. Such a modelling approach is

important for diagnosing the hydrological responses from a glacierized basin in the context of climate change and variability and change in glacier configuration.

Acknowledgements

Very special thanks to Prof John Pomeroy for his all guidance, help, encouragement throughout the PhD program. I have not only learnt many things in my research topic, but also, in my academic career. My knowledge has increased by many folds during this research period. His support and his mentorship during my family's stay in Canada were invaluable as well.

My committee members Prof Alec Aitken, Prof Bram Nobel (committee chair), Prof Dirk de Boer, Prof Shawn Marshall, Dr Warren Helgason and Prof Martin Sharp (external examiner) are highly appreciated for their comments and edits. They helped me transform this thesis into a clearer form.

A special thanks to Carol Mayne, who not only helped me to edit my English, but also motivated me to keep moving. I am indebted to Prof Suresh Raj Chalise, Dr Madan Lall Shrestha and Prof Gordon Young for their motivation and encouragement. I am also indebted to Dr Joseph Shea, Mike Demuth and Dr D. Scott Munro for meteorological and glaciological data and science discussions on glaciology.

My colleagues in the Centre for Hydrology were very valuable to me for motivation and solving technical problems. Some were teaching me; some were encouraging me. I would like to list them here. Dr Abbas Fayad, André Bertoncini, Caroline Aubry-Wake, Dr Chris DeBeer, Dr Chris Marsh, Daniel Günther, Dominic Demand, Emily Anderson, Evan (Pradhananga) Siemens, Dr Jonathan Conway, Dr Kabir Rasouli, Dr Keith Musselman, Xing (Logan) Fang, Dr Lucia Scaff, Dr Nik Aksamit, Dr Nicholas Kinar, Dr Nicolas Leroux, Dr Nicholas Wayand, Paul Whitfield, Dr Philip Harder, Robert Sandford, Dr Sebastian A. Krogh, Yohann Videla-Giering, Dr Zhibang Lv, and Dr Zhihua He. My colleagues, especially, Arun Bhattarai, Jeeban Panthi, Nammy Hang Kirant, Nicky Shree Shrestha, Niranjan Bista, Piyush Dahal, in the Small Earth Nepal were also very supportive to this journey.

Thanks to Angus Duncan, Greg Galloway and Xiu Juan (May) Guan for their help with fieldwork and all those long and fun hours in the field. Thanks to Joni Onclin and Phyllis Baynes for their administrative and logistical help. Funding for this research was from the Canada Research Chair

in Water Resources and Climate Change and from Global Institute of Water Security. I also received a Saskatchewan Innovation and Opportunity Scholarship to support the research.

Through this program, I have had opportunities to learn several tools and applications for research, starting from proposal writing, refining my English writing to many computer languages and software packages. I have become familiar with GIS and remote sensing software, R, and many more. Tom Brown tirelessly coded glacier and avalanche modules in CRHM and provided user support for the model. Dr Kevin Shook helped me on statistical analysis and on R codes. He developed many R-packages (CRHMr, Reanalysis, MSCr) as needed for this study.

My PhD was a long and painful journey. Nepal experienced the earthquake disaster in 2015 while I was in Canada. I needed to rush to Nepal in 2016 when my father was sick, and sadly I lost him. But I had my family and friends supporting me all the time. I acknowledge my mother, wife and son for tolerating me while I was focusing on my PhD. Anup Banepali, Bijesh Charan Raya, Denesh Amatya, Dr Jagadish Karmacharya, Sagar Manandhar, Suresh Kayastha and other friends in Nepal were also always motivating me and taking care of my needs in Nepal so that I could focus on my PhD. Marilyn Pomeroy comforted and helped me and my family to settle in Canmore, Udeep Tandukar, Rajeena Shrestha and other friends in SK and AB supported me and my family whenever needed. For me, it is not me who did my PhD, they did it.

I dedicate this dissertation to my father who passed away in 2016 before I completed my PhD, and to my mother, wife and son.

Table of Contents

List of Tables

List of Figures

List of Abbreviations

AAR	Accumulation Area Ratio
ACIS	Alberta Climate Information Service
AD	Annandale
ADV	Acoustic Doppler Velocimeter
AGRB	Athabasca Glacier Research Basin
ALPINE3D	Three-dimensional distributed energy-budget snowmelt model
AWS	Automatic Weather Station
BC	Bristow and Campbell
CCMEO	Natural Resources Canada, Government of Canada
CCRN	Changing Cold Regions Network
CDED	Canadian Digital Elevation Data
CDEM	Canadian Digital Elevation Model
CDSM	Canadian Digital Surface Model
CFSR	Climate Forecast System Reanalysis
CRHM	Cold Region Hydrology Modelling platform
CRHO	Canadian Rockies Hydrological Observatory
DEM	Digital Elevation Model
DT	Daily temperature range
ECMWF	European Centre for Medium-Range Weather Forecasts
ELA	Equilibrium Line Altitude
ENSO	El Nino and Southern Oscillation
GCW	Global Cryosphere Watch
GDB	Geospatial Data Base
GEE	Google Earth Engine
GIS	Geographical Information System
GLCF	Global Landcover Facilities
GWF	Water Global Futures
HRU	Hydrological Response Unit
HS	Hargreaves
IHD	International Hydrological Decade
IP3	Improving Processes & Parameterization for Prediction in Cold Regions Hydrology
IPCC	Intergovernmental Panel on Climate Change
LiDAR	Light Detection and Ranging
MATLAB	Matrix Laboratory
MBE	Mean Bias Error
MERRA-2	Modern-Era Retrospective analysis for Research and Applications, version 2
NARR	North American Regional Reanalysis
NCAR	National Center for Atmospheric Research
NCEP	National Center for Environmental Prediction
NDSI	Normalized-Difference Snow Index
NDWI	Normalized-Difference Water Index

NHRI	National Hydrology Research Institute
NTDB	National Topographic Data Base
P	Pressure
PBSM	Prairie Blowing Snow Model
PDO	The Pacific Decadal Oscillation
PGRB	Peyto Glacier Research Basin
Ppt	Precipitation
Q_{li}, Q_{lo}	Incoming and outgoing longwave radiation
Q_{si}, Q_{so}	Incoming and outgoing shortwave radiation
RADAR	Radio Detecting and Ranging
RH	Relative humidity
RMSE	Root Mean Square Error
Sd	Snow depth
Snobal	Snowcover energy and mass-balance model
SR50A	Campbell Scientific Sonic Ranger
SWE	Snow Water Equivalent
Ta	Air temperature
TBRG	Tipping Bucket Rain Gauge
T/RH	Temperature and relative humidity
Tmax	Daily maximum temperature
Tmean	Daily mean temperature
Tmin	Daily minimum temperature
TOA	Top-of-Atmosphere
Ts	Soil/snow/firn/ice temperature
WATCH	Water and Global Change
WBI	Wang-Bovik index
Wd	Wind direction
WECC	Water, Ecosystem, Cryosphere and Climate
WFDEI	WATCH Forcing Data ERA-Interim
WGMS	World Glacier Monitoring Service
WMO	World Meteorological Organization
Ws	Wind speed

CHAPTER 1: Introduction

1.1 Background and literature review

Glaciers and glacierized basins are important components of the hydrological cycle of Canadian high mountain regions. Glaciers play an important role in regulating downstream water supply, both seasonally and annually. Mountain glacier hydrology is expected to change in response to climate change and, in turn, to impact water availability downstream. Studies on the impact of climate change on glaciers have generally focussed on changes in glacier mass and relate how glacier growth and shrinkage are linked to climatic forcing. Hydrological responses to climate change of mountain glaciers depend on glacier mass and energy balance. The general objective of this study is to investigate the combined effect of climate change and changes in glacier accumulation and ablation on the hydrology of a glacier basin.

This section reviews the current understanding of mountain glacier hydrology, focussing on the impact of climate change on snow/ice accumulation and ablation and on resulting streamflow.

1.1.1 Motivation

The Canadian Rocky Mountains constitute the headwaters of most of the major rivers of western Canada, for example, the North and South Saskatchewan Rivers, the Fraser River and the Columbia River. Mountain streamflow profoundly affects the amount and quality of runoff in these rivers, along with their seasonal variability in downstream regions, particularly in arid and semiarid regions of western North America (Marks *et al.*, 2008). The contribution of glacial meltwater to total streamflow discharging from a river basin decreases with downstream distance from the glacier because the non-glacierized area of the basin increases downstream. Glaciers, however, tend to contribute significantly to streamflow volume during warm and dry periods and, in doing so, moderate inter-annual variability in streamflow far downstream of their locations (Fountain and Tangborn, 1985; Hopkinson and Young, 1998; Comeau *et al.*, 2009).

North American mountain glaciers are retreating (Munro, 2000; Moore and Demuth, 2001; Arendt *et al.*, 2002; Marks *et al.*, 2002; Demuth and Pietroniro, 2003; Berthier, 2004; Demuth and Keller, 2006; DeBeer and Sharp, 2007; Schiefer *et al.*, 2007; Berthier *et al.*, 2010; Derksen *et al.*, 2012; Tennant and Menounos, 2013; Clarke *et al.*, 2015). Vincent *et al.* (2015) analysed Canada's climate trends and found increasing temperature and precipitation, with the largest warming in winter and spring and more spatial variability in precipitation than in temperature trends. DeBeer *et al.* (2016) noted similar changes in temperature and precipitation in western Canada. They also noted a decrease in the fraction of precipitation falling as snow and widespread decreases in snow depth, snow cover extent and duration, and an increase in glacier melt. Clarke *et al.* (2015) projected that the glaciers in western Canada are expected to lose 60 to 80% of their combined volume compared to 2005, while many of them in the Rockies disappear by 2100.

High elevation cold regions are sensitive to climate change and, thus, are excellent indicators of climate change (Oerlemans, 2001, 2005; Hopkinson and Demuth, 2006; Demuth *et al.*, 2008; Kohler and Maselli, 2009). There is rapid glacier retreat (Demuth and Pietroniro, 2003; Berthier, 2004; Kaser *et al.*, 2004; Anderson *et al.*, 2006; Ohmura, 2006; Schiefer *et al.*, 2007; Haeberli *et al.*, 2007; Arendt *et al.*, 2009; Moore *et al.*, 2009; Bolch *et al.*, 2010; Hirabayashi *et al.*, 2010; Diolaiuti *et al.*, 2011; Fujita and Nuimura, 2011; Naz *et al.*, 2014; Shea *et al.*, 2015a; Zemp *et al.*, 2015), shrinking seasonal snowcover at higher elevations in the northern hemisphere (Mote *et al.*, 2005; IPCC, 2007; Adam *et al.*, 2009; Fujita and Nuimura, 2011) and declining streamflow (Demuth and Pietroniro, 2003; Stahl and Moore, 2006; Demuth *et al.*, 2008; Rood *et al.*, 2008; Immerzeel *et al.*, 2010; Kienzle *et al.*, 2012; Naz *et al.*, 2014) or, in some cases, increasing streamflow (Lutz *et al.*, 2014; Van Pelt and Kohler, 2015). Although many glaciers began to retreat after the Little Ice Age ended in the early 1800s, the rate of glacier retreat in recent decades is higher than in the past (Barry, 2006; Riedel *et al.*, 2015).

This study will investigate the influence of snow and glacier hydrology in determining water availability under changing climate and glacier conditions in mountain sites. It will use a physically based hydrological modelling platform that implements a robust energy budget melt model, and a snow redistribution and sublimation model within a mountain basin hydrology model.

1.1.2 Hydrological processes in mountain glaciers

Some uncertainties arise with hydrological responses to glacial change. It is generally accepted that, with climate warming, runoff originating from glaciers increases for a time due to increased melt rate, then declines when the mass of ice decreases substantially (Moore *et al.*, 2009). The duration and timing of this change, from increasing to decreasing flow, however, will be regionally variable (Casassa *et al.*, 2009). In addition, a few recent studies have projected a different future of streamflow in the Himalayas than in the study by Moore *et al*. (2009). For example, Immerzeel *et al.* (2013) used predictions of a warmer and wetter future for the Himalayas. They argued that increasing precipitation in the region would compensate for declining contributions of glacier melt on river flow in the future. Luo *et al.* (2013) indicated that glacier melt was less sensitive to precipitation change than to temperature change in northwest China and suggested further modelling of the effects of climate change, with increasing temperatures and decreasing precipitation. It is not yet understood how a glacier behaves with changing precipitation and temperature, along with a changing glacier configuration. Continuous mass loss from a glacier leads to reduction in the glacier-covered area, an increase in ice exposure and changes to the elevation and slope of the glacier surface. These changes alter the near-surface distribution of temperature and precipitation, as well as the surface radiation budget of the glacier and the turbulent transfer of mass and energy to the glacier surface.

Stahl and Moore (2006) observed that British Columbia streams originating from glacierized mountain basins show a decreasing phase in the runoff due to a decline in late-summer flow, and most glaciers have already completed a phase of increased flow, due to global warming. The observed decrease in glacier mass in the Canadian Rockies has been caused by an increase in average annual air temperatures and a reduction in winter snowfall since the mid-1980s (Demuth and Keller, 2006, Moore and Demuth, 2001). The Bow River at Banff also experienced declining flows over the past century (Whitfield and Pomeroy, 2016).

Demuth and Keller (2006) conducted a detailed assessment of the mass balance variation of Peyto Glacier in Alberta from 1966-1995. Winter snow accumulation was a bigger influence on year to year variability in annual net mass balance than was summer balance. They attempted to establish the mass balance trend, including reference to shifts in synoptic weather patterns related to changes

in sea surface temperature, atmospheric circulation, seasonal snowcover and glacier ice. The Pacific Decadal Oscillation (PDO) and the El Nino Southern Oscillation (ENSO) were found to be correlated with the winter mass balance. The study inferred a loss of ~70% of glacier volume during the last century. Kienzle *et al.* (2012) projected a shift in streamflow in Alberta's Cline River basin in western Canada, higher flow during October-June, and lower flow during July-September, exacerbated by reduced glacier volume, in terms of both depth and area, during 2010-2099 compared to the baseline period (1961-1990). They projected earlier snowmelt, lower summer flow, an extended low-flow late-summer period and greater autumn precipitation. Similarly, Marshall *et al.* (2011) projected glacier volumes of the Canadian Rockies (eastern slopes) for the next century. Their projected values are alarming, as they indicate a 40% loss of glacier volume in the 21st century if the present climate stabilizes, and a loss of ~85% if the climate changes as projected in IPCC's A1b and B1 climate scenarios. Similarly, Clarke *et al.* (2015) used a high resolution glacier model forced by the 21st century climate scenarios ensembled by global climate models to simulate future of the glaciers in western Canada. They projected the loss of the glacier in 2100 by about 70% of the volume relative to 2005 with the maximum rate of ice volume loss during 2020–2040 and thus this period to be peak input of deglacial meltwater to the runoff.

To better understand glacier melting processes and how they are impacted by changes in climate and glacier configurations, more appropriate models are required. Investigations in different climatological regions, additional meteorological measurements and experiments, mesoscale modelling of atmospheric dynamics (Kaser *et al.*, 2004), replacement of empirical knowledge with improved process understanding (Haeberli *et al.*, 2007) and a combination of energy balance data and further field validation (Hopkinson *et al.*, 2010) must also be considered.

Energy budget and mass balance models use a digital elevation model (DEM) to distribute shortwave irradiance based on slope and aspect, and distribute temperature and precipitation based on elevation. Most models developed for snowmelt, however, may not adequately consider the environment of a glacierized basin or address the ice melting process. Redistribution of snow due to blowing snow and avalanches and the spatial and temporal variability of the components of the full surface energy budget of the glacier are not normally included in glacio-hydrology models.

Because snow drifting processes and sublimation significantly affect snow accumulation, models that ignore these processes do not accurately simulate the runoff and mass balance of a glacierized basin.

1.1.3 Temperature index models are not the solution

It is well established that the energy balance is fundamental for understanding the links between glaciers and the climate of a region. Due to limited data availability and other reasons, many models use the temperature index method to simulate snow and glacier melt (Hock, 2005). These models lump all components of the surface energy budget into a degree-day factor, which is a proportionality coefficient that calculates melt rates based on air temperature (normally in excess of a defined threshold value). Air temperature in these models is considered representative for the main terms of the energy budget. Oerlemans (1989) emphasized the radiation balance as the primary factor in the mass balance, with temperature as a secondary factor. Munro and Young (1982) stated that net shortwave radiation should be a main component of a glacier melt model. Arendt (1999) suggested considering diurnal fluctuations in the glacier surface albedo while applying energy budget melt models. Magnusson *et al.* (2011) compared an uncalibrated energy budget snowmelt model (ALPINE3D) and a calibrated temperature index model to simulate runoff from a partly glacierized Swiss watershed. The former approach better simulated snowmelt compared to the latter during the snowmelt-dominated period, but performance was not equally favourable during the glacier ice melt period. They suggested direct measurement on the glacier to accurately simulate turbulent heat fluxes and the net radiation budget. They concluded that snow distribution and redistribution were significant to variation in the glacier albedo and, thus, the performance of runoff simulations. Albedo is an important part of the surface energy budget of snow and glacier and thus for their melt processes (Oerlemans *et al.*, 2009). Therefore, the temperature index model is insufficient to capture processes such as snow redistribution and change in surface albedo, which alter the surface energy budget. A similar comparative study conducted by Guðmundsson *et al.* (2009) concluded that degree-day models were less accurate compared to the energy budget approach in daily melt simulation. They suggested, however, that degree-day models were successful in simulating seasonal variations in melting.

In summary, while temperature index models are comparatively simple and widely used because of limited data requirements, energy budget models provide a more accurate solution and more temporal and spatial transferability due to their physical basis. Though most models use an empirical temperature index approach due to unavailability of high altitude observations of radiation, alternative proven approaches can be used to simulate these data (Walter *et al.*, 2005; Sicart *et al.*, 2006; Shook and Pomeroy, 2011; Pomeroy *et al.*, 2013) to drive physically based energy budget melt models. Daily global shortwave irradiance can be estimated with reasonable accuracy from latitude, altitude, time of year, time of day and air temperature variations (Annandale *et al.,* 2002, Hargreaves and Samani, 1982). Once daily shortwave irradiance is simulated, it can be distributed to hourly time steps using the method detailed in Shook and Pomeroy (2011).

1.1.4 Estimating shortwave irradiance for high mountain glacier environments

Shortwave irradiance is the main energy source that drives the other components of radiation balance (Garnier and Ohmura, 1968). Munro and Young (1982) showed that net shortwave radiation is the energy source for modelling glacier melt. However, a major component in energy budget models, the net radiation, is often not measured. It is either estimated or empirically computed (Shook & Pomeroy, 2011; Besharat *et al.* 2013) or calculated as an output of reanalysis products (Boilley and Wald, 2015).

Shortwave irradiance linked to other components of the radiation balance through the influence of atmospheric transmittance on longwave radiation (Garnier and Ohmura, 1968). Shortwave irradiance is, therefore, sometimes used to simulate net radiation through empirical (Gray and Landine, 1988) or physically based approaches (Pomeroy *et al.* 2007). Accurate estimation of shortwave irradiance is, therefore, crucial for hydrological modeling.

Besharat *et al.* (2013) undertook a comprehensive review of empirical models for estimating solar irradiance based on various meteorological parameters. They classified the models into four major categories: sunshine-based, cloud-based, temperature-based and other meteorological parameter-based models. The first three methods are commonly used, based on data availability. Cloud

information data from satellite observation is available, to some extent, over ice sheets and ice caps, but not over valley glaciers (Oerlemans, 2001). Since sunshine data and cloud observations are not readily available in most locations, the third approach, based on temperature, is the most applicable method to empirically estimate shortwave irradiance (Besharat *et al.*, 2013).

Empirical methods based on daily air temperature range - the difference between daily maximum and minimum temperature - have been continuously developed and tested in different environments, from coastal and lowland environments to highlands, and at different latitudes (Bristow and Campbell, 1984; Meza and Varas, 2000; Samani, 2000; Wu *et al.*, 2007; Bandyopadhyay *et al.*, 2008; Rahimikhoob, 2010; Samani *et al.*, 2011; Shook and Pomeroy, 2011). Shook and Pomeroy (2011) showed that empirical methods based on temperature were not reliable in mountains, although they were reliable in other cold regions in Canada. They suggested the need to improve empirical approaches for high mountains.

Shea (2010) considered vapour pressure and formulated a new algorithm to simulate atmospheric transmittance, based on observations made at four glacier sites in western Canada. This is yet to be tested globally and compared with globally available reanalysis data. Reanalysis products have now become an alternative meteorological forcing data source for hydrological modeling, but with a bias correction scheme (Berg *et al.*, 2005). Several attempts have been made (e.g., Boilley & Wald 2015) to evaluate reanalysis products of daily shortwave irradiance at the surface, mainly focusing on lowlands and tropical regions. There is a need to find appropriate approaches to estimate shortwave irradiance in mountainous cold regions and to evaluate reanalysis products.

1.1.5 Snow redistribution and sublimation

In open, wind-swept cold regions, the spatial and temporal distributions of snowfall, wind redistribution, and mass loss due to sublimation are important components of the snow mass balance (Tabler *et al.*, 1990). The distribution of snow water equivalent (SWE) controls the volume of snowmelt (Pomeroy and Gray, 1995). Snowcover significantly alters the winter surface characteristics in many ways, such by increasing surface albedo and decreasing roughness height (Déry and Tremblay, 2004), impacting local-scale wind speeds, burying ice or bare surfaces,

smoothing out surface topography and isolating sub-surface topography from the atmosphere (Berry, 1981). SWE distribution, therefore, is very important for simulating snow and ice melt runoff. As well, blowing snow redistribution contributes to highly variable patterns of snow depth and water equivalent over a basin (MacDonald *et al.*, 2010).

Snow redistribution occurs due to wind and steep slopes and must be considered in calculating snow accumulation and ablation. Pomeroy *et al.*(1993) and Pomeroy and Li (2000) emphasized the importance of wind on the evolution and redistribution of SWE in prairie and Arctic environments. Wind not only redistributes the snow but also modifies the physical properties of a snowpack; it can harden and increase the density of a snowpack, as well as change the shape, size and other physical properties of snow crystals. Pomeroy and Gray (1995) and Pomeroy *et al.* (1998) emphasized that loss of snow mass due to blowing snow sublimation must also be considered in snow hydrology. Sublimation from blowing snow is greater than that from *in situ* surface snowpacks. Snow crystals undergo greater exposure and ventilation when blown by wind than when snow settles on the surface (Pomeroy *et al.*, 1998). Reba *et al.* (2012) found the sublimation rate, over a season at open sites well exposed to wind, was significantly (almost three times) higher than at sheltered sites. Melt models should consider the role of redistribution, as well as sublimation of snow, during blowing snow.

1.1.6 Cold Regions Hydrological Modelling platform (CRHM)

The Cold Regions Hydrological Modelling platform (CRHM; Pomeroy *et al.*, 2007) is a physically based distributed hydrological modelling system based on a modular design. CRHM is a useful research tool for diagnosing and predicting hydrological process functions over a river basin in cold regions (Pomeroy *et al.*, 2007). CRHM has been used successfully for hydrology modelling in many cold regions, from prairies to alpine environments, in Asia, Europe, and South and North America (Ellis *et al.*, 2013; Fang *et al.*, 2013; Rasouli *et al.*, 2015; Zhou *et al.*, 2014; Rasouli *et al.*, 2014; Armstrong *et al.*, 2015; Dumanski *et al.*, 2015; Krogh *et al.*, 2015, 2017; Weber *et al.*, 2016; Fang and Pomeroy, 2016; López-Moreno *et al.*, 2016; Cordeiro *et al.*, 2017). Beckers *et al.* (2009) reviewed 30 hydrological models and suggested CRHM's strength in blowing snow and

cold regions modelling. They also suggested CRHM's limitation in its applicability to small and medium-sized basins due to its basic streamflow routing module.

Saltation and suspension are the two primary modes of transport of snow by blowing processes (Pomeroy *et al.*, 1997). The Prairie Blowing Snow Model (PBSM, Pomeroy and Li, 2000, Pomeroy, 1989) simulates snow transportation by saltation and suspension, as well as sublimation rates. Surface characteristics of high elevation mountains differ from lowlands in several respects. Two phenomena are prominent in mountains for snow redistribution: blowing snow due to wind action and snow redistribution by avalanches along steep slopes. Snow is transported from smoother to rougher surfaces and topographic depressions (Essery and Pomeroy, 2004). MacDonald *et al*. (2009) showed that the physically based blowing snow model developed for prairie landscapes could be successfully applied over mountains for blowing snow redistribution, with minor modifications. Gravitational snow transport is also important in steep terrain and the process leads to a relocation of snow from high to low elevations (Bernhardt and Schulz, 2010). Bernhardt and Schulz (2010) developed the avalanche model (*SnowSlide*) that is parameterized using a threshold snow depth and slope angle. It has yet to be tested on a mountain glacierized basin, with snow redistribution by wind and avalanches, and snow and firn/ice melt energetics to simulate glacier mass balance and glacier-fed runoff.

In summary, the mountain glaciers in the Canadian Rockies are retreating, there is a reduction in snow accumulation in the region, and streamflows from these glacierized basins are changing. There is also change in spatial and temporal variations of temperature and precipitation. This means there are observed changes both in glacier configurations and in the climate of the region. However, there is a lack of clear understanding of how these changes are interrelated. There is a need for a physically based glacier hydrological model, and an energy budget approach coupled with snow redistribution by wind and gravity to study impacts of changes in climate and glacier configuration on glacierized mountain hydrology. The model must simulate the hydrology of both glacierized and glacier-free areas within the basin. Physically based energy budget models are not commonly used in glacierized mountain basins because of the limited availability of radiation observations. There are reanalysis products and empirical approaches to estimate shortwave irradiance, but there is uncertainty in estimating radiation on mountain terrain, and reanalysis

products have yet to be evaluated in these basins. One of the intentions of this work, therefore, is to improve daily shortwave irradiance simulation for mountain sites and to compare the suitability of using reanalysis products with temperature based shortwave irradiance models.

1.2 Objectives

The aim of the study is to model of snow and glacier ablation and accumulation dynamics by improving hydrological modeling capacity in high mountain cold regions and diagnosing the impacts of changes in climate and glacier configuration on headwater hydrology. Three specific objectives are proposed to fulfil the research aim.

(1) Develop a new atmospheric transmittance model to estimate shortwave irradiance from temperature and humidity observations and evaluate reanalysis data.

Empirical relations between melt and temperature have often been preferred over physical energy budget calculations for snow and glacier melt in high mountain basins because of the lack of observations of shortwave irradiance and uncertainty in estimating irradiance from other variables. There are empirical methods for the estimation of shortwave irradiance that are primarily based on air temperature and have been developed for lower elevations. They need to be tested at high elevations. There is also a need to evaluate reanalysis shortwave irradiance data, and the reanalysis temperature and humidity data as inputs for the empirical methods for estimating shortwave irradiance over mountains.

(2) Couple snow redistribution and surface energy and mass budgets in a glacier hydrological modelling platform and test the model at two glacier research basins in the Canadian Rockies.

Redistribution of snow due to blowing snow and avalanches and the spatial and temporal distributions of the surface energy and mass budgets are not normally coupled in glacio-hydrology models. It is hypothesized that the simulation of mass and energy budgets will be more process based when snow redistribution by wind and gravity and sublimation of blowing snow are included.

(3) Diagnose the individual and combined impacts of changes in climate and glacier configurations on headwater hydrology.

Glacio-hydrology studies mainly focus on the impact of warming climate on glacier mass and runoff, and these studies primarily use empirical models. The individual and joint impacts of changes in glacier configurations and climate on the headwater hydrology have not been studied.

The research findings from this study are expected to be relevant to water resource management, particularly in determining the influence of changing climate on water availability from glacier streams. Models of non-glacierized and recently de-glacierized parts of a mountain glacial basin can also be used to determine the role of deglaciation in the hydrology of the basin.

1.3 Organization of chapters

This thesis consists of an introduction, four chapters in the form of journal articles, and a concluding chapter. Chapter 1 introduces the study's background, objectives and comprehensive literature review. Chapters 2, 3, 4 and 5 consist of four manuscripts designed for submission to peer-reviewed journals. Chapter 2 provides glaciological, hydrological, meteorological and geophysical datasets for Peyto Glacier Research Basin. Chapter 3 describes a global radiation model to estimate daily shortwave irradiance for cold regions and mountains (Objective 1). Chapter 4 describes the development and testing of the glacier hydrology model within the CHRM platform (Objective 2). Chapter 5 addresses the application of the CRHM-glacier hydrology model to diagnose the impact of climate change and change in glacier configuration on the hydrology of the headwaters (Objective 3). Chapter 6 synthesizes the findings and the conclusions drawn from the last five chapters.

CHAPTER 2 : Hydrometeorological, glaciological and geophysical research data from the Peyto Glacier Research Basin in the Canadian Rockies

Paper manuscript status

Contents of this chapter have been compiled as a data paper to the Earth System Science Data (ESSD) – INARCH special Issue.

Author contributions: Dhiraj Pradhananga collected, analysed and prepared data, and drafted the manuscript. John W. Pomeroy, D. Scott Munro, Caroline Aubry-Wake and Joseph Shea revised the manuscript. D. Scott Munro collected and cleaned meteorological data prior to 2012; Caroline Aubry-Wake collected and analysed streamflow data [2013-2018]; Michael N. Demuth collected glaciological data. Nammy Hang Kirat prepared 1966 (from topographic map) and 2014 DEMs and coding in Google Earth Engine for landcover mapping; Brian Menounos and Kriti Mukherjee prepared DEMs of 1966 (from aerial photographs), 1986 and 2017 and co-registered the DEMs [1966, 1986, 2006] with 2017 as the master DEM.

Peyto Glacier Research Basin (PGRB) in the Canadian Rockies is one of the glacier basins that USask has been monitoring in western Canada to study the impact of climate change on glacier hydrology. The other basins are Robertson, Athabasca and Bologna glaciers. Meteorological data from these glaciers and Peyto Glacier were used in Chapter 3 for developing and testing a new model based on temperature and humidity to simulate shortwave irradiance and for evaluating shortwave irradiance data from reanalysis data products. CRHM-glacier, a physically based energy and mass balance model, was developed in the Cold Region Hydrological Modelling platform and tested over PGRB and the Athabasca Glacier Research Basin (AGRB) in Chapter 4. Preparation of meteorological data to both drive and evaluate such a hydrology model is a critical step in achieving the objectives of this thesis.

2.1 Abstract

This chapter presents hydrological, meteorological, glaciological and geophysical data of PGRB. Peyto Glacier has been of great interest to glaciological and hydrological research since the 1960s, when it was chosen as one of five glacier basins in Canada for the study of mass and water balance during the International Hydrological Decade (IHD, 1965-1974). Intensive studies of the glacier and observations of the glacier mass balance are ongoing till now, whereas the initial meteorological and hydrological observations were discontinued. In the late 1980s, meteorological observations resumed, and streamflow measurements restarted more recently. The Centre for Hydrology at the University of Saskatchewan has continued these hydro-meteorological observations since 2012. During these periods, Peyto Glacier has lost significant mass and a mostly negative mass balance has been consistently observed since the mid-1970s. Hourly meteorological data are available from 1987 to the present, but precipitation data collected within the basin are not reliable. Therefore, precipitation data from the Environment Canada's Bow Summit station, ~5 km away from the basin, are used as a substitute. A long-term (1979-2018) forcing data set with hourly time step have also been prepared from four bias-corrected reanalysis products (ERA-Interim, WFDEI, NARR, and CFSR). These data are crucial for studying climate change and variability in the basin and for the application of process-based hydrological models to study the hydrological responses of the basin to both glacier and climate change.

2.2 Introduction

Peyto Glacier (Figure 2-1) in Banff National Park is a valley outflow glacier of the Wapta Icefield in the Waputik Mountains in the Canadian Rockies – in the headwaters of the Columbia and Saskatchewan-Nelson river systems in western Canada. The meltwater from the glacier contributes to the North Saskatchewan River. These water sources are important to downstream water supply for industrial, agricultural, hydropower, environmental and drinking purposes. The meltwater from this glacier and others in the region is crucial to the supply, specifically during the dry late summer season (Hopkinson and Young, 1998; Comeau *et al*., 2009).

Although the first record of Peyto Glacier goes back to a photograph by Walter D. Wilcox taken in 1896, significant research of the glacier began in 1965, when it was selected as one of the research sites for the International Hydrological Decade (IHD). The scope and observational resources have improved progressively since then (Munro, 2013). Young and Stanley (1976) documented the glaciological and hydro-meteorological data collected within the glacier basin during the IHD. Past studies over the glacier are also well documented in 'Peyto Glacier: One Century of Science' (Demuth *et al.*, 2006). The edited book provides details on the mass balance data (until 1995) along with the hypsometry of the glacier. The first-ever measurements of the position of the glacier terminus were made by the team of J.M. Thorington and H.S. Kingman of the Canadian Alpine Club in 1933 (Ommanney, 1972). Since 1945, glacier front variation data have been collected regularly, while mass balance and runoff data have been recorded since the early IHD period. Mass balance observations have been continued till now. However, discharge observations were discontinued when the stream gauge was washed away by a flood in July 1983. Since 2013, discharge measurements have resumed, recorded by the Centre for Hydrology at the University of Saskatchewan (USask), with a new gauging site located 1.5 km upstream from the previous location. A year-round automatic weather station, operating since 1987 (Munro, 2013), was upgraded in 2012 and is now operated by USask.

Collecting data from remote, difficult-to-access alpine glacier basins can be daunting and can give rise to a host of other difficulties. For example, Lafrenière and Sharp (2003) and Rasouli *et al*. (2018) noted the impact of power source failures on automatic weather station (AWS) records, such as to cause significant data gaps. High accumulation of snow during winter can bury on-ice AWS and riming can compromise instrument performance. In turn, high summer melt can cause on-ice stations to tilt or fall over. Climate data availability and accuracy in the PGRB suffer from many such irregularities. Therefore, affected data must be infilled or corrected before the datasets can be used for medium and long-term studies.

The World Glacier Monitoring Service (WGMS) has listed Peyto Glacier as a 'reference glacier' for mass balance, in consideration of its mass balance data record of over 30 years. PGRB can be considered an outdoor laboratory for conducting hydrological research, as proposed by Seyfried (2003); however, a single document to list these hydro-meteorological datasets is needed.

This paper details the meteorological forcing datasets that were created for driving hydrological models of Peyto Glacier, along with the related hydrological and geophysical datasets that can be used for model evaluation, mainly for three time periods: 1965-1974, 1987-2012 and 2013-2018. These datasets include historical archived data from the IHD period and recent data from both on-ice and off-ice stations. Glaciological mass balance measurements, using ablation stakes and snow pits, have been carried out continuously since the beginning of the IHD period. A comprehensive account of the first 14 years mass balance results can be found in Young (1981). The mass balance data have been used by many researchers (Østrem, 1973; Letréguilly, 1988; Letréguilly and Reynaud, 1989; Bitz and Battisti, 1999; Watson *et al.*, 2006; Shea and Marshall, 2007; Matulla *et al.*, 2009; Marshall *et al.*, 2011) as reference data for the region. However, the meteorological, hydrological and geophysical datasets of the basin have not yet published.

2.3 Peyto Glacier Research Basin

The PGRB is in the Canadian Rockies, on the eastern side of the Continental Divide, at latitude 51°40'N and longitude116°33'W. Ranging in elevation from 1907 to 3152 m, this heavily glacierized basin is 23.6 km^2 in area. It is a sub-basin of the Mistaya River Basin in Banff National Park, Alberta, and is located in a predominantly sedimentary geological region, with surrounding mountains formed from hard, resistant dolomite (Young and Stanley, 1976). The basin has been well monitored over a 50-year observational period (Shea *et al.*, 2009). During the 1960s, the area of the glacier was 13.4 km^2, but it has been continuously losing mass and area since the mid-1970s, shrinking to an area of 9.87 km^2 as of 2018 (Figure 2-1). A new proglacial lake formed at the tongue of the glacier increases in size every year and has been informally named ‘Lake Munro’ by USask to honor D. Scott Munro’s research contribution to the glacier basin. Peyto Creek flows out of Lake Munro, draining PGRB into Peyto Lake and thus supplying water to the Mistaya River, a tributary of the North Saskatchewan River.

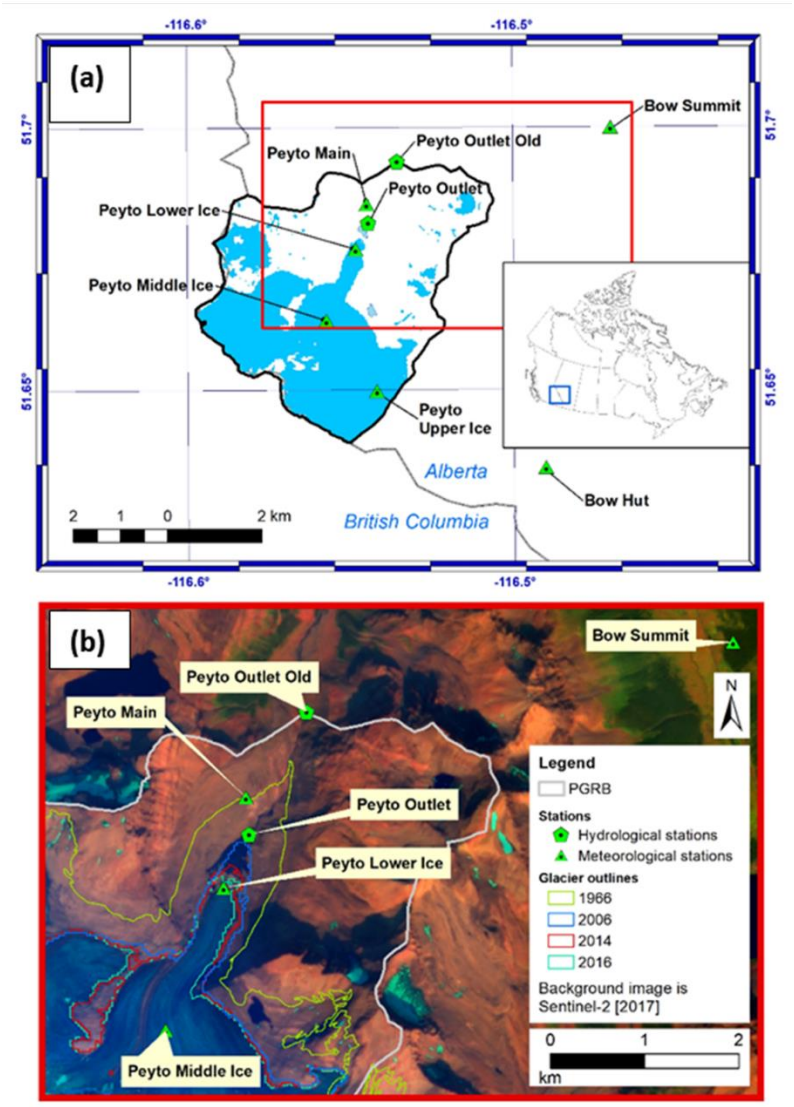

Figure 2-1: Peyto Glacier Research Basin (PBRB). (a) locations of PGRB and the hydro-meteorological stations, (b) past and present glacier extents.

2.3.1 Meteorological sites

Meteorological observations were initiated for the summer months (June – September) during the IHD at the Peyto Creek Base Station adjacent to the glacier terminus, now renamed as Peyto Main (Figure 2-1). After becoming dormant, the station was re-established at the same location in September 1987 as an AWS. Table 2-2 details the meteorological variables and instruments to record them at the station during the IHD and the post-IHD period. Three AWS were also established on the glacier surface in different elevation zones - namely, the Lower, Middle and

Upper ice stations - for post-IHD micrometeorological studies by D. Scott Munro. These were originally positioned to represent different glacier dynamical zones – ablation zone, equilibrium line zone and accumulation zone. Since 2012, these stations have been continued by USask, with new instruments, but they have been relocated to accommodate changing glacier geometry and shifts in the dynamical zones. These data, however, are not continuous and only the Lower Ice station was continued after 2013.

2.3.2 Hydrological sites

Peyto Outlet is a hydrometric station that measures glacier meltwater runoff at the outlet of Lake Munro. The Old Gauge (Peyto Outlet Old) was about 1.5 km downstream of the New Gauge (Peyto Outlet) (Figure 2-1).

The AWS sites in the PGRB are now a part of the cryospheric surface observation network (CryoNet) of the World Meteorological Organisation (WMO) Global Cryosphere Watch (GCW) http://globalcryospherewatch.org/cryonet. Peyto Main and Peyto Lower Ice are listed as Reference CryoNet stations, whereas the others are Contributing CryoNet Stations of the GCW. Figure 2-1, Figure 2-2, Figure 2-3 and Table 2-1 contain the locational information, data period, and data collection details of the stations.

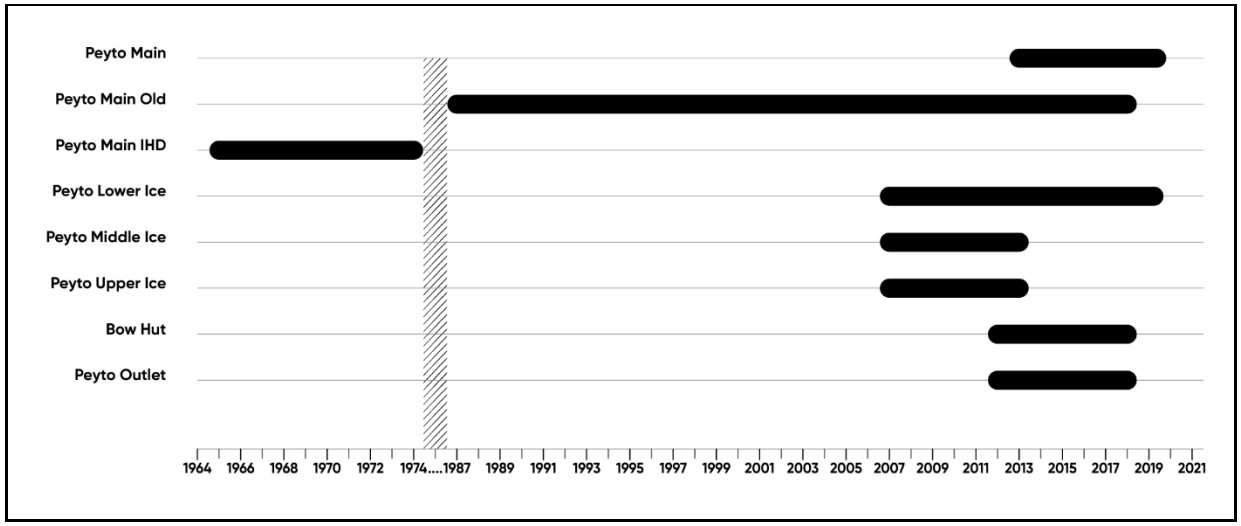

Figure 2-2: Data collection periods for each of the 8 CryoNet stations in PGRB.

Table 2-1: CryoNet station data

Station Name	Station Type^	Geographical Coordinates Elevation above sea level	Variables	Data Period
Peyto Main	Reference	51°41'07.78"N 116°32'41.81"W 2240 m	Ta, RH, Ws, Wd, Ts, Q_{si}, Q_{so}, Q_{li}, Q_{lo}, Ppt, Sd	July 2013 – Aug 2019[+]
Peyto Main Old	Reference	51°41'07.49"N 116°32'40.82"W 2240 m	Ta, RH, Ws, Wd, Ts, Q_{si}, Q_{li}, P, Ppt,	Sept 1987 – July 2018[%#]
Peyto Main IHD	Reference	51°41'07.78"N 116°32'40.81"W 2240 m	Ta, RH, Ws, O_{si}	1965 – 1974*
Peyto Lower Ice[&]	Reference	51°40'36.10"N 116°32'02.35"W 2173-2183 m	Ta, RH, Ws, Sd, Ts, Q_{si}, Q_{so}	Jan 2007 – Aug 2019[@]
Peyto Middle Ice[&]	Contributing	51°39'46.54"N 116°33'27.13"W 2454-2461 m	Ta, RH, Ws, Sd, Ts, SWE	Jan 2007 – Sept 2013[%]
Peyto Upper Ice[&]	Contributing	51°38'57.47"N 116°32'11.43"W 2709 m	Ta, RH, Ws, Sd, Ts, SWE	Aug 2007 – Sept 2013[%]
Bow Hut	Primary	51°38'06.61"N 116°29'25.12"W 2421 m	Ta, RH, Ws, Wd, Sd	Oct 2012 – Sept 2018[+]
Peyto Outlet	Primary	51°40'52"N 116°32'41"W 2150 m	Ta, Runoff	June 2013 – Sept 2018[+]

Ta = air temperature, RH = relative humidity, Ws = wind speed, Wd = wind direction, Ts = soil/snow/firn/ice temperature, Q_{si}, Q_{so} = incoming and outgoing shortwave radiation, Q_{li}, Q_{lo} incoming and outgoing longwave radiation, Ppt = precipitation, P = air pressure, Sd = snow depth (SR50), SWE = snow water equivalent.

[^]Station type according to CryoNet

[+]recorded at fifteen-minute intervals

[%]recorded hourly until September 2008, at thirty-minute intervals then after

*daily data for the summer months

[#]Q_{li} is available, beginning September 1998

[@]hourly until September 2008, then at 30-minute intervals to 2015, 15-minute intervals 2015-2019. Q_{si} and Q_{so} data from 2007 to 2008; Q_{si} measurements available again since 2015

[&]snowpack glacier accumulation and ablation data are also available; Ice stations have several data gaps, mainly in middle and upper ice station records

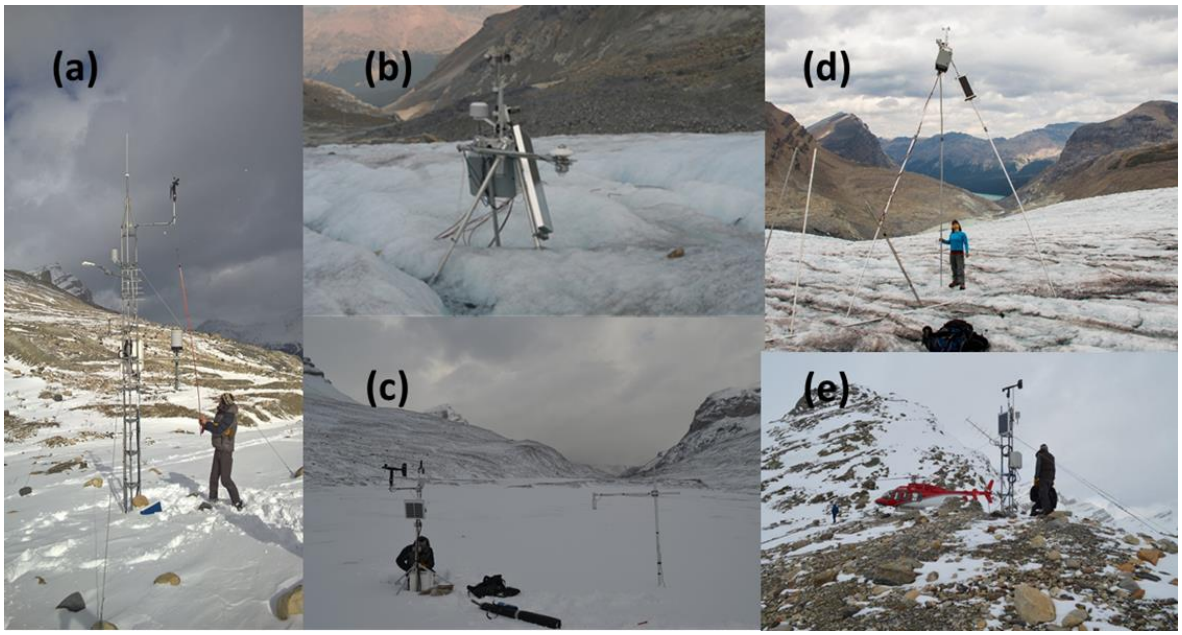

Figure 2-3: Photographs of selected CryoNet stations at PGRB. (a) Peyto Main, (b) Peyto Lower Ice (2009), (c) Peyto Lower Ice (2016), (d) Peyto Middle Ice (2015), and (e) Bow Hut. [Photo (d) by – Angus Duncan; (b) by D. Scott Munro; and the rest by the author]

2.4 Data availability

2.4.1 Meteorological data – historical and present

The National Hydrology Research Institute (NHRI) publication titled, 'Peyto Glacier: A Compendium of Information Prepared for Parks Canada,' by Ommanney (1987), provided meteorological and mass balance data until 1984. It stated that the meteorological station at the base camp documented as 'Peyto Creek Base Station', now renamed Peyto Main Old AWS, took observations for temperature, humidity, precipitation and cloud cover from 1965 to 1984 and for wind speed, sunshine hours and incoming solar radiation from 1967 to 1984. These historic data are, however, not readily available. A segment of the data (1965-1974) was obtained by abstraction from the published graphs (daily values) in the report prepared by Young and Stanley (1976). Air temperature, relative humidity, global radiation, sunshine duration, cloud cover, wind and precipitation were observed and recorded during the summer months only. The details of data and instruments used were documented in publications by the Inland Waters Directorate of Environment Canada (Goodison, 1972; Young and Stanley, 1976).

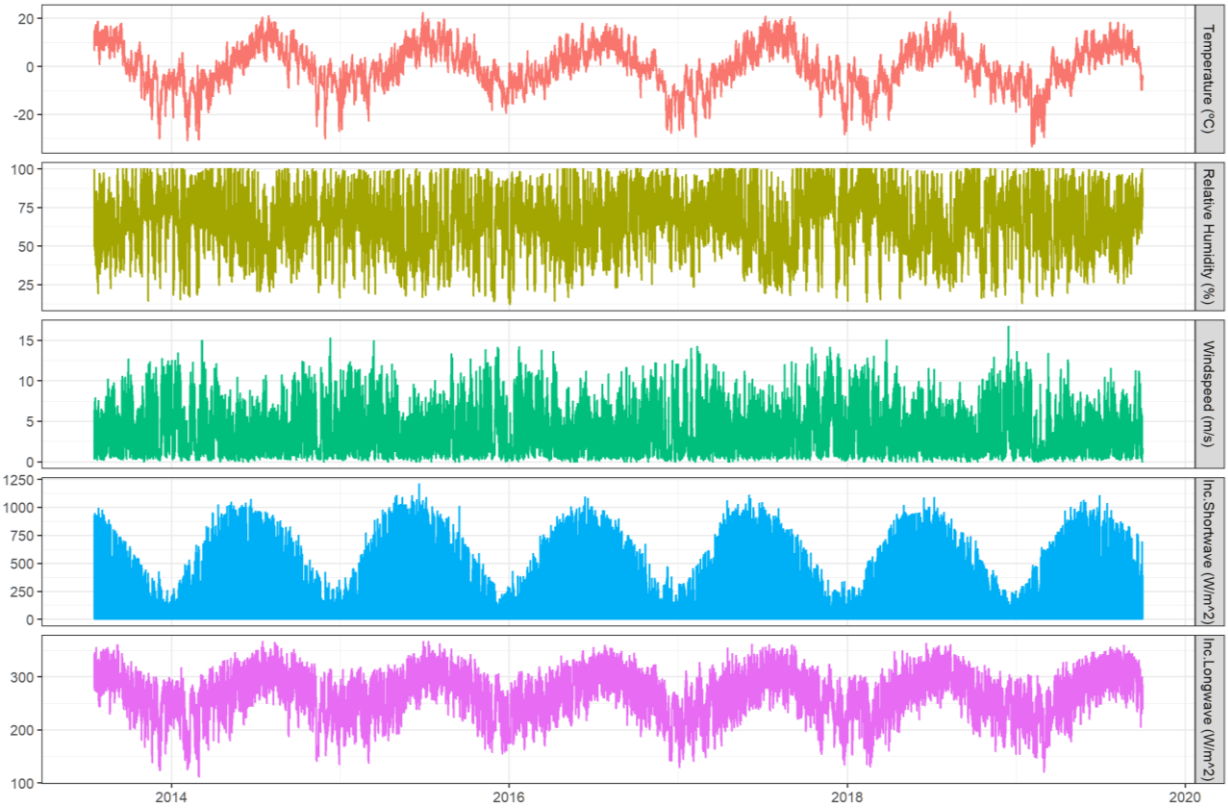

Figure 2-4: Hourly values of meteorological variables recorded at Peyto Main AWS between July 2013 and September 2019.

Automatic weather stations were first installed at on- and off-glacier sites for micrometeorological studies and retained over the long term. The Peyto Main station was installed near Peyto Main Old in 2013, with new instruments and settings. The data from these stations are hourly prior to September 2008, sub-hourly there after, and available from 1987 to 2018 from Peyto Main Old, and from 2013 to 2019 from Peyto Main (Figure 2-4). Some data (2002-2007) for Peyto Main Old were published (Munro, 2011a) in support of the IP3 initiative: *Improving Processes & Parameterization for Prediction in Cold Regions Hydrology*. The details of the IP3 project and AWS data from the Peyto Main Old (Table 2-2) are available at (http://www.usask.ca/ip3/data.php).

The nearest AWS outside the basin boundary is operated by USask at Bow Hut (Figure 2-1), established in October 2012 and continuously monitored since then. Air temperature, humidity, wind and snow depth data are available from the station. The moraine AWS (Peyto Main and Bow

Hut) were connected to telemetry in 2015 and can be monitored remotely. Near real-time data by telemetry, extending back one week can be viewed on the website: http://www.usask.ca/hydrology/CRHOStns.php.

Table 2-2: Details of hourly PGRB meteorological data referred to in Goodison (1972) and Munro (2011b).

Variables	**Instruments**	
	Peyto Main Old	**Peyto Main IHD (June – August)**
Air temperature and relative humidity	Vaisala HMP35/45, YSI[%] thermistor	Lambrecht 252 Thermo-Hygrograph, CMS[#] max. and min. thermometers
Ground/snow temperatures	YSI thermistor	N/A
Wind speed and direction	RM Young	MK II totalizing anemometer
Precipitation	Geonor gauge*, CMS tipping bucket	Pluvius/CMS 3" rain gauge
Sunshine hours		Campbell-Stokes sunshine recorder
Incoming longwave radiation	Epply pyrgeometer	
Incoming shortwave radiation	Kipp & Zonen CM6/11 pyranometer	Belfort 5-3850 pyranograph
*standard recording precipitation gauge with Alter wind shield after April 2002; custom adapted Fischer-Porter gauge with Alter shield prior to that time. [%]YSI stands for Yellow Springs Instruments. [#]CMS stands for Canadian Meteorological Service (now MSC, the Meteorological Service of Canada)		

Meteorological data from the Peyto Ice stations (Upper, Middle and Lower) are not continuous because of difficulties in operating the stations on glacier ice, but periods of synchronous observational data are available. The three stations were operational at the same time for brief periods between 2007 and 2013 (Table 2-1). Peyto Lower Ice has been maintained for a longer period than Middle and Upper Ice, collecting both incoming and outgoing shortwave radiation data until August 2010. Peyto Lower Ice and the two moraine stations (Peyto Main Old and Peyto Main) are currently operational. Peyto Lower Ice was updated with new instruments in October 2015. The details of data availability from these stations are presented in Table 2-1.

2.4.2 Precipitation

Precipitation at the Main Old station was measured by a Geonor T-200B, a recording precipitation gauge with Alter wind shield, beginning in April 2002; and a CMS tipping bucket rain gauge (TBRG) operating nearby (Figure 2-5 and Table 2-1). Both instruments, however, might be malfunctioning. When compared to the new TBRG at the Peyto Main station, 20 metres west of the old station (Figure 2-4), both the Geonor and the old TBRG recorded significantly less precipitation. The Geonor rainfall record was less (by 112 to 153 mm) than that from the new TBRG over four months (June – Sept, Figure 2-5). The old TBRG and Geonor may have developed mechanical faults in this harsh location. Winter precipitation recorded by the single alter-shielded Geonor was also very low compared to the Bow Summit station (Figure 2-5), which is located nearby (Figure 2-1).

Precipitation records at the Peyto Main was first segregated to rainfall and snowfall by applying the precipitation phase determination algorithm developed by Harder and Pomeroy (2013). Snowfall was bias-corrected for wind-induced under catch (Smith, 2007) and rainfall was corrected with a catch efficiency of 0.95 (Pan *et al*. 2016). Bow Summit data were accepted as recorded because the surrounding trees (Figure 2-7) act as a double fence shield around the single Alter-shielded precipitation gauge at Bow Summit, thus making the site ideal for precipitation measurement.

Mean monthly recorded precipitation data (averaged over seven years from 2010-2016) from Peyto Main and Bow Summit stations were compared (Figure 2-9). Similar values were recorded during the summer months (May-October), with June-September as the months with the most rainfall. The differences, however, were larger during the months with the most snowfall during winter, fall and spring (November to April). Therefore, the winter precipitation recorded at Peyto was comparatively less than that at Bow Summit (Figure 2-9). The precipitation gauge may have been under catching a large portion of the solid precipitation. In addition, the empirical bias correction method developed for prairie snowfall under-catch due to wind (Smith, 2007) may need to be improved for use in a mountain environment.

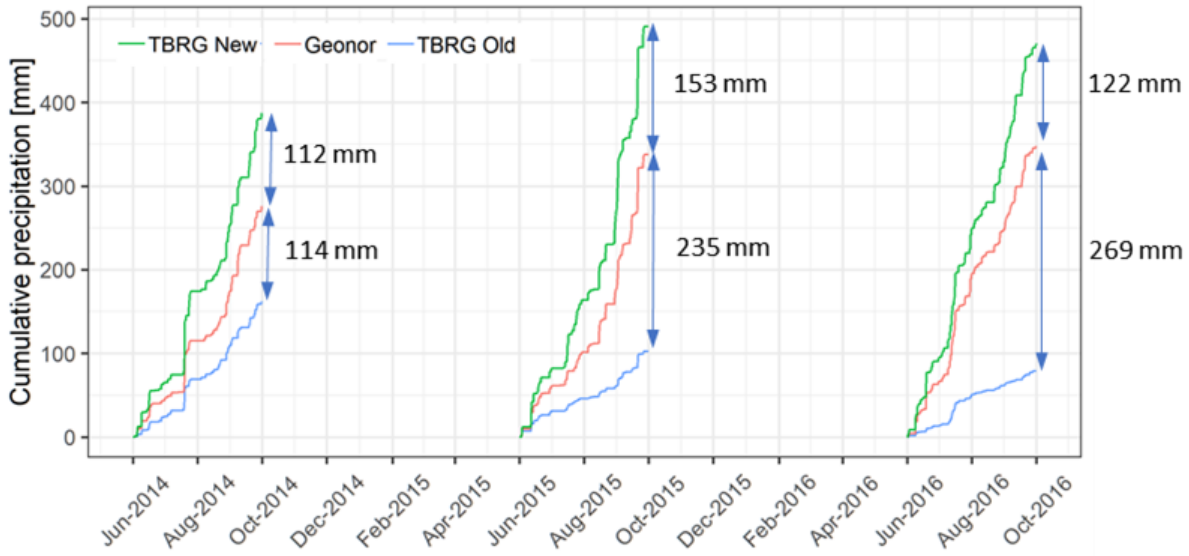

Figure 2-5: Comparison of cumulative liquid precipitation at the Peyto Main station.

Note: Both the Geonor and the old TBRG recorded less rainfall compared to the new TBRG during summer months (June, July, August, and September)

The precipitation data recorded at Bow Summit (51°42'00"N, 116°28'00"W, Elevation 2080 m, Climate ID: 3050PPF) are, therefore, considered the most suitable to represent precipitation over PGRB. Bow Summit data can be downloaded from Alberta Climate Information Service (ACIS, http://agriculture.alberta.ca/acis/). Quality-controlled hourly temperature and precipitation data are available continuously from 1 November 2008 to the present; continuous daily data are available from 23 March 2006 to the present. The hourly temperature and precipitation data (from 1 November 2008 to 31 December 2019) are plotted in Figure 2-10. Because earlier data are not continuous, they are disregarded for use in this study.

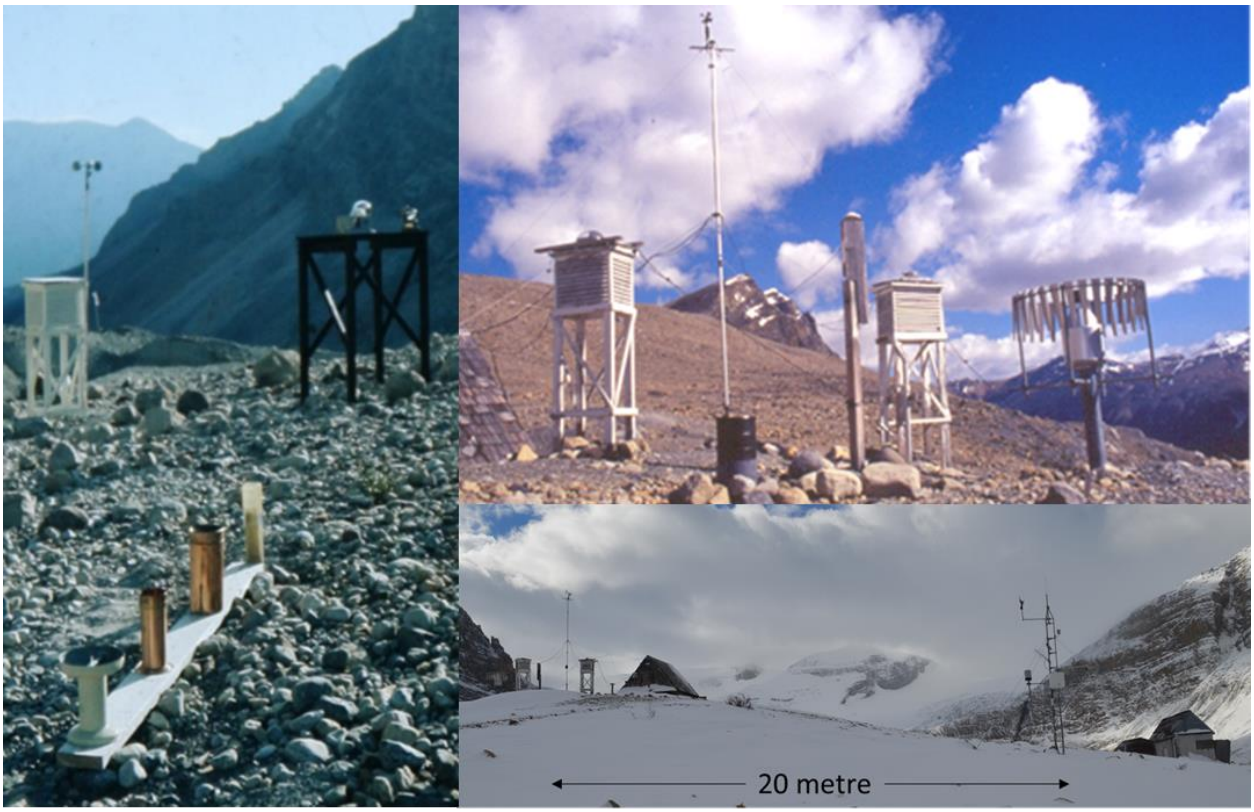

Figure 2-6: The base camp stations – Peyto Main IHD (left), Peyto Main Old (top), Peyto Main and Peyto Main Old (bottom). [Photos, left and top by D. Scott Munro, bottom by the author]

Figure 2-7: Bow Summit station. [Photo by the author]

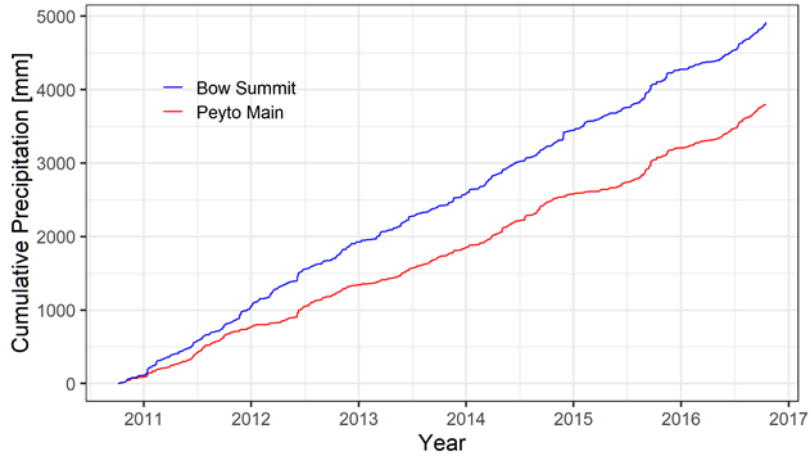

Figure 2-8: Cumulative precipitation from Bow Summit and Peyto Main from October 2010 to September 2016.

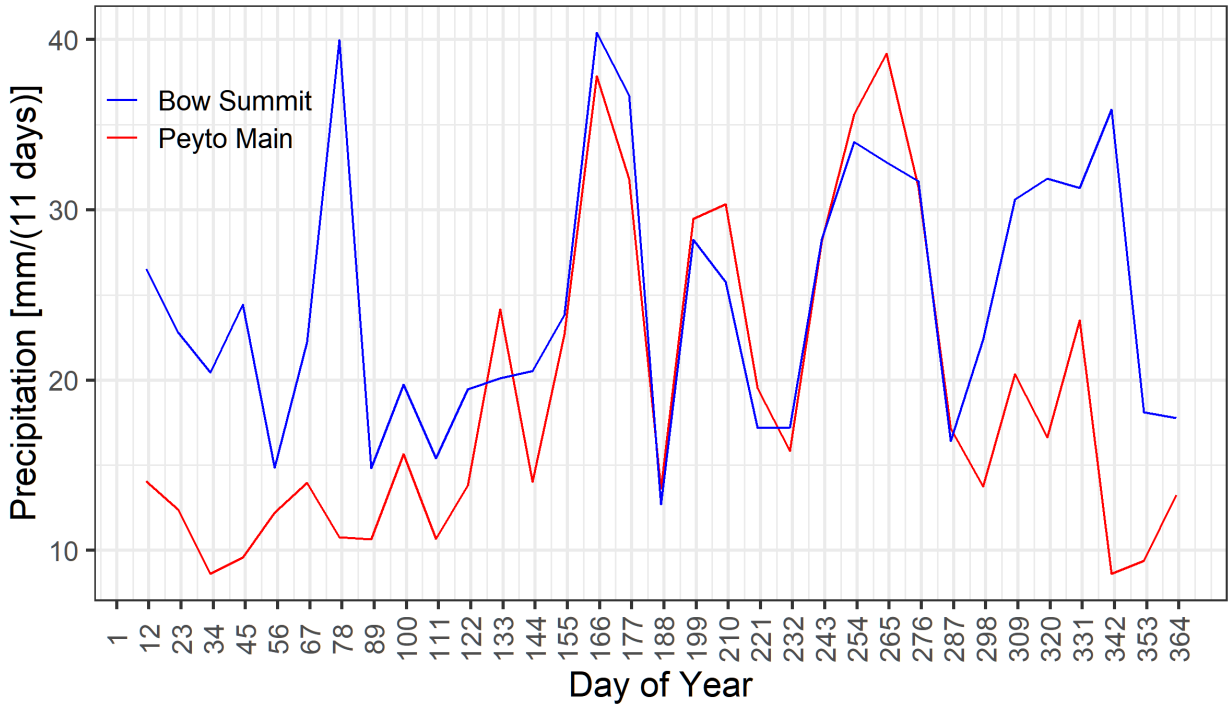

Figure 2-9: Comparison of precipitation (11-day total values averaged over the period from 2010 to 2016) recorded at Bow Summit and Peyto Main.

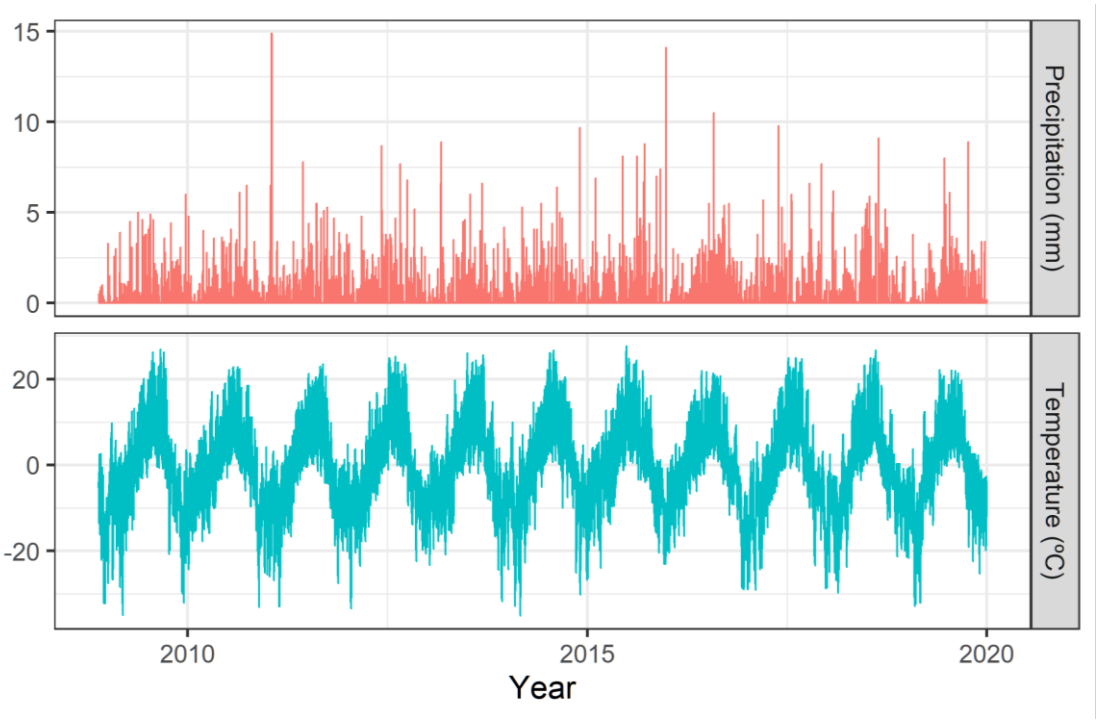

Figure 2-10: Hourly temperature and precipitation recorded at Bow Summit.

2.4.3 Data cleaning and gap infilling

Meteorological data were recorded at 15-minute (new stations – Bow Hut, Peyto New, Lower Ice after 2013) and 30-minute (old stations – Peyto Old, ice stations) intervals and were aggregated to hourly intervals, thus corresponding to the AWS recording interval used prior to September 2008. Raw data were thoroughly checked for errors and erroneous data were removed. Missing data were filled in by either linear interpolation or linear regression to data from the stations within the basin. Linear interpolation was chosen when the data gaps were less than or equal to four hours, and linear regressions were applied when data gaps were more than four hours. These data cleaning processes were followed in a sequence by applying various R functions along with the CRHMr package (Shook, 2016a). Details on CRHMr and guidance to install the r package are available at the GitHub https://github.com/CentreForHydrology/CRHMr. The data processing steps for quality assurance and control are listed below [the corresponding r functions in the CRHMr package are listed in the brackets]:

1. Read the raw data files. [CRHMr:: readCampbell]
2. Remove duplicate data. [CRHMr::findGaps and deDupe]
3. Check for inconsistencies by plotting each data column for initial quality control. [CRHMr::plotObs]
4. Remove spikes and outliers. [CRHMr::minObs and maxObs]
5. Fill in the missing data by interpolation if the gap is less than 4 hours. [CRHMr::interpolate]
6. Fill in the missing data (gap > 4 hours) by nearby stations with monthly regression equations. [CRHMr::regress and impute]
7. Aggregate cleaned sub-hourly data to hourly. [CRHMr::aggDataframe]

Despite two data gaps 6-8 months long and five more that span periods of 15-45 days, the Peyto Main Old record is over 91% complete between 1987 and 2012. Gap fill-ins and corrections to key elements, such as air temperature and solar radiation, were done with flags to aid judgement on data suitability. Recent data from Peyto Main Old (4 October 2010 to 31 July 2018) and Peyto Main (17 July 2013 to 1 Oct 2019) are almost continuous, except for two short gaps in 2013 for Peyto Main Old (13 hours total) and five brief gaps in 2013, 2015, and 2016 for Peyto Main (5.5 hours total) – each a gap of less than four hours. The wind data from Peyto Main Old were not correct from 17 July 2017 to 8 March 2018. Also, the temperature and humidity probes at Peyto Main were not functioning properly for longer periods during 2016-2018. The temperature probe at Peyto Main recorded 10 ^{o}C less than that of Peyto Main Old from 22 November 2016 to 8 March 2018 due to a coding error in the datalogger program; the humidity probe was not functioning well from 20 September 2016 to 20 March 2017. These differences were detected by plotting the data and comparing them with data from Peyto Main Old.

Table 2-3 shows the regression results and Figure 2-11 shows the systematic bias in Peyto Main air temperature data before and after a 10 ^{o}C correction. The erroneous humidity data were corrected from the Peyto Main Old station data using monthly regressions (Table 2-4). In addition, Peyto Main station data for all the variables were extended back to 2010 using monthly regressions with data from the Peyto Main Old.

Table 2-3: Hourly regression results for Peyto Main and Peyto Main Old

Variables	From	To	Slope	Intercept	R^2
Air temperature	2013-07-17	2018-06-13	1.00	0.23	1.00
Vapour pressure	2013-07-17	2018-06-13	0.91	0.02	0.99
Wind	2013-07-17	2018-06-13	0.84	-0.14	0.96
Incoming shortwave	2013-07-17	2018-06-13	1.01	2.04	0.97
Incoming longwave	2013-07-17	2018-06-13	0.95	21.12	0.96

Table 2-4: Regression results for Peyto Main and Peyto Main Old hourly data.

Month	Air temperature		Vapour pressure	Wind	Incoming shortwave	Incoming longwave	
	Slope	Intercept	Slope	Slope	Slope	Slope	Intercept
Jan	1.00	0.23	1.01	0.83	1.07	0.93	23.58
Feb	1.00	0.20	0.99	0.83	1.05	0.95	18.08
Mar	1.00	0.24	0.99	0.84	1.03	0.94	20.58
Apr	0.99	0.21	0.97	0.83	1.02	0.92	29.25
May	0.99	0.34	0.94	0.83	1.01	0.92	30.64
Jun	0.99	0.32	0.94	0.81	1.01	0.91	32.44
Jul	0.99	0.35	0.93	0.79	0.99	0.86	48.38
Aug	0.98	0.44	0.93	0.79	0.99	0.87	45.11
Sep	0.98	0.36	0.95	0.80	1.02	0.89	37.77
Oct	0.99	0.23	0.96	0.81	1.03	0.93	25.24
Nov	1.00	0.23	1.01	0.82	1.05	0.90	29.71
Dec	1.00	0.19	1.01	0.82	1.06	0.91	27.57

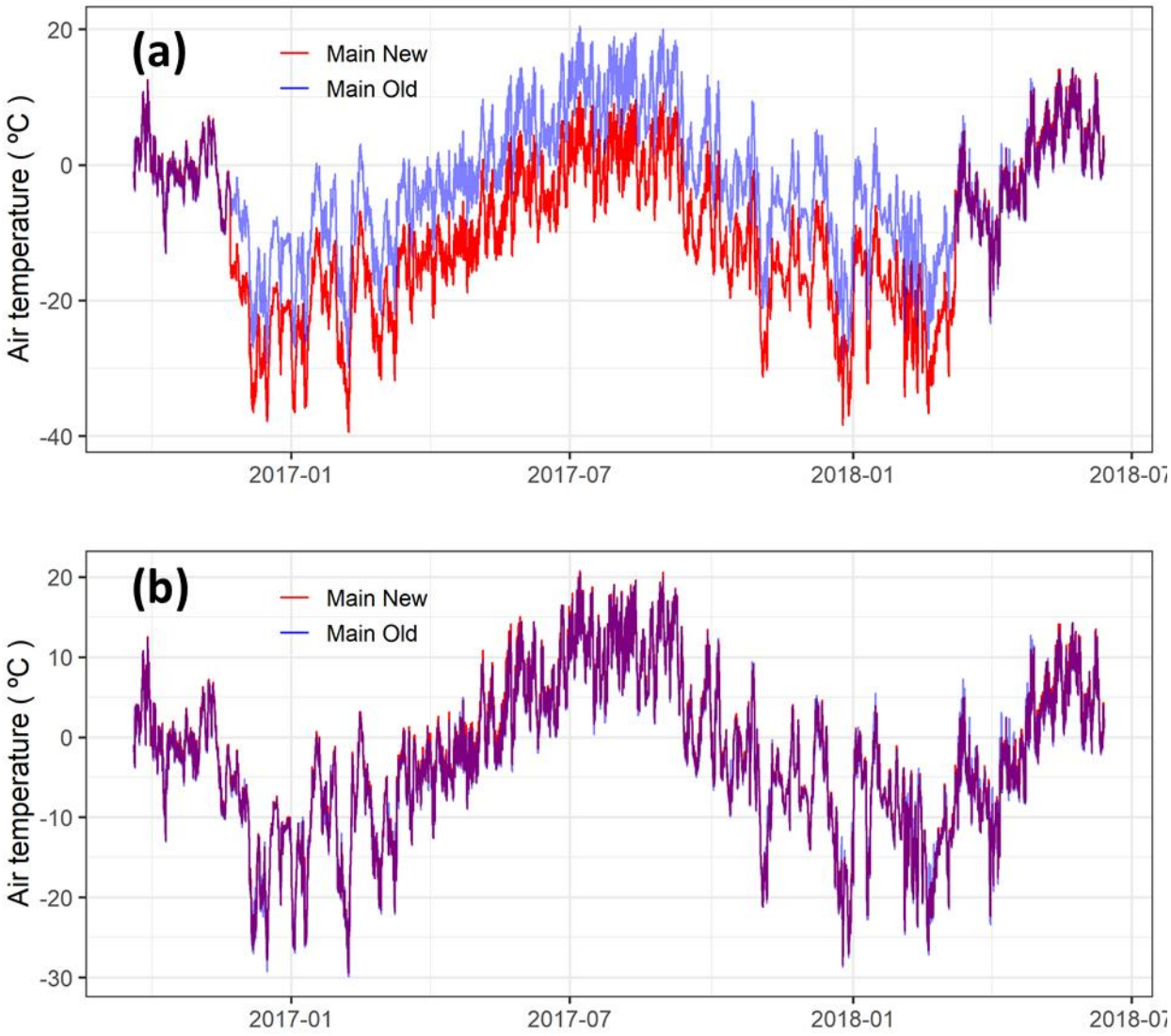

Figure 2-11: Air temperature recorded at the Peyto Main stations (Main and Main Old) (a) before bias correction to Peyto Main; (b) after bias correction. Where the values overlap, they appear in purple.

2.4.4 Reanalysis forcing data

Bias-corrected reanalysis data are also included as model forcing data for running glacio-hydrological models for longer periods. Four gridded reanalysis products were bias-corrected to the *in-situ* observations at PGRB:

1. ERA-Interim is the European Centre for Medium-Range Weather Forecasts (ECMWF) interim reanalysis (Dee *et al.*, 2011);

2. Water and Global Change (WATCH) product, WFDEI (WATCH Forcing Data ERA-Interim) (Weedon *et al.*, 2011);
3. North American Regional Reanalysis (NARR) (Mesinger *et al.*, 2006); and
4. Climate Forecast System Reanalysis (CFSR) (Saha *et al.*, 2010).

These products are available at different spatial and temporal resolutions and for different time periods. WATCH, ERA and CFSR are global datasets, whereas NARR covers only North America. Evaluation of these datasets are provided in Appendix B. While comparing the three reanalysis products, ERAI was found the best compared to NARR and WFDEI for air temperature, vapour pressure, shortwave irradiance, longwave irradiance and precipitation. WFDEI was found the best for wind speed in comparison to ERAI and NARR.

ERA-Interim is available from January 1979 to August 2019, with the original resolution of 0.7^{o} at the Equator (Dee *et al.*, 2011). WFDEI (Weedon *et al.*, 2011) is available at a spatial resolution of 0.5^{o} x 0.5^{o} from January 1979 to December 2019. NARR (Mesinger *et al.*, 2006) is available at 3-hourly temporal and 32 km spatial resolutions from January 1979 to January 2017. CFSR, which is developed by the National Centers for Environmental Prediction-National Center for Atmospheric Research (NCEP-NCAR), is available at an hourly time resolution and a horizontal resolution of $0.5° \times 0.5°$ for the period from 1979 to 2009 (Saha *et al.*, 2010).

All gridded reanalysis data were first extracted for the Peyto Main station coordinates. ERA-Interim, WFDEI, and NARR data were interpolated to hourly time periods. The R-package, Reanalysis (Shook, 2016b) was used for extracting and interpolating ERA-Interim, WFDEI, and NARR datasets. Air temperature, vapour pressure, wind, precipitation, incoming longwave and incoming shortwave radiation data were interpolated linearly from 3 or 6 hours to hourly time intervals. Total precipitation (3 or 6 hours) was distributed evenly to hourly time intervals. MATLAB (MATrix LABoratory) codes (Krogh *et al.*, 2015) were used to extract CFSR values, which were already at hourly time intervals. The hourly data were bias-corrected to the *in-situ* observations at the main station using quantile mapping technique with parameters calibrated for

each month from the common data periods using qmap package in r (Gudmundsson, 2016). ERA-Interim data from January 1979 to August 2019 are presented in Figure 2-12.

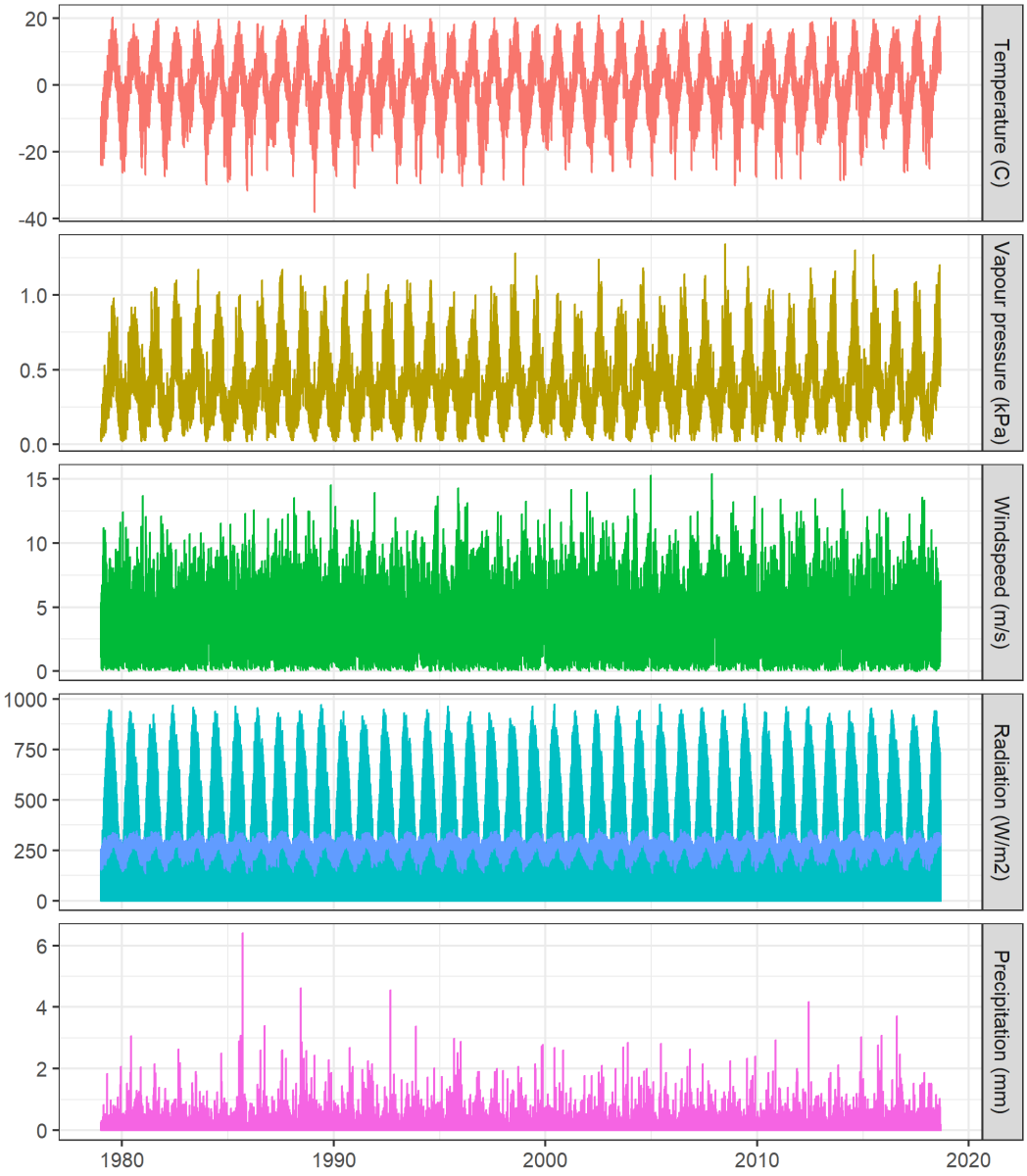

Figure 2-12: Bias-corrected ERA-Interim hourly data for PGRB.

2.4.5 Hydrological data – historical and present

Historical observed daily outflows from the glacier at Peyto Creek are available for 1967 to 1977, from the Water Survey of Canada (WSC, http://www.ec.gc.ca/rhc-wsc/). They are also available at 15-minute intervals from 1970 to 1977 by accessing the Peyto Glacier runoff archive housed at the University of Waterloo (Munro, 2011b). The gauge station (ID 05DA008) was established in 1966 for the IHD program and maintained by WSC. It consisted of a float-activated continuous stage recorder (Table 2-5) mounted on a stand pipe ~500 m from the glacier tongue (Figure 2-13).

Flow measurement at Peyto Creek was a challenge due to unstable cross sections, occasional flash floods and lack of direct discharge measurements during high flows. Goodison (1972) reported that the discharge records from 1967 were not reliable and he did not consider the observation data for his study. The stage gauge was washed out during a flood in August 1967. As reported by Ommanney (1987), heavy precipitation and a resulting landslide caused two major flood waves in July 1983. The instantaneous discharge during the flood was estimated to be in the range of 200 to 300 $m^3 s^{-1}$ (Johnson and Power, 1985), depositing an estimated 6000 m^3 of debris, approximately 3 m thick, in the valley near the gauging site. A similar event in September 2010 deposited a thick debris cover over the original gauge area, thus changing the trail into the glacier.

A new hydrometric station (Table 2-5) at Peyto Creek, at the outflow of Lake Munro (on the bedrock near the glacier snout at the glacier terminus) was installed in 2013 by the Centre for Hydrology to resume flow measurements. It is nearly 1.5 km upstream from the old gauging site. Both locations are shown in Figure 2-1. The new station is equipped with a Campbell Scientific Sonic Ranger (SR50A) to monitor water stage. This gauge data is temperature-corrected using air temperature measured below the SR50A. In the summer of 2018, an automated salt dilution system and a stage level measurement using a level logger were installed approximately 100 m downstream of the SR50A. Between 14 May 2018, and 10 September 2018, 43 streamflow discharge measurements were performed with automated and manual salt dilutions. One manual streamflow measurement was conducted with an FT2 handheld Acoustic Doppler Velocimeter (ADV) on 1 August 2018. Early season measurements were taken when the stream upstream of

the survey site was still snow-covered. Sudden drops in stage were observed during that period, likely due to temporary ice jamming. Therefore, two rating curves were developed for the 2018 season (Sentlinger *et al.*, 2019), one for the early season when the stream was still snow-covered, and the other for the melt season, when the stream was snow-free. For the 2018 season, the shift between early and late rating curves happened on 12 June. When using this rating curve to obtain streamflow for 2013-2017, only the late season curve is used, as the SR50A site became snow covered and measurements were only available after snowmelt exposed the stream. The daily mean basin runoff averaged over the historical 11-year period, 1967-1977) and the present 5-year period (2013-2017) are presented in Figure 2-14.

Table 2-5: Hydrometric station information.

Hydrometric station	**Geographical coordinates**	**Drainage area**	**Elevation above sea level**	**Stage recording instrument and rating curve method**	**Discharge data period of record**
Old gauge: Peyto Creek at Peyto Glacier (05DA008)	51°41'37" N 116°32'08" W	23.6 km^2	1951 m	Stevens A-35 water-level recorder; rating curve data from current meter for low flows, salt dilution or Rhodamine dye injection for high flows (Goodison, 1972)	1967-1977 (June – Sept)
New gauge: Lake Munro outlet	51°40'52" N 116°32'41" W	18.3 km^2	2150 m	Campbell Scientific SR50 ranger; rating curve data from salt dilution method	2013-2018 (June – Sept)

Figure 2-13: Left: old IHD hydrometric gauge on Peyto Creek (photo by D. Scott Munro). Right: new hydrometric station at the Lake Munro outlet (photo by Angus Duncan).

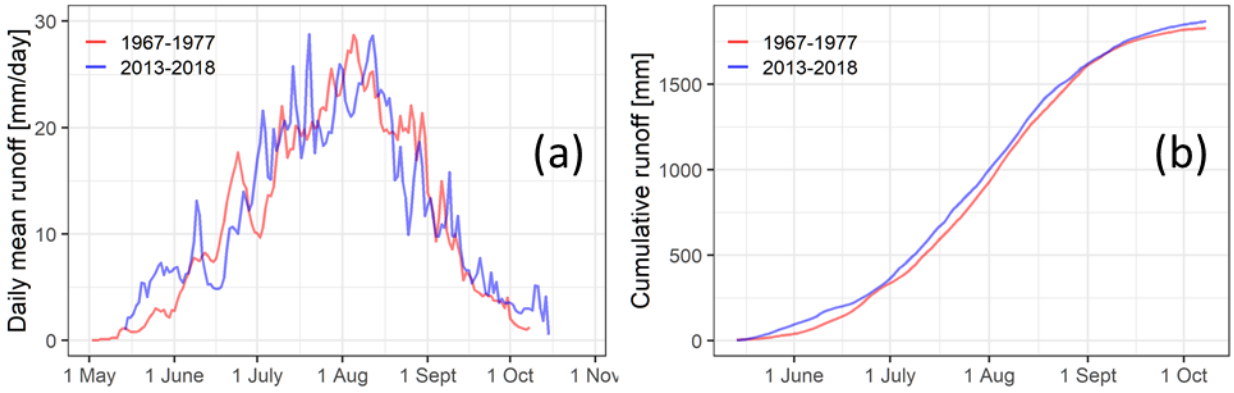

Figure 2-14: (a) Daily mean basin streamflow (expressed as a depth of runoff per day, mm/day) averaged during the historical (1967-1977) and present (2013-2018) periods at the gauging stations of the time. (b) Cumulative annual depth of runoff averaged over the periods.

2.4.6 Glaciological data

Glaciological mass balance measurements, using ablation stakes and snow pits, have been taken semi-annually since 1965, when the IHD program began (Østrem, 1966). Mass balance data for 11 elevation bands, 100 m in width, are reported in several publications (Young and Stanley, 1976; Young, 1981; Ommanney, 1987; Meier and Dyurgerov, 2002; Demuth and Keller, 2006). The recent mass balance data are available from the WGMS (http://www.wgms.ch). The WGMS

(2019) has also compiled datasets from 1966 to 2017. The available mass balance data are plotted in Figure 2-15 (1991-1992 mass balance year missing). Specific winter and summer mass balance data for 11 elevation bands covering an elevation range from 2100 to 2703 m are also available for the period 2003-2018 and presented in this study. The winter, summer and annual point balances have been calculated for the middle of each elevation band, from 2150 to 2650 m above sea level, using a local polynomial regression technique.

The dataset also includes front variation, equilibrium line altitude (ELA), accumulation area ratio (AAR), glacier mass balance (winter, summer, annual) and repeat photographs (WGMS, 2019). Radio detection and ranging (RADAR) measurements of ice thickness for Peyto Glacier in the 1980s were reported by Holdsworth *et al*. (2006). Ground-penetrating radar surveys of ice thickness across the glacier tongue in 2008-10 were reported by Kehrl *et al*. (2014) in their study of volume loss from the lower Peyto Glacier area between 1966 and 2010.

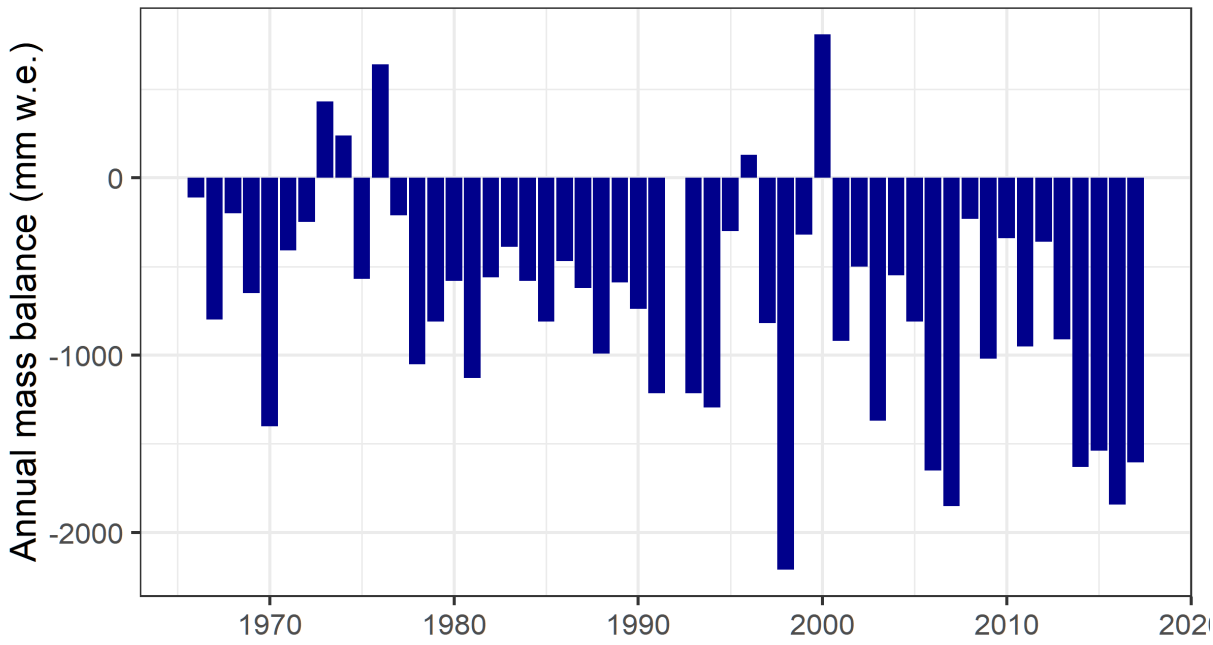

Figure 2-15: Mass balance data for Peyto Glacier. Data source: WGMS (2019).

2.4.7 Geophysical data

A geographical information system (GIS) and remote sensing were used to prepare geophysical data describing the PGRB. ESRI ArcGIS (ArcMap, ArcScan and ArcPy modules) and R were used while working with the time series datasets of Landsat images, digital elevation models (DEM), scanned topographic maps and data tables, using various tools and functions available in the software modules. Google Earth Engine (GEE) was also used for the spatial and temporal analysis of annual landcover mapping from Landsat images. Landcover maps from the satellite images were prepared according to classifications by the normalized-difference snow index (NDSI), albedo and the normalized-difference water index (NDWI). As datasets extracted from different sources have different projection systems, they were re-projected to NAD 1983 UTM Zone 11 (EPSG: 26911).

2.4.7.1 Digital elevation models (DEM)

To detect changes in glacier configurations, DEMs of the PGRB from 1966, 1978, 1986, 2000, 2006, and 2014 were analysed and presented in tif format. DEMs of 1978, 1986 and 2000 were collected from the Canadian Digital Elevation Data (CDED) sources of Natural Resources Canada, (Natural Resources Canada, 1986, 2000; CCMEO, 1997). The 2006 DEM was from airborne light detection and ranging (LiDAR) measurements (Demuth and Hopkinson, 2013) obtained from the Geological Survey of Canada and the Canadian Consortium for LiDAR Environmental Applications Research; the 2014 DEM was prepared by photogrammetry using aerial photographs taken during July and September 2014. The 1966 DEM was developed from a scanned topographic map of Peyto Glacier, which was produced from aerial photographs taken on 22 and 24 August 1966 (Sedgwick and Henoch, 1975). DEM preparation and sources are presented in Appendix A.

2.4.7.2 Basin delineation and landcover classification

The watershed of PGRB was delineated from the 1966 DEM. Google Earth Engine (GEE) was used for the landcover classification of Landsat images of each year, from the 1980s to the present.

Landcover information was extracted from Landsat 5 and Landsat 8 top-of-atmosphere (TOA) reflectance images. Landsat 5 images were used for the years 1984 to 2011, Landsat 8 images from 2013 to 2016.

Landsat satellite images are freely available and accessible through EarthExplorer (http://earthexplorer.usgs.gov) and Global Landcover Facilities (GLCF, http://lcluc.umd.edu/). The images are available at 30 m spatial resolution and 16-day temporal resolution. Two criteria governed image acquisition: (a) an image date between 15th July and 15th September, (b) minimal or no cloud cover, at least inside the PGRB boundary. Landsat images used to create landcover classification of PGRB appear in Table 2-6. Landsat 5 images were from Thematic Mapper (TM) sensor, and Landsat 8 images were from Operational Land Imager (OLI). Images for the years 1992, 1995, 1999 and 2012 are missing due to failure to meet the criteria. A landcover map for 1966 was created from the topographic map of Sedgwick and Henoch (1975).

Four types of landcover classes were identified: (1) firn/snow (accumulation area), (2) ice (ablation area), (3) bare (non-glacierized area) and (4) water body. Snow and non-snow covered areas of bare landcover were differentiated by the NDSI (Hall *et al.*, 2002) and NDWI (Gao, 1996; McFeeters, 1996). Snow and firn areas within firn/snow landcover were classified by their albedo (Liang, 2000; Smith, 2010). The NDSI, NDWI and albedo for the images were obtained from the Raster Calculator and further classified in an ArcPy environment into four categories:

1. **Bare**: all snow-free non-glacierized areas identified by the NDSI
2. **Firn/Snow**: glacierized areas with albedo greater than 0.4 and NDWI lower than 0.4
3. **Ice**: glacierized areas with albedo lower than 0.4 and NDWI lower than 0.4
4. **Waterbody**: Areas with NDWI greater than 0.4

After GEE export to Google Drive the images were downloaded from the drive and converted to a shape file using Raster to Polygon tool in ArcMap.

Table 2-6: Satellite images for generating landcover maps of the PGRB

Mission	**Year**	**Month/Date of acquisition**	**Image ID**
Landsat 5	1984	August 15	LT50430241984228PAC00
	1985	August 2	LT50430241985214PAC02
	1986	August 28	LT50440241986240XXX01
	1987	August 8	LT50430241987220XXX02
	1988	September 2	LT50440241988246XXX01
	1989	August 13	LT50430241989225XXX02
	1990	August 7	LT50440241990219PAC00
	1991	September 4	LT50430241991247XXX02
	1993	August 15	LT50440241993227PAC03
	1994	August 11	LT50430241994223PAC02
	1996	August 23	LT50440241996236PAC00
	1997	August 3	LT50430241997215PAC03
	1998	August 29	LT50440241998241PAC03
	2000	August 18	LT50440242000231XXX01
	2001	August 14	LT50430242001226LGS02
	2002	August 24	LT50440242002236LGS01
	2003	August 20	LT50430242003232PAC02
	2004	August 13	LT50440242004226EDC00
	2005	August 9	LT50430242005221PAC01
	2006	August 28	LT50430242006240PAC01
	2007	August 15	LT50430242007227PAC01
	2008	August 17	LT50430242008230PAC02
	2009	August 27	LT50440242009239PAC01
	2010	August 14	LT50440242010226PAC01
	2011	August 26	LT50430242011238PAC01
Landsat 8	2013	August 22	LC80440242013234LGN00
	2014	August 18	LC80430242014230LGN00
	2015	August 12	LC80440242015224LGN00
	2016	August 30	LC80440242016243LGN00

2.5 Summary

This chapter describes the hydro-meteorological, glaciological and geophysical data collected at PGRB over the past five decades. The meteorological data are from six AWS sites, three on the glacier and three near the glacier. These stations are listed as CryoNet stations of the WMO GCW. Near real-time data from Peyto Main and Bow Hut are accessible through telemetry.

Several examples of data cleaning approaches are presented. The Main station was operational during the summer months of the IHD and re-established as an AWS in 1987. New instruments and dataloggers were added in 2012-2013 by the Centre for Hydrology, University of Saskatchewan. The meteorological data include hourly air temperature, humidity, wind speed, incoming shortwave and longwave radiation, and precipitation. These data are available for a period longer than two decades from the Main station, more than one decade from the on-ice stations. ERA-Interim (European Centre for Medium-Range Weather Forecasts interim reanalysis), WFDEI (Water and Global Change Forcing Data ERA-Interim), NARR (North American Regional Reanalysis), and CFSR (Climate Forecast System Reanalysis) reanalysis data were also bias-corrected for running hydrological models for longer periods.

Glaciological data are published by the WGMS and updated annually. Details of these data were previously described in several publications. Specific mass balance data at different elevation zones, available from 2003 to 2018, are included in this paper. On-ice station data include glacier surface elevation change due to ablation and accumulation, as measured by sonic rangers at three ice stations. The three ice stations, each in a different elevation zone, have been operational for various time periods, the first starting in 1995 with long gaps in the records becoming less frequent over time, especially after 2007. Geophysical data include information on basin boundary, drainage area, landcover, and locations of hydrometric sites. Both historical and contemporary discharge data are included. The flow data and hourly surface elevation change data in different elevation zones are useful for model validation. The long-term mass balance data are a valuable research asset for model development, analysis of climate change, and study of impacts on glacier mass balance and hydrology.

The datasets compiled in this chapter were used for the next three chapters as one of the meteorological datasets to develop and test T/RH models (Chapter 3); to drive and test the CRHM-glacier model described in the Chapter 4; and to diagnose the impact of changes in climate and glacier mass on the hydrology of the headwaters (Chapter 5).

CHAPTER 3: Estimation of shortwave irradiance from temperature and humidity records in cold region and mountain environments

Paper manuscript status

Contents of this chapter are in revision process as a research paper.

Author contributions: Dhiraj Pradhananga and John W. Pomeroy conceptualized the research. Dhiraj Pradhananga analysed data and drafted the manuscript. Joseph Shea, Juan I. López-Moreno, Antoine Rabatel and Jean Emmanuel Sicart provided data and revised the manuscript.

There is a need to find appropriate approaches to estimate shortwave irradiance in mountainous cold regions and to evaluate reanalysis products. This chapter develops new approaches for estimating shortwave irradiance and evaluates two reanalysis products (WFDEI and ERA-Interim) fulfilling the first objective of the research.

3.1 Abstract

Empirical methods for the estimation of shortwave irradiance are based primarily on air temperature and have been developed at lower elevations for snowmelt energy budget, soil thaw or evapotranspiration calculations. This study evaluates existing empirical methods and two reanalysis products for estimating atmospheric transmittance, and then proposes a modified method that can be applied with greater confidence at high elevations and in other cold regions. Observations from thirty snow-dominated and/or glacierized sites in North America, Europe, South America and the Himalayas were used to develop an atmospheric shortwave radiation transmittance model based on air temperature and humidity, which, when coupled with existing extraterrestrial shortwave radiation models, permits a more accurate estimation of shortwave irradiance than was previously possible. Humidity has a higher correlation with atmospheric transmittance than daily temperature range. The models simulated shortwave irradiance better when observed clear sky transmittance were included in the models. The globally available

reanalysis products provided good estimates of shortwave irradiance for a site at lower elevation (<3000 m.a.s.l.) but did not provide robust results at higher elevations.

3.2 Introduction

Key hydrological processes such as evapotranspiration and snow and ice melt are controlled by the surface energy balance, while incoming shortwave irradiance being a key energy input. Most of the components in energy budget models - for example, net radiation - often are not measured but are either estimated or empirically computed (Shook & Pomeroy, 2011; Besharat *et al.* 2013). Another option is to use numerical weather model reanalysis products (Boilley and Wald, 2015). In recent decades, these reanalysis products have gained reliability and higher spatial resolution by using different downscaling techniques.

While temperature index models are comparatively simple and widely used because of their limited data requirements, energy budget models provide a more accurate solution to modelling snow and glacier melt and more temporal and spatial transferability due to their physical basis. Even though many glacier models use an empirical temperature index approach (Réveillet *et al.* 2017) due to unavailability of high elevation observations of radiation, there are proven approaches that can be used to simulate radiation (Walter *et al.* 2005; Sicart *et al.* 2006; Shook & Pomeroy 2011; Pomeroy *et al.* 2013). These simulated radiation data could be used to drive physically based energy budget melt models.

Shortwave irradiance is the largest single flux for glacier and snow surface energy balance, and it is also linked to other components of the surface radiation balance through the influence of atmospheric transmittance on incoming longwave radiation (Garnier and Ohmura, 1968). The radiation balance is the dominant in the energy balance components (Male and Granger, 1981; Munro and Young, 1982b; Dozier, 1987). Shortwave irradiance is sometimes used to simulate net radiation through empirical (Gray and Landine, 1988) or physically based approaches (Pomeroy *et al.* 2007), so it must be accurately estimated.

Several algorithms are available to determine shortwave irradiance. Besharat *et al.* (2013) conducted a comprehensive review of empirical models based on various meteorological variables. They classified the models into four major categories: sunshine hour-based, cloud-based, temperature-based and other meteorological variable-based models. It has been shown that daily shortwave irradiance can be estimated empirically with reasonable accuracy from latitude, altitude, time of year, and daily air temperature range (Hargreaves & Samani 1982; Annandale *et al.* 2002) for low and moderate elevations. Shook and Pomeroy (2011) tested the empirical models and two reanalysis data and suggested the need to improve empirical approaches for high mountains. They suspected that the relatively poor performance of the empirical models over the mountains might be due to the models not being able to account the effects of complex mountain weather systems on atmospheric transmittance. Therefore, they suggested that the physically based simulations of reanalysis data could provide better estimation of transmittance.

Empirical methods for simulating atmospheric transmittance, based on the difference between maximum and minimum temperature, have been developed and tested in different environments, from coastal and lowland environments to high elevation sites, and at different latitudes (Bristow & Campbell 1984; Meza & Varas 2000; Samani 2000; Wu *et al.* 2007; Bandyopadhyay *et al.* 2008; Rahimikhoob 2010; Samani *et al.* 2011; Shook & Pomeroy 2011). Shook and Pomeroy (2011) showed that temperature-based empirical methods were reliable in the continental climate of the Canadian Prairies. Shea (2010) considered vapour pressure observations and formulated a statistical relationship to simulate atmospheric transmittance at the four glaciers (Bridge, Place, Weart and Helm) in western Canada. The relationship, however, has not been tested globally or compared with reanalysis data. Several attempts have been made (e.g., Boilley & Wald 2015) to evaluate reanalysis products of daily shortwave irradiance at the surface, mainly focusing on lowlands and tropical regions. There remains a need to find appropriate approaches to estimate shortwave irradiance in mountainous cold regions. This work aims to improve shortwave irradiance simulation for mountain sites. Once daily shortwave irradiance is simulated, it can be distributed to hourly time-steps using the method detailed in Shook and Pomeroy (2011).

The objectives of this study are (1) to develop and test a new empirical model for atmospheric shortwave irradiance transmittance in high mountain environments; (2) to compare shortwave

irradiance estimation from empirical models and reanalysis products with *in-situ* monitored data; and (3) to examine the global transferability of the new transmittance model.

3.3 Study sites, data and methods

3.3.1 Study sites

Cold region mountain environments were the focus of this study. Daily shortwave irradiance observations, measured at 30 automatic weather stations (AWS) distributed across North America, South America, Europe and the Himalayas, were considered for developing and evaluating transmittance models and reanalysis data. Figure 3-1 shows geographical locations of observational sites used in this study. Table 1 lists the stations' locations and the length of the time series with available data.

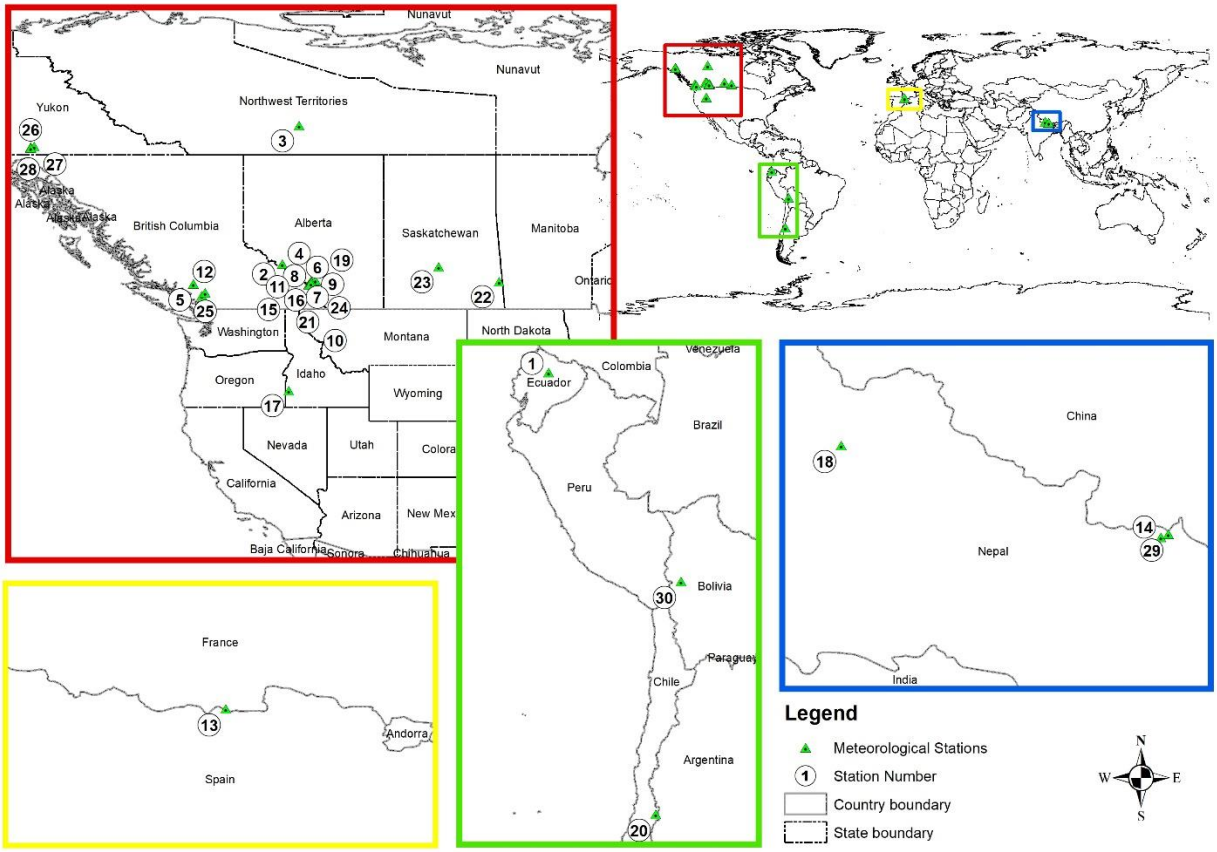

Figure 3-1: Observation sites considered for the study. Meteorological stations are numbered (in circles) as per the list in Table 3-1. Base map for country/state boundary is from https://www.naturalearthdata.com/

Table 3-1: List of the sites and data periods.

SN	Station Names	Elevation (m.a.s.l.)	Latitude (º)	Longitude (º)	Data Period		Country
					From	To	
1	Antisana	4860	-0.47	-78.15	22/12/2004	31/12/2012	Ecuador
2	Athabasca	1974	52.22	-117.23	12/09/2014	31/12/2016	Canada
3	Bologna	2159	62.11	-116.06	18/07/2014	01/10/2016	Canada
4	Bonsai	2099	50.82	-115.21	26/07/2014	03/10/2016	Canada
5	Bridge	1745	50.81	-123.60	02/09/2006	14/08/2008	Canada
6	Burstall	2243	50.76	-115.37	25/03/2014	31/12/2016	Canada
7	Centennial Ridge	2468	50.94	-115.19	18/04/2014	31/12/2016	Canada
8	Fisera Ridge	2325	50.96	-115.20	15/09/2011	31/12/2016	Canada
9	Fortress Ridge	2323	50.84	-115.22	01/11/2013	31/12/2016	Canada
10	Hay Meadow	1436	50.94	-115.14	14/09/2011	31/12/2016	Canada
11	Helen Lake	2545	51.69	-116.42	17/02/2014	31/12/2016	Canada
12	Helm	2192	49.96	-122.98	02/08/2006	19/09/2008	Canada
13	Izas	2056	42.70	0.40	01/10/1996	27/09/2009	Spain
14	Kyanging	3862	28.21	85.56	22/03/2012	29/12/2014	Nepal
15	Peyto Main	2240	51.69	-116.54	18/07/2010	31/12/2016	Canada
16	Power Line	2136	50.83	-115.20	07/02/2013	31/12/2016	Canada
17	Reynold	2094	43.19	-116.78	01/10/1983	30/09/2008	USA
18	Rikha Samba	5310	28.80	83.51	12/10/2012	30/12/2014	Nepal
19	Robertson	2064	50.76	-115.34	26/06/2010	17/03/2012	Canada
20	San Francisco	2154	-33.81	-70.07	01/01/2013	01/02/2015	Chile
21	Sibbald	1490	51.06	-114.87	07/11/2012	10/11/2015	Canada
22	Smith Creek	517	50.97	-101.78	31/10/2007	29/09/2013	Canada
23	St. Denis	554	52.03	-106.10	29/01/1999	29/06/2006	Canada
24	Upper Clearing	1845	50.96	-115.18	01/01/2010	18/10/2012	Canada
25	Weart	2168	50.16	-122.76	21/07/2006	18/09/2008	Canada
26	Wolf Creek Alpine	1760	60.55	-135.19	01/10/1993	30/12/2011	Canada
27	Wolf Creek Forest	706	60.60	-134.95	01/10/1993	30/12/2011	Canada
28	Wolf Creek Subalpine	1250	60.51	-135.20	01/10/1993	30/12/2011	Canada
29	Yala	5090	28.23	85.61	06/06/2012	16/12/2014	Nepal
30	Zongo	5050	-16.25	-68.17	26/08/2003	28/08/2012	Bolivia

3.3.2 Data

The empirical methods and the reanalysis products were evaluated by comparing their predictions against 30 *in-situ* quality controlled observed data series (Table 3-1). Hourly and daily temperature (daily temperature range is plotted in Figure 3-2), humidity (Figure 3-3) and shortwave irradiance (Figure 3-4) observations were used for this study. Some of the datasets used in this study are published and can be accessed online. Data from Wolf Creek (Wolf Creek Alpine, Subalpine and Forest) and Marmot Creek (Centennial Ridge, Fisera Ridge and Hay Meadow) research basins were published by Rasouli *et al*. (2019) and Fang *et al*. (2019). Similarly, data from glaciers in Nepal (Kyanging, Rikha Samba and Yala) were used in Shea *et al.* (2015) and are available from the International Centre for Integrated Mountain Development (ICIMOD) (Shea 2016). Meteorological data from glaciers in the Coast Mountains of British Columbia, Canada (Bridge, Helm, and Weart glaciers) were previously published in Shea (2010) and Trubilowicz *et al.* (2016). Station data from Reynolds Mountain East basin, Idaho, USA were published by Reba *et al.* (2011).

This study considered only the last two years of the time series available at each site; half the data were used for parameter calibration, and the remainder were used for model evaluation. If a time series was less than two years, all the data were considered. Bologna, Robertson, Rikha Samba, San Francisco and Yala have less than two years of data. Even days were used to calibrate the parameters; odd days were used to evaluate the models and reanalysis products.

To simulate atmospheric transmittance, temperature and humidity were also obtained from the same stations. Reanalysis data consisting of temperature, humidity and shortwave irradiance were also obtained for the grid cell encompassing each site. Reanalysis datasets were from ERA-Interim reanalysis of the ECMWF (European Centre for Medium-range Weather Forecast, Dee *et al.* 2011) and WFDEI (WATCH Forcing Data methodology applied to ERA-Interim data, Weedon *et al.* 2014). WFDEI, available for the period of 1979-2016, is a bias adjustment of ERA-Interim. The ERA-Interim source is http://apps.ecmwf.int/datasets/data/interim-full-daily/levtype=sfc/ and WFDEI source is ftp://ftp.iiasa.ac.at/WFDEI/. Details of these datasets are also provided by Jones *et al.* (2017). Temperature and humidity data from reanalysis products were bias adjusted to the *in-situ* observations on a monthly basis using the statistical package, CRHMr in R (Shook, 2016a).

Monthly biases, obtained by considering the values of odd days, were applied to adjust reanalysis data of even days. The analysis was repeated with bias-corrected ERA-Interim temperature and relative humidity data.

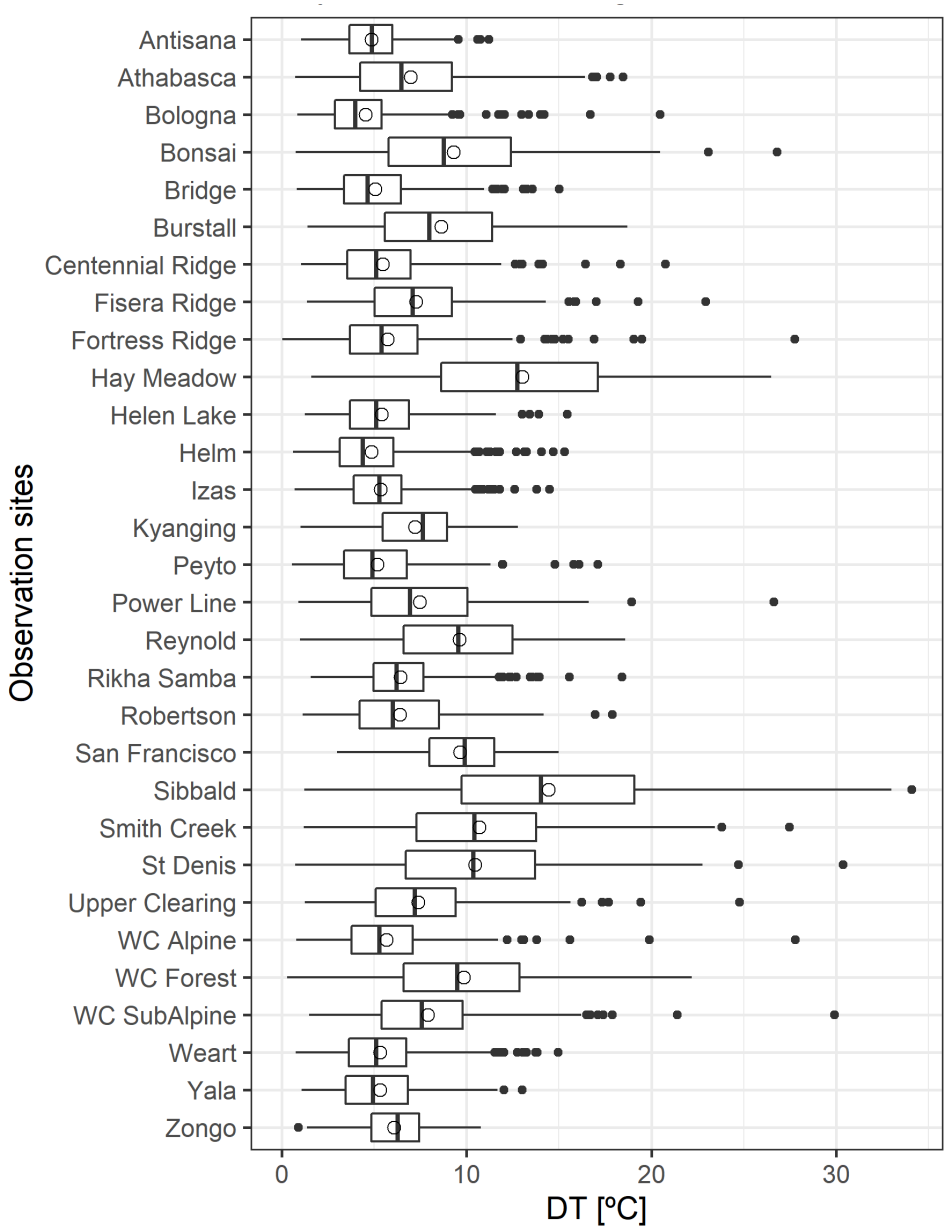

Figure 3-2: Daily temperature range [DT] measured at the thirty observation sites.

Note: The boxes represent the interquartile ranges for each site; the vertical lines and circles within the boxes represent the medians and the means, respectively. Left and right horizontal lines extend to capture values ±1.5 times the 75th and 25th percentiles, respectively. Dots represent extreme outliers beyond this range.

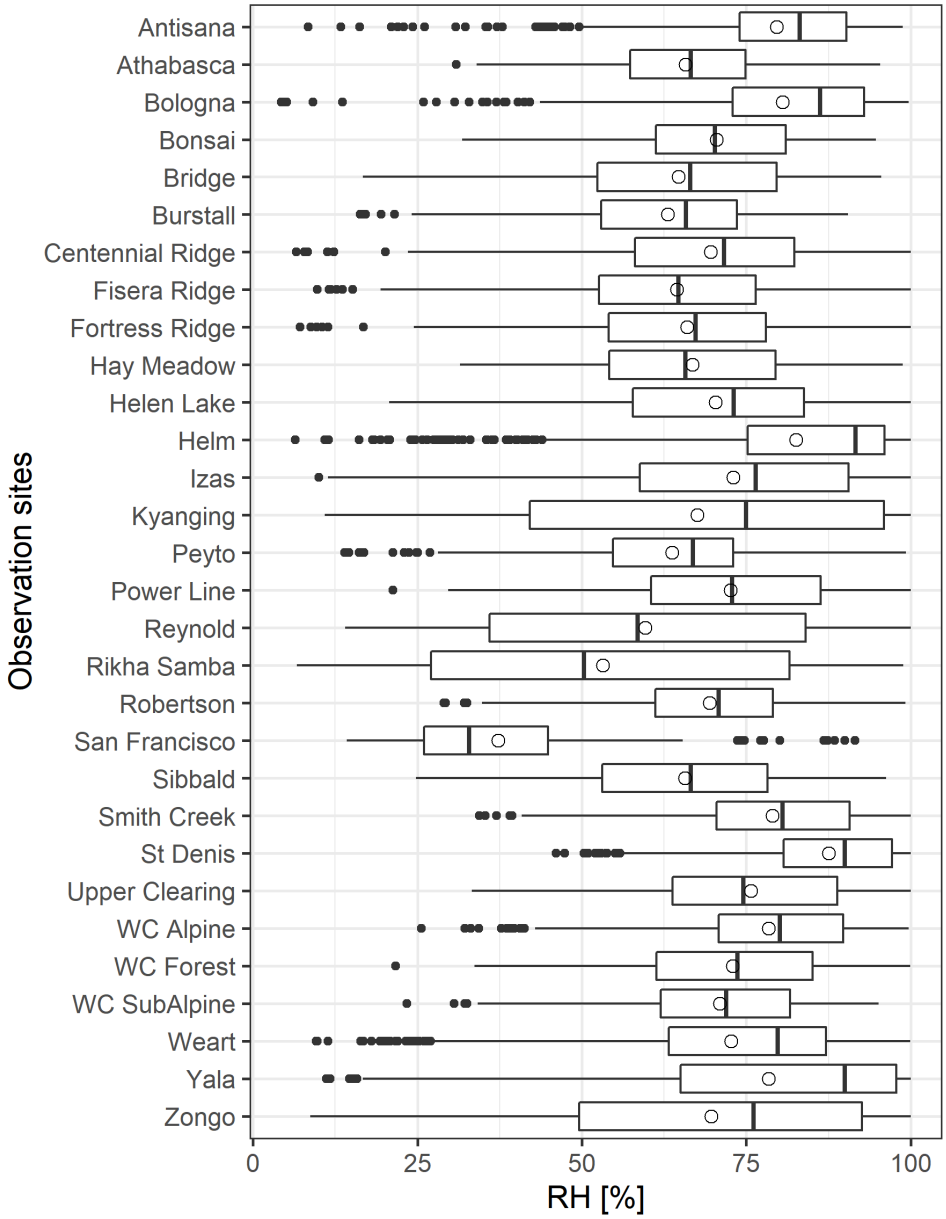

Figure 3-3 Daily mean relative humidity from the thirty observation sites.

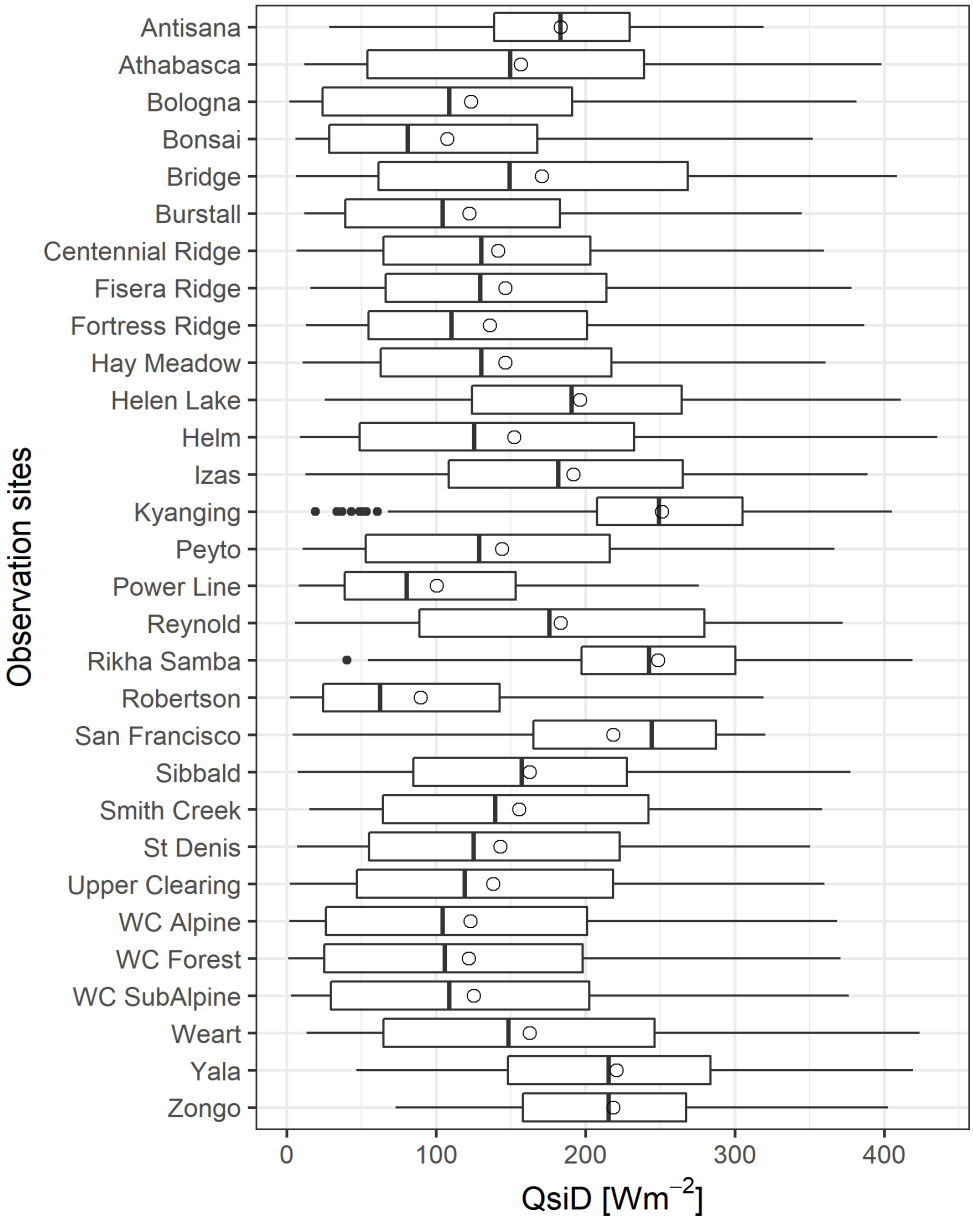

Figure 3-4: Daily mean shortwave irradiance measured at the thirty observation sites.

3.3.3 Methodology

Atmospheric transmittance (τ) is defined as:

$$\tau = \frac{Q_{si}}{K_{ext}} \quad (3.1)$$

K_{ext} is extraterrestrial shortwave irradiance at the top of the atmosphere (W m^{-2}) and Q_{si} is irradiance measured at the site (W m^{-2}). The atmospheric transmittance is a measure of clearness of the atmosphere; higher values of τ indicate a clearer atmosphere. During clear-sky conditions, the clear-sky transmittance (τ_{cs}) is the ratio of shortwave irradiance on clear-sky days to extra-terrestrial irradiance. Therefore, the transmittance (τ_{cs}) is

$$\tau_{cs} = \frac{\tau}{\tau_{cloud}} \quad (3.2)$$

where τ_{cloud} is the transmittance when clouds are present. Bojanowski *et al*. (2013) considered mean of τ_{cs} from 3% of the highest τ values (assuming these are clear sky days). In this study, the 97th percentile of τ was considered as the τ_{cs} for the site (Figure 3-5). The 97th percentile was chosen after plotting various percentile values of τ over the distributions of τ for all the sites. However, τ_{cs} estimated from the 97% percentile of τ may not work for all the sites. For example, τ_{cs}= 0.86 estimated for Zongo in this study from the 97% percentile of τ is very close to τ_{cs}= 0.87 obtained by Sicart *et al*. (2015). However, the value of τ_{cs} found for Antisana (0.70) from the 97% percentile of τ seems low for a high elevation site, but the range of observed values for Q_{si} at this site (Figure 3-4) indicates that clear sky days are rare. Therefore, it is difficult to calibrate clear-sky parameters for such sites.

Since air temperature data are readily available, in comparison with other meteorological data, empirical methods based on air temperature data were evaluated for estimating the daily mean atmospheric transmittance. Three atmospheric transmittance algorithms based on temperature were considered for this study: Hargreaves, Bristow and Campbell, and Annandale.

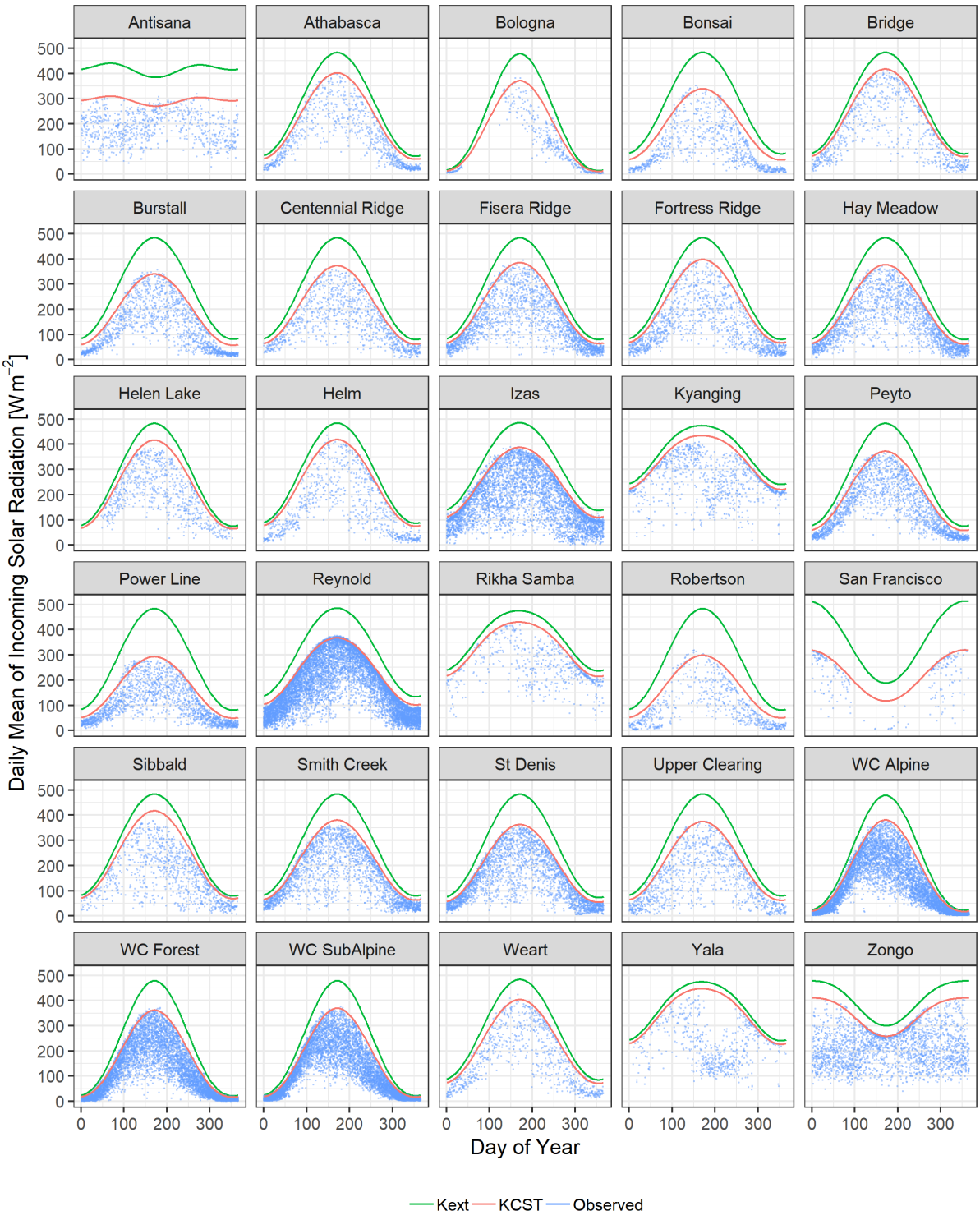

Figure 3-5: Plot of shortwave irradiance (blue) observed at each site.

Note: Data periods are shown in Table 3-1. Green is Kext, extraterrestrial shortwave irradiance at the top of the atmosphere and red (KCST) is the potential irradiance on clear days obtained from clear sky transmissivity, τ_{cs}. τ_{cs} is obtained from the highest 3% of τ at each site.

HS: Hargreaves *et al.* (1985)

A simple linear relationship between the daily atmospheric transmittance and daily range of air temperature was proposed by Hargreaves and Samani (1982). Later, Hargreaves *et al.* (1985) improved the relationship as follows:

$$\tau = a_{HS} \cdot \sqrt{DT} + b_{HS} \quad (3.3)$$

a_{HS} and b_{HS} are the empirical site-dependent coefficients; the two subscripts represent the model in abbreviation. DT is the daily temperature range (°C).

BC: Bristow and Campbell (1984)

Bristow and Campbell (1984) presented an exponential relationship between the daily atmospheric transmittance and daily range of air temperature:

$$\tau = a_{BC} \cdot \left(1 - exp(-b_{BC} \cdot [DT^{c_{BC}}])\right) \quad (3.4)$$

a_{BC}, b_{BC}, and c_{BC} are the empirical coefficients; the two subscripts represent the model in abbreviation.

AD: Annandale *et al.* (2002)

Several researchers suggested that the thickness of atmosphere be considered, due to site elevation (Annandale *et al.* 2002) or atmospheric pressure (Allen, 1995). Annandale *et al.* (2002) proposed including the effect of altitude (E, in metres above sea level) as:

$$\tau = a_{AD} \cdot \left(1 + 2.7 \cdot 10^{-5} \cdot (E)\right) \cdot \sqrt{DT} \quad (3.5)$$

a_{AD} is the empirical coefficient; the two subscripts represent the model in abbreviation.

Shea (2010) considered vapour pressure (e_a) and formulated a new algorithm to simulate atmospheric transmittance based on observations made at four glaciers (Place, Helm, Bridge and Weart) in western Canada:

$$\tau = a \cdot \left(1 - exp\left(b \cdot \left[\frac{DT}{e_a}\right]^c\right)\right) \quad (3.6)$$

where a, b, and c are empirical coefficients, similar to those in Equation 3.4. This model provided better results at the study sites than those from Hargraves and Samani (1982), Bristow and Campbell (1984) and Donatelli and Marletto (1994). However, in this study it was found that relative humidity (RH) is a better predictor than vapour pressure (details are provided in Appendix C). Inclusion of altitude and latitude did not improve the model's performance. Therefore, three new algorithms (N1, N2 and N3) were developed, introducing RH in the HS and BC models, to simulate transmittance from temperature and humidity for application in cold region mountain environments.

N1: Tau [T/RH] model 1

$$\tau = a_{N1} \cdot \left(1 - exp\left(-b_{N1} \cdot \left[\frac{\sqrt{DT}}{RH}\right]^{cN1}\right)\right) \tag{3.7}$$

N2: Tau [T/RH] model 2

$$\tau = a_{N2} \cdot \left(1 - exp\left(-b_{N2} \cdot \left[\frac{\sqrt{DT}}{RH}\right]\right)\right) \tag{3.8}$$

N3: Tau [T/RH] model 3

$$\tau = a_{N3} \cdot \left[\frac{\sqrt{DT}}{RH}\right]^{c_{N3}} + b_{N3} \tag{3.9}$$

where, τ is atmospheric transmittance, DT and RH are daily temperature range and relative humidity respectively; a_{N1}, b_{N1}, c_{N1}, a_{N2}, b_{N2}, a_{N3}, b_{N3} are empirical coefficients; the two subscripts indicate the respective transmittance algorithms considered in abbreviation. The new temperature- and humidity-based models (N1, N2, N3) and the two reanalysis products (ERA-Interim and WFDEI) were compared to observed transmittance, along with the performances of the three existing temperature-based models (HS, BC and AD).

Curve fitting and statistical analysis were carried out in R (R Core Team, 2017) using RStudio platform (RStudio, 2017). The nlsLM function of the Levenberg–Marquardt algorithm, in the R package minpack.lm was used for fitting nonlinear curves (Elzhov *et al.* 2016).

3.3.4 Calibration approaches

Empirical methods generally need calibration for site-specific coefficients based on the measured values of shortwave irradiance. The model parameters were calibrated in this study according to three different approaches (AP 1-3, Table 3-2). First, the calibration of the parameters was conducted at individual sites (AP1). Second, all the stations were considered to calibrate the parameters globally (AP2). Third, only high elevation sites above 3000 m.a.s.l. were considered and the parameters calibrated (AP3). The three calibrations were analysed with and without considering τ_{cs}.

Table 3-2: Calibration approaches to evaluate the empirical methods

Calibration Approach	**Details**
AP1	Individual stations
AP2	Global data
AP3	High elevation sites (greater than 3000 m.a.s.l.) altogether, not site by site

Model coefficients of the algorithms were fit in each scheme by using the nonlinear curve fitting method. As previously mentioned, data were divided into two subsets: odd days were used for model calibration and even days for model validation.

3.3.5 Evaluation of model performance

Model performance was evaluated using three statistical indicators – mean bias error (MBE) (W m^{-2}), the root mean square error (RMSE) (W m^{-2}), standard error of estimate (SEE) (W m^{-2}) and Wang-Bovit index (WBI). The lower the values of MBE, RMSE and the higher the WBI, the better the model is. MBE was not considered for evaluation with mean values from the sites (Table 3-3). It was, however, considered in the box plots to show the spread of MBE values. Agreement between simulated and observed values was described by MBE, RMSE, and SEE as follows:

$$MBE = \frac{1}{n}\sum_{i=1}^{n}(x_i - y_i) \tag{3.10}$$

$$RMSE = \sqrt{\frac{1}{n}\sum_{i=1}^{n}(x_i - y_i)^2} \tag{3.11}$$

$$SEE = \sqrt{\frac{1}{n-2}\sum_{i=1}^{n}(x_i - y_i)^2} \quad (3.12)$$

Here x_i and y_i are measured and predicted daily shortwave irradiance, respectively, at i^{th} day, and n is number of observation values. In addition, the WBI, proposed by Wang and Bovik (2002) and reformulated by Mo *et al*. (2014) for application to hydrometeorological data, was also used. The WBI, which varies between 0 and 1, measures similarities between modeled and observed variables in terms of pattern association and differences in the means and variances (Mo *et al*., 2014).

$$WBI = [m_{xy}][v_{xy}][R_{xy}] \quad (3.13)$$

where, m_{xy} and v_{xy} are the measures of differences in means and variances, respectively. R_{xy} is the Pearson correlation coefficient. These three components are defined as:

$$m_{xy} = \left[\frac{2(\bar{x}-\psi_{xy})(\bar{y}-\psi_{xy})}{(\bar{x}-\psi_{xy})^2+(\bar{y}-\psi_{xy})^2}\right] \quad (3.14)$$

$$v_{xy} = \left[\frac{2\sigma_x\sigma_y}{\sigma_x^2+\sigma_y^2}\right] \quad (3.15)$$

$$R_{xy} = \left[\frac{\sigma_{xy}}{\sigma_x\sigma_y}\right] \quad (3.16)$$

where, ψ_{xy} = min(x_i, y_i | i=1, 2, 3, ……n); $\bar{x}$ and $\bar{y}$ are means of x_i and y_i respectively; σ_x and σ_y are standard deviances, and σ_{xy} is co-variance. All statistical analyses were carried out in R (R Core Team, 2017) in the RStudio platform (RStudio, 2017). The code for WBI was provided by Paul Whitfield of the University of Saskatchewan Centre for Hydrology and Environment and Climate Change Canada (personal communication, 4 April 2017); other codes were used from the R package *sirad* (Bojanowski, 2016). The Wilcoxon signed-rank test (Wilcoxon, 1945) (*wilcox.test* in R) was considered to evaluate statistical significance of the model's performance. The paired test was used at 5% level of significance.

3.4 Results and discussion

Atmospheric transmittance depends on the atmosphere's thickness and properties. One of the major controlling factors is cloud cover, for which the temperature range is a proxy indicator.

Other factors that influence transmittance are the atmosphere's moisture, aerosol and dust content. Daily mean transmittance was better associated with daily mean relative humidity than with daily temperature range or vapour pressure (Appendix C, Figure C.9) while the influences of aerosol and dust were kept constant for each site.

3.4.1 Model performance

Simulated shortwave irradiance from the six calibrated models was tested against observed shortwave irradiance data reserved for validation. The evaluation considered models calibrated at individual sites (AP1), at all sites (AP2), and at high elevation sites only (AP3). Model inputs included temperature and humidity from *in-situ* observations and from bias-adjusted reanalysis data. MBE, RMSE and WBI were calculated based on the comparison to observed daily shortwave irradiance data, which was not used for model calibration.

Table 3-3 presents comparisons amongst the *in-situ* observations of shortwave irradiance and that estimated by the six empirical approaches and the two reanalysis products at the 30 AWS sites. The statistical test was with H1: T/RH method is better than T-method and the reanalysis data. The statistical values in Table 3-3 are average values of 30 sites in the cases of the AP1 and AP2 calibration schemes, whereas only 5 sites, above 3000 m.a.s.l., were considered for the AP3 scheme. p-values are tabulated in Appendix C. Similarly, Figure 3-6 to Figure 3-8 are box plots of three statistical measures: MBE, RMSE and WBI. Figure 3-6 is for the AP1 evaluation approach: calibration of parameters at individual sites. Figure 3-6 (A) uses temperature and humidity from the *in-situ* observations; Figure 3-6 (B) uses outputs from ERA-Interim datasets.

Table 3-3: Comparison between empirical methods, reanalysis products and *in-situ* observations of daily mean values of shortwave irradiance.

Calibration Scheme	τ_{cs}	**Models**	***In-situ* observation [t, RH]**		**Bias-corrected ERAI [t, RH]**	
			RMSE (W m^{-2})	**WBI**	**RMSE (W m^{-2})**	**WBI**
All sites (reanalysis)		ERAI	**49.8**	0.82	**50.7**	**0.82**
		WFDEI	51.4	0.82	52.4	**0.82**
AP1 (calibration at individual sites)	Without τ_{cs}	HS	46.9	0.82	46.2	0.82
		BC	46.5	0.82	46.2	0.82
		AD	47.6	0.81	47.4	0.81
		N1	**39.9**	**0.88**	**44.0**	**0.83**
		N2	40.7	0.87	44.3	**0.83**
		N3	41.7	0.85	44.7	0.82
	With τ_{cs}	HS	47.0	0.82	46.2	0.82
		BC	46.6	0.82	46.2	0.82
		AD	47.6	0.81	47.4	0.81
		N1	**39.9**	**0.88**	**44.0**	**0.83**
		N2	40.7	0.87	44.3	**0.83**
		N3	41.8	0.85	44.7	0.82
AP2 (global calibration)	Without τ_{cs}	HS	58.0	0.74	57.0	0.76
		BC	57.5	0.76	57.0	0.76
		AD	61.3	0.77	60.7	0.77
		N1	51.9	0.82	55.3	0.77
		N2	51.8	**0.83**	55.2	0.78
		N3	52.4	0.81	55.5	0.77
	With τ_{cs}	HS	54.0	0.76	52.2	0.77
		BC	53.1	0.77	52.3	0.77
		AD	56.0	0.78	54.6	0.79
		N1	**45.6**	0.84	**49.6**	0.79
		N2	**45.6**	0.84	49.7	0.79
		N3	46.4	0.83	50.0	0.78
High-elevation sites (reanalysis)		ERAI	74.1	0.45	74.3	0.45
		WFDEI	71.8	0.51	71.9	**0.51**
AP3 (calibration on high-elevation sites only)	Without τ_{cs}	HS	59.5	0.63	64.3	0.50
		BC	59.2	0.64	64.2	**0.52**
		AD	61.8	0.57	64.5	0.49
		N1	**53.1**	**0.71**	**61.5**	0.50
		N2	54.2	0.67	61.8	0.47
		N3	57.6	0.59	64.8	0.36
	With τ_{cs}	HS	56.4	0.61	62.0	0.48
		BC	55.8	0.63	61.5	0.50
		AD	57.7	0.57	62.0	0.49
		N1	**48.1**	**0.72**	**58.0**	**0.51**
		N2	50.0	0.66	58.5	0.47
		N3	54.4	0.57	62.3	0.35

Note: Best values in the categories are in bold. Cells marked in green indicate that the difference of T/RH method to all the T-methods and the reanalysis data is statistically significant ($p < 0.05$)

for the Wilcoxon test for paired samples. Cells marked in blue indicate that the difference of T/RH to all the T-methods is significant, and those in purple indicate that the difference of T/RH to the reanalysis data is significant.

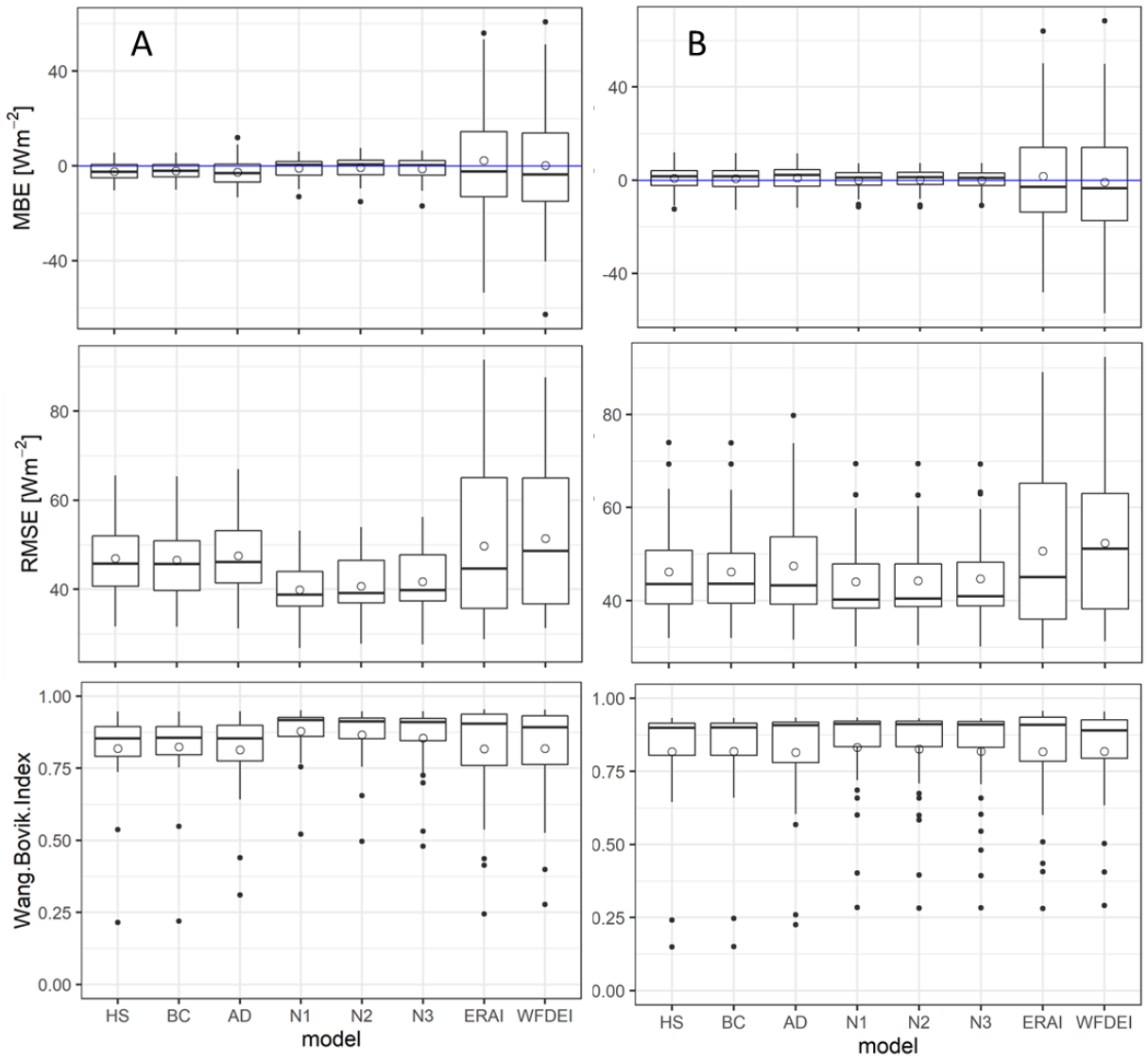

Figure 3-6: Box plots of the performance statistics for prediction of shortwave irradiance by the six models with calibration of coefficients at the individual sites (AP1) and by the reanalysis products. In "A" the models are driven by *in-situ* observation of temperature and humidity; in "B" the models are driven by ERA-Interim outputs of temperature and humidity.

Note: The boxes represent the interquartile ranges for each site; the horizontal lines and circles within the boxes represent the medians and the means, respectively. Upper and lower vertical lines extend to capture values ±1.5 times the 75th and 25th percentiles, respectively. Dots represent extreme outliers beyond this range. Wang-Bovik Indices have values from 0 to 1.

In the case of AP1, N1 provided the best performance amongst all the empirical approaches and in comparison to the reanalysis data. This was true whether the models were driven by temperature and humidity either by the *in-situ* observation or by those from ERA-Interim outputs. Biases were higher for either of the reanalysis estimations (Figure 3-6). Therefore, it can be suggested that if a site has a year of measurements, the T/RH algorithm [N1] provides the best simulation of shortwave irradiance, either with observed or reanalysis temperature and humidity data.

In the case of AP2, with parameters calibrated globally, considering all 30 sites (Figure 3-7), the performance of the T/RH approaches are comparable to the reanalysis products. The median RMSE of ERA-Interim is the lowest and that of WBI is the highest; however, the spread is larger. ERA-Interim provided reliable results in several sites (Figure 3-7). The results were improved from the empirical approaches, however, with the inclusion of τ_{cs} in the algorithms (Table 3-3). τ_{cs} filtered out the impact of factors other than cloud and, therefore, improved the predictability of the models.

This suggests that if a site does not have any *in-situ* observation of shortwave irradiance, T/RH algorithms can be applied; but, the reanalysis data also provides solid results similar to the empirical approaches when global coefficients were fixed for all sites. In the study by Boilley and Wald (2015), ERA-Interim did not provide good simulations of shortwave irradiance. However, the reanalysis outputs provided useful results in the cold regions considered in this study.

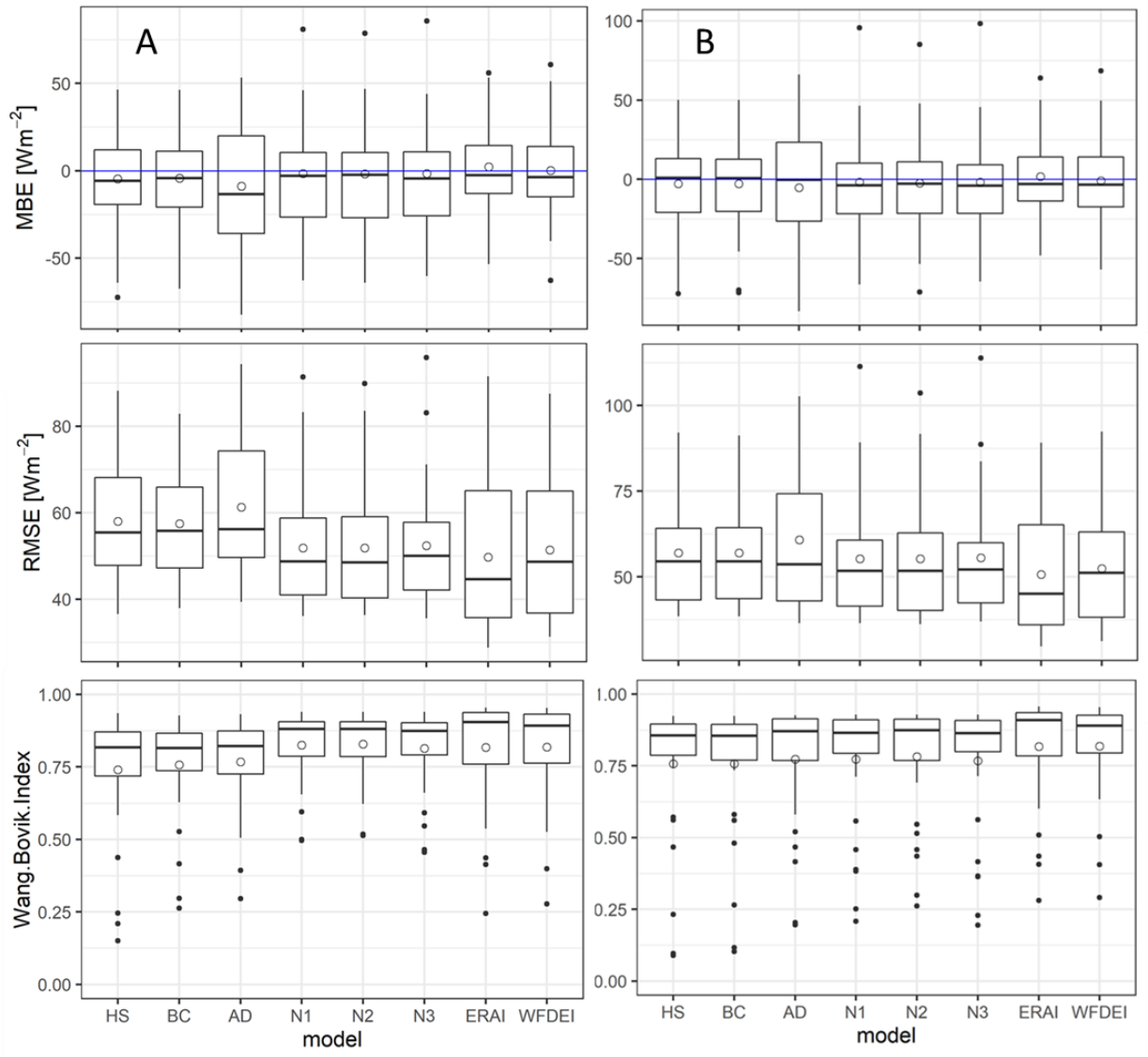

Figure 3-7: Box plots of the performance statistics for prediction of shortwave irradiance by the six models with calibration of coefficients globally (AP2) and by the reanalysis products. In "A" the models are driven by *in-situ* observation of temperature and humidity; in "B" the models are driven by ERA-Interim outputs of temperature and humidity.

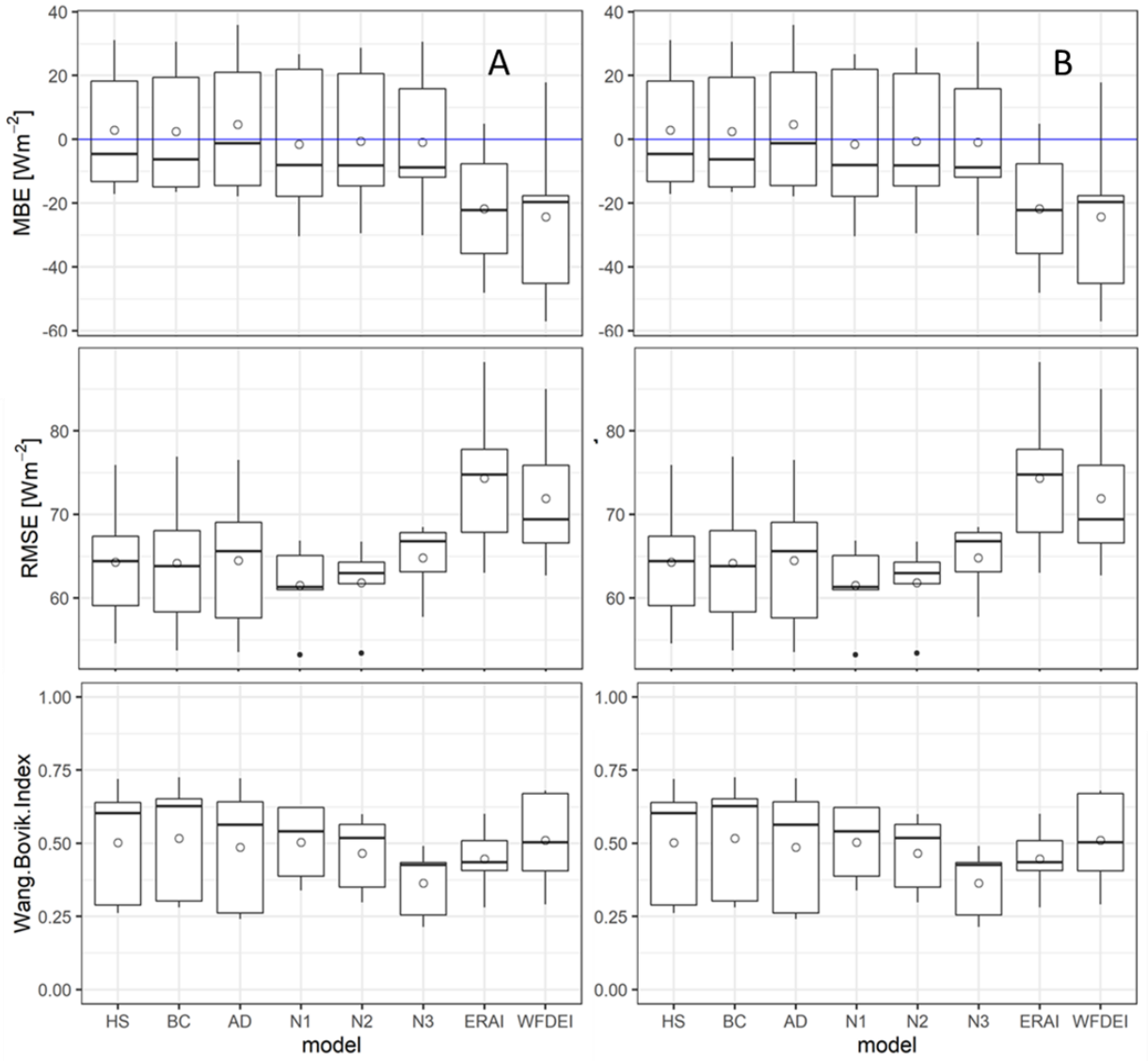

Figure 3-8: Box plots of the performance statistics for prediction of shortwave irradiance by the six models with calibration of coefficients globally to high elevation sites only (AP3) and by the reanalysis products. In "A" the models are driven by *in-situ* observation of temperature and humidity; in "B" the models are driven by ERA-Interim outputs of temperature and humidity.

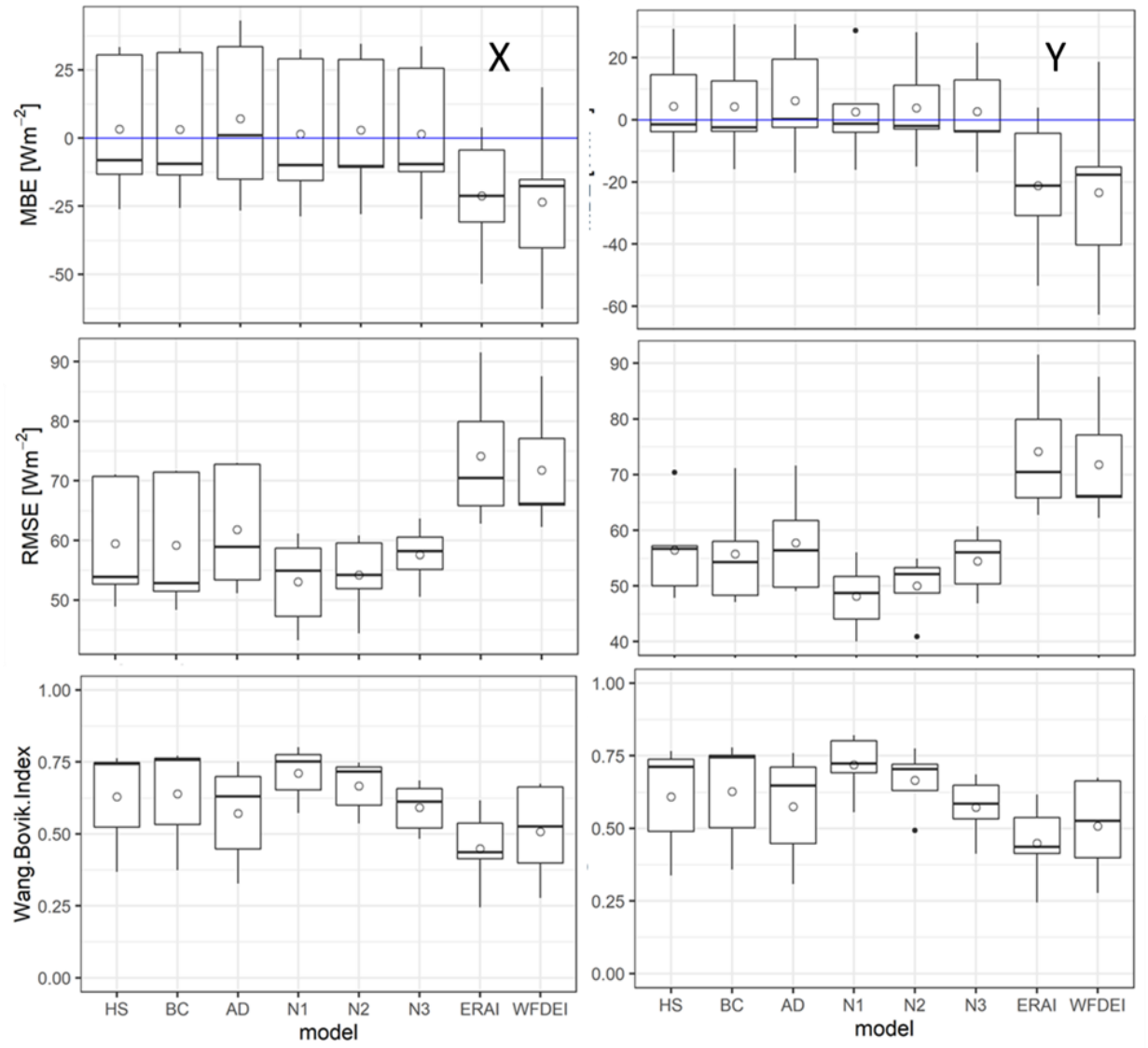

Figure 3-9: Box plots of the performance statistics for prediction of shortwave irradiance by the six models with calibration of coefficients globally to high elevation sites only (AP3) and by the reanalysis products. In "X" the models are without τ_{cs}; in "Y" the models are with τ_{cs}.

In the case of AP3, with the parameters calibrated globally but using only the five high elevation sites, the temperature- and humidity-based approaches – specifically, N1 - provided the best results in all cases (Figure 3-8 and Table 3-3). Inclusion of τ_{cs} in the algorithms reduced MBE and RMSE (Figure 3-9). In the high elevation sites, the reanalysis products considered in this study did not provide robust results; they were largely biased negatively. The results suggest that the new T/RH algorithms should be used in these environments.

The empirical methods provided better simulation of shortwave irradiance than did the reanalysis products, as evidenced by the MBE and RMSE statistics. The new approaches, temperature- and humidity-based (N1, N2, N3), provided the best results amongst the empirical approaches. The performance of the empirical approaches declined when the parameters were calibrated globally (Figure 3-7). When the parameters were calibrated globally to high elevation sites only (Figure 3-8), the simulated values from the empirical approaches were closer to the *in-situ* observations than was the reanalysis data.

The lowest mean values of RMSE were obtained from the temperature- and humidity-based approaches. Among the three new methods, N1 has the best RMSE and WBI values. Only when the empirical model parameters were calibrated globally did the reanalysis products provide equally good estimates of shortwave irradiance.

3.5 Conclusions

This study compared the performance of six empirical relations for estimating atmospheric transmittance for shortwave irradiance calculations. Three existing methods based on air temperature and three new methods based on air temperature and relative humidity were used, along with two reanalysis data products, at over 30 sites in different cold regions around the world. The temperature and humidity data used to drive the empirical model predictions of shortwave irradiance were drawn from both *in-situ* observed values and the WFDEI and ERA-Interim reanalysis products, bias-corrected to the observations using monthly biases. The calibration of site-dependent coefficients in the statistical relationships was done using six approaches: at individual sites; globally, considering all the sites; globally, considering high elevation sites only. All these approaches were repeated with and without considering clear sky transmittance. The following conclusions can be drawn from the study.

- Inclusion of relative humidity in the relationships used to estimate atmospheric transmittance improved the prediction of shortwave irradiance. In general, the Tau [T/RH] model N1 performed the best amongst all the empirical models considered in this study for prediction of shortwave irradiance.

- Bounding the empirical models by using regional differences in τ_{cs} provided an improvement in transmittance estimation for non-clear conditions, as suggested by Bojanowski *et al.* (2013). Therefore, if a site has some observations of shortwave irradiance to estimate τ_{cs}, the new T/RH models with τ_{cs} provide better predictions for non-clear sky shortwave irradiance. This can be very useful when gap-filling station observational radiation datasets using only temperature and humidity data.
- If a site is at lower elevation and does not have any observations of shortwave irradiance, the reanalysis products can provide good estimates of this variable. The globally available reanalysis products present high potential for application to large-scale hydrological models and at remote sites.
- If a site is at higher elevation and has only sparse observations of shortwave irradiance, the new (T/RH) algorithms should be used to gap-fill the irradiance dataset for the period of study. The reanalysis products, however, were not suitable for the high elevation sites. The empirical coefficients of the new models calibrated globally to high elevation sites (>3000 m.a.s.l.) or, better, to local stations, provided the best results for such sites in comparison to the ERA-Interim and WFDEI, and should be used for mountain snow and glacier hydrology studies.

In summary, a very good estimation of shortwave irradiance is based on sunshine duration, but this is generally not measured at cold regions or high elevation sites. Models based upon temperature and humidity are the alternatives as these variables are more readily available than any other meteorological parameters. Reanalysis products also provide a good alternative.

CHAPTER 4: Physically based glacier hydrology model

Paper manuscript status

Contents of this chapter have been drafted as a research paper manuscript for submitting to the Journal of Hydrology.

Author contributions: Dhiraj Pradhananga and John W. Pomeroy conceptualized the research. Tom Brown coded the model in the CRHM platform. Dhiraj Pradhananga built the model and tested it at the research basins and prepared the manuscript. John W. Pomeroy revised the manuscript.

This chapter addresses the second objective of the study, *Couple snow redistribution and full energy and mass budget in a glacier hydrological modelling platform and test the model at two glacier research basins in the Canadian Rockies.* It shows the development of a physically based, integrated glacier hydrology model in the CRHM platform. The CRHM-glacier model considers snow redistribution by wind and avalanches and has separate processes for firn/ice melt and snowmelt and routing of meltwater through the glacier. The model was tested in two glacierized basins in the Canadian Rockies against observations of radiation, albedo, point and aggregated surface mass balances, and streamflow.

4.1 Abstract

A novel glacier hydrology model was developed within the Cold Regions Hydrological Modelling Platform (CRHM) by including new modules to represent snow and ice energy budget, mass balance and runoff, and snow redistribution by avalanches. These new modules were coupled to existing modules for radiation estimation, wind flow over complex terrain, elevational lapse of temperature, humidity and precipitation, snow redistribution and sublimation by wind, meltwater routing, non-glacier surface evapotranspiration and sub-surface storage and flow modules. A physically based glacier hydrology model created from these modules in CRHM was capable of

simulating the hydrology of both ice-covered and ice-free areas in the Peyto and Athabasca glacier research basins in the Canadian Rockies. It was tested against observed radiation and albedo, point and aggregated surface mass balance, and streamflow. This model successfully simulated snow and glacier accumulation and ablation and predicted mass balance and streamflow, both with in-situ observations and reanalysis forcing data. The model could simulate both past and present discharges from the basins. There was an increase in discharge in the present time compared to the 1960s due to increased meltwater contribution from glacier firn and ice.

4.2 Introduction

Snow and glacier melt models range from complex energy budget models (Oerlemans, 1991; Klok and Oerlemans, 2002; Munro, 2004, 2011b; Hock and Holmgren, 2005; Munro and Marosz-Wantuch, 2009; Naz *et al.*, 2014; Shea *et al.*, 2015a) to more simplified degree-day models (Hock, 1999; Anderson *et al.*, 2006; Immerzeel *et al.*, 2012). Most glacier hydrology models use simple conceptual melt models that are based on temperature and precipitation observations and are calibrated from past conditions (see Hock, 2005 for review). Examples include statistical and temperature index models (Hock, 1999, 2003; Hannah and Gurnell, 2001; Verbunt *et al.*, 2003; Singh and Bengtsson, 2005; Shea and Marshall, 2007; Stahl *et al.*, 2008; Fujita and Nuimura, 2011; Luo *et al.*, 2013). These empirical models do not consider the redistribution of snow by wind and mass movement, and the full radiation energetics that are critical to the survival of small mountain glaciers (Déry *et al.*, 2010). Because high altitude observations of shortwave irradiance are limited, empirical techniques that rely upon commonly measured variables, such as air temperature, have led to the popularity of the temperature-index model and its wide use to simulate glacier snow and ice melt (Hock, 2005). These empirical methods are unlikely to be reliable for future conditions, as they have been calibrated on past behaviour (Poulin *et al.*, 2011). Walter *et al.* (2005), however, demonstrated that a physically based energy budget melt model does not require more input data than most temperature-index methods. An example of this is Energy Budget Snowmelt Model (EBSM) (Gray and Landine, 1988). Pomeroy *et al.* (2013) showed that shortwave and net radiation can be simulated from temperature and humidity data and geographical location. Moreover, reanalysis products are now commonly being used to force hydrological models (Krogh *et al.*, 2015).

Recent work has attempted to couple basin hydrology modelling with glacier dynamics to assess the impact of glacier retreat on streamflow (Huss *et al.*, 2008; Huss, 2011; Immerzeel *et al.*, 2012; Finger *et al.*, 2013; Naz *et al.*, 2014; Shea *et al.*, 2015a). These and other studies have not considered many of the important cold region hydrological processes, including the evolution, ablation and redistribution of snow. Snow storage, redistribution of snow by wind and gravity, and sublimation rates in high latitude alpine mountains are crucial considerations when determining water contribution to the basin (Strasser *et al.*, 2008; Bernhardt and Schulz, 2010; MacDonald *et al.*, 2010; Ayala Ramos, 2017; Bravo *et al.*, 2017). Despite significant advances in the areas of blowing snow redistribution and sublimation over alpine landscapes (Déry *et al*., 2010; Doorschot *et al*., 2001; Essery and Pomeroy, 2004; Liston and Elder, 2006; MacDonald *et al*., 2009; Pomeroy and Li, 2000), these processes have not yet been fully included in mountain glacier melt studies in the Canadian Rocky Mountains. They have been considered in mass balance and melt studies over Icelandic and polar glaciers, as well as in studies of Antarctic and Arctic sea ice and ice-sheets (Bintanja and Reijmer, 2001, Bintanja, 2001, Dery and Tremblay, 2004, Gallée *et al*., 2012, Liston and Hiemstra, 2011, Mernild *et al*., 2007, 2008, Thiery *et al*., 2012). Bernhardt *et al*. (2009, 2010) found significant redistribution of snow due to blowing snow over an alpine glacier in Germany. Snow redistribution, snow sublimation and other hydrological processes may also contribute significantly to the mass and energy budget of mountain glaciers in western Canada.

There is a need to develop a glacial melt model that utilizes an energy budget approach, physically measurable inputs, and a snow redistribution approach that accounts for the complex mass transport present in mountainous regions. It is hypothesized that the simulation of water contributions from glacial ablation will be more accurate when snow redistribution by wind and gravity, sublimation and surface energy budget energetics are included. This study develops and tests a physically based and spatially distributed model of glacier snow and ice hydrology. The model includes redistribution of snow by wind and avalanches, an energy budget melt model for snow, firn and ice, consideration of slope and aspect for radiation distribution, and runoff routing.

4.3 Study sites and data

4.3.1 Two alpine glacier basins in the Rocky Mountains

The CRHM-glacier model was tested over the Peyto Glacier Research Basin (PGRB, latitude: 51°40'N and longitude:116°33'W) in Banff National Park and the Athabasca Glacier Research Basin (AGRB, Latitude: 52°11'N and Longitude:117°16'W) in Jasper National Park (Figure 4-1). PGRB, with the outlet at the old gauging site (Figure 4-6), covers an area of 22.43 km^2, which includes 9.9 km^2 of glacier as of 2016. AGRB consists of a basin area of 29.3 km^2, including 16.9 km^2 of glacier in 2016. Peyto Glacier in PGRB is a valley outflow glacier of the Wapta Icefield in the Waputik Mountains. Athabasca Glacier in AGRB is a valley outflow glacier of the Columbia Icefield. Streamflow out of PGRB flows east into, Mistiya River Basin, a headwater of North Saskatchewan River and eventually into the Hudson Bay via Nelson; and that out of AGRB flows north through Sunwapta River, a headwater of Athabasca River and eventually into Beaufort Sea of Arctic Ocean via Mackenzie. Table 4-1 provides the general physical characteristics of these two research basins. These basins were recently equipped in 2013-2014 with new automatic weather stations (AWS) at on-ice and off-ice sites. The instrumentation and range of parameters measured, and the logging frequency of these AWS are presented in Table 2-1 and Appendix E.

These glaciers have been losing mass continuously since the mid-1970s (Demuth and Keller, 2006; Tennant and Menounos, 2013; Kehrl *et al.*, 2014). In the case of Peyto Glacier, the new proglacial lake, "Lake Munro", formed at the tongue of the glacier is increasing in size every year. Peyto Creek, flowing out of Lake Munro, drains the meltwater from the glacier and discharges to Peyto Lake, which has outflow into the Mistaya River, one of the tributaries of the North Saskatchewan River. The first record of Peyto Glacier goes back to 1897 (photograph by Walter D. Wilcox). Significant research over the glacier started in 1965 when it was selected as one of the research sites for the International Hydrological Decade (IHD). Scope and observational instruments improved progressively since then (Munro, 2013). As reported by Meek (1948), the surveys covering recession and flow of Athabasca Glacier began in 1945.

Table 4-1: Physical characteristics of the study basins

Basin configuration	**PGRB**	**AGRB**
Basin Area	22.43 km^2	29.3 km^2
Glacier Area	9.9 km^2 [44%] as of 2014	16.9 km^2 [58%] as of 2014
Elevation range of basin	1907 – 3152 m as of 2014	1926 – 3459 m as of 2011
Location	$51^0$40’N, $116^0$33’W Banff National Park, Alberta	$52^0$11’N, $117^0$16’W Jasper National Park, Alberta
Mean elevation of glacier	2615 m [2014 DEM and Landcover]	2826 m [2011 DEM, 2014 Landcover]
Basin outlets	Old gauge: 51°41'37"N; 116°32'08"W New gauge: 51°40'52"N; 116°32'41"W	52°12'58"N; 117°13'55"W

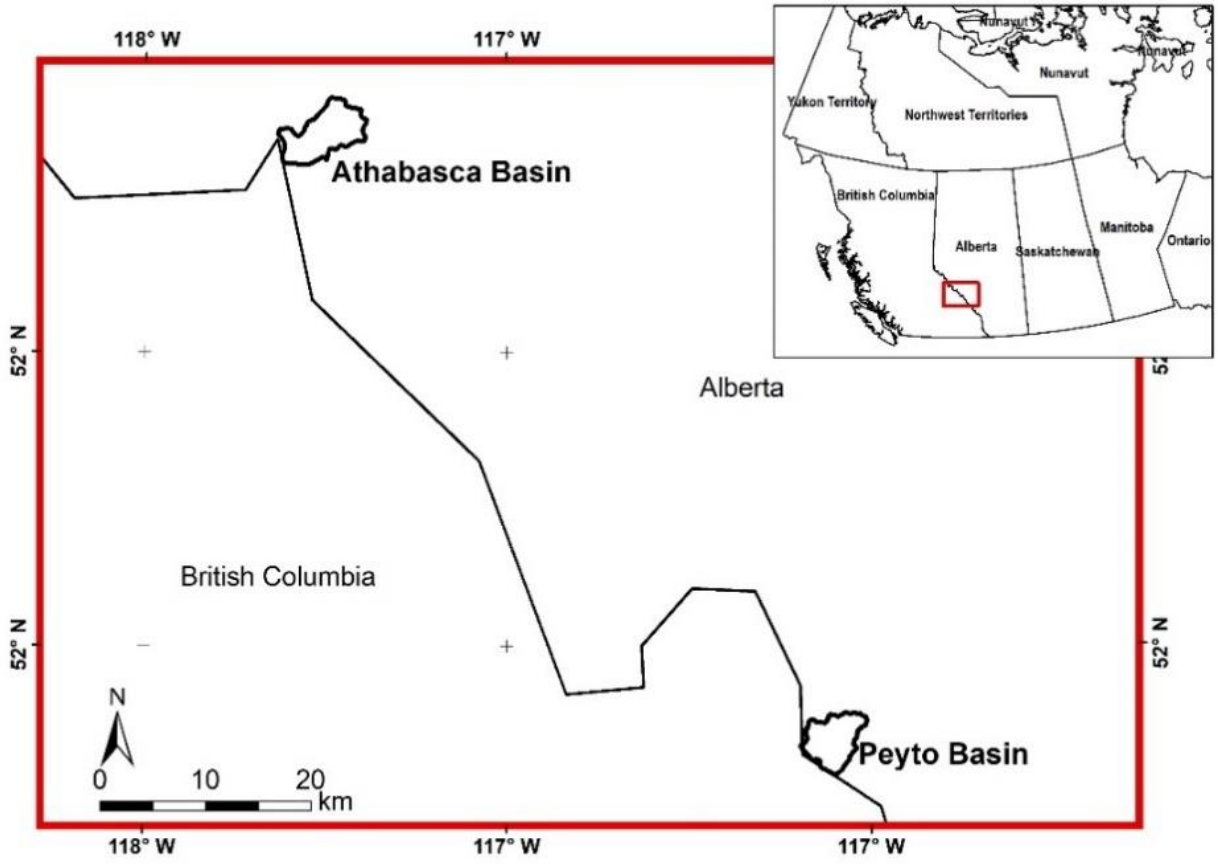

Figure 4-1: Location map of Peyto and Athabasca glacier research basins

4.3.2 Data

4.3.2.1 Topography

Several digital elevation models (DEM) from different years, topographical maps and satellite images were used for both the basins. In the case of Peyto Glacier, 20 m horizontal resolution DEMs of 1978, 1986 and 2000 were collected from the Canadian Digital Elevation Data (CDED) sources of Natural Resources Canada (CCMEO, 1997; Natural Resources Canada, 2000, 1986). The 2006 DEM (10 m resolution) was obtained from airborne LiDAR measurements (Demuth and Hopkinson, 2013); the 2014 DEM was prepared at 10 m resolution from the aerial photogrammetry taken during July and September 2014. The 1966 DEM (10 m resolution) and 1994 DEM (40 m resolution) were developed from scanned topographic maps of Peyto Glacier. The 1966 topographic map was produced from the aerial photographs from August 1966 (Sedgwick and Henoch, 1975) and the 1994 map of Blaeberry River was from Natural Resources Canada.

For Athabasca Glacier, DEMs from 1983, 2000 and 2011, all at 20 m horizontal resolution, were available. The aerial photos from 2014 over Athabasca Glacier were not good enough to create a DEM. The details of the DEM preparation and their sources are presented in Appendix A. Landcover maps were generated from the Landsat images, Landsat 5 and Landsat 8 top-of-atmosphere (TOA) reflectance images, using Google Earth Engine (GEE). Landsat 5 images were used for the years 1984 to 2011 and Landsat 8 images were used from 2013 to 2017. The images acquired for this study were taken between 15th July to 15th September each year and with minimum or no cloud cover inside the basin boundaries. Dates of the images used in the study are listed in Appendix A.

4.3.2.2 Glaciology and hydrology

Past studies of Peyto Glacier are well documented in the book ‘Peyto Glacier: One Century of Science’ edited by Demuth *et al*. (2006). The edited book also provides details of the mass balance data, along with hypsometry of the glacier. Long-term glacier mass balance records are available for Peyto Glacier from 1965, with a data gap in 1991 and 1992. Glaciological mass balance measurements using ablation stakes and snow pits have been performed continuously since the

IHD period. Mass balance data for 11 elevation bands were published (with a data gap for 1991-1992) in several publications (Demuth and Keller, 2006; Ommanney, 1987; Young and Stanley, 1976). Though winter (Bw) and summer (Bs) balance records were available until 1994, annual glacier net mass balance (Bn) data were available after 1994 (WGMS, 2019) for this study. Mass balance data for Athabasca Glacier were not available for this study.

PGRB was gauged (old gauge shown in Figure 2-1) during the IHD period and then discontinued. In the summer of 2013, the Centre for Hydrology, University of Saskatchewan established a gauging site in the basin, about 1.5 km upstream from the site used in the IHD (new gauge shown in Figure 2-1). Discharge data from the IHD period are available for an 11-year period (1967-1977) and those from the recent period are available for 6 years (2013-2018). Discharge data from the outlet of Athabasca Glacier are available from 1948 up to the present, with a data gap from 1997 to 2004. Historical discharge data of PGRB and AGRB were obtained from the Water Survey of Canada; the recent preliminary discharge data of AGRB from 2005-2019 were obtained from the Environment and Climate Change Canada (email communication with Samantha Hussey and Dennis Lazowski) and the Alberta Environment and Parks (https://rivers.alberta.ca).

4.3.2.3 Meteorological forcing datasets

AWSs were installed at on ice and off-glacier sites of Peyto and Athabasca glaciers by the Centre for Hydrology, University of Saskatchewan in 2013-2014. The archived hourly meteorological observations from the AWS at the Peyto Glacier main station are available from 1987 (Munro, 2011) along with periodical observations made on the ice since 2007. Climatological data for the stations near PGRB (Figure 4-2) were obtained from the Parks Canada and Environment Canada (http://climate.weather.gc.ca/).

Climate data preparation to force a hydrology model presents several challenges. Climate data collection from an alpine glacier basin is not an easy task due to its location, difficulty in accessibility and many other difficulties. For example, Lafreniere and Sharp (2003) experienced failure of their power source. Higher accumulation during winter often buries on-ice stations, and

higher melt causes the stations to tilt or fall during summer (Figure 4-3). Climate data availability in PGRB and AGRB is impacted by many of these irregularities.

Therefore, climate stations located within and near the basin, along with reanalysis data, were used to prepare the climate forcing datasets. The ERA global reanalysis datasets (Weedon *et al*., 2011) were first bias-corrected to the single point at the main stations by comparing with the *in-situ* observations at these sites. They were described in Section 2.4.4 and details of evaluation of ERA with the other reanalysis datasets are in Appendix B. Accessibility of the datasets and its applications in CRHM are discussed by previous studies (eg. Krogh *et al.*, 2015, 2017; Anderson, 2017; Krogh and Pomeroy, 2018). In the second stage, these data were distributed to the basin using algorithms and macros in CRHM (Pomeroy *et al*., 2007). The 'Observation module' adjusts temperature and precipitation with elevation, the 'Radiation module' distributes global radiation to HRUs based on latitude, elevation, ground slope and azimuth. Details of these modules are provided by Fang *et al.* (2013).

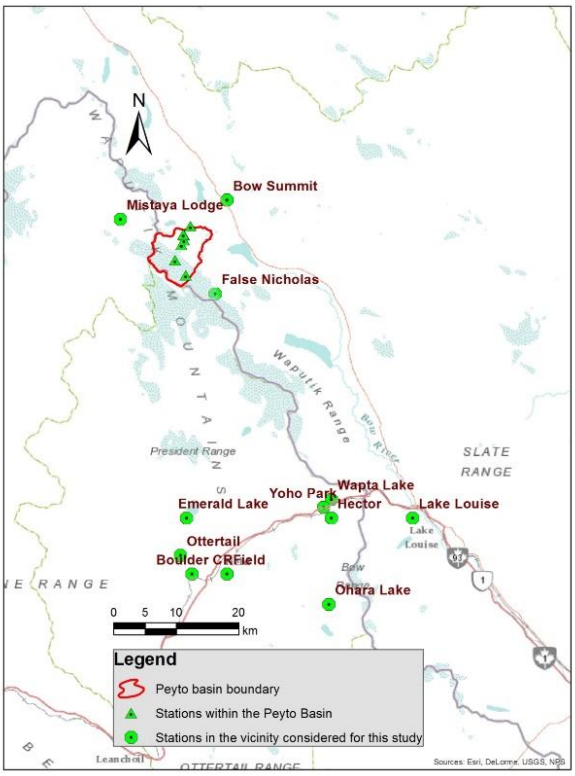

Figure 4-2: Climate stations near PGRB.

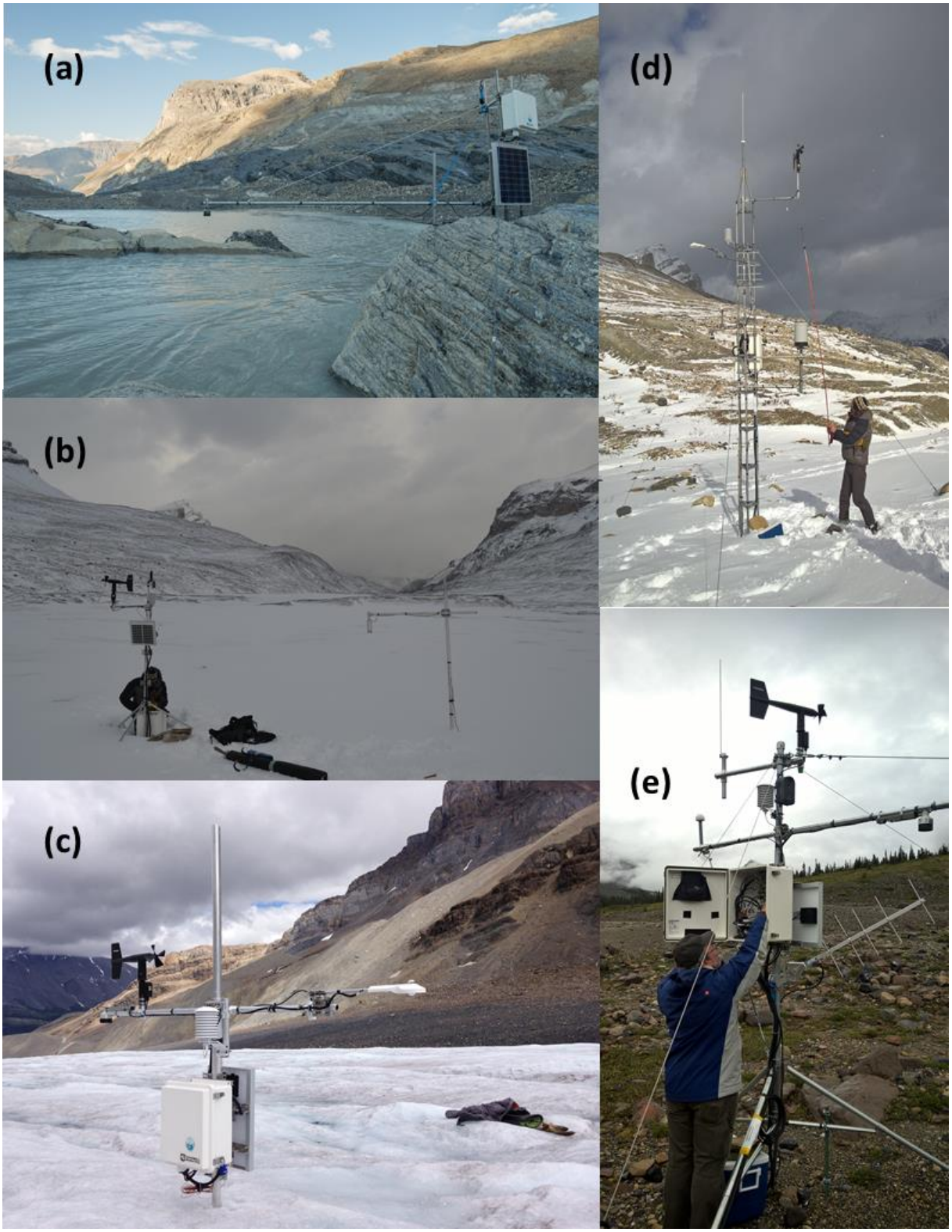

Figure 4-3: AWSs in AGRB and PGRB. (a) New gauging station at the outlet of Munro Lake, (b) Lower Ice station in PGRM, (c) Ice station in AGRB, (d) Peyto Main New station, (e) Athabasca Moraine station. [Photo (a) by May Guan; the rest by the author]

4.4 CRHM-glacier

CRHM (Pomeroy *et al*., 2007) is a flexible, object-oriented, process-based modelling platform that runs on spatially distributed of hydrological response units (HRU) at sub-daily or sub-hourly timesteps. It simulates several cold region hydrological processes including blowing snow and sublimation, infiltration into frozen soils, radiation exchange to complex terrain, snow accumulation and ablation (Pomeroy *et al*., 2007; Fang *et al*., 2013). The model runs through interactions of the four components - observations, parameters, set of modules, and variables and states. Through these interactions, CRHM links atmospheric data inputs and hydrologic information outputs. Minimum climate inputs required for CRHM are air temperature, humidity, wind speed and precipitation either from automatic weather stations or from atmospheric model outputs for the surface level. CRHM has been successfully applied in many places, ranging from the Canadian prairies to high altitude mountains in South America and Asia (e.g., Fang and Pomeroy, 2007; MacDonald *et al.*, 2009b; Ellis *et al.*, 2010; Fang *et al.*, 2010; Rasouli *et al.*, 2014; Zhou *et al.*, 2014; Krogh *et al.*, 2015; Stone *et al.*, 2019).

Processes were incorporated within CRHM to create CRHM-glacier, a model suitable for alpine glacier basins. These modules are linked in a sequential manner to simulate hydrological processes for a glacierized basin; the flow diagram of these modules is shown in Figure 4-4. The most relevant modules for an alpine glacier are described in the following sub-sections, along with the new glacier module. This section details the development of a distributed, physically based, numerical model to simulate glacier mass and energy fluxes.

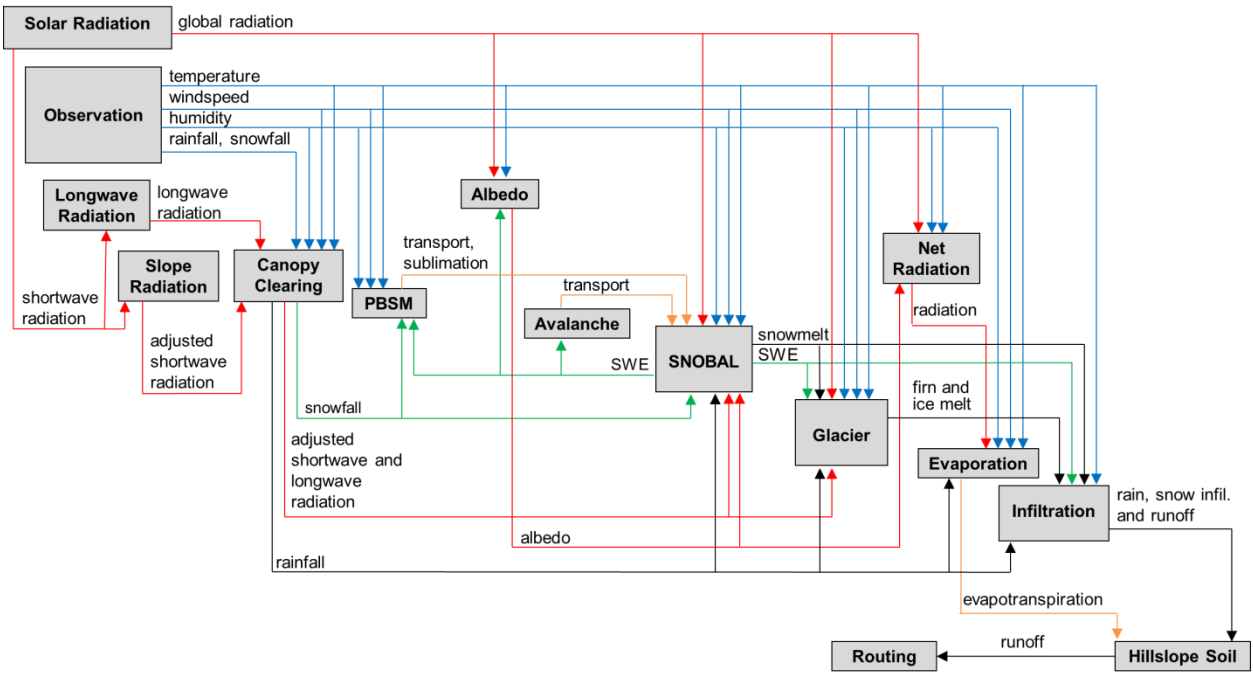

Figure 4-4: Modular structure of CRHM-glacier modified from Pomeroy *et al*. (2016). Red linking arrows are radiation terms; blue lines are climate observations; orange lines are mass transport; green and black lines are model outputs or processed variables of water equivalents, in solid and liquid forms, respectively.

4.4.1 Snow redistribution and sublimation

Many glacier models neglect blowing snow and sublimation (e.g., Naz *et al.*, 2014; Shea *et al.*, 2015a). Snow redistribution by both wind and avalanches is important in mountain glaciers due to high wind speed and steep topography. It significantly alters the mass balance and, thus, melting processes (Wayand *et al*., 2018). The blowing snow module (Pomeroy, 1989; Pomeroy & Li, 2000) calculates snow transport and sublimation from wind speed, air temperature and relative humidity at the interval of observations. Horizontal snow redistribution by wind from one HRU to another is determined by surface roughness. Saltation and suspension are the two primary modes of transport of snow by blowing processes, where either surface snow or falling snow or both act as sources of blowing snow (Pomeroy *et al*., 1997). Three factors are needed for a blowing snow event to occur – wind, open snow surface with good exposure to wind, and supply of erodible snow. The details of the blowing snow model in CRHM are provided in Pomeroy *et al*. (1993) and its test over a mountain region is detailed in MacDonald *et al*. (2009).

In addition to blowing snow, snow is redistributed from higher to lower elevations on steep surfaces, described by an avalanche module (named as 'SWESlope' in CRHM) based on Bernhardt and Schulz (2010). Snow slides if a minimum snow holding depth (H_d) and a minimum slope angle (S_m) are exceeded. They suggested values of H_d and S_m as 50 mm of SWE and 250 of surface slope, respectively. For slopes steeper than S_m, snow holding depth decreased exponentially. The best fit regression line (Equation 4.1) as developed by Bernhardt and Schulz (2010) for the curve of H_d [m] and S_m [0] was used in the avalanche module.

$$H_d = 3178.4\, S_m^{-2} \tag{4.1}$$

4.4.2 Energy balance

The energy available for snow, firn and ice melt (Q_M [W m^{-2}]) is the sum of fluxes due to radiation, turbulence, advection, and conduction (Pomeroy *et al*., 1998):

$$Q_M = Q_n + Q_h + Q_e + Q_p + Q_g - \frac{dU}{dt}, \tag{4.2}$$

where dU/dt is the change in internal energy of the snow/ice; Q_M is the energy available for melt, Q_p is the advection energy from precipitation, Q_g is the heat flux due to conduction, Q_e and Q_h are turbulent fluxes of latent heat and sensible heat, respectively and Q_n is the net radiation expressed as:

$$Q_n = K_n + L_n = (K_{in} - K_{out}) + (L_{in} - L_{out}) = (1 - \alpha)K_{in} + L_{in} - \varepsilon\sigma T_s^4, \tag{4.3}$$

where, K_n is the net shortwave radiation, L_n is the net longwave radiation; K_{in} and K_{out} are incoming and outgoing solar radiation; L_{in} and L_{out} are incoming and outgoing longwave radiation. All these energy components have units of W m^{-2}. T_s is the surface temperature in Kelvin and ε is the emissivity of the surface. The available energy for melt, Q_M, can be converted to a melt rate, M (m s^{-1}) as:

$$M = \frac{Q_M}{\rho_w L_f}, \tag{4.4}$$

where, ρ_w is the density of water and L_f is the latent heat of water fusion at freezing temperature. Energy balance glacier melt modelling in CRHM-glacier consists of two separate melt algorithms, giving distinct calculations for snow and firn/ice surfaces. The energy and mass balance snowmelt

model - Snobal (Marks *et al*., 1999; Marks *et al*., 1998), was incorporated in CRHM-glacier for modelling snowmelt processes. It simulates the energy and mass balance of deep snowpacks in mountains over glacierized and non- glacierized surfaces. Internal energy exchange is through cold content based on two layers: a) surface-shallow and fixed-thickness active layer, and b) lower deep snowpack. The model solves for temperature and specific mass [kg m^{-2}], which is the product of snow depth and snow density. Accumulated energy is the energy available after satisfying the cold content and runoff of accumulated melt and liquid content exceeding a specified threshold. The turbulent heat fluxes are obtained using an approach adopted from Brutsaert (1982) by Marks and Dozier (1992). Details are in Marks *et al.* (1998). A single layer, daily time step, energy budget melt model, originally developed by Gray & Landine (1988) for shallow prairie snowpacks and adopted by Ellis *et al*., (2010), was customized to ice and firn melt by adjusting its albedo routine and assuming glacier ice and firn are isothermal, so all internal energy change goes to melt.

The radiation module in CRHM simulates incoming shortwave (global) radiation adjusted to slope and aspect. Similarly, in the absence of observation, longwave irradiance can be estimated from shortwave transmittance and air temperature using the algorithm proposed by Sicart *et al*. (2006) that modified Brutsaert's clear sky longwave algorithm for cloudy conditions. Terrain emission of longwave is also included in the Sicart's model. Influence of the longwave irradiance from the surrounding terrain is significant in mountains (Plüss and Ohmura, 1997). The albedo module of snow evolution by Verseghy (1991) adopted by Essery and Etchevers (2004) based on the age, depth, density and temperature of the snow layer is used to simulate albedo of snow.

4.4.3 Mass balance

CRHM-glacier simulates the mass balance for snow/firn/ice water equivalents for glaciers, as the variables of snow water equivalent (SWE [mm]), firn water equivalent (FWE [mm]), and ice water equivalent (IWE [mm]). The mass balance of a glacier (MB [mm]), also referred to as the mass budget, is expressed as:

$$MB = SWE + FWE + IWE, \quad (4.5)$$

where the three terms are expressed as:

$$SWE = SWE_0 + P + H_{in} - H_{out} - S - M, \quad (4.6)$$

$$FWE = FWE_0 + V_{in} - V_{out} - S - M, \text{ and} \quad (4.7)$$

$$IWE = IWE_0 + V_{in} - S - M. \quad (4.8)$$

SWE_0, FWE_0, IWE_0 are the initial water equivalents of snow, firn and ice, respectively. P is the amount of precipitation. H_{in} and H_{out} are horizontal incoming and outgoing mass flows due to blowing snow and avalanches, whereas, V_{in} and V_{out} are vertical incoming and outgoing mass flows due to snow and firn densifications. S is the mass loss by sublimation, and M is loss by melting from snow, firn, and ice. The units for these variables are mm. Many models do not consider firn separately (e.g., Li *et al.*, 2015; Naz *et al.*, 2014). Firn has properties that are significant in the model. The albedo of firn is lower than that of snow, but it is higher than that of ice. Secondly, it is important for meltwater routing, which is slower in firn than in ice (Hannah and Gurnell, 2001). This is because of macro-scale permeability within ice in the form of englacial and subglacial meltwater channels that are connected to the surface via crevasses and/or moulins. Thirdly, the model adds water equivalent of firn and ice in the hydrological processes so that it simulates changes in glacier surface elevation. Glacier surface elevation change (ΔE) at each time step can be obtained as:

$$\Delta E = \left(\frac{\Delta SWE}{\rho_s} + \frac{\Delta FWE}{\rho_f} + \frac{\Delta IWE}{\rho_i}\right)\rho_w \quad (4.9)$$

Here, ρ_s , ρ_f, ρ_i, and ρ_w are the densities of snow, firn, ice, and water, respectively. The densities are modelled through multilayer snow (Pomeroy *et al.*, 1998) and firn (Herron and Longway, 1980) densification. ΔSWE, ΔFWE, and ΔIWE are changes in water equivalents of snow, firn and ice, respectively.

4.4.4 Hydrological modules

CRHM is built from models assembled from the library of physically based hydrological and energy balance process modules. The model considers delayed interflow through snow, firn, ice and subsurface, as well as groundwater flow, using lag and storage parameters, which are empirical

parameters derived from analysis/fitting of runoff hydrograph. The concept of linear storage routing was used in several glacio-hydrological studies (e.g., Engelhardt *et al*., 2014; Hannah & Gurnell, 2001; Huss *et al*., 2008; Magnusson *et al*., 2011; Oerter *et al*., 1981, Jansson *et al*., 2003). de Woul *et al*. (2006) proposed variable snow and ice reservoirs whilst keeping the firn reservoir constant. They considered snow-covered firn to be part of the firn reservoir, however if ice was covered by snow, they considered a distinctive snow reservoir in their model. In CRHM-glacier, meltwater is therefore routed from one HRU to the other until it reaches the outlet by means of three storage constants - ice, firn and snow. Once the meltwater and rain reach the ground surface, three modules (infiltration, hillslope and routing) estimate their storage and flow through three different strata – surface, subsurface and groundwater. The model considers delayed interflow through snow, firn, ice and subsurface and groundwater flows, using lag and storage parameters, which could be determined either by literature/measurements or by calibration.

Either the Muskingum streamflow routing module (Chow, 1959) or Clark's lag and route surface runoff routing module (Clark, 1945) can be chosen in CRHM for calculating surface runoff. Infiltrated water is calculated by hillslope soil module by Fang *et al*. (2013), based on the soil module by Leavesley *et al*. (1983), which was progressively developed by Dornes *et al*. (2008) and Fang *et al*. (2010). The hillslope soil module deals with depression storage, subsurface runoff, groundwater recharge, and groundwater flows between HRUs. Water moisture loss from the natural unsaturated surface by evaporation is estimated by Granger's evaporation expression (Granger and Gray, 1989; Granger and Pomeroy, 1997) using an energy budget and extension of Penman's equation, whereas evaporation from saturated surfaces is simulated by the evaporation expression developed by Priestley and Taylor (1972).

4.4.5 Hydrological response units (HRUs)

The meteorological forcing data and distribution of climate data over the basin are based on slope, aspect, elevation and landcover of each HRU. ArcMap was used to prepare HRUs of both basins. The steps in the flowchart shown in Figure 4-5 (example for PGRB) were followed for the two research basins, PGRB (Figure 4-6) and AGRB (Figure 4-7). Two landcovers, 2014 and 1966 in the case of PGRB and 1984 and 2014 in the case of AGRB were used. Since the gauging sites

were at different locations during the IHD period and the present time, two separate basin maps were prepared for PGRB. The catchment area at the new gauging site is about 4 km^2 smaller than at the old gauging site.

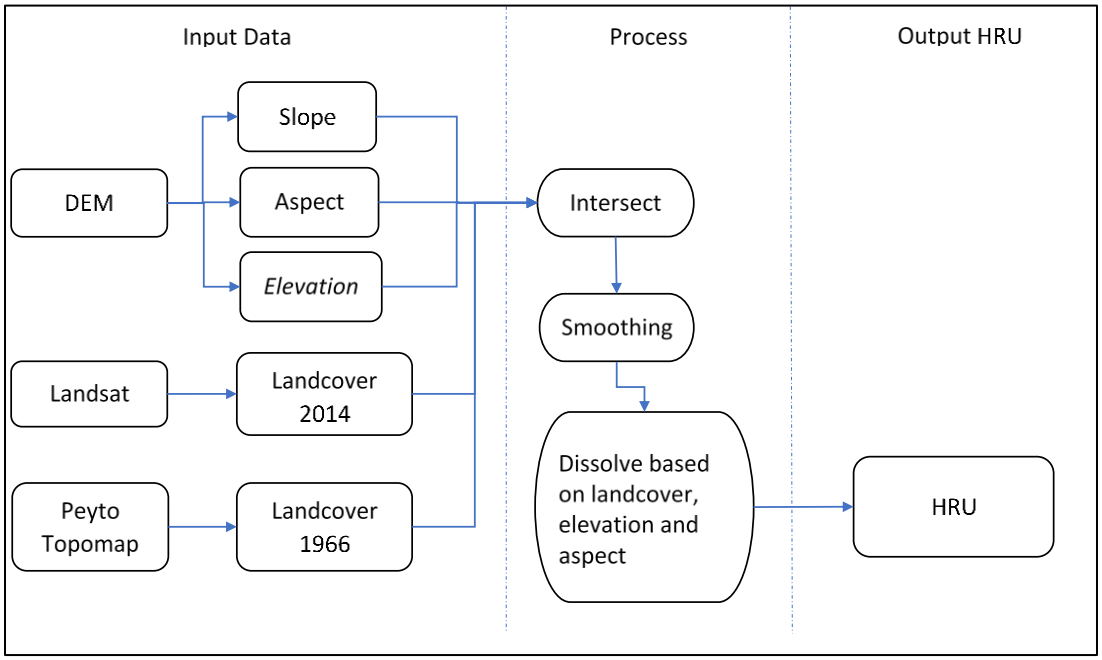

Figure 4-5: Flowchart showing the process for delineating HRUs.

The physiographic parameters required by CRHM-glacier include the following: area, latitude, average elevation, average ground slope, average aspect and average terrain view factor (TVF). Except for TVF, all parameters were calculated in R for each available DEM. TVF was obtained in SAGA GIS as a sub-product of the sky view factor under the terrain analysis. The major landcover of each HRU in each year was calculated using Zonal Statistics with Table. The majority of landcovers from 1966, and 1984-2017, in the case of PGRB, and those from 1984-2017, in the case of AGRB were calculated by using the raster iterator operator in a model builder of ArcGIS 10.3.1.

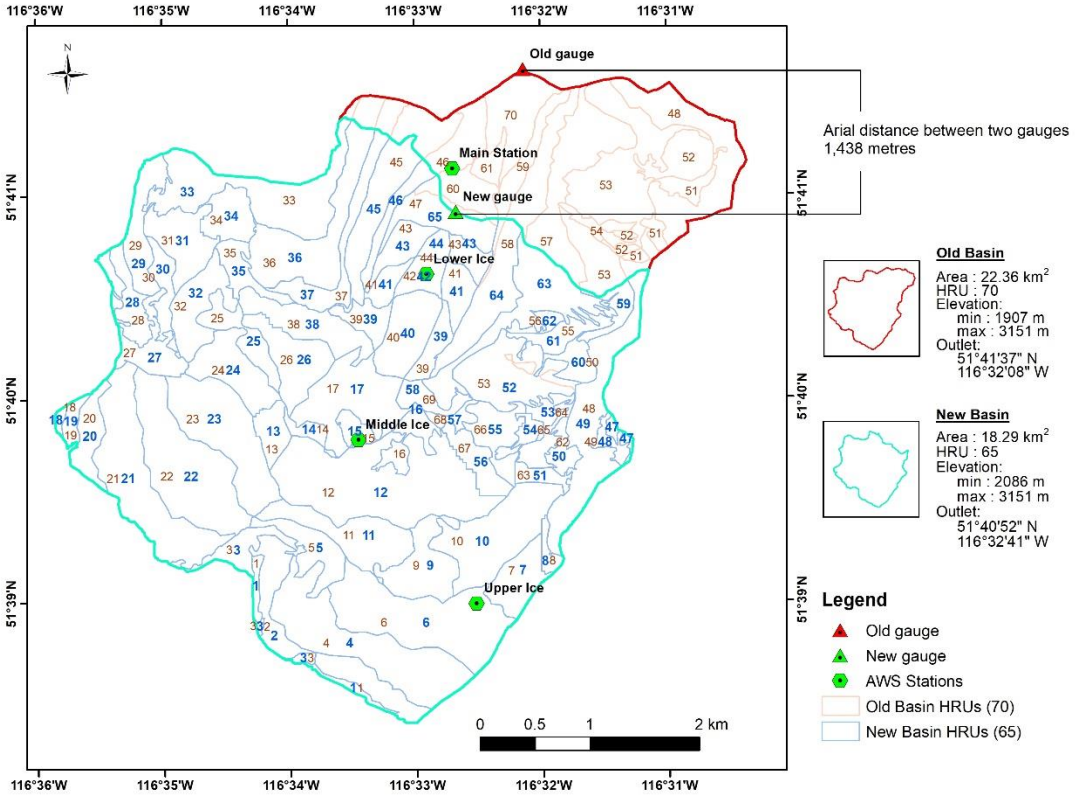

Figure 4-6: PGRB with two outlets

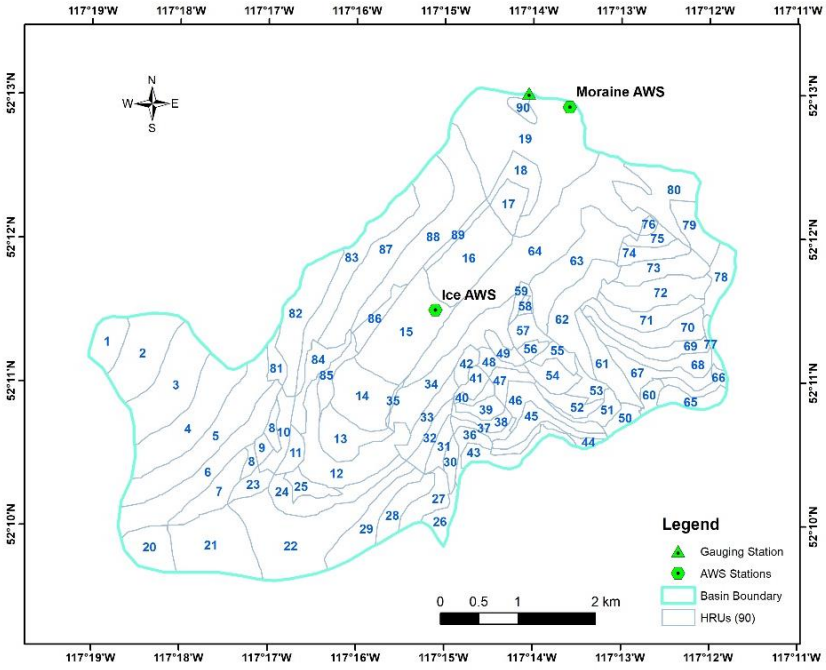

Figure 4-7: AGRB with 90 HRUs

4.4.6 Spatial distribution of temperature, precipitation and other meteorological variables

The model input data files were prepared using the R packages developed in the Centre for Hydrology by Kevin Shook - CRHMr (Shook, 2016a); archived data from Environment and Climate Change Canada were obtained by the package MSCr (Shook, 2015); and reanalysis data were obtained and interpolated using the package Reanalysis (Shook, 2016b). CRHMr was also used for pre-processing meteorological forcing data, post processing and analysing model outputs.

Monthly lapse rates of temperature were obtained from the four AWSs at different elevations within PGRB (Figure 4-6). For precipitation, the four stations (Helen Lake, Bow Summit, Saskatchewan River Crossing and Lake Louise) near to PGRB were considered. Temperature and precipitation were distributed by the elevation of each HRU based on the monthly lapse rates. Wind speed change due to local topography is adjusted by the Walmsley's wind flow module (Walmsley *et al.*, 1989). Incoming shortwave and incoming longwave radiation were distributed considering slope and aspect and terrain view factors of HRUs. The parameters were set primarily by knowledge of physical processes or measurement, and calibration is optional (Pomeroy *et al*., 2007).

4.5 Testing model performance

A series of simulations were designed for testing model performance. Fist, the model was evaluated for distribution of meteorological variables to HRUs. Gridded meteorological reanalysis data were compared with *in-situ* measurement data for air temperature, vapour pressure, wind speed, incoming shortwave and longwave radiations, and precipitation. Model runs from *in-situ* observations and the reanalysis data were also compared.

Model simulations were compared with the available hydro-meteorological and glaciological observations at the two basins, AGRB and PGRB to evaluate the CRHM-glacier model. The model was evaluated for albedo simulation, accumulation and ablation, and runoff generation comparing with the *in-situ* measurements over the two basins. Incoming and outgoing shortwave radiation measured by AWS on glacier ice and moraine provided observed albedo. Measured daily albedo

was obtained as a ratio of the daily amount of outgoing shortwave radiation to the daily amount of incoming shortwave radiation (Oerlemans and Knap, 1998). Daily observed and simulated albedo values were compared for the four sites for five years except Peyto Glacier Lower Ice AWS, which had both incoming and outgoing shortwave radiation measurements during 2007-2008 only.

Modelled surface accumulation and ablation processes over the glacier were compared with surface height changes (Figure 4-8) that were measured by SR50 at the three ice stations in PGRB. The advantage of comparing surface elevation change over comparing water equivalent change is that the former provides additional comparison of density simulation in the model (Garen and Marks, 2005). This process also validates the surface elevation change modelled by the accumulation and ablation process at the surface.

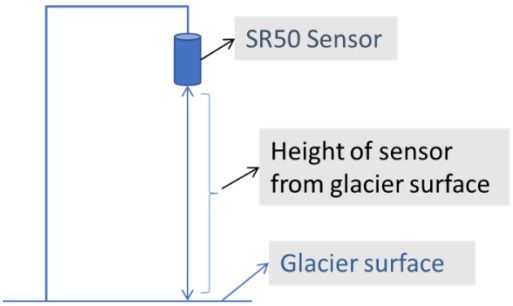

Figure 4-8: Schematic diagram of SR50 on glacier surface measuring change in glacier surface elevation.

In CRHM, most of the parameters were set by knowledge and understanding of the basin, instead of optimizing in comparison with the observation, as stated in Section 4.4.6. Though calibration is sometimes inevitable, it can be reduced with advancements in hydrological science. Ommanney (2002) summarized the studies made by Derikx (1975) and Collins (1982) who found that the meltwater reaches the outlet at a very short time, from 2 to 5 hours. Munro (2011a) and Munro (2013) also considered the runoff delay, and found it varied from a few hours to half a day. Given the daily time step of discharge, calibration of model routing parameters was not done in this study. No parameters whatsoever were calibrated in this study. The model simulated discharges of the two basins for two different time slices were compared with observations over daily periods for the present (2014-2019 for AGRB; 2013-2018 for PGRB) and past datasets (1967-1977 and 1980-1989 for AGRB; 1967-1977 for PGRB).

CRHM-glacier considered redistribution of accumulated snow by two processes, blowing snow and avalanche. Blowing snow includes the effect of blowing snow sublimation losses. The effects of adding blowing snow and avalanche were investigated using the model falsification, with and without these processes, and comparing the model outputs to the observations. First, the model was tested for glacier surface elevation changes on Peyto Glacier at three sites. Second, it was tested for streamflow simulations from the two basins, AGRB (for 2014-2019) and PGRB (2013-2018) with forcing meteorological data from bias-corrected ERA-Interim and *in-situ* observed data. The following four model scenarios were considered to examine the impacts of snow redistribution on streamflow.

1. Without blowing snow and without avalanche [scenario S_0]
2. With blowing snow and with avalanche [scenario S_BsAv]
3. With blowing snow, but without avalanche [scenario S_Bs]
4. Without blowing snow, but with avalanche [scenario S_Av]

Based on these four experimental scenarios, three comparison tests were employed to evaluate the two snow redistribution modules. Wilcoxon Signed-Rank test in the R environment (R Core Team, 2017) was applied to test the significance of the changes between the model scenarios. All tests were conducted at the 5% level of significance.

Test 1: compare scenario S_BsAv and scenario S_0
Test 2: compare scenario S_Bs and scenario S_0
Test 3: compare scenario S_Av and scenario S_0

Agreement between simulated and observed values was evaluated by using both traditional and non-traditional statistical indices. Nash-Sutcliffe efficiency (NSE, Nash and Sutcliffe, 1970), mean bias error (MBE) and the root mean square error (RSME) were used, along with the Wang-Bovik Index (WBI). Details of the WBI and statistical analyses (R packages) are provided in section 3.3.5. The additional code used from the R packages was *hydroGOF* (Mauricio, 2014). The analysis results are presented in graphs and tables. Performance rating based on the values of NSE (following Dahal *et al.* (2020)) was considered as 'very good' [NSE > 0.65], 'adequate' [0.65 => NSE > 0.54], and 'satisfactory' [0.54 => NSE > 0.50].

4.6 Results and discussion

Unlike other glacier hydrological models, the model parameters in CRHM-glacier are determined by observations when available and by knowledge and experiments from the previous studies, as mentioned in Section 4.4.6. As such there are no calibration and validation periods to compare. The model results are presented in the following subsections.

4.6.1 Model validation

The model was tested against observations of meteorological variables, albedo, mass balance and discharge. Model performance was evaluated by means of visual as well as statistical interpretations.

4.6.1.1 Albedo

Net shortwave radiation is the most important energy component over glaciers (Munro and Young, 1982a). Therefore, accurate parameterization and modelling of surface albedo are crucial for computing the energy and mass balance of the glaciers. The model was validated to recent measurements of surface albedo at four locations - two sites in PGRB and two sites in AGRB. The CRHM-glacier albedo module was used to simulate albedo on glacier ice and off glacier surfaces over both basins. The comparisons were made at daily values with point AWS measurements (Figure 4-9) and their statistical measures for model performance are presented in Table 4-2.

The model captured the variation of albedo both on-ice and off-ice sites with WBI higher than 0.85, RMSE less than 0.17 and the highest MBE being 0.063. Though these point observations do not represent all basin areas, they represent storm events and snow decay conditions. Since a single value of albedo was used for snow-free conditions, the variation of albedo during ice melt was not represented. However, transition of albedo from snow-covered to snow-free and vice versa were well captured at both on-ice and off-ice sites (Figure 4-9). Both glacier and moraine sites presented cycles of snow-covered and snow-free times, with albedo values reaching 0.9 and 0.3 in the case

of ice surfaces, and 0.15 at moraines. The ice-exposed periods with lower albedo values were well simulated by the model. The modelled albedo decay over the Athabasca Moraine station was slower than the observed values. The albedo of Athabasca Ice during snow free time in the recent years (2017-2019) was lower (< 0.25) than the previous years (Figure 4-9a), and this could be investigated further and may be influenced by upwind forest fires.

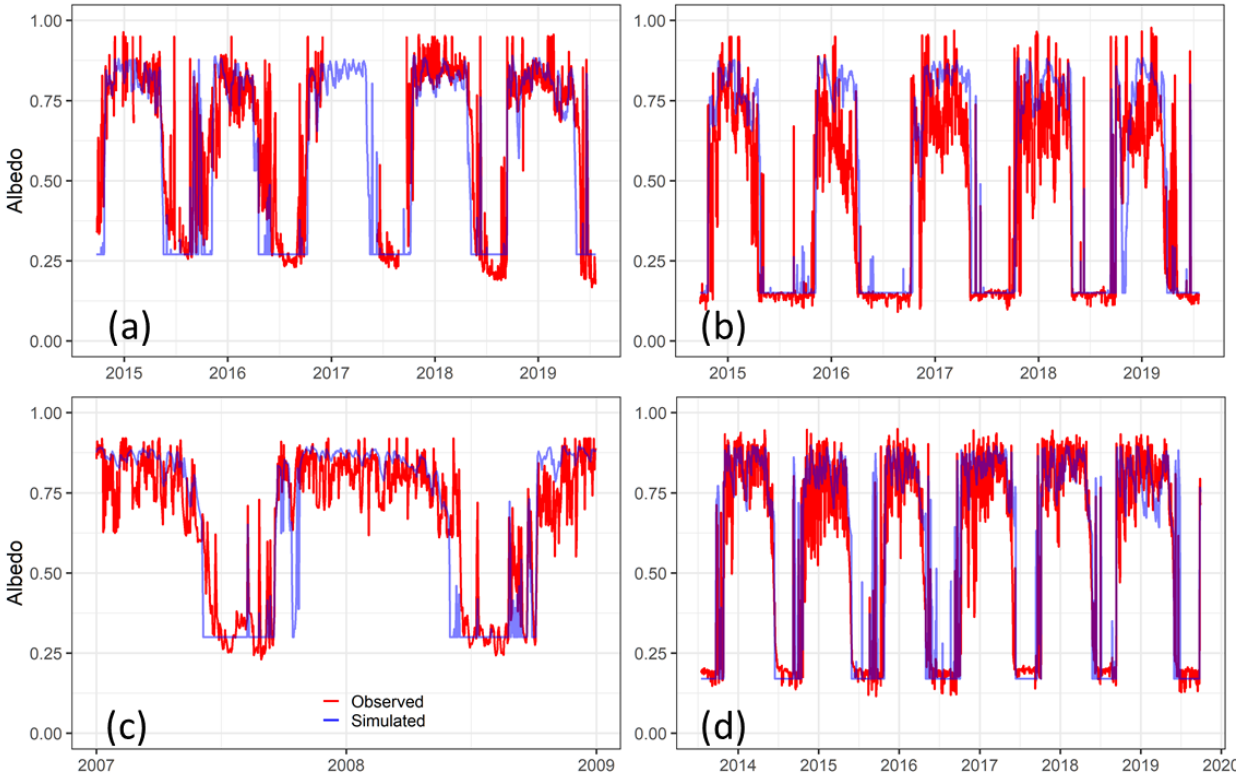

Figure 4-9: Albedo simulations, measured (red lines) and simulated (blue lines). (a) Athabasca Glacier at the Ice station (2014-2019); (b) Athabasca Glacier at the Moraine station (2014-2019); (c) Peyto Glacier at the Lower Ice station (2007-2008); (d) Peyto Glacier at the Main station (2013-2019).

Table 4-2: Comparison of *in-situ* observed, and CRHM-glacier simulated albedo

Research site	Surface type	Elevation (m)	Data period (number)	MBE	RMSE	WBI
AGRB	Ice	2177	2014-2019 (1475)	-0.047	0.142	0.86
	Moraine	1974	2014-2019 (1760)	0.063	0.170	0.85
PGRB	Ice	1973	2007-2008 (731)	0.007	0.117	0.88
	Moraine	2250	2013-2019 (2266)	0.030	0.129	0.91

4.6.1.2 Glacier mass balance

The surface accumulation and ablation simulations from CRHM-glacier were tested with the surface mass balance measurements by bass balance stakes and ultrasonic sensors (SR50) installed at various points over Peyto Glacier.

4.6.1.2.1 Surface point mass balance

Figure 4-10 shows the time series of simulated and observed changes in the height of the glacier surface with respect to the SR50 sensors during the recent decade. The comparisons were limited to the periods when SR50 data were available. The distance between the sensor and the glacier surface are shown in negative values. An increase in distance means lowering of the glacier surface, whereas a decrease in distance represents an increase in glacier surface elevation. Performance of the model along with meteorological forcing data were evaluated by statistical parameters presented in Table 4-3.

All the sites had at least one continuous data for two years showing the model's capability to capture accumulation and ablation. The best match between simulated and observed surface heights was at the lower station. However, performance diminished with elevation. The model accumulated more mass during the two-year period than the measured mass balance at the Upper Ice station (MBE = 0.26 m) with the measured model forcing data from the Peyto Main. However, the accumulation was less from the ERA-Interim data (Table 4-3).

The point mass balance evaluation shows that model simulation is better when the mass balance measurement site is closer to the meteorological observation station, suggesting a need for improvement in distributing meteorological variables to basin HRUs.

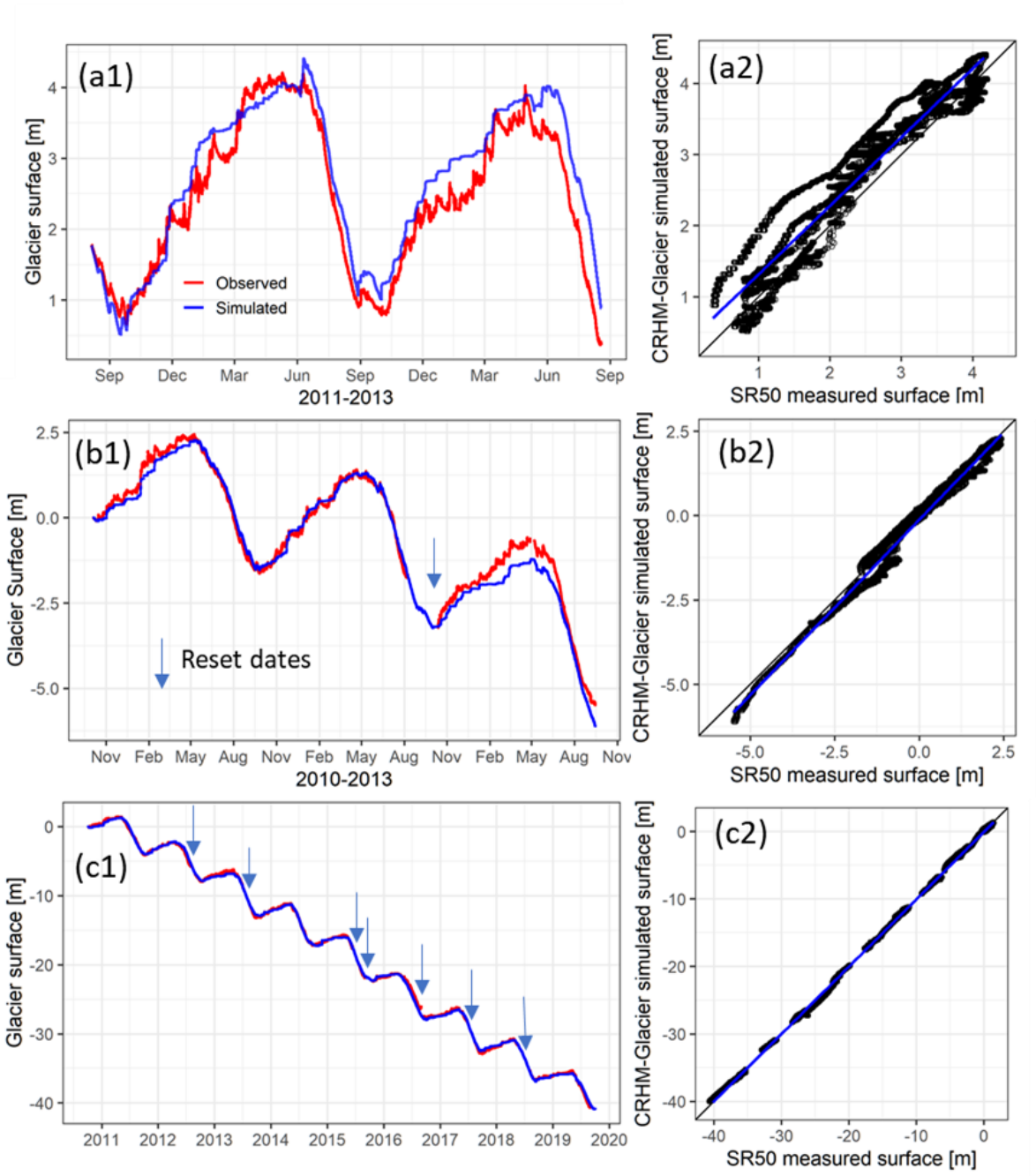

Figure 4-10: Simulated surface accumulation and ablation averaged to daily values as represented by the change in glacier surface elevation with respect to the height of sonic ranger sensor at the ice stations of Peyto Glacier. (a) Upper Ice station, (b) Middle Ice station, and (c) Lower Ice station. a2, b2, and c2 are scatter plots between measured and simulated surface heights.

Note: Resets are the adjustments of the SR50 to new heights, and they are brought to coincide with the simulated values of the same dates. Blue is model simulated height and red is the measured height from SR50.

Table 4-3: Statistical matrix of mass balance simulation at different sites using *in-situ* and ERA-Interim data

Site	Data period (number)	Forcing data	Slope	Intercept (m)	WBI	NSE	RMSE (m)	MBE (m)
Peyto Upper Ice station	2011-2013 (17855)	*In-situ*	0.96	0.35	0.96	0.863	0.39	0.26
		ERA-I	1.02	-0.74	0.91	0.424	0.80	-0.69
Peyto Middle Ice station	2010-2013 (23235)	*In-situ*	1.04	-0.13	0.99	0.975	0.27	-0.14
		ERA-I	1	-0.38	0.98	0.943	0.48	-0.38
Peyto Lower Ice station	2010-2019 (63630)	In-situ	1	0.23	1	0.998	0.36	0.23
		ERA-I	1	0.25	1	0.998	0.40	0.21

4.6.1.2.2 Aggregated glacier mass balance

Model-simulated hourly/daily mass balance for Peyto Glacier was converted to seasonal and annual mass balances to compare with the measured values obtained from the ablation stakes (Figure 4-12). The simulated seasonal glacier mass balances exclude Dragan Glacier and other small ice patches in the northeast part of the basin for the period from 1965 to 1995. Figure 4-12 shows that the model did not simulate the aggregated seasonal mass balance as well as it simulated point mass balances, as presented in section 4.6.1.2.1. Several factors could have contributed to the reduced performance at the glacier scale. Firstly, none of the model parameters were calibrated to simulate mass balance, although there is a practice of calibrating mass balance against *in-situ* observations (e.g., Giesen and Oerlemans, 2012; Radić and Hock, 2011; Shannon *et al.*, 2019). Secondly, the model performed less well at the Upper Ice Station compared to the Middle and Lower ice stations (Figure 4-10). Another reason could be the difference in approaches to obtain the seasonal mass balance. The observed values of seasonal mass balance were obtained from a series of transects of ablation stakes, distributed over half of the glacier area at lower elevations (Figure 4-11), and these values were linearly extrapolated to higher elevation bands, as there were not any mass balance stake measurements above 2700 m (details are in Demuth and Keller, 2006). The modeled seasonal mass balance was calculated from the HRUs distributed over the glacier.

This could be why the mass balances simulated at lower elevation bands matched closer to the observations (not shown here) than did those simulated at higher elevation bands.

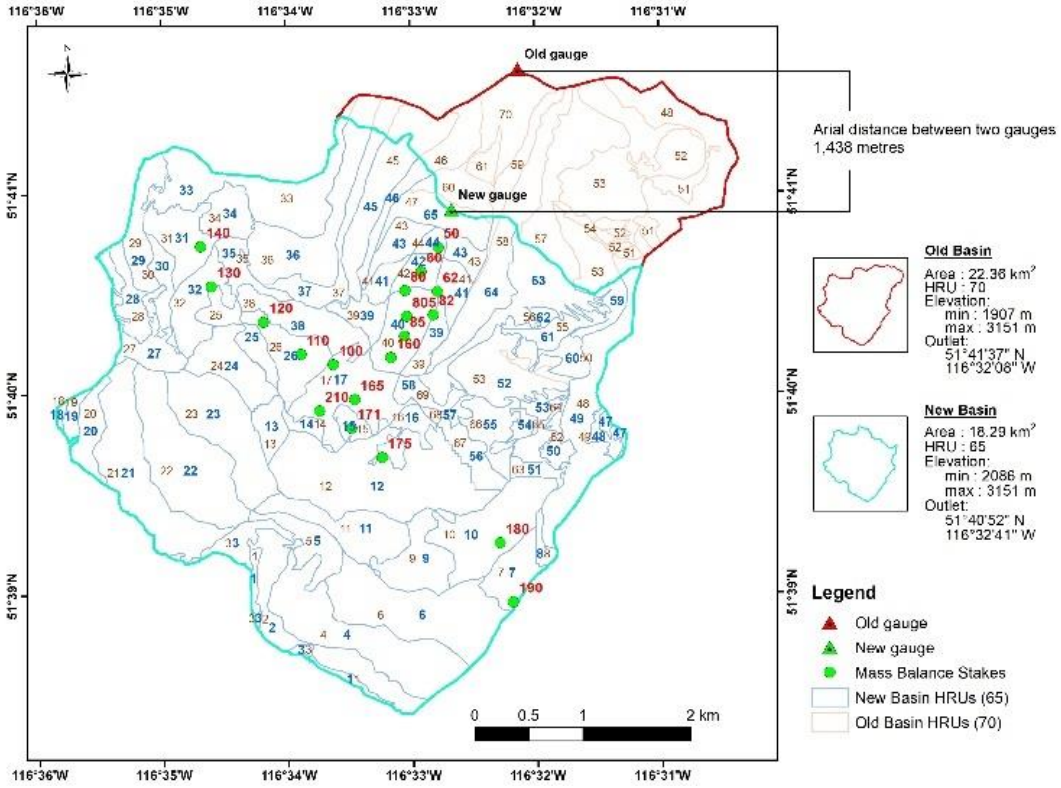

Figure 4-11: Location of mass balance stakes on Peyto Glacier

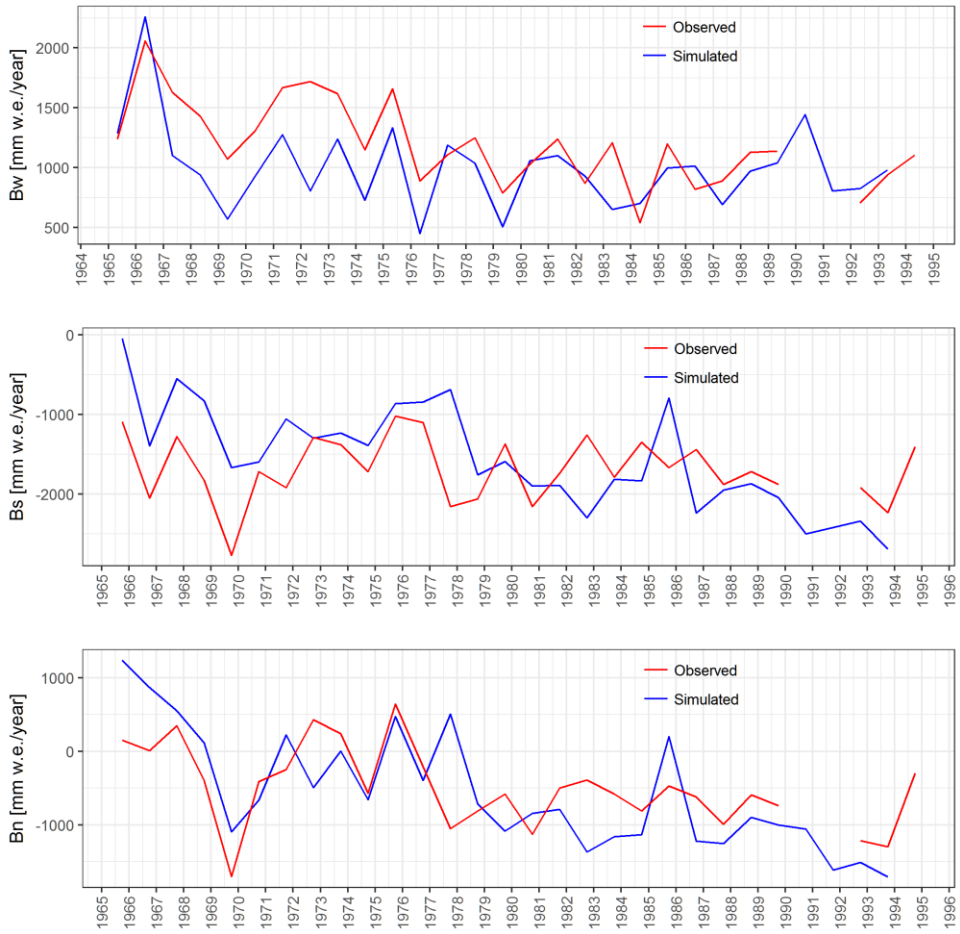

Figure 4-12: Mass balance simulation for the Peyto Glacier. Bw: winter balance, Bs: summer balance, Bn: net mass balance. Blue is simulated, and red is observed.

4.6.1.3 Streamflow

Model performance metrics for both basins are provided in Table 4-4 and from Figure 4-13 to Figure 4-16. The performance of the model can be rated as ‘very good’ with NSE equal to 0.71 and 0.77 for AGRB for the period 2014-2019 with meteorological forcing data from in-situ observation and from ERA-Interim, respectively. The model performance of AGRB with ERA-40 forcing data was also ‘very good’ for the past records, 1967-1977 (NSE = 0.75) and 1980-1989 (NSE = 0.73). However, the model performance is ‘good’ only with NSE equal to 0.68 and 0.67 for PGRB with meteorological forcing data from in-situ observation and from ERA-Interim, respectively. WBI values are 0.86 and 0.87 for AGRB and 0.80 for PGRB. However, PGRB had

lower MBE values (-0.06 and -0.01 m^3/s) and RMSE values (1.19 and 1.2 m^3/s) than AGRB (MBE, 0.28 and -0.11 m^3/s; RMSE, 1.29 and 1.14 m^3/s).

The model also performed well for the past records with bias-corrected ERA-40. NSE values of AGRB are 0.75 and 0.73 and WBI are 0.89 and 0.87 for the periods 1967-1977 and 1980-1989 respectively. The NSE value of PGRB (1967-1977) is 0.61 with the bias corrected ERA-40. The model was also tested with Lake Louise precipitation data for PGRB (1967-1977). The model driven by ERA-40 data provided a better simulation than did that driven by ERA-40 with Lake Louise precipitation data (Figure 4-15, Table 4-4).

Table 4-4: Statistical matrix for the streamflow simulations

Research basins	Meteorological forcing data	Simulation periods	MBE [m^3s^{-1}]	RMSE [m^3s^{-1}]	WBI	NSE
AGRB	In-situ	2015-2019	0.28	1.28	0.86	0.71
	ERA-Interim	2015-2019	0.11	1.14	0.87	0.77
	ERA-40	1967-1977	0.19	1.09	0.89	0.75
	ERA-40	1980-1989	0.17	1.14	0.87	0.73
PGRB	In-situ	2013-2018	-0.06	1.19	0.80	0.68
	ERA-Interim	2013-2018	-0.01	1.20	0.80	0.67
	ERA-40	1967-1977	-0.45	1.74	0.76	0.61
	ERA-40 and Lake Louise (ppt)	1967-1977	-0.42	1.87	0.73	0.56

Generally, the model simulated streamflow well while comparing with the observed records with WBI values higher than 0.8 except for PGRB in the past (1967-1977) with WBI equaled to 0.76. WBI evaluates similarity in modelled and simulated values in terms of not only correlation, but also mean and variance (Mo *et al.*, 2014). The model performed better in AGRB compared to PGRB. Moreover, the streamflow simulations were better in the present period compared to the past for PGRB. This could be due to the quality of streamflow data at PGRB in the past. Flow measurement at the Peyto outlet during the IHD (1967-1977) was a challenge due to unstable cross section, occasional flash floods, and lack of direct discharge measurements during high flows. Goodison (1972) reported that the discharge records from 1967 were not reliable and he did not use this data for his study. The streamflow stage gauge was washed out during a flood in August

1967. Occasional flash floods were reported in the stream by Ommanney (1987) and Johnson and Power (1985). However, model performance statistics show a good ability to simulate streamflow both in the past and present time periods from the bias-corrected reanalysis data for both basins.

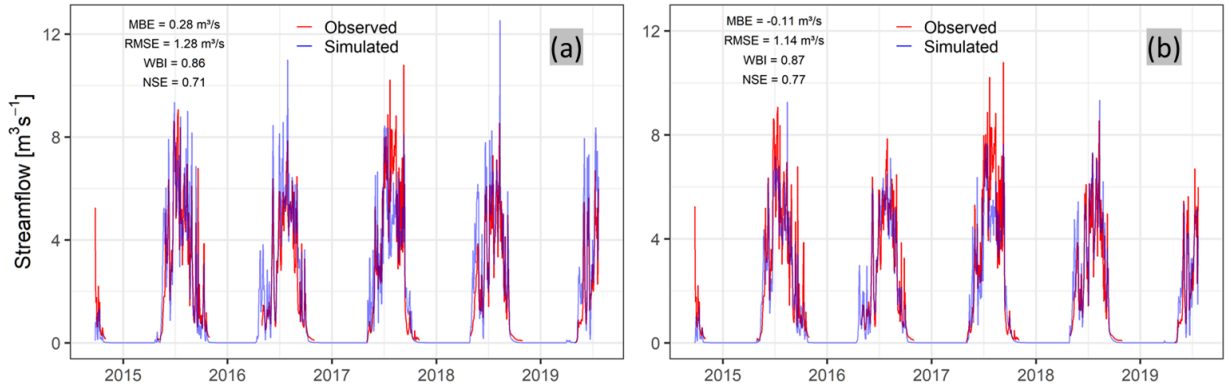

Figure 4-13: Daily mean streamflow at Athabasca Glacier outlet [2014-2019], (a) simulated from *in-situ* observed meteorological forcing data (b) simulated from the bias corrected ERA-Interim.

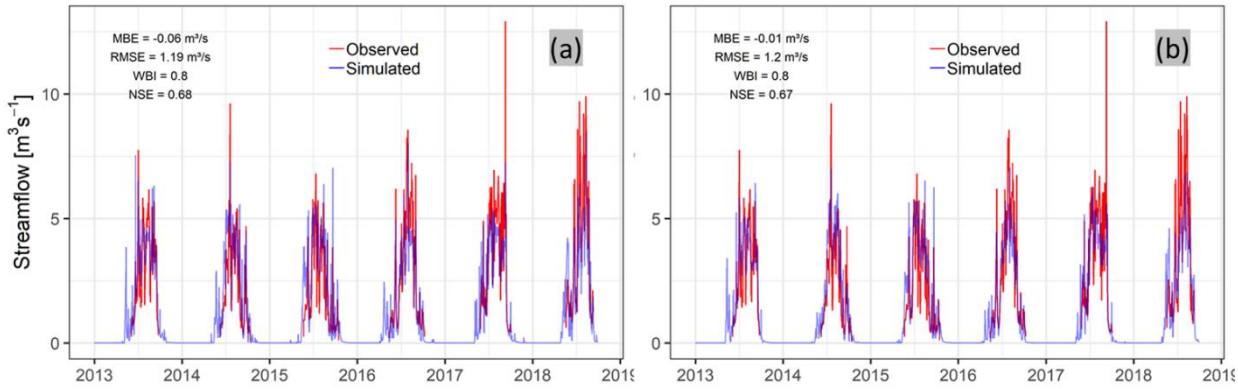

Figure 4-14: Daily mean streamflow at the Peyto Glacier outlet [2013-2018], (a) simulated from *in-situ* observed meteorological forcing data measured at Peyto Main (t, rh, u, Q_{si}, Q_{li}) and Bow Summit (ppt) (b) simulated from the bias corrected ERA-Interim meteorological forcing data.

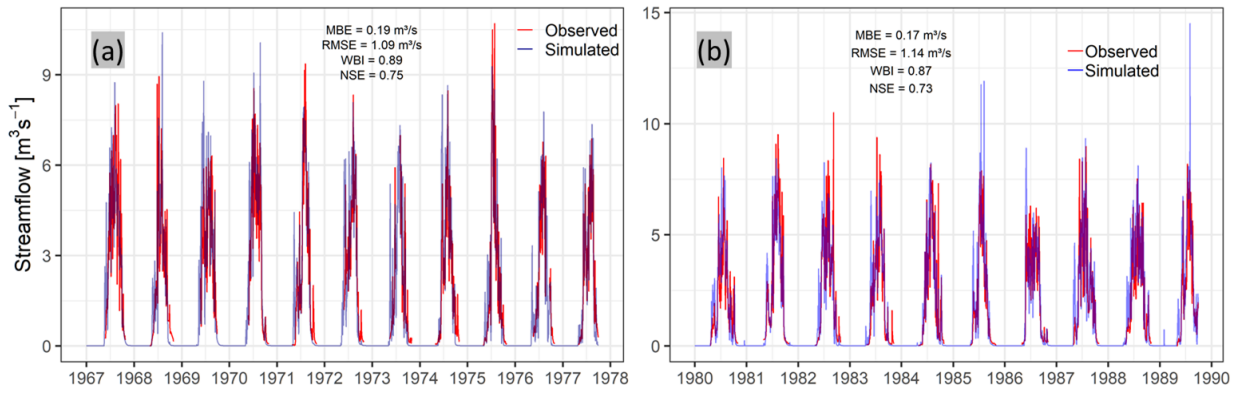

Figure 4-15: Daily mean streamflow at the Athabasca Glacier outlet simulated from the bias corrected ERA-40 forcing data; a) [1967-1977] and b) [1980-1989].

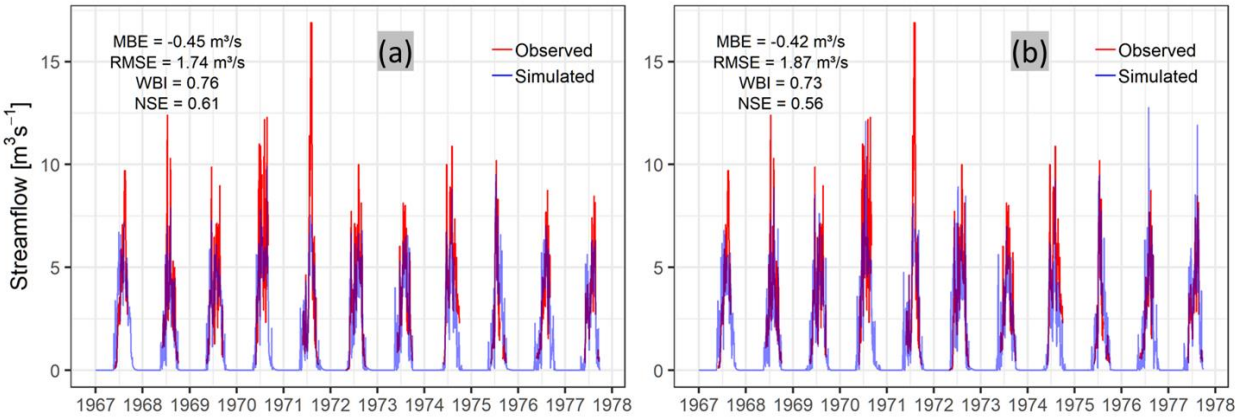

Figure 4-16: Daily mean streamflow at the Peyto Glacier outlet [1967-1977], (a) simulated from the bias corrected ERA-40, (b) simulated from the bias corrected ERA-40 (t, rh, u, Q_{si}, Q_{li}) and bias corrected Lake Louise [ppt].

The test runs were also carried out to see the impacts of glacier and snow redistribution processes with a model falsification approach. The model was run three times, first with both glacier and snow redistribution processes. The second run was with the glacier, but without snow redistribution processes, and the third one was with snow redistribution, but without the glacier. Figure 4-17 shows the comparisons of these simulations with the observed streamflow at the Peyto Glacier outlet. Hydrological simulations without the glacier generated almost half the streamflow compared to the observed streamflow. Similarly, streamflow simulations without snow redistribution overestimated streamflow, and the overestimation was reduced when snow

redistribution processes were included. More details on the impact of snow redistribution are provided in section 4.6.1.4.

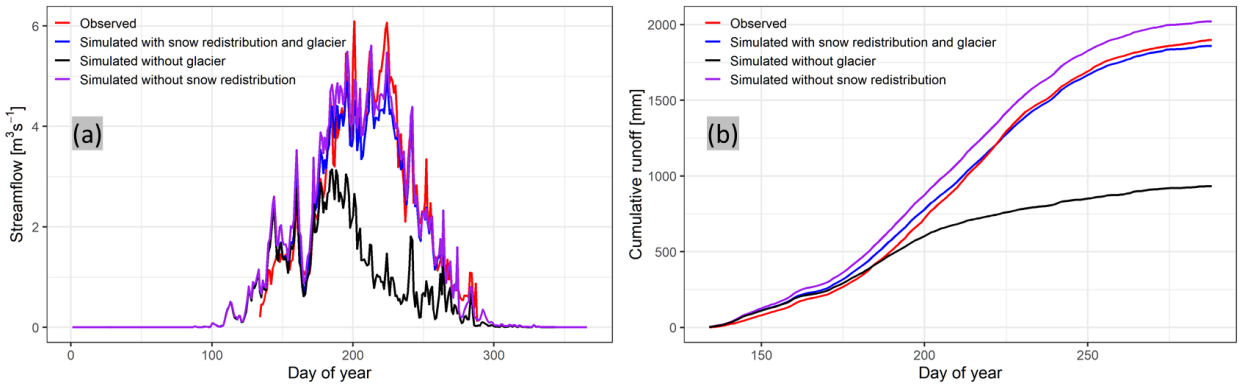

Figure 4-17: Simulation of streamflow of PGRB with and without glacier and snow redistribution; (a) daily averaged values for the period, 2013-2018, (b) averaged cumulative values.

4.6.1.4 Snow redistribution

Table 4-5 presents statistical measures of the model's performance in simulating glacier surface elevation with and without snow redistribution. Simulated values were compared to the measurements at three sites over PGRB: for 2 years at the Peyto Upper Ice station, 3 years at the Peyto Middle Ice station, and for 9 years at the Peyto Lower Ice station. The differences between the simulated glacier surface elevation with and without the blowing snow module were statistically significant at the Peyto Upper Ice and Peyto Lower Ice stations [p = 0, at 5% level of significance]. However, the difference was not statistically significant at the Peyto Middle Ice station [p = 0.455, at 5% level of significance]. Figure 4-18, Figure 4-19 and Table 4-5 show that the simulated glacier surface elevation at the Peyto Upper Ice station was closer to the observed data [WBI = 0.96, NSE = 0.863, MBE = 0.26 m, RMSE = 0.39 m] when the blowing snow module was included in the CRHM-glacier model. The model without blowing snow process simulated more accumulation than was observed [WBI = 0.81, NSE = -0.219, MBE = 0.99 m, RMSE = 1.16 m] (Table 4-3). Inclusion of the blowing snow module made a slightly adverse impact in the case of the Peyto Lower Ice station. MBE and RMSE were 0.23 m and 0.36 m respectively for the Lower Ice station with blowing snow module, whereas they were -0.05 m and 0.26 m respectively without blowing snow module. However, there were not much difference in WBI and NSE. The difference was negligible at the Peyto Middle Ice station.

Table 4-5: Statistical measure of mass balance simulation for improvement in model performance with snow redistribution

Site	Data period (number)	Snow Redistribution	Slope	Intercept (m)	WBI	NSE	RMSE (m)	MBE (m)
Peyto Upper Ice station	2011-2013 (17855)	Yes	0.96	0.35	0.96	0.863	0.39	0.26
		No	1.1	0.73	0.81	-0.219	1.16	0.99
Peyto Middle Ice station	2010-2013 (23235)	Yes	1.04	-0.13	0.99	0.975	0.27	-0.14
		No	1.04	-0.12	0.99	0.974	0.28	-0.13
Peyto Lower Ice station	2010-2019 (63630)	Yes	1	0.23	1	0.998	0.36	0.23
		No	1	-0.12	1	0.999	0.26	-0.05

Table 4-6: Statistical measure of streamflow for improvement in model performance with snow redistribution

Site	Data period	Forcing data	Snow Redistribution		R^2	WBI	NSE	RMSE (m^3/s)	MBE (m^3/s)
			Blowing Snow	Avalanche					
AGRB	2014-2019 (823)	*In-situ*	No	No	0.71	0.81	0.53	4.82	1.95
			Yes	Yes	0.75	0.86	0.70	3.82	0.95
			No	Yes	0.69	0.81	0.51	4.92	1.96
			Yes	No	0.75	0.86	0.70	3.83	0.94
		ERA-I	No	No	0.75	0.86	0.72	1.25	0.23
			Yes	Yes	0.77	0.87	0.77	1.14	-0.09
			No	Yes	0.74	0.86	0.71	1.28	0.25
			Yes	No	0.77	0.87	0.77	1.15	-0.10
PGRB	2013-2018 (785)	*In-situ*	No	No	0.66	0.81	0.65	1.25	0.20
			Yes	Yes	0.68	0.80	0.68	1.19	-0.06
			No	Yes	0.65	0.80	0.64	1.26	0.15
			Yes	No	0.68	0.80	0.68	1.19	-0.10
		ERA-I	No	No	0.67	0.80	0.67	1.21	0.03
			Yes	Yes	0.67	0.80	0.67	1.20	-0.01
			No	Yes	0.68	0.81	0.68	1.19	0.07
			Yes	No	0.67	0.80	0.67	1.20	-0.03

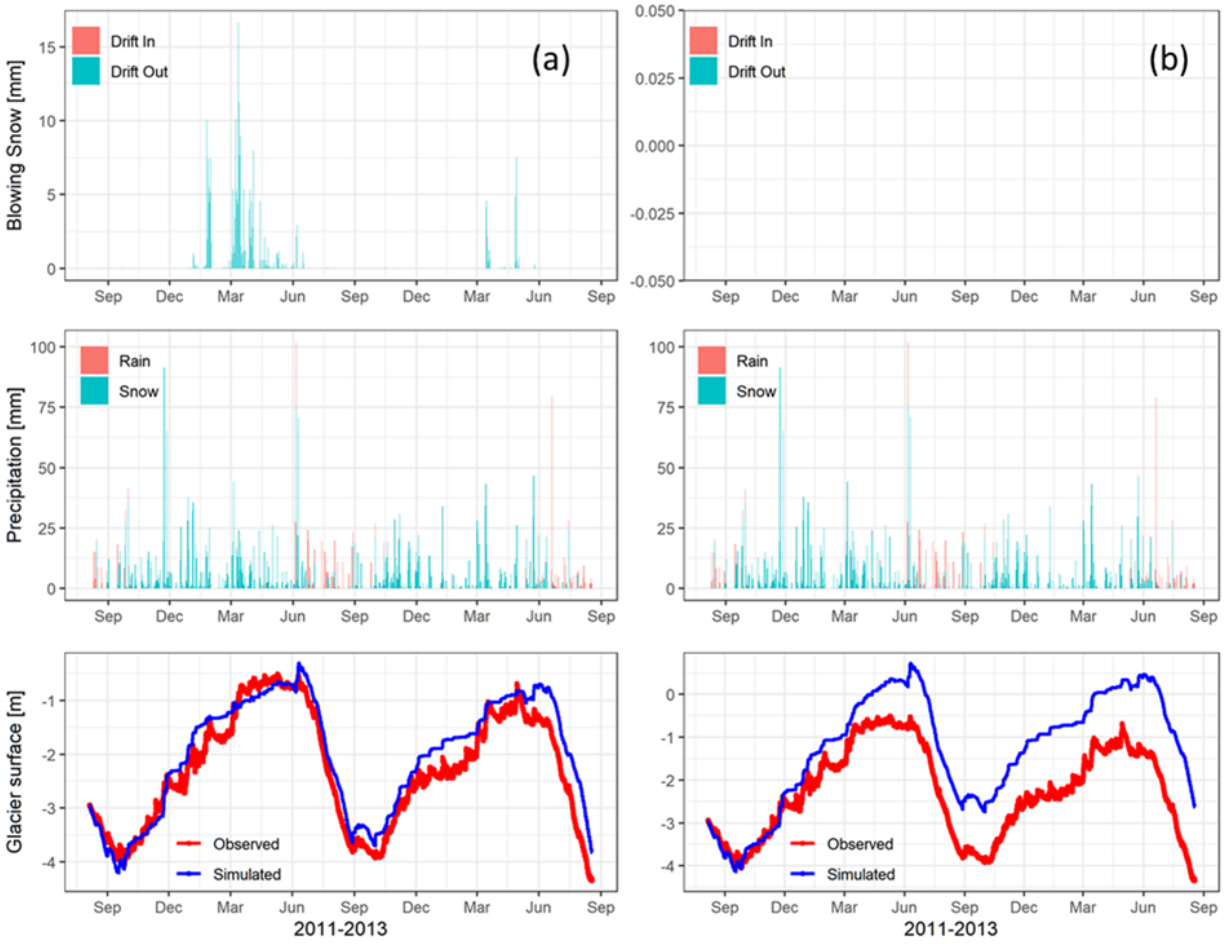

Figure 4-18: Simulated surface accumulation and ablation averaged to daily values as represented by the change in glacier surface elevation with respect to the height of SR50 at the Peyto Upper Ice station. (a) Model outputs with blowing snow module (b) model outputs without blowing snow module.

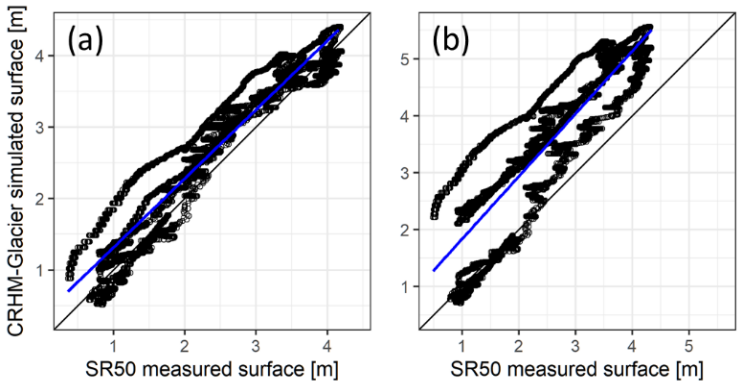

Figure 4-19: Observed and simulated glacier surface elevation at the Peyto Upper Ice station. (a) Model outputs with blowing snow module (b) Model outputs without blowing snow module.

Streamflow simulations of the two basins with and without snow redistribution are presented in Figure 4-20 and Figure 4-21, respectively. The models were run with both in-situ observation and bias-corrected ERA-Interim data. Their averaged values are plotted in Figure 4-22 for AGRB and in Figure 4-17 for PGRB. Their model performance statistics are presented in Table 4-6. Changes in streamflow simulations were tested as per the schemes designed in Section 4.5. All the changes were statistically significant at 5% level of significance, except the Test 3 (between Scenario S_0 and S_Av) of PGRB with ERA-Interim ($p = 0.278$). Inclusion of both snow redistribution processes (Scenario S_BsAv) and inclusion of blowing snow alone (Scenario S_Bs) improved the model performance in all the cases in comparison to the model without snow redistribution (Scenario S_0). Interestingly, the statistical measures have similar values for the two scenarios (Scenario S_BsAv and Scenario S_Bs). However, inclusion of snow redistribution by avalanche process alone (Scenario S_Av) worsened the result in comparison to the model without snow redistribution (Scenario S_0). Model performance improved more when including blowing snow compared to avalanche processes.

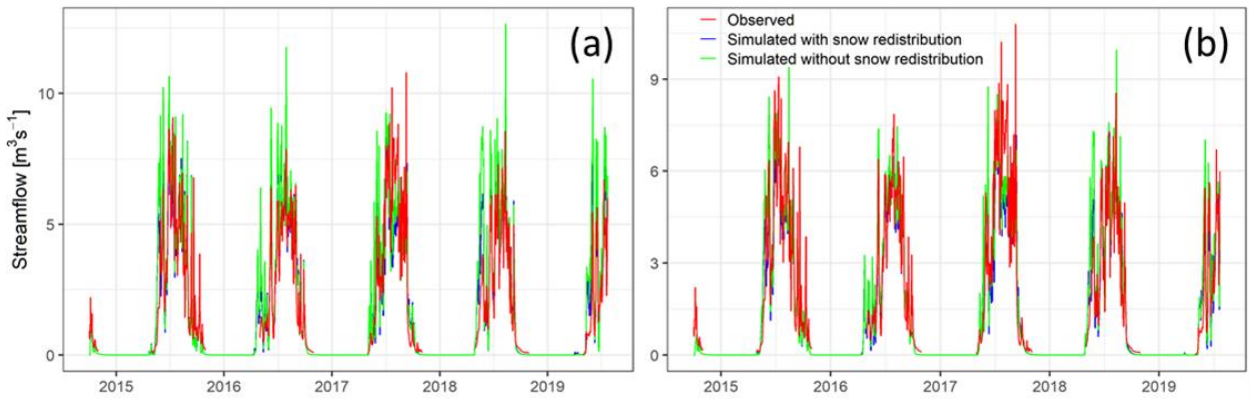

Figure 4-20: Hydrographs for AGRB with and without snow redistribution and compare with observation. (a) *In-situ* observation data (b) ERA-Interim meteorological forcing data.

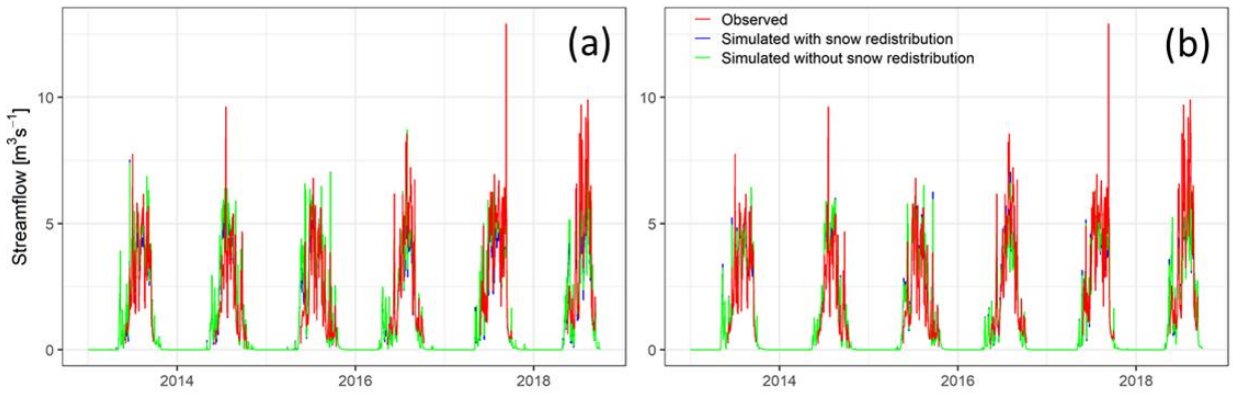

Figure 4-21: Runoff simulation for PGRB with and without snow redistribution and compare with observation. (a) *In-situ* observation data (b) bias corrected ERA-Interim meteorological forcing data.

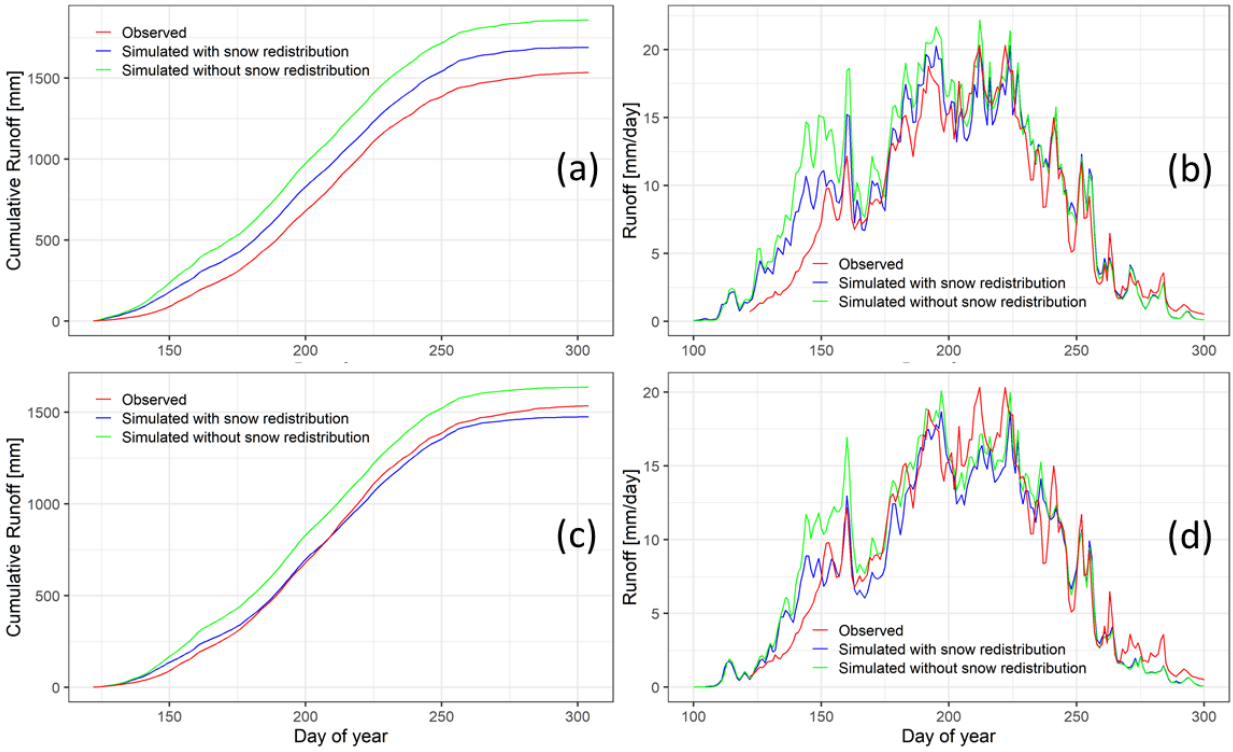

Figure 4-22: Runoff simulation for AGRB with and without snow redistribution. Values are averaged over 2014 - 2019. (a) and (b) are with *in-situ* forcing data. (c) and (d) are with ERA-Interim.

4.6.2 Streamflow components

The validated CRHM-glacier model was used to determine various components of runoff and their changes during a period of five decades. Simulated components of runoff are shown in Figure 4-23; their values are given in Table 4-7. These are average annual values of the period from 2013 to 2018. This shows the importance of glacier firn and ice melt (38-50%) to total runoff. Glacier ice and firn melt do not include snowmelt on the glaciers. The contribution of glacier melt increased by 6-7% in the recent decade (2006-2017) compared to the past (1966-1977). Total precipitation decreased in both basins, with an increase in rainfall ratio, and total runoff. This was balanced by an increase in glacier ice melt.

Table 4-7: Annual water fluxes averaged over the periods of simulation

Research basin	**Water fluxes (mm)**	**Past (1966-1977)**	**Present (2006-2017)**
PGRB	Rain (rainfall ratio)	325 (0.31)	354 (0.43)
	Precipitation	1435	1209
	Evaporation and sublimation	97	87
	Snowmelt	1091	914
	Firnmelt	170	162
	Icemelt	465	665
	Basin flow	1597	1857
	% flow from glacier firn/ice melt	38%	44%
AGRB	Rain (rainfall ratio)	132.3 (0.10)	173.0 (0.15)
	Precipitation	1433	1318
	Evaporation and sublimation	324	387
	Snowmelt	1091	1040
	Firnmelt	177	174
	Icemelt	532	696
	Basin flow	1612	1700
	% flow from glacier firn/ice melt	43%	50%

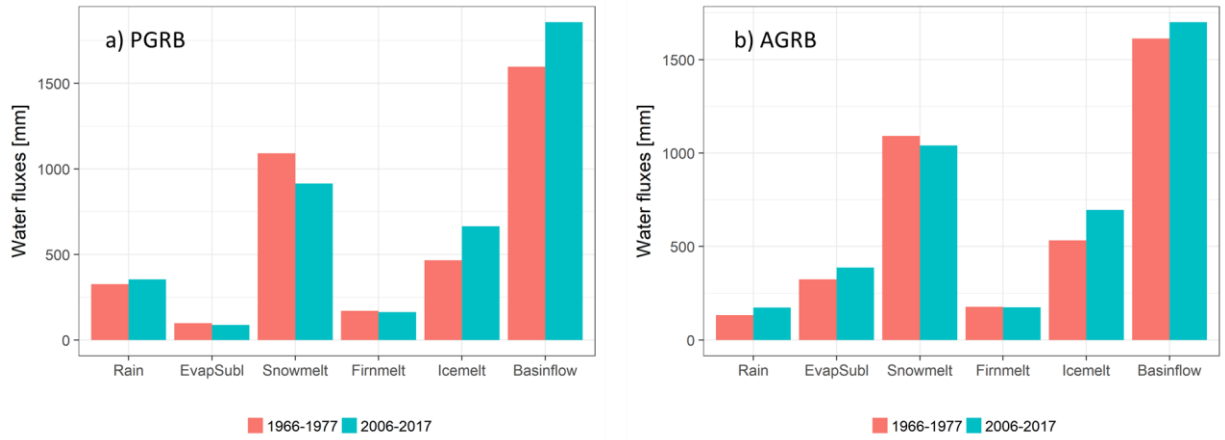

Figure 4-23: Simulated annual water fluxes comparison between past (average of the period 1966-1977) and present (average of 2006-2017) periods for (a) PGRB and (b) AGRB.

Note: EvapSubli is sum of all evaporation and sublimation processes from surfaces of snow, firn, ice and blowing snow.

Though the model performed well in most tested metrics, there are some limitations that could be improved in future studies. CRHM-glacier was constrained by the driving meteorology used as input data and the suite of processes that were included in the model. Several uncertainties in the input data drove the uncertainties in model outputs. Precipitation is critical for CRHM-glacier. Precipitation measurements at the moraine stations in the study basins were not reliable due to high wind speeds. Therefore, precipitation measured at Bow Summit, outside PGRB, was used to evaluate model performance and to bias correct reanalysis data. The temperature and precipitation lapse rates were set by observations made at different elevations.

Another important meteorological variable is shortwave irradiance. The model corrects radiation by self-shading for each HRU due to slope and aspect while distributing shortwave and longwave radiation. However, it does not consider shading from surrounding topography, consideration of which may improve melt calculations mountains as shown by Marsh *et al*. (2012) in a nearby deglaciated mountain basin. Hopkinson *et al.* (2010) neglected reflected shortwave irradiance but considered direct bean shortwave irradiance by obstruction from surrounding terrains for their study over Peyto Glacier. They emphasized the importance of higher resolution DEMs for incorporating local shadow conditions and suggested that the lower resolution DEMs caused over-estimation of melt in the ablation zone and an under-estimation of melt in the accumulation zone.

Moreover, there are potential errors in global radiation measurement. Average global radiation was measured with a Kipp and Zonen CM-11 pyranometer and a CNR-4 in the main stations. Snow accumulation and frost on the pyranometer dome certainly occurred at times.

Similarly, several processes such as ice flow, glacier surges, ice falls, evolution of vegetation cover at the lower elevation of the basin, and evolution of drainage patterns were not considered in the model. Debris-covered ice is common in mountain glaciers, particularly at the terminus. Currently, these areas are not treated distinctively, apart from assigning low albedo values. The debris cover may alter the surface energy balance due to the low thermal conductivity of debris (Vincent *et al*., 2016). The model also did not consider short-term impacts of meltwater refreezing in glacier ice (Naz *et al.*, 2014).

4.7 Conclusions

Most mountain glaciers lack on-ice weather data (Clarke *et al*., 2009) and, as such, validation of climate models in high mountains is difficult (Karmalkar *et al*., 2011). Therefore, the result of CRHM-glacier over Peyto and Athabasca glaciers is encouraging, in that both off-ice station and reanalysis data have potential for use in glacier hydrology modelling in mountain glaciers. Bias-corrected reanalysis data and data from off-ice stations were used to drive the model, and on-glacier station data were used to validate the model. Hydrometeorological, streamflow and glaciological observations from the 1960s to recent times at Peyto Glacier and new observations at Athabasca Glacier were used to quantify change, suggest model development, verify model operation, and drive models of glacier hydrology change. Model performance improved in terms of glacier surface elevation change at accumulation zone and runoff generation at the basin outlet when snow redistribution processes were included in the model.

Cold region hydrological modelling must include a glacier component to simulate the hydrology of glacierized basins. Additional algorithms and processes were incorporated in the CRHM platform to more fully describe glaciological components of the hydrological processes. CRHM-glacier, a physically based energy budget and mass balance, distributed glacier hydrology model can simulate streamflow of a mountain glacier, by using coupled mass and energy budgets, along

with snow redistribution by wind and gravity. When driven with locally measured meteorological data or bias-corrected reanalysis data and tested against specialized on-ice snow and ice surface height measurements, the model was able to simulate both accumulation and ablation of snow and ice. Inclusion of snow redistribution improved the model simulation of surface mass balance in the accumulation zone but did not improve the simulation in the ablation zone. In the case of streamflow, inclusion of snow redistribution by both processes (blowing snow and avalanches), or blowing snow alone improved the model simulation. This suggests a need to improve the avalanche module or assess the role of avalanches on snow distribution in these basins in more detail than was possible here.

The validated model was used to simulate runoff components of both study basins for two time periods, past (1966-1977) and present (2006-2017). There was an increase in streamflow in the more resent period. This was due to increased meltwater contribution from glacier firn and ice, which was a major runoff component during late summer.

In summary, this chapter described extension of the CRHM platform with a physically based distributed glacio-hydrological model. CRHM-glacier considers the hydrological processes in a glacierized basin from precipitation to runoff and includes most of the important processes in the alpine hydrological cycle, including snow redistribution by wind and avalanches. It considers the processes of snow, firn and ice melt; sublimation and evaporation; snow and firn densification; snow, ice, soil and groundwater storage; and surface, sub-surface and groundwater flow, and routing of meltwater through the glacier. CRHM-glacier handles snowmelt and ice melt separately, and it can be used in basins that are glacierized, partly glacierized, or de- glacierized. Thus, it can be used for long-term study of a basin that is undergoing transitional phases from glaciation to deglaciation. The model was tested in two glacierized basins in the Canadian Rockies. The model with snow redistribution could successfully simulate both accumulation and ablation of snow and ice on a glacier surface and streamflow from the basins. The model is suitable for both ice-covered and ice-free areas within a mountain basin. No parameters were calibrated. The physical basis of this model and the identifiability of its parameters reduces uncertainty in long-term simulations, including those for future climates.

CHAPTER 5: Hydrological response of glaciers in the Canadian Rockies to changing climate and glacier configuration

Paper manuscript status

Contents of this chapter is ready as a paper manuscript for submission to Hydrology and Earth System Sciences (HESS). The paper was presented during the AGU Fall 2018.

Author contributions: Dhiraj Pradhananga analysed model outputs and drafted the manuscript. John W. Pomeroy revised the manuscript.

This chapter addresses the third objective of the study. CRHM-glacier module was used to diagnose the hydrological response to the warming climate and changes in glacier configuration. This research outputs could be useful to water resource planners and managers who wish to determine changes in streamflow resulting from climate warming and associated glacier recession.

5.1 Abstract

Mountain snow and ice greatly influence the hydrological cycle of alpine regions by regulating both the quantity and seasonal variations of water availability downstream. This study considers the combined impacts of climate and glaciers changes due to recession on the hydrology and water balance of two high-elevation basins in the Canadian Rockies. A distributed, physically based glacier hydrology model developed in the Cold Regions Hydrological Modelling platform (CRHM) was used to simulate the hydrology of Peyto and Athabasca Glacier research basins in Alberta. Bias-corrected reanalysis data were used to drive the model. The model calculates the water balance of a glacierized basin, influenced by the surface energy and mass balance, and considering redistribution of snow by wind and avalanches. It was set up using hydrological response units based on elevation bands, surface slope and aspect, as well as changing land cover. Aerial photos, satellite images and Digital Elevation Models (DEM) were assimilated to represent the changing configurations of glacier area and the exposure of ice and firn. Observations of glacier

mass balance, snow and glacier ice surface elevation changes at glacier and alpine tundra meteorological stations and streamflow discharge at the glacier outlets were used to evaluate the model performance. Model results indicated that both basins have undergone continuous glacier loss over the last three to five decades, leading to a 6-31% reduction in glacierized area, a 78-109% increase in ice exposure, and changes to the elevation and slope of the glacier surfaces. Diurnal temperature ranges are increasing, mainly due to increasing summer maximum daily temperatures. Annual precipitation is not changing much, but rainfall ratios are increasing. Basin hydrology was simulated over two periods, 1965-1975 and 2008-2018, using observed glacier configurations. The results show that changes in both climate and glacier configuration cause changes in melt rates and runoff, and a shift of peak flows from August to July. Glacier melt contributions increased from 27-61% to 43-59% of annual discharges. Recent discharges were 3-19% higher than in the 1960s and 1970s. The results suggest that increased exposure of glacier ice and lower surface elevation due to glacier thinning were less influential in increasing streamflow than climate warming. Streamflow from these glaciers continues to increase.

5.2 Introduction

Changes in alpine snow and glacier influence both the timing and magnitude of the streamflow and thus impacting the water supply for downstream industrial, agricultural, hydropower and drinking purposes. The notable change in most glaciers is the rise in their equilibrium line altitudes (ELA) due to climate warming (Malecki, 2015; Van Pelt and Kohler, 2015; Zemp *et al.*, 2015). The influence of glacier snow and ice melt dominates the seasonality of runoff from mid-latitude mountains more than that from low-latitude high mountains (Kaser *et al*., 2003). Glacier runoff also strongly influences the temperature and nutrient loading of downstream water (Hood and Berner, 2009). However, observations suggest that there is a pronounced acceleration in glacier retreat in the Canadian Rockies (Moore *et al.*, 2009), which is very noticeable at Peyto Glacier (e.g., Demuth and Keller, 2006; Kehrl *et al*., 2014). Changes in glacier mass, area, shape, and their contribution to water resources have been observed in North America (Reynolds and Young, 1997; Barry, 2006; Hopkinson and Demuth, 2006), and these changes in glacier elevation and volume are related to changes in air temperature and precipitation (Tennant and Menounos, 2013). However, there is no clear understanding of how these changes are interrelated and how they are

responding to the changing climate. It is essential to understand how shrinking alpine snowcover and shrinking glacier mass in the mountains influence downstream water supply. A model of the changing characteristics of the alpine cryosphere can help to predict the future availability of water resources.

Canada is experiencing a warming climate, with increased precipitation and greater spatial and seasonal variability (Derksen *et al.*, 2012; Vincent *et al.*, 2015). Derksen *et al.* (2012) reported increasing surface temperatures over the Canadian Arctic over the last four decades, increasing mass loss from glaciers, and a reduction in snow cover extent and duration. Vincent *et al.* (2015) reported increasing temperature and precipitation trends in Canada, with the greatest warming in winter and spring and more spatial variability in precipitation trends than in temperature trends.

There are some uncertainties with the hydrological response to glacial change. It is generally accepted that flow originating from glaciers will increase for a certain time due to increased melt rate, then decline when the mass of ice in the landscape decreases significantly (Moore *et al.*, 2009). The duration and timing of this change from increasing to decreasing flow, however, will be regionally dependent (Casassa *et al.*, 2009). In addition, recent studies have projected a different future of streamflow in the Himalayas than Moore *et al (2009)*. For example, Immerzeel *et al.* (2013) predicted a warmer and wetter future for the Himalayas. They argued that increasing precipitation in the region would compensate for declining contributions of glacier melt to river flow in the future. Luo *et al.* (2013) indicated that glacier melt was less sensitive to precipitation change than to temperature change in northwest China and suggested further modelling of the effects of climate change with increasing temperatures and decreasing precipitation.

Stahl and Moore (2006) observed that British Columbia streams originating from glacierized mountain basins have shown a decreasing phase (in late summer flow) and indicated that most glaciers had already completed the phase of increased flow due to global warming. Kienzle *et al.* (2012) projected decreased summer and fall streamflow, exacerbated by reduced glacier flows, in Alberta's Cline River watershed in western Canada. They observed earlier snowmelt, lower summer flow, an extended low-flow late summer period and greater autumn precipitation. The observed decrease in glacier mass in the Canadian Rockies has been caused by an increase in

average annual air temperatures and a reduction in winter snowfall since the mid-1980s (Demuth and Keller, 2006, Moore and Demuth, 2001).

Demuth and Keller (2006) conducted a detailed assessment of the mass balance variation of Peyto Glacier in Alberta from 1966-1995 and its change due to regional climate variability and climate change. They found that winter snow accumulation was a dominating factor for annual net mass balance. They attempted to establish the mass balance trend with shifts in synoptic climate variation, considering sea surface temperature, atmospheric circulation, seasonal snow and perennial ice. The Pacific Decadal Oscillation (PDO) and the El Nino Southern Oscillation (ENSO) were found to correlate with the winter mass balance. The study showed there has been a loss of ~70% of glacier volume during the last century. Marshall *et al.* (2011) projected glacier volumes of the Canadian Rockies (eastern slopes) for the next century. Their projected values are alarming, as they indicate a further ~85% loss of glacier volume by 2100 and an order of magnitude decrease in glacier contribution to streamflow in Alberta from 1.1 km^3 per year at present to 0.1 km^3 per year at the end of this century. Similarly, Clarke *et al.* (2015) projected the loss of the glaciers in western Canada by about 75% at the end of the 21st Century compared to the glacier mass in 2005.

Therefore, there are changes in both climate and glacier configuration with glacier retreat. However, it is yet to be understood how a glacier behaves with changing precipitation and temperature, along with changes in glacier configuration. Continuous glacier mass loss leads to a reduction in glacier-covered area, an increase in ice exposure and changes to the elevation and slope of the glacier surface. These changes alter the near-surface distribution of temperature and precipitation, as well as radiation and turbulent transfer of mass and energy to snow and ice. This study investigates the individual and combined impacts of the changing climate and receding glaciers on headwater hydrology in glacierized basins.

5.3 Methodology and data

To diagnose the impacts of climate change and changing glacier configurations on mountain headwater hydrology, experiments were conducted, applying CRHM-glacier, a glacio-hydrological model. This was done in two research basins (AGRB and PGRB) in the Canadian Rockies considering climate of two periods (1965-1975 and 2008-2018) and glacier configurations of two periods, past (1966 for PGRB and 1981 for AGRB) and present (2011 for AGRB and 2014 for PGRB).

5.3.1 CRHM-glacier model development

The CRHM-glacier model (Pradhananga and Pomeroy, in preparation), developed in the Cold Regions Hydrological Modelling Platform (Pomeroy *et al*., 2007) was applied in this study to evaluate the impacts of changes in climate and in glacier configuration on the hydrology of glacierized basins. CRHM-glacier is a physically based, flexible, multi-physics hydrological model. It distributes meteorological variables (shortwave and longwave radiation, air temperature, relative humidity, wind speed, precipitation and its phase) to slope, aspect and elevation within hydrological response units (HRU). CRHM-glacier models the hydrology of both glacierized and non-glacierized areas in a basin. It redistributes snow by coupling the blowing snow process and avalanching. Melt energies for snow and ice melt are calculated separately, based on *Snobal* and energy budget glacier melt modules, respectively. Meltwater routing is through three glacier reservoirs (snow, firn, and ice) modified to de Woul *et al*. (2006) approach as described in the section 4.4.4. Once water leaves the glacier boundary, rain and meltwater are routed further into the soil surface, subsurface and groundwater (Fang *et al.*, 2013).

The CRHM-glacier model was validated in two basins in western Canada – Peyto Glacier Research Basin (PGRB) in Banff National Park and Athabasca Glacier Research Basin (AGRB) in Jasper National Park (Pradhananga and Pomeroy, in preparation). Previous research has successfully applied CRHM over several mountain sites (Rasouli *et al.*, 2014; Zhou *et al.*, 2014; Krogh *et al.*, 2015; Pomeroy *et al.*, 2015) and glacierized basins (Anderson, 2017).

5.3.2 Study sites

Two alpine glacier basins in the Canadian Rockies, PGRB and AGRB (Figure 4-1), were chosen for this research. The details of these basins are provided in Table 4-1. Both glaciers have been losing mass continuously since the mid-1970s (Reynolds and Young, 1997; Demuth and Keller, 2006; Tennant and Menounos, 2013; Kehrl *et al.*, 2014). Clarke *et al*. (2015) projected that AGRB will lose half its glacier coverage by 2050. Kehrl *et al*. (2014) estimated that Peyto Glacier may lose about 85% of its present-day mass by 2100. Both glaciers are gauged at the outlets of their pro-glacial lakes.

5.3.3 Modelling approaches (scenarios)

CRHM-glacier was run to simulate the hydrological responses of the two glacier research basins to four experimental scenarios (Table 5-1 and Figure 5-1). The glacier configuration in each basin was considered for two periods, past and present. The model was run for two climate periods, past (1965-1975) and present (2008-2018). A novel approach was used - past and present climate forced to both past and present glacier configurations. Therefore, there were a combination of four model simulations using two separate decades of climate data from past and present periods, with past and present glacier configurations. Simulated runoff from these model outputs was examined to diagnose the hydrological response to both glacier change and climate change.

Glacier configuration maps for the two periods were prepared according to the availability of DEM and landcover information (Table 5-1). A topographic map of Peyto Glacier from 1966 (Sedgwick and Henoch, 1975) was used to prepare a past glacier configuration. Both the 1966 DEM (10 m resolution) and the 1966 landcover map were developed from the topographic map, which was produced from aerial photographs taken in August 1966. The 2014 DEM was prepared at 10 m resolution from airborne Lidar measurements taken during July and September 2014. The landcover map for the present basin was prepared based upon a Landsat image from 2014. Bolch *et al*. (2010) found only 1.7% deviation in these two approaches (aerial photo and satellite images) for Peyto Glacier from the same year 2005.

For AGRB, two DEMs, each at 20 m horizontal resolution, from 1983 and 2011, were used. Landsat images from 1984 (Landsat 5) and 2014 (Landsat 8) were used to prepare past and present landcover maps.

Table 5-1: DEM and landcover maps of two periods.

		Climate	**Glacier Configuration**	
			DEM	**Landcover**
Present	Athabasca	2008-2018	2011	2014
	Peyto		2014	2014
Past	Athabasca	1965-1975	1983	1984
	Peyto		1966	1966

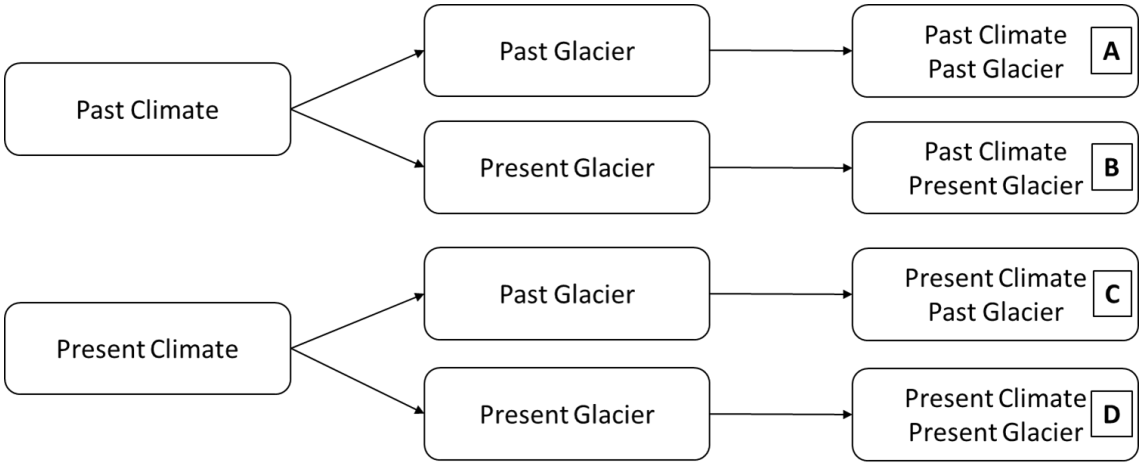

Figure 5-1: Four model scenarios combining past and present climate and glacier

Based on these four experimental scenarios, five comparison schemes (Table 5-2) were employed to diagnose the impacts of climate and glacier changes on streamflow. S1 represents realistic conditions of both climate and glacier configuration; it compares model scenarios A and D, i.e., past climate – past glacier with present climate – present glacier. The other schemes are falsified modeling experiments to segregate the impacts of changing climate and glacier configuration. S2 and S5 scenarios consider change in glacier configuration, while keeping climate the same, either

past or present. S3 and S4 schemes compare the impacts from changing climate while keeping glacier configuration constant, either past or present glacier.

Student's t-test and the Wilcoxon Signed-Rank test in the R environment (R Core Team, 2017) were applied to test the significance of the changes between model scenarios. All tests were conducted at the 0.05 level of significance.

Table 5-2: Schemes for comparison of model outputs

Schemes	**Comparison of model scenarios**		
S1	Past Climate-Past Glacier [A]	*VERSUS*	Present Climate-Present Glacier [D]
S2	Past Climate-Past Glacier [A]	*VERSUS*	Past Climate-Present Glacier [B]
S3	Past Climate-Past Glacier [A]	*VERSUS*	Present Climate-Past Glacier [C]
S4	Past Climate-Present Glacier [B]	*VERSUS*	Present Climate-Present Glacier [D]
S5	Present Climate-Past Glacier [C]	*VERSUS*	Present Climate-Present Glacier [D]

5.3.4 Meteorological forcing datasets

Bias-corrected ERA-40 (Uppala *et al.*, 2005) and ERA-Interim reanalysis data (Dee *et al.*, 2011) were used to force the model. These ERA global reanalysis products were bias-corrected to *in-situ* observational datasets at single points near the glaciers (Athabasca Moraine Station for AGRB and Peyto Main Station for PGRB, Figure 5-6). The meteorological variables that were used to run CRHM-glacier were air temperature, vapour pressure, wind speed, precipitation, and incoming short- and longwave radiation. In the second stage, these data were distributed to the basin HRUs using built-in algorithms and macros in CRHM (Pomeroy *et al*., 2007). The HRUs of these basins are presented in Pradhananga and Pomeroy (2020).

For PGRB, ERA-Interim data were bias-corrected to Peyto Main Station observations from 2013-2018 and ERA-40 data were bias-corrected to the archived observations from the station for the common overlap period of 1992-2001 (Munro, 2011). For AGRB, ERA-Interim data were bias-corrected to Athabasca Moraine Station. No *in-situ* observations available for the period before 2014 from AGRB. Therefore, ERA-40 data for 1965-1975 were bias-corrected using ERA-Interim

data for the period of 1979-2002, similar to Krogh and Pomeroy (2018), using quantile mapping approach with monthly bias correction factors.

5.4 Results and discussion

Changes in climate (temperature and precipitation), changes in glacier configuration, and impacts on changes in runoff and glacier mass balance are discussed below for both AGRB and PGRB.

5.4.1 Change in climate

Air temperature and precipitation over PGRB and AGRB were analysed for the two periods – 1965-1975 and present 2008-2018. Daily mean (Tmean), maximum (Tmax), and minimum (Tmin) temperature (Figure 5-2 and Appendix F) and monthly precipitation and cumulative precipitation (Figure 5-3 and Appendix F), averaged and aggregated over the two climatic periods, were compared using scheme S1. Daily mean temperatures were obtained by averaging 24 hourly temperature values (Bernhardt *et al*., 2018).

Except during the summer maximum over AGRB, temperatures generally increased in the present decade compared to the past, for both annual and seasonal averages. Analysis at monthly time periods also shows that temperature at both glaciers increased significantly, except for a few months. The exceptions in AGRB were Tmax in May, June and September; Tmin in February, October, November and December; and Tmean in February, May, June, October and December, when the present temperature values were either equal to or less than the past temperature values. The exceptions in PGRB were Tmax in December; Tmin in February and November; and Tmean in February and December. Temperature increments are significantly different from zero and evident in more of the temperature variables in PGRB than in AGRB.

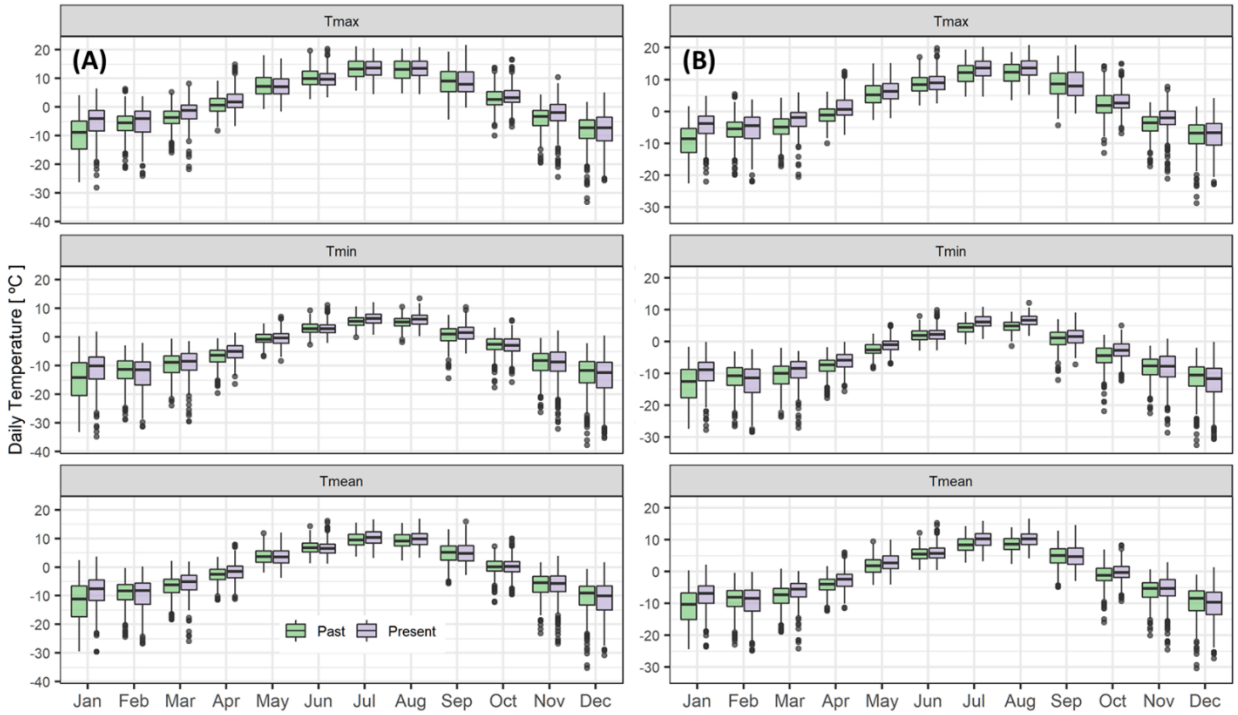

Figure 5-2: Seasonal daily maximum, minimum and mean temperature comparison between two periods, past (1965-1975) and present (2008-2018). (A) AGRB (B) PGRB.

The precipitation data show that there was a slight increase in total annual precipitation in the present decade compared to the past over both basins (Figure 5-3). The monthly precipitation breakdown shows that winter (December - February) precipitation over both basins has decreased, but that precipitation in the other seasons has increased. Statistical analysis of seasonal precipitation change showed that an increase in summer precipitation in both basins and a decrease in winter precipitation in AGRB were statistically significant, at the 5% level of significance (Appendix F). The other changes in precipitation were not significant. Instead, there was an increase in rainfall ratio, for both present climate and present glacier configuration, compared to the past climate and past glacier configuration in both research basins (Figure 5-4). Increases in the rainfall ratio in these basins are consistent with other studies, for example, in Europe by Hynčica and Huth (2019).

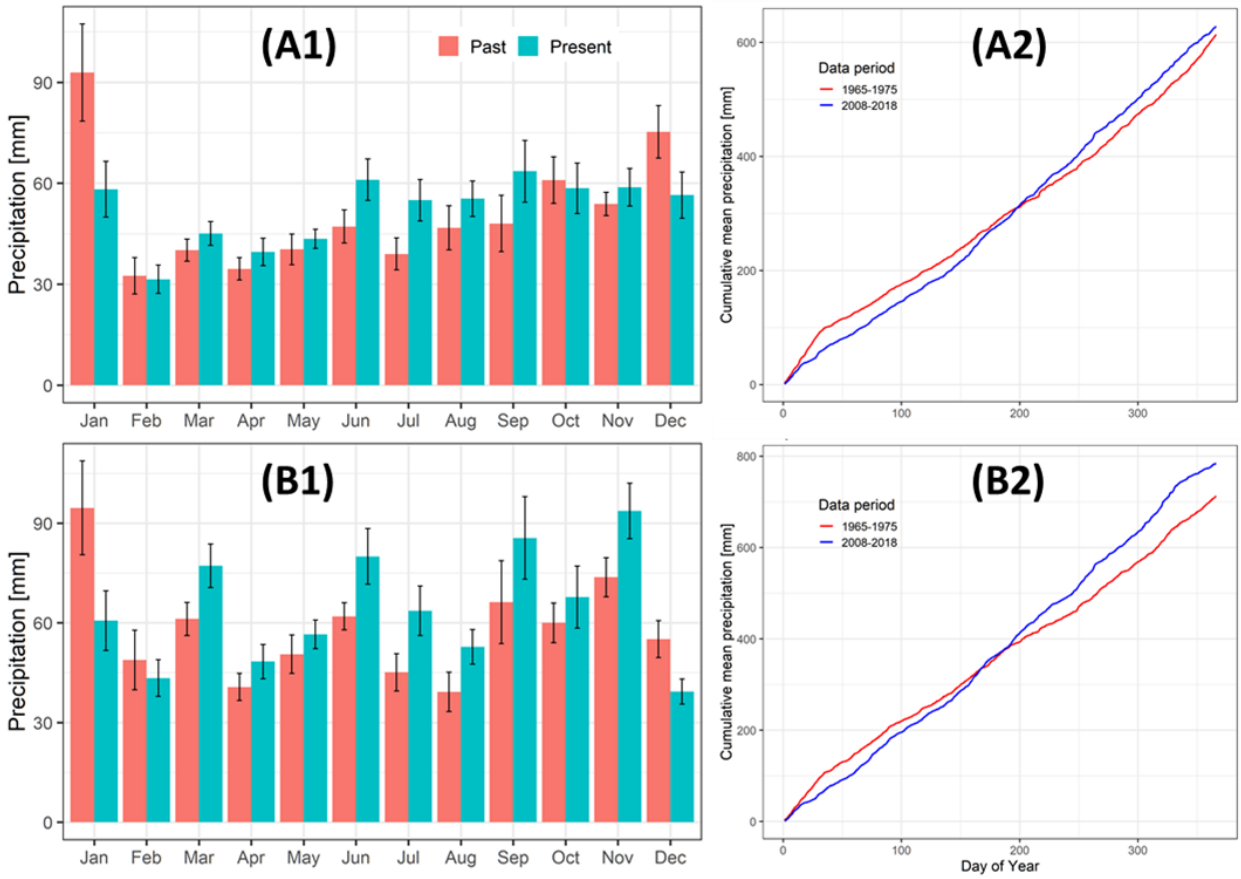

Figure 5-3: Monthly and cumulative daily mean precipitation averaged over the two periods, past (1965-1975) and present (2008-2018). (A) AGRB (B) PGRB. A1 and B1 are monthly totals, red is for the past and blue is for the present. A2 and B2 are the averaged cumulative precipitation.

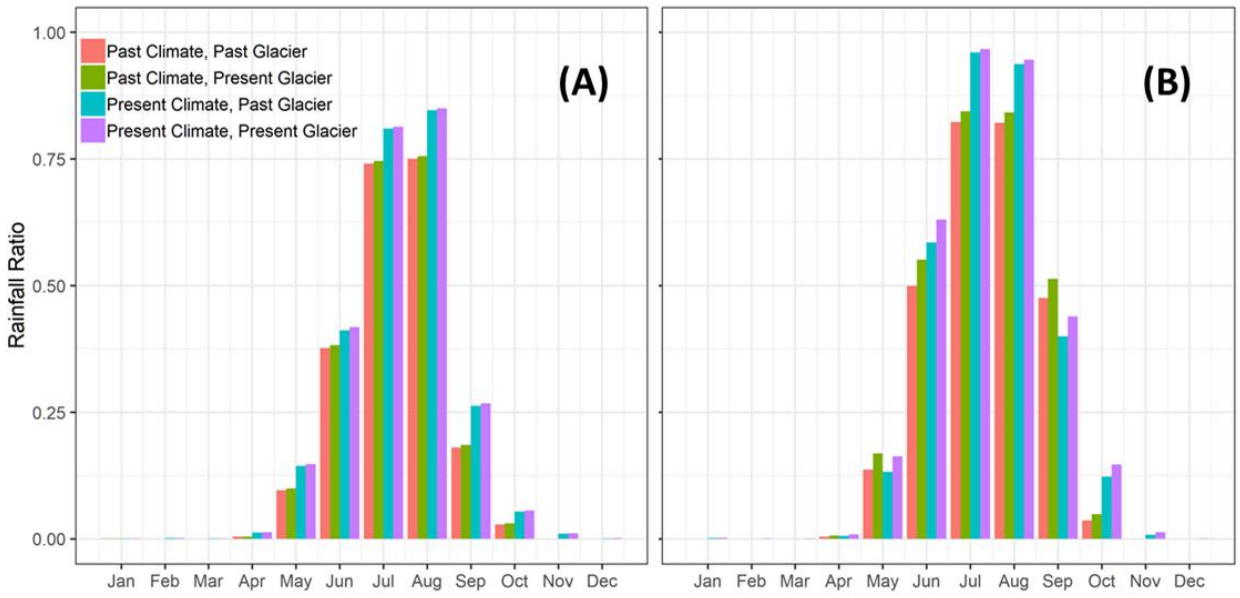

Figure 5-4: Mean-monthly rainfall ratios simulated for the four model run scenarios. (A) AGRB, (B) PGRB.

5.4.2 Change in glacier configuration

The glaciers have undergone significant mass loss in the last five decades, which is very noticeable at Peyto Glacier (e.g., Demuth and Keller, 2006; Kehrl *et al.*, 2014) and comparatively less so at Athabasca Glacier (Tennant and Menounos, 2013).

During the period 1966-2014, Peyto Glacier shrank in area from 14.4 km^2 (64.6% of the total basin area of 22.3 km^2) to 9.9 km^2 (44.4% of the basin area) and the accumulation area ratio (AAR) of the glacier dropped from 0.75 to 0.35, exposing more ice in 2014, more than double the area exposed in 1966. The exposed ice area increased from 3.6 km^2 to 6.4 km^2, whereas the firn area decreased from 10.8 km^2 to 3.5 km^2.

Though to a lesser degree than Peyto Glacier, the area of Athabasca Glacier has also decreased in the last three decades (1984-2014) from 18 km^2 (61.4% of the total basin area of 29.3 km^2) to 16.9 km^2 (57.7% of the total basin area), and AAR decreased from 0.76 to 0.47. The exposed ice area increased from 4.3 km^2 to 9.0 km^2, and the firn area decreased from 13.6 km^2 to 7.9 km^2.

The firn line has moved to a higher elevation on both glaciers, and glacier surfaces have become steeper. The other change in the two glacier configurations was in surface elevation; the mean surface elevation of Peyto Glacier has decreased (from 2628 m to 2615 m) while that of Athabasca Glacier has increased (from 2799 m to 2826 m). In summary, less glacier area is in the present compared to the past, but firn area reduced, and ice-exposed area increased in the present compared to the past. The details are in Table 5-3 and Figure 5-5 - 5.8.

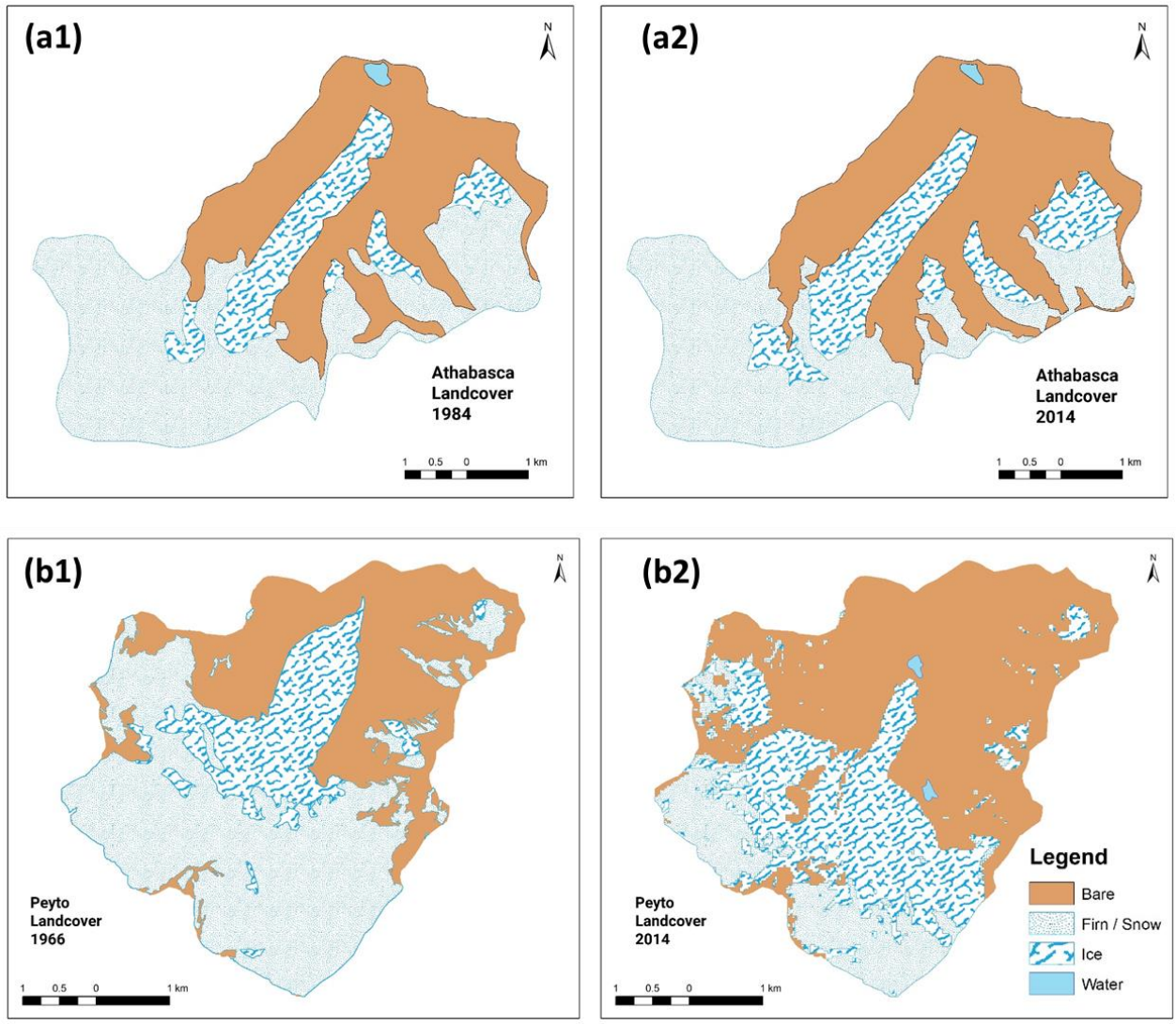

Figure 5-5: Change in landcover between the glaciers in past and present. (a) AGRB (b) PGRB. (a1) and (a2) are AGRB in 1984 and 2014, respectively. (b1) and (b2) are PGRB in 1966 and 2014, respectively.

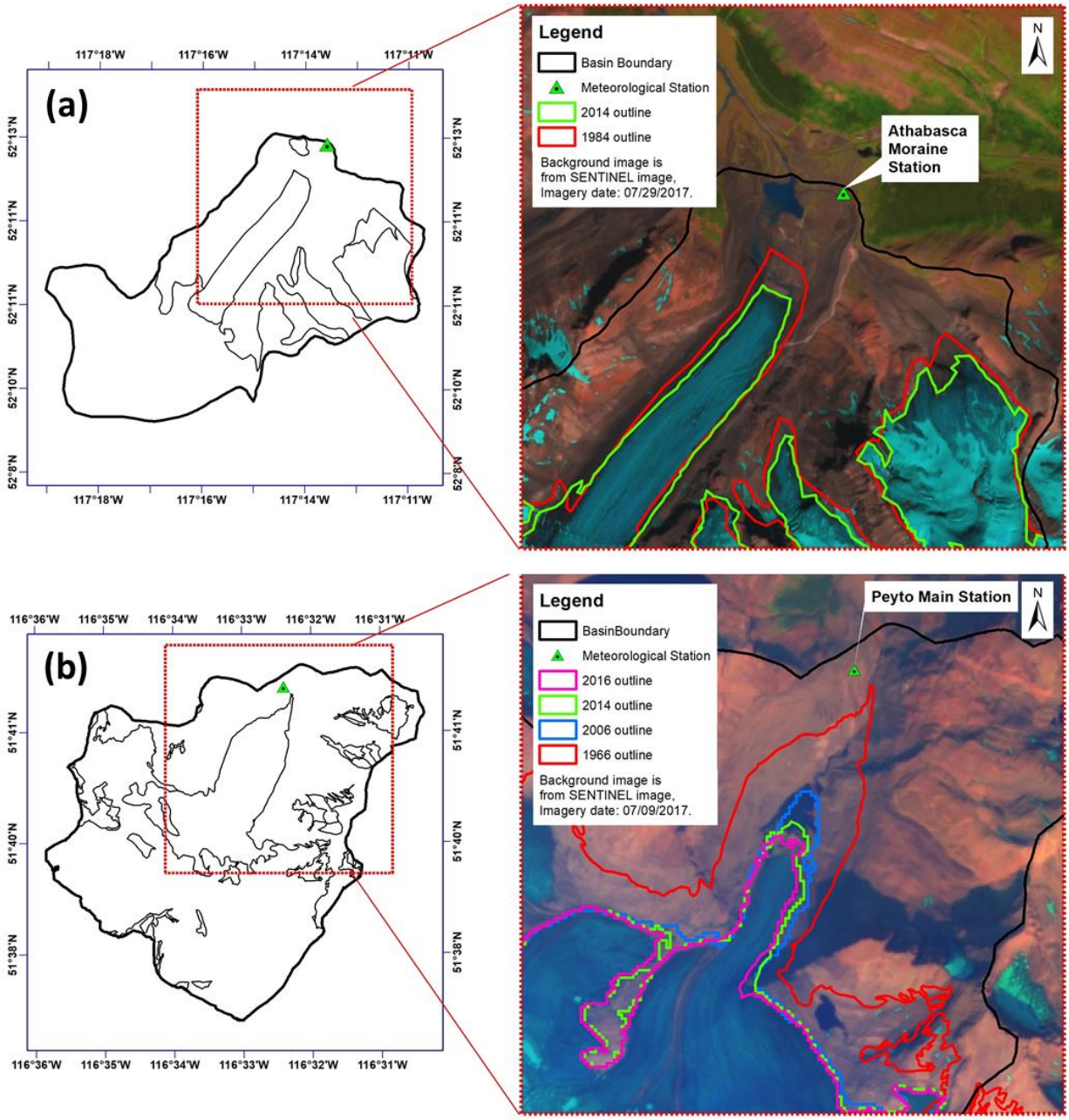

Figure 5-6: Change in landcover between the glaciers in past and present. (a) AGRB (b) PGRB.

Table 5-3: Changes in glacier configurations.

Landcover	Athabasca		Peyto	
	1984	2014	1966	2014
Firn area (km^2)	13.6	7.9	10.8	3.5
Exposed ice (km^2)	4.3	9.0	3.6	6.4
Glacier[#] (km^2)	18.0	16.9	14.4	9.9
Accumulation Area Ratio (AAR)	0.76	0.47	0.75	0.35
Non-glacial area (km^2)	11.3	12.4	7.9	12.4
Total basin area[&] (km^2)	29.3	29.3	22.3	22.3
Mean glacier elevation (m)	2798.9	2825.5	2627.6	2615.1
Slope (°)	21.1	21.6	19.9	22.0

[#]Glacier area is the sum of firn area and ice exposed area.
[&]Total basin area is the sum of glacier area and nonglacial area.

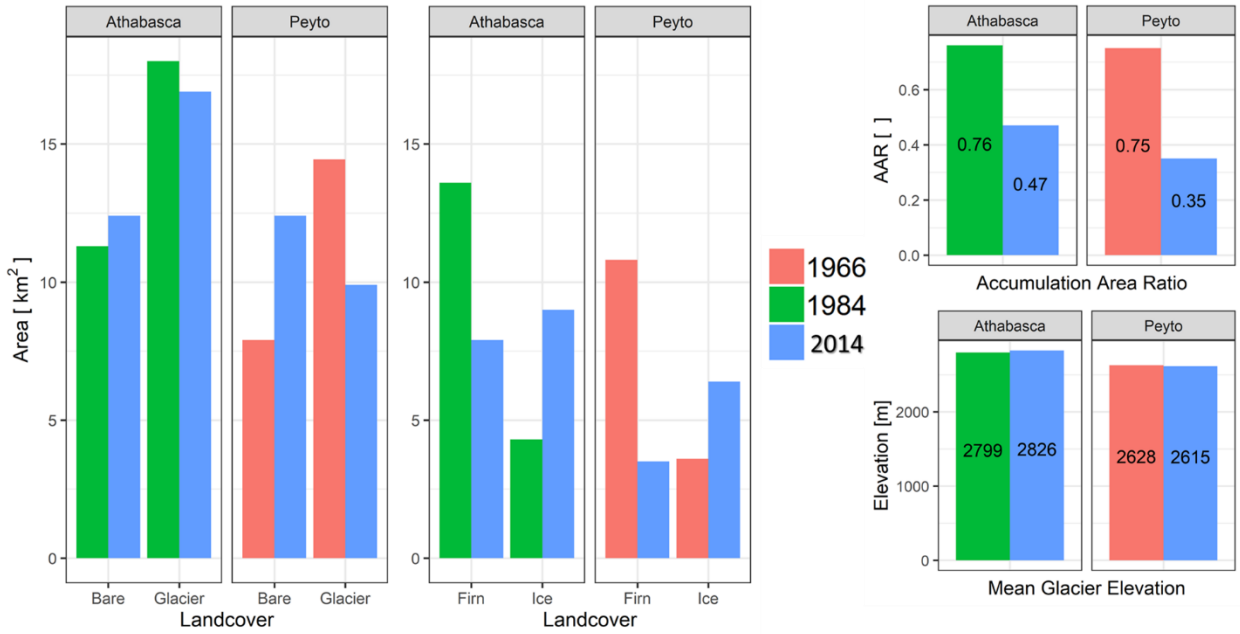

Figure 5-7: Comparison of glacier configurations at two times. PGRB is compared in between 1966 and 2014, AGRB is compared in between 1984 and 2014. Red is for 1966, green is for 1984, and blue is for 2014.

5.4.3 Change in runoff

Figure 5-8 shows runoff and melt components from AGRB and PGRB with the two model scenarios, A and D (scheme S1). Snowmelt runoff dominated both the basins, in comparison to rainfall runoff, icemelt runoff, and firnmelt runoff. The present climate and present glacier

configurations (model scenario A) produced more runoff than the past climate and past glacier configurations (model scenario D). There was a 19% increase significant at α=5% (p=0.005, Table F.5) in annual mean runoff, from 1581 mm to 1888 mm in PGRB (scheme S1, Figure 5-8). This was mainly due to an increased contribution from icemelt, from 265 mm to 667 mm (p=0, Table F.6). There was a decrease in mean annual snowmelt, from 1105 mm to 974 mm, but the change in this and the other fluxes were statistically insignificant. The increase in runoff was insignificant at α=5% (p=0.578, Table F.6) in the case of AGRB, from 1320 mm to 1365 mm, though there was a significant increase in rainfall, from 175 mm to 262 mm. AGRB experienced increased snowmelt and firnmelt but decreased icemelt.

In the case of AGRB, only increases in rainfall in the S3 and S4 schemes and in snowmelt in S4 were significant. More rainfall occurred with both past and present glacier configurations. There were significant changes in runoff, firn melt and snow melt for PGRB, suggesting that the increase in runoff over time (S3 and S4) was due to an increase in firn melt and ice melt. The large loss of firn in PGRB resulted in a decrease of firn melt by 65% (from 414 mm to 146 mm) when the past glacier configuration was replaced by the present one with the climate for both glacier configurations held constant at the present climate.

Monthly averaged runoff from the four model scenarios is presented in Figure 5-9. There was a reduction in peak flows from both glaciers as glacier mass declined over time with the climate held constant. However, with changing climate only, peak flows increased over time. The peak flow of PGRB also shifted from August to July as climate shifted. This is in line with the prediction by Kienzle *et al.* (2012) for the Cline River watershed that spring runoff and peak streamflow would shift four weeks advance in the 21st century compared to the baseline period (1961-1989). The combination of moving from past to present climate and changing glacier configuration shifted peak flows forward by a month, however, the impact of changing climate was greater than that of the changing glacier configuration.

The warmer temperatures and increased rainfall ratio in the present climate led to increased glacier runoff from both basins. However, the reduced glacier extent in the present glacier configuration

resulted in decreased runoff in both basins, counteracting the direct climate change impact on the basin.

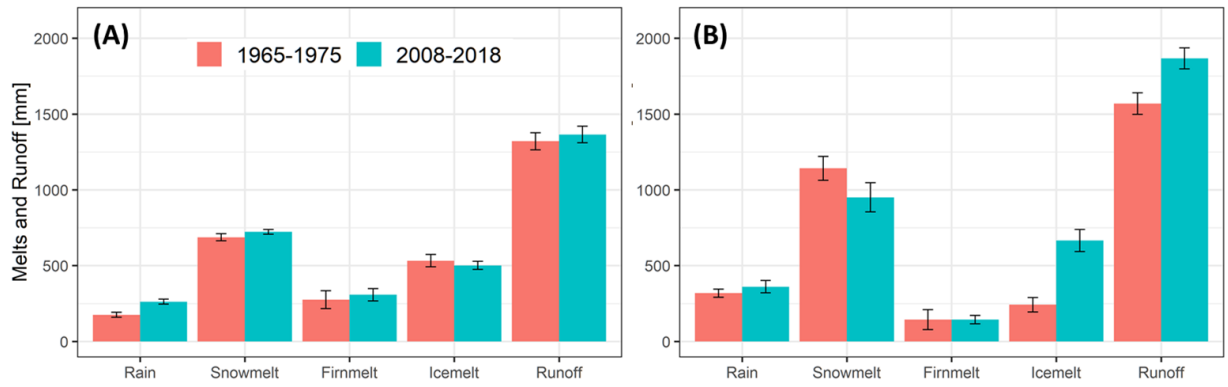

Figure 5-8: Mean annual melt and runoff in the past and the present. Error bars show the annual variability, defined as the standard error between years. (A) AGRB (B) PGRB.

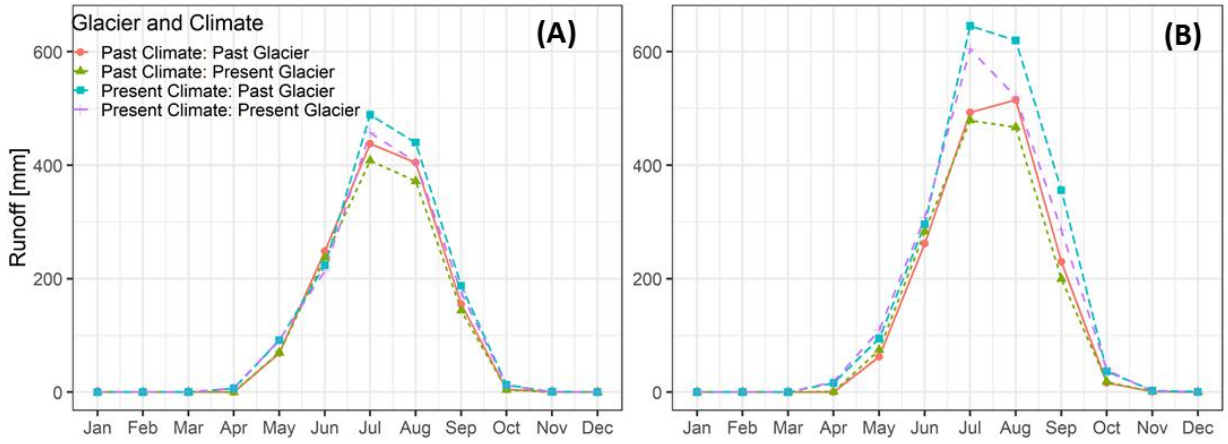

Figure 5-9: Monthly averaged runoff from the four model scenarios. (A) AGRB (B) PGRB.

5.4.4 Change in glacier mass balance

Seasonal and annual mass balances for AGRB and PGRB resulting from the four model scenarios, A-D, are presented in Figure 5-10. The results from the statistical analysis are presented in Table F.7. Except for the change in winter mass balance between model scenarios A and D (scheme S1), the mass balance changes are not statistically significant in AGRB. There was a significant change in winter and annual mass balances between past and present climates and glaciers in PGRB (S1). Mean annual winter accumulation decreased from 586 mm [averaged over the past climate, 1965-1975] to 324 mm [averaged over the present climate, 2008-2018], resulting in negative mean

annual mass balances, from -271 mm in the past climate to -733 mm in the present climate (Table F.5). These changes are due more to the change in climate than the change in glacier configuration. Summer ablation increased significantly with present climate for both past and present glacier configurations (S3 and S4 scenarios). The changes are not significant in model runs using the S2 and S5 scenarios. However, the past glacier configuration resulted in greater winter snow accumulation in both basins for both past and present climates.

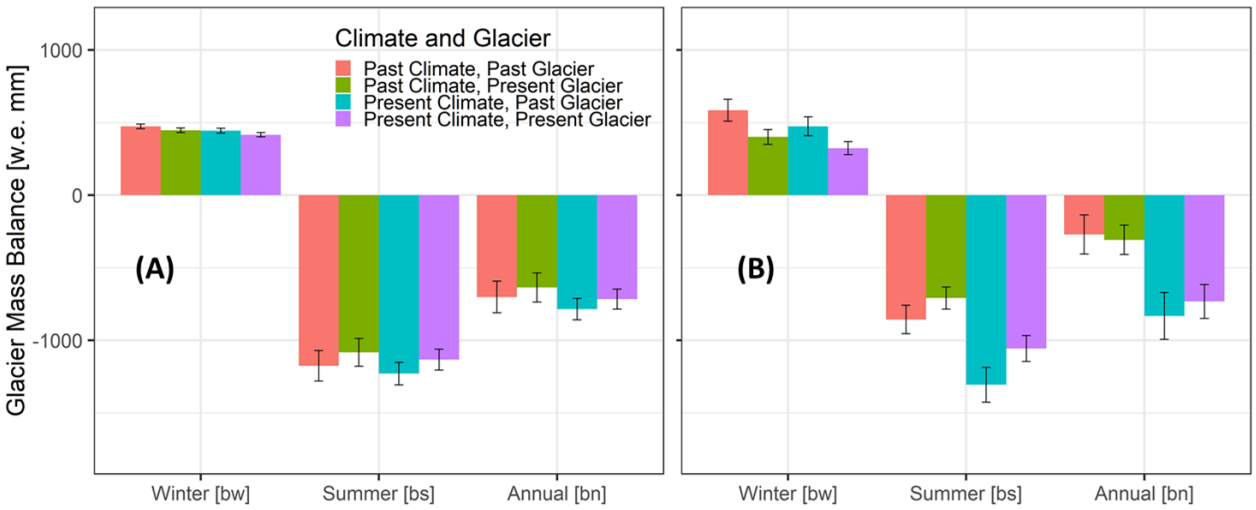

Figure 5-10: Glacier mass balance – winter, summer and annual, from the four model scenarios. (A) AGRB and (B) PGRB.

In summary, the outputs show that changes in climate and basin configuration are both causing changes in the melt rate and runoff. Compared to past climate and past glacier configuration, present climate and present glacier configuration provided more runoff in both basins, although they are resulting in significant losses of glacier mass.

5.5 Conclusion

This study investigated the influence of snow and glaciers on headwater hydrology in two mountain basins in the Canadian Rockies, where a warming climate and glacier retreat continue to cause concern about changes in high mountain hydrology.

There was an increase in air temperature, mainly in daily maximum and winter minimum temperatures. Total precipitation has not increased, but the rainfall ratio has increased with the shift in climate. Decreases in winter precipitation were balanced by increased precipitation in the other seasons. Both mass balance observations and analysis of satellite imagery show that the glaciers are losing mass, and that the exposure of ice at glacier surfaces has increased. The rate of these changes is lower in AGRB than in PGRB. The retreat of the glaciers has led to reductions in glacierized areas and changes in elevation and slope of the glacier surfaces. The decreases in AAR over time as the glacier changed configuration, caused increases in both proportional and areal ice exposure.

The study used a novel approach to apply present climate to feed past glacier configuration and past climate to feed present glacier configuration, so that the impacts of changes in glacier configuration and climate on glacier hydrology could be explicitly separated. The modelling results presented here show that glacier retreat and ablation are due to the joint effect of warming climate and an increase in ice exposure, which increased both seasonal melt and runoff. Increased streamflow discharge was due to climate warming and is limited somewhat by glacier retreat. Model results indicated that streamflow from the glaciers was still increasing in the present climate (2008-2018) compared to the past climate (1965-1975) despite reductions in glacier area and volume. Such a modelling approach is important for diagnosing the hydrological responses from a glacierized basin in the context of climate change and variability.

CHAPTER 6: Synthesis and conclusions

The results and discussions from Chapters 1-5 are synthesized in this chapter. The conclusions were drawn from the results of each chapter. This work investigated the hydrological response of a mountain glacier to climate change and change in glacier configuration. The main conclusions from each chapter are summarised below. Recommendations for further studies, resulting from this research, are also outlined.

6.1 Synthesis

Chapter 1 reviewed literature on mountain glacier hydrology and found three key research gaps. In high mountain basins, empirical relations between snow and ice melt and air temperature have often been preferred over physical energy budget calculations as a basis for computing snow and glacier melt. Major reasons for this are cited as the lack of high-elevation observations of shortwave irradiance and uncertainty in estimating irradiance from other variables. Empirical methods for the estimation of shortwave irradiance are based primarily on air temperature and have been developed at lower elevations for calculating the snowmelt energy budget, soil thaw, or rates of evapotranspiration. Similarly, glacier hydrology models need to be physically based, using an energy budget approach coupled with snow redistribution. Furthermore, studies of the impact of climate change on glaciers have generally focussed on changes in glacier mass and how this relates to climate forcing. Hydrological responses of glacierised mountain headwater basins to climate change depend on precipitation, snow and ice dynamics, hydrology of the deglacierized terrain and the mass and energy balance. There is a research gap in our understanding of how climate change and transient glacier retreat work together to influence the hydrology of glacierized basins. The four chapters (2-5) address these research gaps, described as follows:

Peyto Glacier in the Canadian Rockies has been the subject of many hydrological and glaciological studies since the 1960s. However, there was a need to compile all these meteorological, hydrological, glaciological, and geographical datasets into a single database for glacio-hydrological modelling studies. Chapter 2 presented hydro-meteorological, glaciological and

geophysical data collected from Peyto Glacier Research Basin (PGRB) in the Canadian Rockies from the 1960s to the present. Several examples of data cleaning approaches and description and methods for producing datasets for model meteorological forcing, parameterization and testing were also provided. Four reanalysis products were bias-corrected to *in-situ* observations for glacio-hydrological model runs. These long-term mass balance records, along with hydrometeorological data, are a great asset for modelling research, along with analysis of climate change and variability impacts on glacier mass balance and hydrology. The streamflow data, along with hourly surface elevation change as measured by sonic rangers at different elevation zones, could be used for model validation for modeling snow and glacier melt and glacier accumulation/ablation, respectively. These approaches for data compilation, data cleaning and preparation of bias-corrected reanalysis datasets were also followed for Athabasca Glacier Research Basin (AGRB). These datasets have been used for developing and testing of shortwave irradiance models (chapter 3) and of the glacier hydrology model, focusing on using reanalysis meteorological forcing data and modelling outputs of glacier surface elevation change and basin runoff while considering snow redistribution in the model (chapter 4) and the application of the glacier hydrology model (chapter 5).

Energy budget melt models are not generally applied in mountain glacier basins due to a lack of observations of incoming shortwave irradiance. A very good estimation of radiation is based on the duration of sunshine and cloud cover, but these are not generally measured in cold region high mountains. Atmospheric transmittance models based on temperature and humidity are the alternatives, as these variables are more readily available than any other meteorological parameters. The other approach could be the use of reanalysis datasets. Chapter 3 presented the new T/RH algorithms for estimating atmospheric transmittance based on temperature and humidity. This fulfills the first objective of the research - *(1) Develop a new atmospheric transmittance model to estimate shortwave irradiance from temperature and humidity observations*. These T/RH models and the reanalysis products along with existing temperature-based models were tested against observed data from thirty stations in North and South America, Europe, and Asia. The evaluation provided confidence in using reanalysis products for forcing the glacier hydrology model with redistribution of snow by wind and avalanches within the study basins (chapter 4) and for running the models for longer periods (chapter 5).

Snow accumulation and redistribution due to wind and gravity are important hydrological processes for an alpine glacier. Chapter 4 shows the development of a physically based, integrated glacier hydrology model in the CRHM platform considering snow redistribution by wind and avalanches and separate processes for firn/ice melt and snowmelt and routing of meltwater through the glacier. The model was tested in two glacierized basins, PGRB in Banff National Park and AGRB in Jasper National Park. The model was tested for change in glacier surface elevation and albedo and in basin runoff with and without snow redistribution by wind and avalanche to validate the model. The simulation of glacier surface elevation at accumulation zone improved while blowing snow model was included. Streamflow simulations were improved when either both snow redistribution processes were included or only blowing snow process was included. Snow distribution by avalanche process alone did not improve model performance. The model was also validated for the model outputs comparing with the *in-situ* observations by forcing the model with both the reanalysis datasets and the observed data measured within the basins. This addresses the second objective - *(2) Couple snow redistribution and full energy and mass budget in a glacier hydrological modelling platform and test the model at two glacier research basins in the Canadian Rockies.* Its potential for long-term study over a basin, undergoing transitional phases from glaciation to deglaciation, is noteworthy.

The glacier hydrology model, CRHM-glacier developed in chapter 4, was used to simulate runoff from Peyto Glacier in Banff National Park and Athabasca Glacier in Jasper National Park to study the impacts of changes in climate and glacier configuration on runoff. The model considered redistribution of snow by wind and avalanches, full radiation and turbulent transfer energetics to snow and ice, and densification of perennial snow. It was set up using hydrological response units that considered elevation bands, surface slope and aspect, as well as landcover and its change in the half-century. Long-term observations of mass balance, snow and surface elevation change and discharge at the glacier outlet were used to evaluate model performance, which was adequate for this purpose. CRHM-glacier was used to diagnose the hydrological response to the warming climate and changes in glacier configuration. This chapter answers the research questions set by the third objective - *(3) Diagnose the individual and combined impacts of changes in climate and glacier mass on headwater hydrology.* This research contributes information to water resource

planners and managers who wish to determine changes in headwater streams resulting from climate warming and associated glacier recession.

This study improved the understanding of snow and glacier ablation and accumulation dynamics, and their impact on high mountain hydrology. It also improved current hydrological modelling capacity in this region. The model could be used to research the impact of past and future climate change on the headwater hydrology of cold region mountains dominated by snow and glaciers.

6.2 Conclusions

The Peyto Glacier Research Basin (PGRB) provided meteorological data from six AWS, three on the glacier ice and three on the glacier moraine. These stations are included in the cryospheric surface observation network of WMO's Global Cryosphere Watch. The present meteorological data collected are hourly air temperature, relative humidity, wind, incoming shortwave and longwave radiation, and daily total precipitation. These data are available for a period of three decades (1987-2019) from the off-ice stations and for twelve years (2007-2019) from the on-ice stations. Bias-corrected reanalysis datasets from ERA-Interim, WFDEI, NARR and CFSR are created for running hydrological models for longer periods. Streamflow data are available for two periods, 1967-1977 and 2013-2018. Geophysical data, which consisted of basin boundary, drainage area, DEM and landcover, were also prepared for the basin. Glaciological data published by WGMS (2019) were available from 1966 to 2017. Glacier surface elevation measured by sonic rangers at three elevations were available for short periods between 2007-2013, and at the Lower Ice station from 2007 to 2019, with a few data gaps.

The new T/RH algorithms for estimating atmospheric transmittance based on temperature and humidity were tested against observed data from thirty stations in North and South America, Europe, and Asia. Daily mean humidity provided a better predictor for atmospheric transmittance than daily temperature range. The new algorithms that considered both temperature and humidity provided better results for all the sites compared to the original empirical approaches based on temperature only. Inclusion of clear sky transmittance also improved the simulation of shortwave irradiance, as it filters out the impact of cloud cover on other atmospheric properties that influence

the transmittance. The new models were also better than the ERA Interim reanalysis data when the parameters were calibrated to the specific sites. However, ERA Interim data provide better simulation when a site completely lacks observations of shortwave irradiance, but only for sites lower than 3000 m. For the higher altitude sites, the new approaches with global calibration still provide better estimation of atmospheric transmittance.

The CRHM-glacier model developed in the CRHM platform considers separate processes for icemelt and snowmelt and routing of meltwater through a glacier. The model includes snow redistribution by wind and avalanches and densification of snow, firn and ice. The model was tested for two glaciers in the Canadian Rockies, Peyto Glacier and Athabasca Glacier using both *in-situ* and reanalysis forcing data. The model could simulate both accumulation and ablation processes on the glacier surfaces, along with runoff from the glaciers. Since the model computes snowmelt and icemelt separately, it can model possible states of mountain glaciers – advancing and receding of the glacier, along with completely de-glacierized condition, in which it is dealt by snowmelt model. The model was also applied to see the impacts of snow redistribution by blowing snow and avalanches. Inclusion of snow redistributions improved the model simulation in mass balance at accumulation zone only and streamflow. When individual impacts of blowing snow and avalanches processes were evaluated for streamflow simulations of the basins, only inclusion of blowing snow process improved the result. Since the model computes snowmelt and icemelt separately, it can model possible states of mountain glaciers – advancing and receding of the glacier, along with completely de-glacierized condition, in which it is dealt by snowmelt model. The model did not, however, simulate continuous ice flow, for which the model needs to be coupled to glacier. The model parameters were physically based obtained by observations and literature. The model could simulate past and present discharges resulting from historical climate change. There was good agreement between simulated and observed streamflow in the two basins when the model was forced by *in-situ* meteorological observations and reanalysis data.

This study considered the combined impacts of climate change and glacier recession on the hydrology and water balance of two glacierized basins in the Canadian Rockies. CRHM-glacier was used to simulate runoff from Peyto Glacier and Athabasca Glacier to study the impacts on runoff of changes in climate and glacier configuration. Using meteorological forcing data from

1965–2018, basin glacier hydrology was simulated using the fixed glacier configurations of past and present. To distinguish the impacts of changes in climate and glacier configuration, past climate was forced to present glacier configuration and present climate was forced to past glacier configuration. The outputs show that both changes in climate and glacier configuration are causing changes in melt rate and streamflow discharge. There was increased discharge recently, compared to the 1960-70s. The results suggest that glacier retreat has attenuated the increased runoff; however, increased exposure of glacier ice and lower surface elevation due to glacier thinning are less influential than climate warming in increasing streamflow over time. As a result, streamflow from these glaciers are still in the increasing phase. The past glacier configuration produced more runoff. Therefore, the runoff from the basins increased more due to warming climate than to the change in glacier configuration. The headwaters streamflows from the glaciers are still in the increasing phase, although glacier shrinkage has already caused a slight reduction in discharge. Such a modelling approach is important for diagnosing the hydrological responses from a glacierized basin in the context of climate change and variability.

6.3 Recommendation for future analyses

One further analysis would involve running the CRHM-glacier model with climate change projection and ice flow dynamics. This could be done by embedding the present glacier configuration in CRHM-glacier and updating the glacier configuration outside the CRHM platform. Investigation of the climate change impact on hydrological components should also be carried out with a projected change in future climate (e.g., Chattopadhyay and Jha, 2016; Rasouli *et al.*, 2019b; Dahal *et al.*, 2020) to project changes in water availability in the mountain headwaters due to change in climate. With retreat of the glaciers, vegetation cover change could be observed. Its effects could also be considered in future modeling scenario. This study showed that there has recently been an increasing rainfall ratio compared to the past in the Canadian Rockies. With warming climate, precipitation phase may also change in future and therefore, the impact of a change in rainfall ratio on the headwater hydrology could be of greater research interest.

The model has been tested over two glacierized basins in the Canadian Rockies and it needs to be tested over other parts of the world, for example, the Himalayan region. The model has been built for Langtang Glacier Research Basin in the Nepal Himalayas. Model calibration and validation are in progress. These glaciers have significant areas of ice covered by debris. Therefore, debris covered glaciers are to be dealt within the model as they have distinctive hydrological behaviour compared to clean glaciers (Fyffe *et al.*, 2019). The other consideration could be the impact of black carbon on the glacier surface. When black carbon or dusts are deposited on snow and ice they may change albedo values of the surface considerably impacting snow and glacier surface melting (Salzmann *et al.*, 2014), for example, the possible impact of the 2017 forest fire during melt season over PGRB (Aubry-Wake *et al.*, 2020). The albedo of glacier ice was lower in 2017-2019 than that in the earlier years as measured at the Athabasca Ice station (section 4.6.1.1).

The new T/RH models for simulating incoming shortwave irradiance have been tested at 30 sites from *in-situ* observation data and from two reanalysis products (WFDEI and ERA-Interim). More station data could be included and an additional global reanalysis product, for example, the Modern-Era Retrospective analysis for Research and Applications, version 2 (MERRA-2, Rienecker *et al.*, 2011) could also be tested.

References

Adam JC, Hamlet AF, Lettenmaier DP. 2009. Implications of global climate change for snowmelt hydrology in the twenty-first century. *Hydrological Processes* **23**: 962–972 DOI: 10.1002/hyp

Allen RG. 1995. Evaluation of procedures for estimating mean monthly solar radiation from air temperature. *Rep. United Nations Food and Agric. Org. (FAO)*

Anderson B, Lawson W, Owens IF, Goodsell B. 2006. Past and future mass balance of'Ka Roimata o Hine Hukatere'Franz Josef Glacier, New Zealand. *Journal of Glaciology* **52** (179): 597–607 DOI: 10.3189/172756506781828449

Anderson ER. 2017. Modelling Changes in Multi-Decadal Streamflow Contributions – Bologna Glacier, Selwyn Mountains, NWT, Canada.University of Saskatchewan. Available at: https://ecommons.usask.ca/handle/10388/7919

Annandale JG, Jovanovic NZ, Benadé N, Allen RG. 2002. Software for missing data error analysis of Penman-Monteith reference evapotranspiration. *Irrigation Science* **21** (2): 57–67 DOI: 10.1007/s002710100047

Arendt A. 1999. Approaches to modelling the surface albedo of a high arctic glacier. *Geografiska Annaler. Series A, Physical Geography* **81** (4): 477–487 Available at: http://www.jstor.org/stable/521487

Arendt A, Echelmeyer K, Harrison W, Lingle C, Valentine VB. 2002. Rapid wastage of Alaska glaciers and their contribution to rising sea level. *Science (New York, N.Y.)* **297** (5580): 382–6 DOI: 10.1126/science.1072497

Arendt A, Walsh J, Harrison W. 2009. Changes of glaciers and climate in northwestern North America during the late twentieth century. *Journal of Climate* **22** (15): 4117–4134 DOI: 10.1175/2009JCLI2784.1

Armstrong RN, Pomeroy JW, Martz LW. 2015. Variability in evaporation across the Canadian Prairie region during drought and non-drought periods. *Journal of Hydrology* **521**: 182–195 DOI: 10.1016/j.jhydrol.2014.11.070

Aubry-Wake C, Pradhananga D, Pomeroy J. 2020. Linking hydrological processes to streamflow temporal variability in a headwater alpine glacierized catchment. *In preperation*

Ayala Ramos AI. 2017. The role of surface sublimation in the summer mass balance of glaciers

in the subtropical semiarid Andes: 220 DOI: 10.3929/ETHZ-B-000000218

Bandyopadhyay A, Bhadra A, Raghuwanshi NS, Singh R. 2008. Estimation of monthly solar radiation from measured air temperature extremes. *Agricultural and Forest Meteorology* **148**: 1707–1718 DOI: 10.1016/j.agrformet.2008.06.002

Barry RG. 2006. The status of research on glaciers and global glacier recession: a review. *Progress in Physical Geography* **30** (3): 285–306 DOI: 10.1191/0309133306pp478ra

Beckers J, Pike R, Werner AT, Redding T, Smerdon B, Anderson A. 2009. Hydrologic models for forest management applications: Part 1: Model selection. *Streamline Watershed Management Bulletin* **13** (1): 35–44

Berg AA, Famiglietti JS, Rodell M, Reichle RH, Jambor U, Holl SL, Houser PR. 2005. Development of a hydrometeorological forcing data set for global soil moisture estimation. *International Journal of Climatology* **25** (13): 1697–1714 DOI: 10.1002/joc.1203

Bernhardt J, Carleton AM, LaMagna C. 2018. A comparison of daily temperature-averaging methods: Spatial variability and recent change for the CONUS. *Journal of Climate* **31** (3): 979–996 DOI: 10.1175/JCLI-D-17-0089.1

Bernhardt M, Schulz K. 2010. SnowSlide: A simple routine for calculating gravitational snow transport. *Geophysical Research Letters* **37** (L11502): 1–6 DOI: 10.1029/2010GL043086

Bernhardt M, Liston GE, Strasser U, Zängl G, Schulz K. 2010. High resolution modelling of snow transport in complex terrain using downscaled MM5 wind fields. *The Cryosphere* **4** (1): 99–113 DOI: 10.5194/tc-4-99-2010

Bernhardt M, Zängl G, Liston GE, Strasser U, Mauser W. 2009. Using wind fields from a high-resolution atmospheric model for simulating snow dynamics in mountainous terrain. *Hydrological Processes* **23**: 1064–1075 DOI: 10.1002/hyp.7208

Berry MO. 1981. Snow and Climate. In *Handbook of Snow: Principles, Processes, Management & Use*, Gray DM, , Male DM (eds).Pergamon; 32–59.

Berthier E. 2004. Recent rapid thinning of the “Mer de Glace” glacier derived from satellite optical images. *Geophysical Research Letters* **31** (17): 2–5 DOI: 10.1029/2004GL020706

Berthier E, Schiefer E, Clarke GKC, Menounos B, Rémy F. 2010. Contribution of Alaskan glaciers to sea-level rise derived from satellite imagery. *Nature Geoscience* **3** (2): 92–95 DOI: 10.1038/ngeo737

Besharat F, Dehghan AA, Faghih AR. 2013. Empirical models for estimating global solar

radiation: A review and case study. *Renewable and Sustainable Energy Reviews* **21**: 798–821 DOI: 10.1016/j.rser.2012.12.043

Bintanja R. 2001. Snowdrift sublimation in a Katabatic wind region of the Antarctic ice sheet. *Journal of Applied Meteorology* **40** (11): 1952–1966 DOI: 10.1175/1520-0450(2001)040<1952:SSIAKW>2.0.CO;2

Bintanja R, Reijmer CH. 2001. A simple parameterization for snowdrift sublimation. **106**: 739–748

Bitz CM, Battisti DS. 1999. Interannual to decadal variability in climate and the glacier mass balance in Washington, Western Canada, and Alaska. *Journal of Climate* **12** (11): 3181–3196 DOI: 10.1175/1520-0442(1999)012<3181:ITDVIC>2.0.CO;2

Boilley A, Wald L. 2015. Comparison between meteorological re-analyses from ERA-Interim and MERRA and measurements of daily solar irradiation at surface. *Renewable Energy* **75**: 135–143 DOI: 10.1016/j.renene.2014.09.042

Bojanowski JS. 2016. sirad: functions for calculating daily solar radiation and evapotranspiration. R package version 2.3-3 Available at: https://cran.r-project.org/package=sirad

Bojanowski JS, Donatelli M, Skidmore AK, Vrieling A. 2013. An auto-calibration procedure for empirical solar radiation models. *Environmental Modelling and Software* **49**: 118–128 DOI: 10.1016/j.envsoft.2013.08.002

Bolch T, Menounos B, Wheate R. 2010. Landsat-based inventory of glaciers in western Canada, 1985–2005. *Remote Sensing of Environment* **114** (1): 127–137 DOI: 10.1016/j.rse.2009.08.015

Bravo C, Loriaux T, Rivera A, Brock BW. 2017. Assessing glacier melt contribution to streamflow at Universidad Glacier, central Andes of Chile. *Hydrology and Earth System Sciences* **21** (7): 3249–3266 DOI: 10.5194/hess-21-3249-2017

Bristow KL, Campbell GS. 1984. On the relationship between incoming solar radiation and daily maximum and minimum temperature. *Agricultural and Forest Meteorology* **31**: 159–166

Brutsaert W. 1982. *Evaporation into the Atmosphere*. D. Reidel, Dordrecht.

Casassa G, Paulina L, Pouyaud B, Escobar F. 2009. Detection of changes in glacial run-off in alpine basins : examples from North America , the Alps , central Asia and the Andes. **41**: 31–41 DOI: 10.1002/hyp

CCMEO. 1997. 082N, GOLDEN, Canadian Digital Elevation Data, Government of Canada; Natural Resources Canada; Earth Sciences Sector; Canada Centre for Mapping and Earth Observation (CCMEO)

Chattopadhyay S, Jha MK. 2016. Hydrological response due to projected climate variability in Haw River watershed, North Carolina, USA. *Hydrological Sciences Journal* **61** (3): 495–506 DOI: 10.1080/02626667.2014.934823

Chow VT. 1959. *Open Channel Hydraulics*. McGraw-Hill, Inc.: New York.

Clark CO. 1945. Storage and the unit hydrograph. *Proceedings of the American Society of Civil Engineering* **69**: 1419–1447

Clarke GKC, Jarosch AH, Anslow FS, Radić V, Menounos B. 2015. Projected deglaciation of western Canada in the twenty-first century. *Nature Geoscience* **8** (5): 372–377 DOI: 10.1038/ngeo2407

Clarke GKCC, Berthier E, Schoof CG, Jarosch AH. 2009. Neural networks applied to estimating subglacial topography and glacier volume. *Journal of Climate* **22** (8): 2146–2160 DOI: 10.1175/2008JCLI2572.1

Comeau LEL, Pietroniro A, Demuth MN. 2009. Glacier contribution to the North and South Saskatchewan Rivers. In *Hydrological Processes*2640–2653. DOI: 10.1002/hyp.7409

Cordeiro MRC, Wilson HF, Vanrobaeys J, Pomeroy JW, Fang X, Team TR-APBM. 2017. Simulating cold-region hydrology in an intensively drained agricultural watershed in Manitoba, Canada, using the Cold Regions Hydrological Model. *Earth Syst. Sci* **21**: 3483–3506 DOI: 10.5194/hess-21-3483-2017

Dahal P, Shrestha ML, Panthi J, Pradhananga D. 2020. Modeling the future impacts of climate change on water availability in the Karnali River Basin of Nepal Himalaya. *Environmental Research* **185**: 109430 DOI: 10.1016/j.envres.2020.109430

DeBeer CM, Sharp MJ. 2007. Recent changes in glacier area and volume within the southern Canadian Cordillera. *Annals of Glaciology* **46** (1): 215–221 DOI: 10.3189/172756407782871710

DeBeer CM, Wheater HS, Carey SK, Chun KP. 2016. Recent climatic, cryospheric, and hydrological changes over the interior of western Canada: a synthesis and review. *Hydrology and Earth System Sciences* **20**: 1573–1598 DOI: 10.5194/hess-20-1573-2016

Dee DP, Uppala SM, Simmons AJ, Berrisford P, Poli P, Kobayashi S, Andrae U, Balmaseda

MA, Balsamo G, Bauer P, et al. 2011. The ERA-Interim reanalysis: Configuration and performance of the data assimilation system. *Quarterly Journal of the Royal Meteorological Society* **137** (April): 553–597 DOI: 10.1002/qj.828

Demuth MN. 2013. Glacier mass balance observations for Peyto Glacier, Alberta, Canada (updated to 2012). Spatially Referenced Data Set contribution to the National Glacier-Climate Observing System, State and Evolution of Canada's Glaciers. *Geological Survey of Canada, Her Majesty the Queen in Right of Canada* Available at: http://pathways.geosemantica.net/WSHome.aspx?ws=NGP_SECG&locale=en-CA

Demuth MN, Hopkinson C. 2013. Glacier elevation data derived from Airborne Laser Terrain Mapper surveys over the reference monitoring glaciers of the Canadian Western and Northern Cordillera, August, 2006.

Demuth MN, Keller R. 2006. An assessment of the mass balance of Peyto glacier (1966-1995) and its relation to Recent and past-century climatic variability. In *Peyto Glacier: One Century of Science*, Demuth MN, , Munro DS, , Young GJ (eds).National Hydrology Research Institute: Saskatoon, Saskatchewan; 83–132.

Demuth MN, Pietroniro A. 2003. The impact of climate change on the glaciers of the Canadian Rocky Mountain eastern slopes and implications for water resource-related adaptation in the Canadian prairies "Phase I " - Headwaters of the North Saskatchewan River Basin Available at: http://www.parc.ca/pdf/research_publications/water1.pdf

Demuth MN, Munro DS, Young GJ (eds). 2006. *Peyto Glacier: one century of science*. National Hydrology Research Institute: Saskatoon, Saskatchewan.

Demuth MN, Pinard V, Pietroniro A, Luckman BH, Hopkinson C, Dornes P, Comeau L. 2008. Recent and past-century variations in the glacier resources of the Canadian Rocky Mountains: Nelson River system. *Terra glacialis* **11** (248): 27–52 Available at: http://scholar.ulethbridge.ca/hopkinson/files/demuthetal_tg11.pdf

Derksen C, Smith SL, Sharp M, Brown L, Howell S, Copland L, Mueller DR, Gauthier Y, Fletcher CG, Tivy A, et al. 2012. Variability and change in the Canadian cryosphere. *Climatic Change* **115** (1): 59–88 DOI: 10.1007/s10584-012-0470-0

Déry SJ, Tremblay L-B. 2004. Modeling the Effects of Wind Redistribution on the Snow Mass Budget of Polar Sea Ice*. *Journal of Physical Oceanography* **34** (1): 258–271 DOI: 10.1175/1520-0485(2004)034<0258:MTEOWR>2.0.CO;2

Déry SJ, Clifton A, MacLeod S, Beedle MJ. 2010. Blowing Snow Fluxes in the Cariboo Mountains of British Columbia, Canada. *Arctic, Antarctic, and Alpine Research* **42** (2): 188–197 DOI: 10.1657/1938-4246-42.2.188

Diolaiuti G, Maragno D, D'Agata C, Smiraglia C, Bocchiola D. 2011. Glacier retreat and climate change: Documenting the last 50 years of Alpine glacier history from area and geometry changes of Dosde Piazzi glaciers (Lombardy Alps, Italy). *Progress in Physical Geography* **35** (2): 161–182 DOI: 10.1177/0309133311399494

Donatelli M, Marletto V. 1994. Estimating surface solar radiation by means of air temperature. In *Proceedings of the 3rd Congress of the European Society for Agronomy*Padova, Italy; 352–353.

Doorschot J, Raderschall N, Lehning M. 2001. Measurements and one-dimensional model calculations of snow transport over a mountain ridge. *Annals of Glaciology* **32** (1): 153–158

Dornes PF, Pomeroy JW, Pietroniro A, Carey SK, Quinton WL. 2008. Influence of landscape aggregation in modelling snow-cover ablation and snowmelt runoff in a sub-arctic mountainous environment. *Hydrological Sciences Journal* **53** (4): 725–740 DOI: 10.1623/hysj.53.4.725

Dozier J. 1987. RecentR esearchin Snow Hydrology. *Reviews of Geophysics* **25** (2): 1983–1986

Dumanski S, Pomeroy JW, Westbrook CJ. 2015. Hydrological regime changes in a Canadian Prairie basin. *Hydrological Processes* **29** (18): 3893–3904 DOI: 10.1002/hyp.10567

Ellis CR, Pomeroy JW, Brown T, MacDonald J. 2010. Simulation of snow accumulation and melt in needleleaf forest environments. *Hydrology and Earth System Sciences* **14** (6): 925–940 DOI: 10.5194/hess-14-925-2010

Ellis CR, Pomeroy JW, Link TE. 2013. Modeling increases in snowmelt yield and desynchronization resulting from forest gap-thinning treatments in a northern mountain headwater basin. *Water Resources Research* **49** (2): 936–949 DOI: 10.1002/wrcr.20089

Elzhov T V., Mullen KM, Spiess A-N, Bolker B. 2016. minpack.lm: R Interface to the Levenberg-Marquardt Nonlinear Least-Squares Algorithm Found in MINPACK, Plus Support for Bounds Available at: https://cran.r-project.org/package=minpack.lm

Engelhardt M, Schuler T V., Andreassen LM. 2014. Contribution of snow and glacier melt to discharge for highly glacierised catchments in Norway. *Hydrology and Earth System Sciences* **18** (2): 511–523 DOI: 10.5194/hess-18-511-2014

Essery R, Etchevers P. 2004. Parameter sensitivity in simulations of snowmelt. *Journal of Geophysical Research* **109** (D20111): 1–15 DOI: 10.1029/2004JD005036

Essery R, Pomeroy J. 2004. Vegetation and topographic control of wind-blown snow distributions in distributed and aggregated simulations for an Arctic tundra basin. *Journal of Hydrometeorology* **5** (5): 735–744 DOI: 10.1175/1525-7541(2004)005<0735:VATCOW>2.0.CO;2

Fang X, Pomeroy JW. 2007. Snowmelt runoff sensitivity analysis to drought on the Canadian prairies. *Hydrological Processes* **21** (19): 2594–2609 DOI: 10.1002/hyp.6796

Fang X, Pomeroy JW. 2016. Impact of antecedent conditions on simulations of a flood in a mountain headwater basin. *Hydrological Processes* **30** (16): 2754–2772 DOI: 10.1002/hyp.10910

Fang X, Pomeroy JW, DeBeer CM, Harder P, Siemens E. 2019. Hydrometeorological data from Marmot Creek Research Basin, Canadian Rockies. *Earth System Science Data* **11** (2): 455–471 DOI: https://doi.org/10.5194/essd-11-455-2019

Fang X, Pomeroy JW, Ellis CR, MacDonald MK, DeBeer CM, Brown T. 2013. Multi-variable evaluation of hydrological model predictions for a headwater basin in the Canadian Rocky Mountains. *Hydrology and Earth System Sciences* **17** (4): 1635–1659 DOI: 10.5194/hess-17-1635-2013

Fang X, Pomeroy JW, Westbrook CJ, Guo X, Minke AG, Brown T. 2010. Prediction of snowmelt derived streamflow in a wetland dominated prairie basin. *Hydrology and Earth System Sciences* **14** (6): 991–1006 DOI: 10.5194/hess-14-991-2010

Finger D, Hugentobler A, Huss M, Voinesco A, Wernli H, Fischer D, Weber E, Jeannin P-Y, Kauzlaric M, Wirz A, et al. 2013. Identification of glacial meltwater runoff in a karstic environment and its implication for present and future water availability. *Hydrology and Earth System Sciences* **17** (8): 3261–3277 DOI: 10.5194/hess-17-3261-2013

Fountain AG, Tangborn W V. 1985. The effect of glaciers on streamflow variations. *Water Resources Research* **21** (4): 579–586 DOI: 10.1029/WR021i004p00579

Fujita K, Nuimura T. 2011. Spatially heterogeneous wastage of Himalayan glaciers. *Proceedings of the National Academy of Sciences* **108** (34): 14011–14014 DOI: 10.1073/pnas.1106242108

Fyffe CL, Brock BW, Kirkbride MP, Mair DWF, Arnold NS, Smiraglia C, Diolaiuti G, Diotri F.

2019. Do debris-covered glaciers demonstrate distinctive hydrological behaviour compared to clean glaciers? *Journal of Hydrology* **570** (January): 584–597 DOI: 10.1016/j.jhydrol.2018.12.069

Gallée H, Trouvilliez A, Agosta C, Genthon C, Favier V, Naaim-Bouvet F. 2012. Transport of Snow by the Wind: A Comparison Between Observations in Adélie Land, Antarctica, and Simulations Made with the Regional Climate Model MAR. *Boundary-Layer Meteorology* **146** (1): 133–147 DOI: 10.1007/s10546-012-9764-z

Gao B. 1996. NDWI—A normalized difference water index for remote sensing of vegetation liquid water from space. *Remote Sensing of Environment* **58** (3): 257–266 DOI: 10.1016/S0034-4257(96)00067-3

Garen DC, Marks D. 2005. Spatially distributed energy balance snowmelt modelling in a mountainous river basin: Estimation of meteorological inputs and verification of model results. *Journal of Hydrology* **315** (1–4): 126–153 DOI: 10.1016/j.jhydrol.2005.03.026

Garnier B, Ohmura A. 1968. A method of calculating the direct shortwave radiation income of slopes. *Journal of Applied Meteorology* **7**: 796–800

Giesen RH, Oerlemans J. 2012. Calibration of a surface mass balance model for global-scale applications. *The Cryosphere* **6** (6): 1463–1481 DOI: 10.5194/tc-6-1463-2012

Goodison B. 1972. *An Analysis of Climate and Runoff Events for Peyto Glacier, Alberta*. Environment Canada: Ottawa, Canada.

Granger RJ, Gray DM. 1989. Evaporation from natural nonsaturated surfaces. *Journal of Hydrology* **111** (1–4): 21–29 DOI: 10.1016/0022-1694(89)90249-7

Granger RJ, Pomeroy JW. 1997. Sustainability of the western Canadian boreal forest under changing hydrological conditions . II . Summer energy and water use. In *Sustainability of Water Resources under Increasing Uncertainty*, Rosjberg D, , Boutayeb N, , Gustard A, , Kundzewicz Z, , Rasmussen P (eds).IAHS Publ. No. 240; 243–249.

Gray DM, Landine PG. 1988a. An energy-budget snowmelt model for the Canadian Prairies. *Canadian Journal of Earth Sciences* **25**: 1292–1303 DOI: 10.1139/e88-124

Gray DM, Landine PG. 1988b. An energy-budget snowmelt model for the Canadian Prairies. *Canadian Journal of Earth Sciences* **25** (8): 1292–1303 DOI: 10.1139/e88-124

Gudmundsson L. 2016. qmap: Statistical transformations for post-processing climate model output. R package version 1.0-4. *R package version 1.0-4*

Guðmundsson S, Björnsson H, Pálsson F, Haraldsson HH. 2009. Comparison of energy balance and degree-day models of summer ablation on the Langjökull ice cap, SW-Iceland. *Jokull* **59**: 1–18

Haeberli W, Hoelzle M, Paul F, Zemp M, Zu C. 2007. Integrated monitoring of mountain glaciers as key indicators of global climate change : the European Alps. *Annals of Glaciology* **46**: 150–160

Hall DK, Riggs GA, Salomonson V V, DiGirolamo NE, Bayr KJ. 2002. MODIS snow-cover products. *Remote Sensing of Environment* **83** (1–2): 181–194 DOI: 10.1016/S0034-4257(02)00095-0

Hannah DM, Gurnell AM. 2001. A conceptual, linear reservoir runoff model to investigate melt season changes in cirque glacier hydrology. *Journal of Hydrology* **246** (1–4): 123–141 DOI: 10.1016/S0022-1694(01)00364-X

Harder P, Pomeroy JW. 2013. Estimating precipitation phase using a psychrometric energy balance method. *Hydrological Processes* **27** (May): 1901–1914 DOI: 10.1002/hyp.9799

Hargreaves GH, Samani ZA. 1982. Estimating potential evapotranspiration. *J. Irrig. Drain. Eng. ASCE* **108** (3): 225–230

Hargreaves GL, Hargreaves GH, Riley JP. 1985. Irrigation water requirements for Senegal River basin. *J. Irrig. Drain. Eng.* **111**: 265–275

Hirabayashi Y, Döll P, Kanae S. 2010. Global-scale modeling of glacier mass balances for water resources assessments: Glacier mass changes between 1948 and 2006. *Journal of Hydrology* **390** (3–4): 245–256 DOI: 10.1016/j.jhydrol.2010.07.001

Hock R. 1999. A distributed temperature-index ice- and snowmelt model including potential direct solar radiation. *Journal of Glaciology* **45** (149): 101–111

Hock R. 2003. Temperature index melt modelling in mountain areas. *Journal of Hydrology* **282**: 104–115 DOI: 10.1016/S0022-1694(03)00257-9

Hock R. 2005. Glacier melt: a review of processes and their modelling. *Progress in Physical Geography* **29** (3): 362–391 DOI: 10.1191/0309133305pp453ra

Hock R, Holmgren B. 2005. A distributed surface energy-balance model for complex topography and its application to Storglaciaren, Sweden. *Journal of Glaciology* **51** (172): 25–36

Holdsworth G, Demuth MN, Beck. TMH. 2006. Radar measurements of ice thickness on Peyto Glacier. In *Peyto Glacier: One Century of Science*, Demuth MN, , Munro DS, , Young GJ

(eds).National Hydrology Research Institute Science Report 8: Saskatoon, Saskatchewan; 59–82.

Hood E, Berner L. 2009. Effects of changing glacial coverage on the physical and biogeochemical properties of coastal streams in southeastern Alaska. *Journal of Geophysical Research* **114** (G3): G03001 DOI: 10.1029/2009JG000971

Hopkinson C, Demuth MN. 2006. Using airborne lidar to assess the influence of glacier downwasting on water resources in the Canadian Rocky Mountains. *Canadian Journal of Remote Sensing* **32** (2): 211–232

Hopkinson C, Young GJ. 1998. The effect of glacier wastage on the flow of the Bow River at Banff, Alberta, 1951-1993. *Hydrological Processes* **12** (10–11): 1745–1762 DOI: 10.1002/(SICI)1099-1085(199808/09)12:10/11<1745::AID-HYP692>3.0.CO;2-S

Hopkinson C, Chasmer L, Munro S, Demuth MN. 2010. The influence of DEM resolution on simulated solar radiation-induced glacier melt. *Hydrological Processes* **24** (6): 775–788 DOI: 10.1002/hyp.7531

Huss M. 2011. Present and future contribution of glacier storage change to runoff from macroscale drainage basins in Europe. *Water Resources Research* **47** (May): 1–14 DOI: 10.1029/2010WR010299

Huss M, Farinotti D, Bauder A, Funk M. 2008. Modelling runoff from highly glacierized alpine drainage basins in a changing climate. *Hydrological Processes* **22** (19): 3888–3902 DOI: 10.1002/hyp.7055

Hynčica M, Huth R. 2019. Long-term changes in precipitation phase in Europe in cold half year. *Atmospheric Research* DOI: 10.1016/j.atmosres.2019.04.032

Immerzeel WW, van Beek LPH, Bierkens MFP. 2010. Climate change will affect the Asian water towers. *Science (New York, N.Y.)* **328** (5984): 1382–5 DOI: 10.1126/science.1183188

Immerzeel WW, van Beek LPH, Konz M, Shrestha AB, Bierkens MFP. 2012. Hydrological response to climate change in a glacierized catchment in the Himalayas. *Climatic Change* **110**: 721–736 DOI: 10.1007/s10584-011-0143-4

Immerzeel WW, Pellicciotti F, Bierkens MFP. 2013. Rising river flows throughout the twenty-first century in two Himalayan glacierized watersheds. *Nature Geoscience* **6** (9): 742–745 DOI: 10.1038/ngeo1896

IPCC. 2007. Working Group II: Impacts, Adaptation and Vulnerability, IPCC Fourth

Assessment Report: Climate Change Available at: http://www.ipcc.ch/publications_and_data/ar4/wg2/en/ch3s3-5-1.html#box-3-1

Jansson P, Hock R, Schneider T. 2003. The concept of glacier storage: a review. *Journal of Hydrology* **282** (1–4): 116–129 DOI: 10.1016/S0022-1694(03)00258-0

Johnson PG, Power JM. 1985. Flood and landslide events, Peyto Glacier terminus, Alberta, Canada, 11-14 July 1983. *Journal of Glaciology* **31** (108): 86–91

Jones PD, Harpham C, Troccoli A, Gschwind B, Ranchin T, Wald L, Goodess CM, Dorling S. 2017. Using ERA-Interim reanalysis for creating datasets of energy-relevant climate variables. *Earth System Science Data* **9** (2): 471–495 DOI: 10.5194/essd-9-471-2017

Karmalkar A V, Bradley RS, Diaz HF. 2011. Climate change in Central America and Mexico: regional climate model validation and climate change projections. *Climate Dynamics* **37** (3–4): 605–629 DOI: 10.1007/s00382-011-1099-9

Kaser G, Hardy DR, Mölg T, Bradley RS, Hyera TM, Molg T, Bradley RS, Hyera TM. 2004. Modern glacier retreat on Kilimanjaro as evidence of climate change: observations and facts. *International Journal of Climatology* **24** (3): 329–339 DOI: 10.1002/joc.1008

Kaser G, Juen I, Georges C, Gómez J, Tamayo W. 2003. The impact of glaciers on the runoff and the reconstruction of mass balance history from hydrological data in the tropical Cordillera Bianca, Perú. *Journal of Hydrology* **282** (1–4): 130–144 DOI: 10.1016/S0022-1694(03)00259-2

Kehrl LM, Hawley RL, Osterberg EC, Winski DA, Lee AP. 2014. Volume loss from lower Peyto Glacier, Alberta, Canada, between 1966 and 2010. *Journal of Glaciology* **60** (219): 51–56 DOI: 10.3189/2014JoG13J039

Kienzle SW, Nemeth MW, Byrne JM, Macdonald RJ. 2012. Simulating the hydrological impacts of climate change in the upper North Saskatchewan River basin, Alberta, Canada. *Journal of Hydrology* **412**–**413**: 76–89 DOI: 10.1016/j.jhydrol.2011.01.058

Klok EJL, Oerlemans J. 2002. Model study of the spatial distribution of the energy and mass balance of Morteratschgletscher, Switzerland. *Journal of Glaciology* **48** (163): 505–518 DOI: 10.3189/172756502781831133

Kohler T, Maselli D (eds). 2009. *Mountains and Climate Change - From Understanding to Action*. Geographica Bernensia with the support of the Swiss Agency for Development and Cooperation (SDC), and an international team of contributors: Bern. Available at:

https://boris.unibe.ch/36553/1/Fullversion_low_Mountains_and _Climate_Change.pdf

Krogh SA, Pomeroy JW. 2018. Recent changes to the hydrological cycle of an Arctic basin at the tundra-taiga transition. *Hydrology and Earth System Sciences* **22**: 3993–4014 DOI: 10.5194/hess-22-3993-2018

Krogh SA, Pomeroy JW, Marsh P. 2017. Diagnosis of the hydrology of a small Arctic basin at the tundra-taiga transition using a physically based hydrological model. *Journal of Hydrology* **550**: 685–703 DOI: 10.1016/j.jhydrol.2017.05.042

Krogh SA, Pomeroy JW, McPhee J. 2015. Physically Based Mountain Hydrological Modeling Using Reanalysis Data in Patagonia. *Journal of Hydrometeorology* **16**: 172–193 DOI: 10.1175/JHM-D-13-0178.1

Lafrenière M, Sharp M. 2003. Wavelet analysis of inter-annual variability in the runoff regimes of glacial and nival stream catchments, Bow Lake, Alberta. *Hydrological Processes* **17** (6): 1093–1118 DOI: 10.1002/hyp.1187

Leavesley G, Lichty R, Troutman B, Saindon L. 1983. Precipitation-runoff modelling system: user's manual.

Letréguilly A. 1988. Relation between the mass balance of western Canadian mountain glaciers and meteorological data. *Journal of Glaciology* **34** (116): 11–18

Letréguilly A, Reynaud L. 1989. Spatial patterns of mass-balance fluctuations of North American glaciers. *Journal of Glaciology* **35** (120): 163–168

Li H, Beldring S, Xu C-Y, Huss M, Melvold K, Jain SK. 2015. Integrating a glacier retreat model into a hydrological model – Case studies of three glacierised catchments in Norway and Himalayan region. *Journal of Hydrology* **527**: 656–667 DOI: 10.1016/j.jhydrol.2015.05.017

Liang S. 2000. Narrowband to broadband conversions of land surface albedo: I. Algorithms. *Remote Sensing of Environment* **76**: 213–238 DOI: 10.1016/S0034-4257(00)00205-4

Liston GE, Elder K. 2006. A distributed snow-evolution modeling system (SnowModel). *Journal of Hydrometeorology* **7**: 1259–1276

Liston GE, Hiemstra CA. 2011. The Changing Cryosphere: Pan-Arctic Snow Trends (1979–2009). *Journal of Climate* **24** (21): 5691–5712 DOI: 10.1175/JCLI-D-11-00081.1

López-Moreno JI, Boike J, Sanchez-Lorenzo A, Pomeroy JW. 2016. Impact of climate warming on snow processes in Ny-Ålesund, a polar maritime site at Svalbard. *Global and Planetary*

Change **146**: 10–21 DOI: 10.1016/j.gloplacha.2016.09.006

Luo Y, Arnold J, Liu S, Wang X, Chen X. 2013. Inclusion of glacier processes for distributed hydrological modeling at basin scale with application to a watershed in Tianshan Mountains, northwest China. *Journal of Hydrology* **477**: 72–85 DOI: 10.1016/j.jhydrol.2012.11.005

Lutz AF, Immerzeel WW, Shrestha AB, Bierkens MFP. 2014. Consistent increase in High Asia's runoff due to increasing glacier melt and precipitation. *Nature Climate Change* **4** (7): 587–592 DOI: 10.1038/nclimate2237

MacDonald MK, Pomeroy JW, Pietroniro A. 2009a. Parameterizing redistribution and sublimation of blowing snow for hydrological models: tests in a mountainous subarctic catchment. *Hydrological Processes* **23** (18): 2570–2583 DOI: 10.1002/hyp.7356

MacDonald MK, Pomeroy JW, Pietroniro A. 2010. On the importance of sublimation to an alpine snow mass balance in the Canadian Rocky Mountains. *Hydrology and Earth System Sciences* **14** (7): 1401–1415 DOI: 10.5194/hess-14-1401-2010

MacDonald RJ, Byrne JM, Kienzle SW. 2009b. A Physically Based Daily Hydrometeorological Model for Complex Mountain Terrain. *Journal of Hydrometeorology* **10**: 1430–1446 DOI: 10.1175/2009JHM1093.1

Magnusson J, Farinotti D, Jonas T, Bavay M. 2011. Quantitative evaluation of different hydrological modelling approaches in a partly glacierized Swiss watershed. *Hydrological Processes* **2084** (February): 2071–2084 DOI: 10.1002/hyp.7958

Male DH, Granger RJ. 1981. Snow surface energy exchange. *Water Resources Research* **17** (3): 609–627 DOI: 10.1029/WR017i003p00609

Malecki J. 2015. Snow Accumulation on a Small High-Arctic Glacier Svenbreen: Variability and Topographic Controls. *Geografiska Annaler, Series A: Physical Geography* **97** (4): 809–817 DOI: 10.1111/geoa.12115

Marks D, Dozier J. 1992. Climate and energy exchange at the snow surface in the alpine region of the Sierra Nevada. *Water Resources Research* **28** (92): 3043–3054

Marks D, Domingo J, Susong D, Link T, Garen D. 1999. A spatially distributed energy balance snowmelt model for application in mountain basins. *Hydrological Processes* **13**: 1935–1959 DOI: 10.1002/(SICI)1099-1085(199909)13:12/13<1935::AID-HYP868>3.0.CO;2-C

Marks D, Kimball J, Tingey D, Link T. 1998a. The sensitivity of snowmelt processes to climate

conditions and forest cover during rain-on-snow: a case study of the 1996 Pacific Northwest flood. *Hydrological Processes* **12** (March): 1569–1587 DOI: 10.3189/172756401781819751

Marks D, Kimball J, Tingey D, Link T. 1998b. The sensitivity of snowmelt processes to climate conditions and forest cover during rain-on-snow: a case study of the 1996 Pacific Northwest flood. *Hydrological Processes* **12** (10–11): 1569–1587 DOI: 10.1002/(SICI)1099-1085(199808/09)12:10/11<1569::AID-HYP682>3.0.CO;2-L

Marks D, Winstral A, Flerchinger G, Reba M, Pomeroy J, Link T, Elder K. 2008. Comparing Simulated and Measured Sensible and Latent Heat Fluxes over Snow under a Pine Canopy to Improve an Energy Balance Snowmelt Model. *Journal of Hydrometeorology* **9** (6): 1506–1522 DOI: 10.1175/2008JHM874.1

Marks D, Winstral A, Seyfried M. 2002. Simulation of terrain and forest shelter effects on patterns of snow deposition, snowmelt and runoff over a semi-arid mountain catchment. *Hydrological Processes* **16** (18): 3605–3626 DOI: 10.1002/hyp.1237

Marsh CB, Pomeroy JW, Spiteri RJ. 2012. Implications of mountain shading on calculating energy for snowmelt using unstructured triangular meshes. *Hydrological Processes* **26** (June): 1767–1778 DOI: 10.1002/hyp.9329

Marshall SJ, White EC, Demuth MN, Bolch T, Wheate R, Menounos B, Beedle MJ, Shea JM. 2011. Glacier Water Resources on the Eastern Slopes of the Canadian Rocky Mountains. *Canadian Water Resources Journal* **36** (March 2010): 109–134 DOI: 10.4296/cwrj3602823

Matulla C, Watson E, Sch W. 2009. Downscaled GCM projections of winter and summer mass balance for Peyto Glacier, Alberta, Canada (2000 – 2100) from ensemble simulations with ECHAM5-MPIOM. *America* **1559** (December 2008): 1550–1559 DOI: 10.1002/joc

Mauricio Z-B. 2014. hydroGOF: Goodness-of-fit functions for comparison of simulated and observed hydrological time series Available at: https://cran.r-project.org/package=hydroGOF

McFeeters SK. 1996. The use of the Normalized Difference Water Index (NDWI) in the delineation of open water features. *International Journal of Remote Sensing* **17** (7): 1425–1432 DOI: 10.1080/01431169608948714

Meek V. 1948. Glacier observations in the Canadian Cordillera Available at: https://wgms.ch/downloads/published/former_data_reports/Meek_IAHS30_1948.pdf

Meier MF, Dyurgerov MB. 2002. Sea level changes. How Alaska affects the world. *Science (New York, N.Y.)* **297** (5580): 350–1 DOI: 10.1126/science.1073591

Mernild SH, Liston GE, Hasholt B. 2007. Snow-distribution and melt modelling for glaciers in Zackenberg river drainage basin , north-eastern Greenland. *Hydrological Processes* **21**: 3249–3263 DOI: 10.1002/hyp.6500

Mernild SH, Liston GE, Kane DL, Knudsen NT, Hasholt B. 2008. Snow, runoff, and mass balance modeling for the entire Mittivakkat Glacier (1998–2006), Ammassalik Island, SE Greenland. *Geografisk Tidsskrift-Danish Journal of Geography* **108** (1): 121–136 DOI: 10.1080/00167223.2008.10649578

Mesinger F, DiMego G, Kalnay E, Mitchell K, Shafran PC, Ebisuzaki W, Jović D, Woollen J, Rogers E, Berbery EH, et al. 2006. North American Regional Reanalysis. *Bulletin of the American Meteorological Society* **87** (March): 343–360 DOI: 10.1175/BAMS-87-3-343

Meza F, Varas E. 2000. Estimation of mean monthly solar global radiation as a function of temperature. *Agricultural and Forest Meteorology* **100**: 231–241 DOI: 10.1016/S0168-1923(99)00090-8

Mo R, Ye C, Whitfield PH. 2014. Application Potential of Four Nontraditional Similarity Metrics in Hydrometeorology. *Journal of Hydrometeorology* **15** (5): 1862–1880 DOI: 10.1175/JHM-D-13-0140.1

Moore RD, Demuth MN. 2001. Mass balance and streamflow variability at Place Glacier, Canada, in relation to recent climate fluctuations. *Hydrological Processes* **15** (18): 3473–3486 DOI: 10.1002/hyp.1030

Moore RD, Fleming SW, Menounos B, Wheate R, Fountain A, Stahl K, Holm K, Jakob M. 2009. Glacier change in western North America : influences on hydrology , geomorphic hazards and water quality. *Hydrological Processes* **23**: 42–61 DOI: 10.1002/hyp.7162

Mote PW, Hamlet AF, Clark MP, Lettenmaier DP. 2005. Declining Mountain Snowpack in Western North America*. *Bulletin of the American Meteorological Society* **86** (1): 39–49 DOI: 10.1175/BAMS-86-1-39

Munro DS. 2000. Progress in glacier hydrology : a Canadian perspective. *Hydrological Processes* **14**: 1627–1640

Munro DS. 2004. Revisiting bulk heat transfer on Peyto Glacier, Alberta, Canada, in light of the OG parameterization. *Journal of Glaciology* **50** (171): 590–600 DOI:

10.3189/172756504781829819

Munro DS. 2011a. Peyto Creek hydrometeorological database (Peyto Creek Base Camp AWS). *IP3 Archive* Available at: www.usask.ca/ip3/data

Munro DS. 2011b. Delays of supraglacial runoff from differently defined microbasin areas on the Peyto Glacier. *Hydrological Processes* **25**: 2983–2994 DOI: 10.1002/hyp.8124

Munro DS. 2013. Creating a Runoff Record for an Ungauged Basin: Peyto Glacier, 2002-2007. In *Putting Prediction in Ungauged Basins into Practice*, Pomeroy JW, , Spence C, , Whitfield PH (eds).Canadian Water Resources Association; 197–204. Available at: http://cwra.org/en/resource-center/publications/bookstore/20-publications/245-putting-prediction-in-ungauged-basins-into-practice

Munro DS, Marosz-Wantuch M. 2009. Modeling Ablation on Place Glacier, British Columbia, from Glacier and Off-glacier Data Sets. *Arctic, Antarctic, and Alpine Research* **41** (2): 246–256 DOI: 10.1657/1938-4246-41.2.246

Munro DS, Young GJ. 1982a. An Operational Net Shortwave Radiation Model for Glacier Basins The model is based upon cioud reflectivity and. *Water Resources Research* **18** (2): 220–230

Munro DS, Young GJ. 1982b. An operational net shortwave radiation model for glacier basins. *Water Resources Research* **18** (2): 220–230 DOI: 10.1029/WR018i002p00220

Nash JE, Sutcliffe J V. 1970. River flow forecasting through conceptual models part I - A discussion of principles. *Journal of Hydrology* **10** (3): 282–290 DOI: 10.1016/0022-1694(70)90255-6

Natural Resources Canada. 1986. The Canadian Digital Elevation Model (CDEM)

Natural Resources Canada. 2000. The Canadian Digital Surface Model (CDSM)

Naz BS, Frans CD, Clarke GKC, Burns P, Lettenmaier DP. 2014. Modeling the effect of glacier recession on streamflow response using a coupled glacio-hydrological model. *Hydrology and Earth System Sciences* **18** (2): 787–802 DOI: 10.5194/hess-18-787-2014

Oerlemans J. 1989. On the response of valley glaciers to climate change. In *Glacier Fluctuations of Climate Change*, Oerlemans J (ed.).Kluwer Academic Publishers; 353–371.

Oerlemans J. 1991. A model for the surface balance of ice masses: part I. Alpine glaciers. *Zeitschrift fur Gletscherkunde und Glazialgeologie* **27/28**: 63–83

Oerlemans J. 2001. *Glaciers and Climate Change*. A.A. Balkema Publishers: Lisse.

Oerlemans J. 2005. Extracting a Climate Signal from 169 Glacier Records. *Science* **308**: 675–677 DOI: 10.1126/science.1107046

Oerlemans J, Knap WH. 1998. A 1 year record of global radiation and albedo in the ablation zone of Morteratschgletscher, Switzerland. *Journal of Glaciology* **44** (147): 231–238

Oerlemans J, Giesen RH, Van Den Broeke MR. 2009. Retreating alpine glaciers: Increased melt rates due to accumulation of dust (Vadret da Morteratsch, Switzerland. *Journal of Glaciology* **55** (192): 729–736 DOI: 10.3189/002214309789470969

Oerter H, Baker D, Moser H, Reinwarth O. 1981. Glacial-hydrological investigations at the Vernagtferner Glacier as a basis for a discharge model. *Nordic Hydrology* **12** (Reinwarth 1972): 335–348

Ohmura A. 2006. Changes in mountain glaciers and ice caps during the 20th century. *Annals of Glaciology* **43** (1): 361–368 DOI: 10.3189/172756406781812212

Ommanney CSL. 1972. Glacier Surveys by District Personnel of the Water Survey of Canada 2. Peyto Glacier. Glacier Inventory Note No. 7. Ottawa, Canada.

Ommanney CSL. 1987. Peyto Glacier: A Compendium of Information Prepared for Parks Canada. Saskatoon, Saskatchewan, S7N 3H5.

Ommanney CSL. 2002. Glaciers of North America — Glaciers of Canada: Glaciers of the Canadian Rockies. In *Satellite Image Atlas of Glaciers of the World*, Williams RS, , Ferrigno JG (eds).J199–J289.

Østrem G. 1966. Mass Balance Studies on Glaciers in Western Canada, 1965. *geographical Bulletin* **8** (1): 81–107

Østrem G. 1973. The transient snowline and glacier mass balance in Southern British Columbia and Alberta, Canada. *Geograpfiska Annaler* **55A** (2): 93–106

Pan X, Yang D, Li Y, Barr A, Helgason W, Hayashi M, Marsh P, Pomeroy J, Janowicz RJ, Li Y. 2016. Bias corrections of precipitation measurements across experimental sites in different ecoclimatic regions of western Canada. *Cryosphere* **10** (June): 2347–2360 DOI: 10.5194/tc-2016-122

Van Pelt W, Kohler J. 2015. Modelling the long-term mass balance and firn evolution of glaciers around Kongsfjorden, Svalbard. *Journal of Glaciology* **61** (228): 731–744 DOI: 10.3189/2015JoG14J223

Plüss C, Ohmura A. 1997. Longwave radiation on snow-covered mountainous surfaces. *Journal*

of Applied Meteorology **36**: 818–824 DOI: 10.1175/1520-0450-36.6.818

Pomeroy JW. 1989. A process-based model of snow drifting. *Annals of Glaciology* **13** (January 1988): 237–240

Pomeroy JW, Gray DM. 1995. *Snowcover: accumulation, relocation and management*. National Hydrology Research Institute: Saskatoon, Saskatchewan.

Pomeroy JW, Li L. 2000. Prairie and arctic areal snow cover mass balance using a blowing snow model. *Journal of Geophysical Research* **105** (D21): 26619–26634 DOI: 10.1029/2000JD900149

Pomeroy JW, Fang X, Marks DG. 2016. The Cold Rain-on-Snow Event of June 2013 in the Canadian Rockies – Characteristics and Diagnosis. *Hydrological Processes* (June 2013) DOI: 10.1002/hyp.10905

Pomeroy JW, Fang X, Rasouli K. 2015. Sensitivity of snow processes to warming in the Canadian Rockies. *72nd Eastern Snow Conference, Sherbrooke, Quebec, Canada*: 22–33

Pomeroy JW, Fang X, Shook K, Whitfield PH. 2013. Predicting in ungauged basins using physical principles obtained using the deductive, inductive, and abductive reasoning approach. In *Putting Prediction in Ungauged Basins into Practice*, Pomeroy JW, , Spence C, , Whitfield PH (eds).Canadian Water Resources Association; 41–62. Available at: https://www.cwra.org/images/BookstorePDFs/2014PuttingPredictioninUngaugedBasinsinPractice/Putting Prediction in Ungauged Basins into Practice_Complete Publication 14-02-11.pdf

Pomeroy JW, Gray DM, Brown T, Hedstrom NR, Quinton WL, Granger RJ, Carey SK. 2007. The cold regions hydrological model: a platform for basing process representation and model structure on physical evidence. *Hydrological Processes* **21** (19): 2650–2667 DOI: 10.1002/hyp.6787

Pomeroy JW, Gray DM, Landline PG. 1993. The Prairie Blowing Snow Model: characteristics, validation, operation. *Journal of Hydrology* **144**: 165–192 DOI: 10.1016/0022-1694(93)90171-5

Pomeroy JW, Gray DM, Shook KR, Toth B, Essery RLH, Pietroniro A, Hedstrom N. 1998. An evaluation of snow accumulation and ablation processes for land surface modelling. *Hydrological Processes* **12** (15): 2339–2367 DOI: 10.1002/(SICI)1099-1085(199812)12:15<2339::AID-HYP800>3.0.CO;2-L

Pomeroy JW, Marsh P, Gray DM. 1997. Application of a distributed blowing snow model to the Arctic. *Hydrological Processes* **11**: 1451–1464 DOI: 10.1002/(SICI)1099-1085(199709)11:11<1451::AID-HYP449>3.3.CO;2-H

Poulin A, Brissette F, Leconte R, Arsenault R, Malo J. 2011. Uncertainty of hydrological modelling in climate change impact studies in a Canadian , snow-dominated river basin. *Journal of Hydrology* **409** (3–4): 626–636 DOI: 10.1016/j.jhydrol.2011.08.057

Pradhananga D, Pomeroy JW. 2020. Glacier Hydrology Model in the Cold Regions Hydrological Modelling platform. *Manuscript in preparation*

R Core Team. 2017. R: A language and environment for statistical computing

Radić V, Hock R. 2011. Regionally differentiated contribution of mountain glaciers and ice caps to future sea-level rise. *Nature Geoscience* **4** (2): 91–94 DOI: 10.1038/ngeo1052

Rahimikhoob A. 2010. Estimating global solar radiation using artificial neural network and air temperature data in a semi-arid environment. *Renewable Energy* **35** (9): 2131–2135 DOI: 10.1016/j.renene.2010.01.029

Rasouli K, Pomeroy JW, Janowicz JR, Carey SK, Williams TJ. 2014. Hydrological sensitivity of a northern mountain basin to climate change. *Hydrological Processes* **28** (14): 4191–4208 DOI: 10.1002/hyp.10244

Rasouli K, Pomeroy JW, Janowicz JR, Williams TJ, Carey SK. 2019a. A long-term hydrometeorological dataset (1993-2014) of a northern mountain basin: Wolf Creek Research Basin, Yukon Territory, Canada. *Earth System Science Data* **11**: 89–100 DOI: 10.5194/essd-11-89-2019

Rasouli K, Pomeroy JW, Marks DG. 2015. Snowpack sensitivity to perturbed climate in a cool mid-latitude mountain catchment. *Hydrological Processes* **29** (18): 3925–3940 DOI: 10.1002/hyp.10587

Rasouli K, Pomeroy JW, Whitfield PH. 2019b. Hydrological responses of headwater basins to monthly perturbed climate in the North American Cordillera. *Journal of Hydrometeorology* **20** (5): 863–882 DOI: 10.1175/JHM-D-18-0166.1

Reba ML, Marks D, Seyfried M, Winstral A, Kumar M, Flerchinger G. 2011. A long-term data set for hydrologic modeling in a snow-dominated mountain catchment. *Water Resources Research* **47** (7): 1–7 DOI: 10.1029/2010WR010030

Reba ML, Pomeroy JW, Marks D, Link TE. 2012. Estimating surface sublimation losses from

snowpacks in a mountain catchment using eddy covariance and turbulent transfer calculations. *Hydrological Processes* **26** (24): 3699–3711 DOI: 10.1002/hyp.8372

Réveillet M, Vincent C, Six D, Rabatel A. 2017. Which empirical model is best suited to simulate glacier mass balances? *Journal of Glaciology* **63** (237): 39–54 DOI: 10.1017/jog.2016.110

Reynolds JR, Young GJ. 1997. Changes in areal extent, elevation and volume of Athabasca Glacier, Alberta, Canada, as estimated from a series of maps produced between 1919 and 1979. *Annals of Glaciology* **24**: 60–65

Riedel JL, Wilson S, Baccus W, Larrabee M, Fudge TJ, Fountain A, Riedel CJL. 2015. Glacier status and contribution to streamflow in the Olympic Mountains , Washington , USA. *Journal of Glaciology* **61** (225): 8–16 DOI: 10.3189/2015JoG14J138

Rienecker MM, Suarez MJ, Gelaro R, Todling R, Bacmeister J, Liu E, Bosilovich MG, Schubert SD, Takacs L, Kim GK, et al. 2011. MERRA: NASA's modern-era retrospective analysis for research and applications. *Journal of Climate* **24** (14): 3624–3648 DOI: 10.1175/JCLI-D-11-00015.1

Rood S, Pan J, Gill K, Franks C, Samuelson G, Shepherd A. 2008. Declining summer flows of Rocky Mountain rivers: Changing seasonal hydrology and probable impacts on floodplain forests. *Journal of Hydrology* **349** (3–4): 397–410 DOI: 10.1016/j.jhydrol.2007.11.012

RStudio. 2017. RStudio: Integrated development environment for R (Version 1.0.143) Available at: http://www.rstudio.org/

Saha S, Moorthi S, Pan HL, Wu X, Wang J, Nadiga S, Tripp P, Kistler R, Woollen J, Behringer D, et al. 2010. The NCEP climate forecast system reanalysis. *Bulletin of the American Meteorological Society* **91** (8): 1015–1057 DOI: 10.1175/2010BAMS3001.1

Salzmann N, Huggel C, Rohrer M, Stoffel M. 2014. Data and knowledge gaps in glacier, snow and related runoff research - A climate change adaptation perspective. *Journal of Hydrology* **518**: 225–234 DOI: 10.1016/j.jhydrol.2014.05.058

Samani Z. 2000. Estimating solar radiation and evapotranspiration using minimum climatological data. *Journal of Irrigation and Drainage Engineering* **126** (4): 265–267

Samani Z, Asce M, Hargreaves G, Asce F, Tran V, Bawazir S. 2011. Estimating Solar Radiation from Temperature with Spatial and Temporal Calibration. *Journal of Irrigation and Drainage Engineering* **137** (11): 692–696 DOI: 10.1061/(ASCE)IR.1943-4774.0000342.

Schiefer E, Menounos B, Wheate R. 2007. Recent volume loss of British Columbian glaciers, Canada. *Geophysical Research Letters* **34** (16): 1–6 DOI: 10.1029/2007GL030780

Sedgwick JK, Henoch WES. 1975. 1966 Peyto Glacier Map, Banff National Park, Alberta. Environment Canada, IWD 1010, 1:10,000.

Sentlinger G, Fraser J, Baddock E. 2019. Salt Dilution Flow Measurement: Automation and Uncertainty. In *HydroSenSoft, International Symposium and Exhibition on Hydro-Environment Sensors and Software.* 8. Available at: http://www.fathomscientific.com/wp-content/uploads/2018/12/HydroSense_AutoSalt_2019_V0.6.pdf [Accessed 31 August 2019]

Seyfried MS. 2003. Distribution and Application of Research Watershed Data. In *First Interagency Conference on Research in the Watersheds.*, Renard K, , McElroy S, , Gburek W, , Canfield H, , Scott R (eds).USDA-ARS: Benson: AZ; 573–578.

Shannon S, Smith R, Wiltshire A, Payne T, Huss M, Betts R, Koutroulis A, Jones D, Harrison S. 2019. Global glacier volume projections under high-end climate change scenarios. *The Cryosphere* **13**: 325–350 DOI: 10.5194/tc-13-325-2019

Shea JM. 2010. Regional-Scale Distributed Modelling of Glacier Meteorology and Melt, southern Coast Mountains, Canada.University of British Columbia.

Shea JM. 2016. Meteorological data from Kyanging automatic weather station. *ICIMOD, Kathmandu, Nepal* Available at: http://rds.icimod.org/ [Accessed 1 January 2019]

Shea JM, Marshall SJ. 2007. Atmospheric flow indices, regional climate, and glacier mass balance in the Canadian Rocky Mountains. *International Journal of Climatology* **27**: 233–247 DOI: 10.1002/joc.1398

Shea JM, Immerzeel WW, Wagnon P, Vincent C, Bajracharya S. 2015a. Modelling glacier change in the Everest region, Nepal Himalaya. *The Cryosphere* **9** (3): 1105–1128 DOI: 10.5194/tc-9-1105-2015

Shea JM, Moore RD, Stahl K. 2009. Derivation of melt factors from glacier mass-balance records in western Canada. *Journal of Glaciology* **55** (189): 123–130 DOI: 10.3189/002214309788608886

Shea JM, Wagnon P, Immerzeel WW, Biron R, Brun F, Pellicciotti F. 2015b. A comparative high-altitude meteorological analysis from three catchments in the Nepalese Himalaya. *International Journal of Water Resources Development* **31** (2): 174–200 DOI: 10.1080/07900627.2015.1020417

Shook K. 2015. MSCr: Downloads daily and hourly MSC data from the webserver. Reads in monthly, daily and hourly MSC data from files. Available at: www.usask.ca/hydrology

Shook K. 2016a. CRHMr: pre- and post- processing for the Cold Regions Hydrological Modelling (CRHM) platform Available at: https://github.com/CentreForHydrology/CRHMr [Accessed 8 January 2019]

Shook K. 2016b. Reanalysis: Creates Cold Regions Hydrological Modelling (CRHM) platform observations files from reanalysis data. Available at: www.usask.ca/hydrology/RPkgs.php/

Shook K, Pomeroy J. 2011. Synthesis of incoming shortwave radiation for hydrological simulation. *Hydrology Research* **42** (6): 433 DOI: 10.2166/nh.2011.074

Sicart JE, Espinoza JC, Quéno L, Medina M. 2015. Radiative properties of clouds over a tropical Bolivian glacier: seasonal variations and relationship with regional atmospheric circulation. *International Journal of Climatology* **36**: 3116–3128 DOI: 10.1002/joc.4540

Sicart JE, Pomeroy JW, Essery RLH, Bewley D. 2006. Incoming longwave radiation to melting snow: observations, sensitivity and estimation in Northern environments. *Hydrological Processes* **20** (17): 3697–3708 DOI: 10.1002/hyp.6383

Singh P, Bengtsson L. 2005. Impact of warmer climate on melt and evaporation for the rainfed, snowfed and glacierfed basins in the Himalayan region. *Journal of Hydrology* **300** (1–4): 140–154 DOI: 10.1016/j.jhydrol.2004.06.005

Smith CD. 2007. Correcting the Wind Bias in Snowfall Measurements Made with a Geonor T-200B Precipitation Gauge and Alter Wind Shield. In *CMOS Bulletin SCMO, 36(5), 162-167.*162–167.

Smith RB. 2010. The heat budget of the earth's surface deduced from space. *Yale University Center for Earth Observation* (0): 1–11 Available at: https://yceo.yale.edu/sites/default/files/files/Surface_Heat_Budget_From_Space.pdf [Accessed 15 February 2018]

Snelgrove KR, Soulis ED, Seglenieks FR, Pietroniro A. 2005. Prediction in Ungauged Basins: Approaches for Canada's Cold Regions. In *Water Research*, Spence C, , Pomeroy JW, , Pietroniro A (eds).Canadian Water Resources Association: Ottawa, Ontario; 139–164.

Stahl K, Moore RD. 2006. Influence of watershed glacier coverage on summer streamflow in British Columbia, Canada. *Water Resources Research* **42** (6): 1–5 DOI: 10.1029/2006WR005022

Stahl K, Moore RD, Shea JM, Hutchinson D, Cannon AJ. 2008. Coupled modelling of glacier and streamflow response to future climate scenarios. *Water Resources Research* **44** (W02422): 1–13 DOI: 10.1029/2007WR005956

Stone LE, Fang X, Haynes KM, Helbig M, Pomeroy JW, Sonnentag O, Quinton WL. 2019. Modelling the effects of permafrost loss on discharge from a wetland-dominated, discontinuous permafrost basin. *Hydrological Processes* **33** (20): 2607–2626 DOI: 10.1002/hyp.13546

Strasser U, Bernhardt M, Weber M, Liston GE, Mauser W. 2008. Is snow sublimation important in the alpine water balance? *Cryosphere* **2** (1): 53–66 DOI: 10.5194/tc-2-53-2008

Tabler RD, Pomeroy JW, Santana BW. 1990. Drifting Snow. In *Cold Regions Science and Hydraulics*, Ryan W, , Crissman R (eds).American Society of Civil Engineers; 95–145.

Tennant C, Menounos B. 2013. Glacier change of the Columbia Icefield, Canadian Rocky Mountains, 1919–2009. *Journal of Glaciology* **59** (216): 671–686 DOI: 10.3189/2013JoG12J135

Thiery W, Gorodetskaya IV, Bintanja R, van Lipzig NPM, van den Broeke MR, Reijmer CH, Kuipers Munneke P. 2012. Surface and snowdrift sublimation at Princess Elisabeth station, East Antarctica. *The Cryosphere* **6**: 841–857 DOI: 10.5194/tc-6-841-2012

Trubilowicz JW, Shea JM, Jost G, Moore RD. 2016. Suitability of North American Regional Reanalysis (NARR) output for hydrologic modelling and analysis in mountainous terrain. *Hydrological Processes* **30** (13): 2332–2347 DOI: 10.1002/hyp.10795

Uppala SM, KÅllberg PW, Simmons AJ, Andrae U, Bechtold VDC, Fiorino M, Gibson JK, Haseler J, Hernandez A, Kelly GA, et al. 2005. The ERA-40 re-analysis. *Quarterly Journal of the Royal Meteorological Society* **131** (612): 2961–3012 DOI: 10.1256/qj.04.176

Verbunt M, Gurtz J, Jasper K, Lang H, Warmerdam P, Zappa M. 2003. The hydrological role of snow and glaciers in alpine river basins and their distributed modeling. *Journal of Hydrology* **282** (1–4): 36–55 DOI: 10.1016/S0022-1694(03)00251-8

Verseghy DL. 1991. CLASS - A Canadian Land Surface Scheme for GCMS. I. Soil Model. *International Journal of Climatology* **11**: 111–133 DOI: 10.1002/joc.3370110202

Vincent C, Wagnon P, Shea JM, Immerzel WW, Kraaijenbrink P, Shrestha D, Soruco A, Arnaud Y, Brun F, Berthier E, et al. 2016. Reduced melt on debris-covered glaciers: investigations from Changri Nup Glacier, Nepal. *The Cryosphere* **10**: 1845–1858 DOI: 10.5194/tc-10-

1845-2016

Vincent LA, Zhang X, Brown RD, Feng Y, Mekis E, Milewska EJ, Wan H, Wang XL. 2015. Observed trends in Canada's climate and influence of low-frequency variability modes. *Journal of Climate* **28** (11): 4545–4560 DOI: 10.1175/JCLI-D-14-00697.1

Walmsley J, Taylor P, Salmon J. 1989. Simple guidelines for estimating windspeed variations due to small-scale topographic features–an update. *Climatol. Bull* **23** (1) Available at: http://scmo.ca/CB/cb230101.pdf

Walter MT, Brooks ES, McCool DK, King LG, Molnau M, Boll J. 2005. Process-based snowmelt modeling: does it require more input data than temperature-index modeling? *Journal of Hydrology* **300**: 65–75 DOI: 10.1016/j.jhydrol.2004.05.002

Wang Z, Bovik AC. 2002. A universal image quality index. *Signal Processing Letters, IEEE* **9** (3): 81–84 DOI: 10.1109/97.995823

Watson E, Luckman BH, Yu B. 2006. Long-term relationships between reconstructed seasonal mass balance at Peyto Glacier, Canada, and Pacific sea surface temperatures. *The Holocene* **16** (6): 783–790 DOI: 10.1191/0959683606hol973ft

Wayand NE, Marsh CB, Shea JM, Pomeroy JW. 2018. Globally scalable alpine snow metrics. *Remote Sensing of Environment* **213** (April): 61–72 DOI: 10.1016/j.rse.2018.05.012

Weber M, Bernhardt M, Pomeroy JW, Fang X, Härer S, Schulz K, Harer S, Schulz K. 2016. Description of current and future snow processes in a small basin in the Bavarian Alps. *Environmental Earth Sciences* **75** (17) DOI: 10.1007/s12665-016-6027-1

Weedon GP, Balsamo G, Bellouin N, Gomes S, Best MJ, Viterbo P. 2014. The WFDEI meteorological forcing data set: WATCH Forcing Datamethodology applied to ERA-Interimreanalysis data. *Water Resources Research* **50**: 7505–7514 DOI: 10.1002/2014WR015638

Weedon GP, Gomes S, Viterbo P, Shuttleworth WJ, Blyth E, Österle H, Adam JC, Bellouin N, Boucher O, Best M. 2011. Creation of the WATCH Forcing Data and Its Use to Assess Global and Regional Reference Crop Evaporation over Land during the Twentieth Century. *Journal of Hydrometeorology* **12** (1963): 823–848 DOI: 10.1175/2011JHM1369.1

WGMS. 2019. Fluctuations of Glaciers Database. *World Glacier Monitoring Service, Zurich, Switzerland* DOI: 10.5904/wgms-fog-2019-12

Whitfield PH, Pomeroy JW. 2016. Changes to flood peaks of a mountain river: implications for

analysis of the 2013 flood in the Upper Bow River, Canada. *Hydrological Processes* **30** (25): 4657–4673 DOI: 10.1002/hyp.10957

Wilcoxon F. 1945. Individual Comparisons by Ranking Methods. *Biometrics Bulletin* **1** (6): 80 DOI: 10.2307/3001968

de Woul M, Hock R, Braun M, Thorsteinsson T, Jóhannesson T, Halldórsdóttir S. 2006. Firn layer impact on glacial runoff: a case study at Hofsjökull, Iceland. *Hydrological Processes* **20** (10): 2171–2185 DOI: 10.1002/hyp.6201

Wu G, Liu Y, Wang T. 2007. Methods and strategy for modeling daily global solar radiation with measured meteorological data – A case study in Nanchang station, China. *Energy Conversion and Management* **48**: 2447–2452 DOI: 10.1016/j.enconman.2007.04.011

Young GJ. 1981. The Mass Balance of Peyto Glacier, Alberta, Canada, 1965-1978. *Arctic and Alpine Research* DOI: 10.2307/1551037

Young GJ, Stanley AD. 1976. Canadian Glaciers in the International Hydrological Decade Program, 1965-1974 No. 4. Peyto Glacier, Alberta - Summary of measurements

Zemp M, Frey H, Gärtner-Roer I, Nussbaumer SU, Hoelzle M, Paul F, Haeberli W, Denzinger F, Ahlstrøm AP, Anderson B, et al. 2015. Historically unprecedented global glacier decline in the early 21st century. *Journal of Glaciology* **61** (228): 745–762 DOI: 10.3189/2015JoG15J017

Zhou J, Pomeroy JW, Zhang W, Cheng G, Wang G, Chen C. 2014. Simulating cold regions hydrological processes using a modular model in the west of China. *Journal of Hydrology* **509**: 13–24 DOI: 10.1016/j.jhydrol.2013.11.013

Appendix A: Sources and resolutions of DEM

Table A.1: sources considered for the Peyto Glacier Research Basin (PGRB)

Year	Resolution	Source and method
1966	10 m	This map is an IHD mandated product based on 1966 aerial photography and enhanced ground control survey at a scale of 1:10,000. It is among the first metric maps produced in Canada, comprising an eight-colour scheme to display terrains, a 50-metre contour interval with 10-metre interval on snow and ice terrains, and is georeferenced to NAD 27. Contour lines, spot heights, stream lines and lake areas digitized from the map were used to interpolate a DEM by using the Topo to Raster tool in ArcMap 10 as follows: 1. ArcScan was used to vectorize contours from the map. Raster layers were symbolized as two-color images to use with ArcScan tools and commands. 2. The scanned map contained full coloured images, with various symbols used to differentiate features and landcover. The raster cleanup process is too complex for ArcMap, so the photo editing software, Adobe Photoshop CS6, was used. 3. In ArcMap, the image was first georeferenced with 9 points and contour lines, which were redrawn in different layers, were vectorized using ArcScan. 4. Spot heights, stream lines and lake areas were manually digitized. 5. Drawing from the digitized data, a DEM was created using Topo to Raster tool of the Spatial Analyst module.
1978	~20 m	CDED consists of an ordered array of ground or reflective surface elevations, recorded in metres, at regularly spaced intervals. The source digital data for CDED is extracted from the hypsographic and hydrographic elements of the National Topographic Data Base (NTDB) at scales of 1:50,000 and 1:250,000, or the Geospatial Data Base (GDB), or various scaled positional data acquired by the provinces and territories or remotely sensed imagery.
1986	~20 m	Canadian Digital Elevation Model (CDEM) is a part of Natural Resources Canada's altimetry system designed to better meet the users' needs for elevation data and products. The CDEM stems from the existing CDED. In these data, elevations can be either ground or reflective surface elevations. The data has an average accuracy spatial resolution of around 20m (0.75 arcsecond) and average accuracy of 25.2 m.
2000	~20 m	Canadian Digital Surface Model (CDSM) was provided by Natural Resources Canada. The CDSM is basically SRTM data re-processed with supplemental information according to Canadian needs. The SRTM data were re-processed from their original form as follows: 1) the data was void-filled using the CDEM; 2) the Vertical Datum was changed from EGM96 to CGVD28; 3) the data was projected to UTM using cubic convolution; 4) the data was smoothened for noise removal; 5) the data was re-projected from WGS84 to NAD83 and aligned to the 0.75-second CDEM grid resolution using cubic convolution; and 6) the waterbodies were re-flattened.

Year	Resolution	Source and method
2006	10 m	This DEM was prepared from LiDAR surveys taken in August 2006 (Demuth and Hopkinson, 2013). The DEM did not cover the whole area of PGRB, the northeast corner of the basin was mosaiced with 2014 DEM data to fill the missing part.
2014	10 m	Aerial photographs of Banff National Park by Geodesy Group Inc. A 3-D model of Peyto was first prepared with Agisoft PhotoScan software, extracting the DEM as follows: 1. A total of 17 images of the PGRB were imported to Agisoft PhotoScan. 2. Each image was provided with coordinates, elevation and Omega, Phi, Kappa (Pitch, Roll, Yaw) values. 3. Import of .csv data from the reference section, with referencing for each image. 4. Coordinate system definition as NAD 83 Zone 11. 5. Photographic alignment, dense cloud creation, DEM assembly and exportation at 10 m resolution.

Appendix B: Evaluation of reanalysis data

ERAI, WFDEI and NARR were evaluated with the in-situ observation at AGRB and PGRB. The availability of the datasets is presented in Table B.1. CFSR was not evaluated here as this dataset is available for the period 1979 to 2010 only. The reanalysis products were bias corrected using *in-situ* observation for the calibration period and evaluated the bias corrected data with the observation for the validation period (Table B.2). The bias corrected technique evaluated was the quantile mapping using the qmap package in R (Gudmundsson, 2016).

Table B.1: Reanalysis datasets considered for evaluation

Dataset	**Source**	**Data period**	**Time step**
ERA Interim	ECMWF	January 1979 – August 2019	3-hour
NARR	NCEP	January 1979 – December 2019	3-hour
WFDEI	WATCH	January 1979 – December 2018	3-hour

Table B.2: observation for calibration and validation

Station	**Calibration Period**	**Validation Period**
Peyto Main	5 Oct 2010 – 30 Sept 2014	1 Oct 2014 – 21 Nov 2018
Athabasca Moraine	1 Oct 2014 – 30 Sept 2016	1 Oct 2016 – 31 Oct 2018

The three reanalysis products were first extracted to the nearest point grid for Athabasca Moraine and Peyto Main stations. They were then linearly downscaled from 3-hour time step to 1-hour. The variables were extracted and downscaled using the 'reanalysis' package (Shook, 2016b) and all the analysis was performed using the R computing software platform (RStudio, 2017).

Table B.3: Comparison between bias corrected hourly reanalysis datasets with in-situ observations for the validity period.

Site	Reanalysis	Variable	MBE	RMSE	Slope	Intercept	WBI
Athabasca	ERAI	Air temperature	-0.23	3.01	1.02	-0.21	0.96
	NARR		0.23	2.99	0.96	0.19	0.96
	WFDEI		0.20	2.91	0.93	0.13	0.96
Peyto	ERAI	Air temperature	-0.10	2.87	0.95	-0.12	0.95
	NARR		0.12	3.26	0.93	0.09	0.93
	WFDEI		0.12	3.34	0.90	0.08	0.93
Athabasca	ERAI	Vapour pressure	-0.01	0.08	1.01	-0.01	0.93
	NARR		0.01	0.10	0.96	0.03	0.90
	WFDEI		-0.01	0.09	0.96	0.01	0.92
Peyto	ERAI	Vapour pressure	0.00	0.07	0.96	0.02	0.94
	NARR		0.01	0.09	0.95	0.03	0.91
	WFDEI		0.00	0.09	0.93	0.03	0.91
Athabasca	ERAI	Wind speed	0.05	2.43	0.53	1.66	0.51
	NARR		0.19	2.74	0.38	2.32	0.37
	WFDEI		0.15	2.37	0.56	1.67	0.54
Peyto	ERAI	Wind speed	0.09	2.54	0.52	1.91	0.55
	NARR		0.07	2.97	0.36	2.50	0.38
	WFDEI		-0.01	2.54	0.53	1.77	0.56
Athabasca	ERAI	Shortwave irradiance	0.80	120.16	0.91	15.03	0.89
	NARR		0.47	220.51	0.62	60.25	0.61
	WFDEI		-2.01	132.9	0.85	21.09	0.86
Peyto	ERAI	Shortwave irradiance	1.00	105.16	0.91	13.35	0.90
	NARR		3.74	201.48	0.65	53.40	0.63
	WFDEI		3.46	112.48	0.91	16.61	0.89
Athabasca	ERAI	Longwave irradiance	-0.90	25.55	0.90	25.69	0.83
	NARR		0.92	30.07	0.81	51.17	0.76
	WFDEI		-1.26	24.66	0.88	31.06	0.84
Peyto	ERAI	Longwave irradiance	1.93	24.85	0.83	47.91	0.83
	NARR		-1.67	28.71	0.82	46.81	0.78
	WFDEI		2.87	25.27	0.78	60.61	0.81
Athabasca	ERAI	Precipitation	0.03	0.59	0.28	0.12	0.25
	NARR		0.06	0.75	0.18	0.17	0.11
	WFDEI		0.49	1.91	0.97	0.49	0.04
Peyto	ERAI	Precipitation	0.03	0.70	0.54	0.08	0.25
	NARR		0.06	0.73	0.33	0.13	0.14
	WFDEI		0.17	1.27	0.89	0.18	0.12

Note: Best statistical values and thus reanalysis data in the categories are in blue for each variable and observation site.

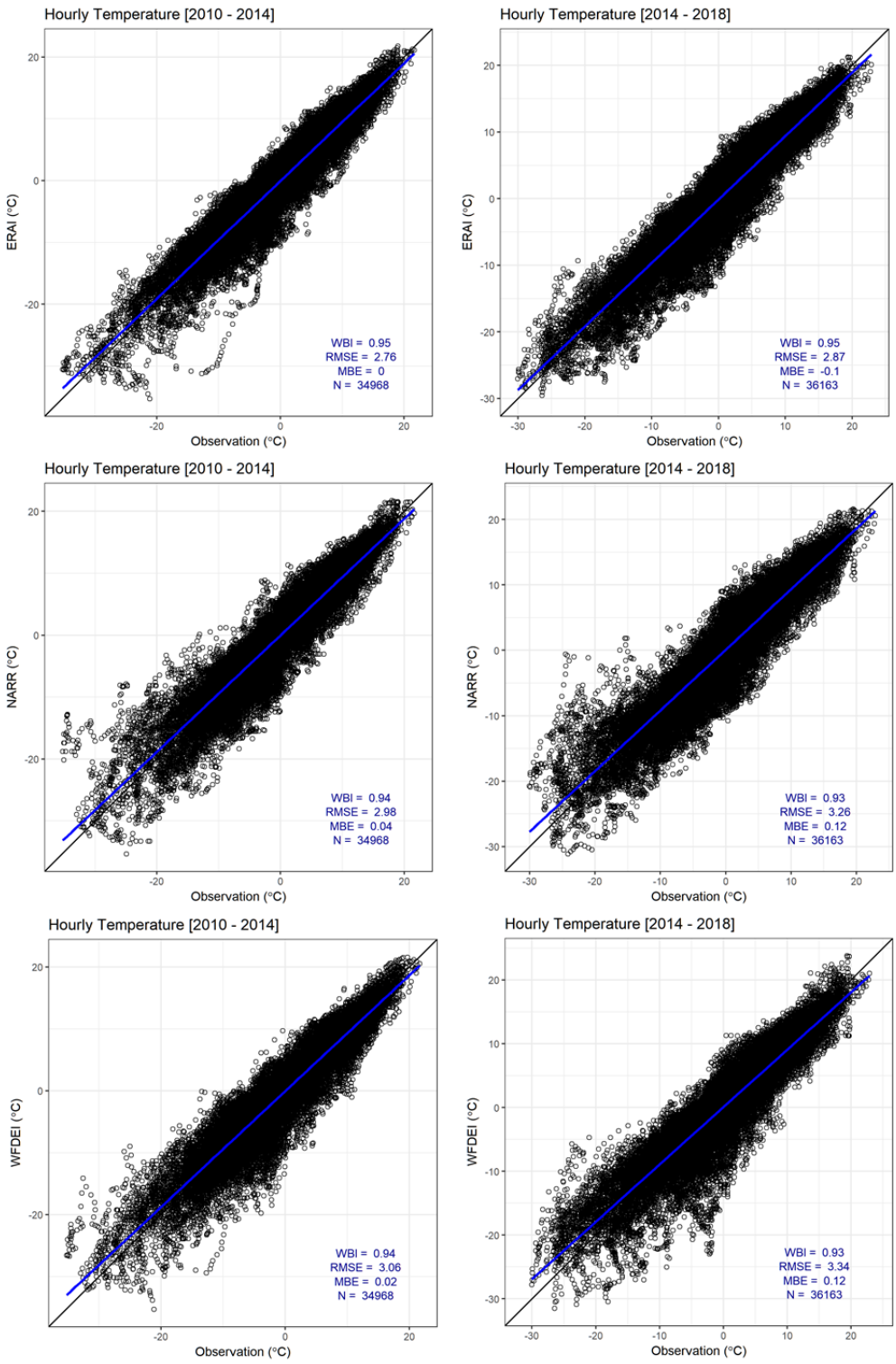

Figure B.1: Comparison of hourly air temperature from the reanalysis datasets with observation at Peyto Main station [left is for calibration, and right is for validation]

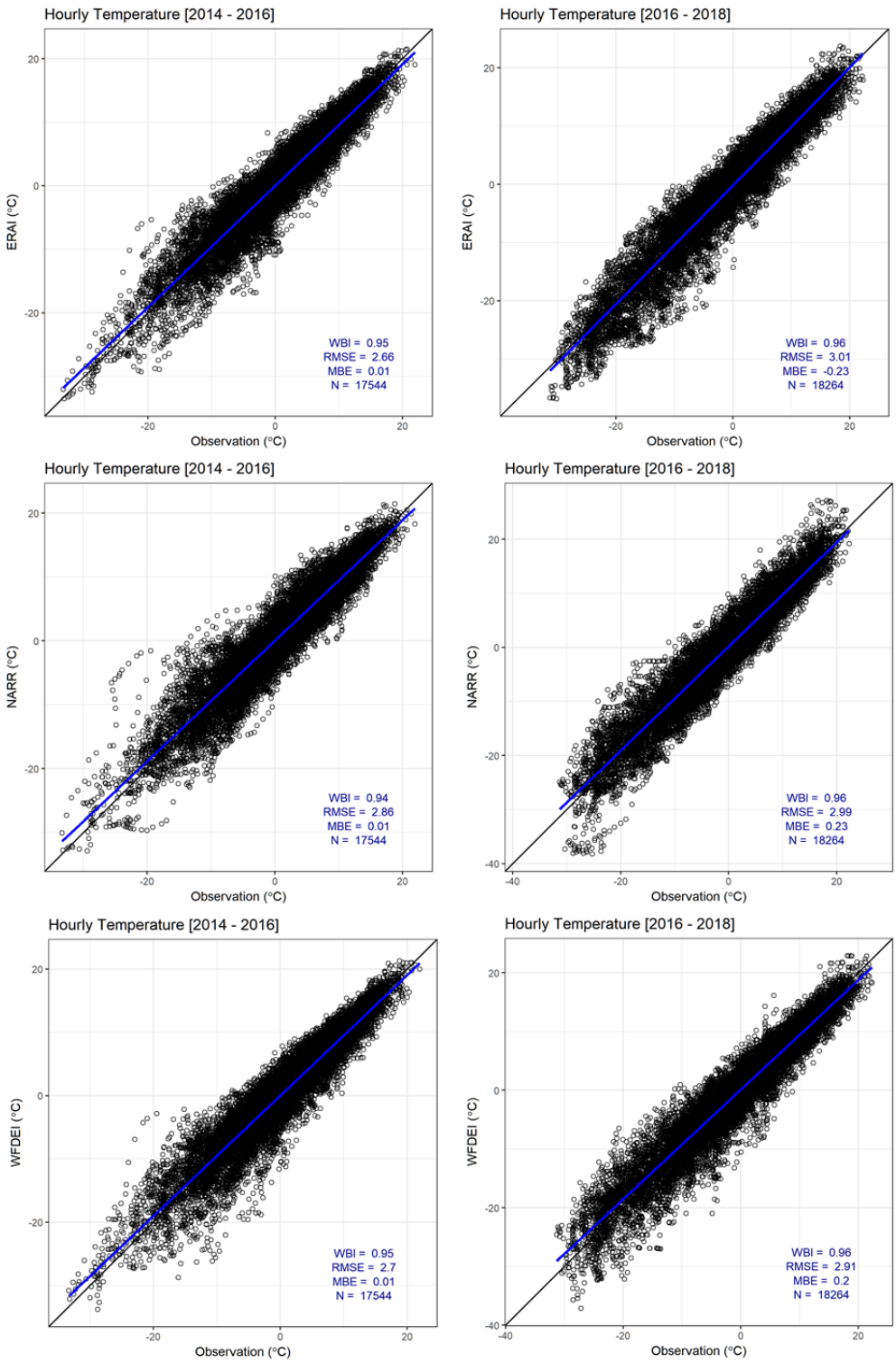

Figure B.2: Comparison of hourly air temperature from the reanalysis datasets with observation at Athabasca Moraine station [left is for calibration, and right is for validation]

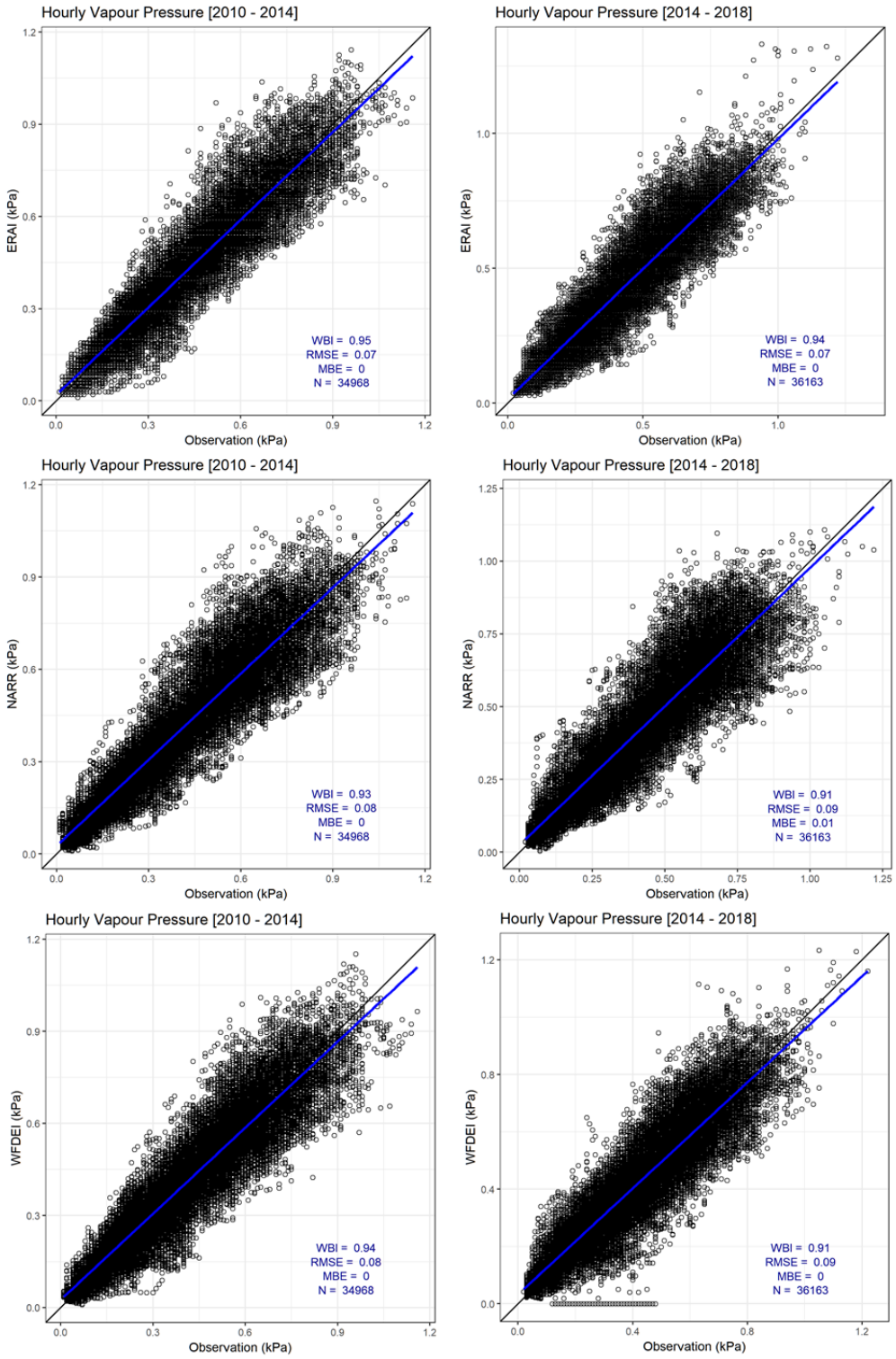

Figure B.3: Comparison of hourly vapour pressure from the reanalysis datasets with observation at Peyto Main station [left is for calibration, and right is for validation]

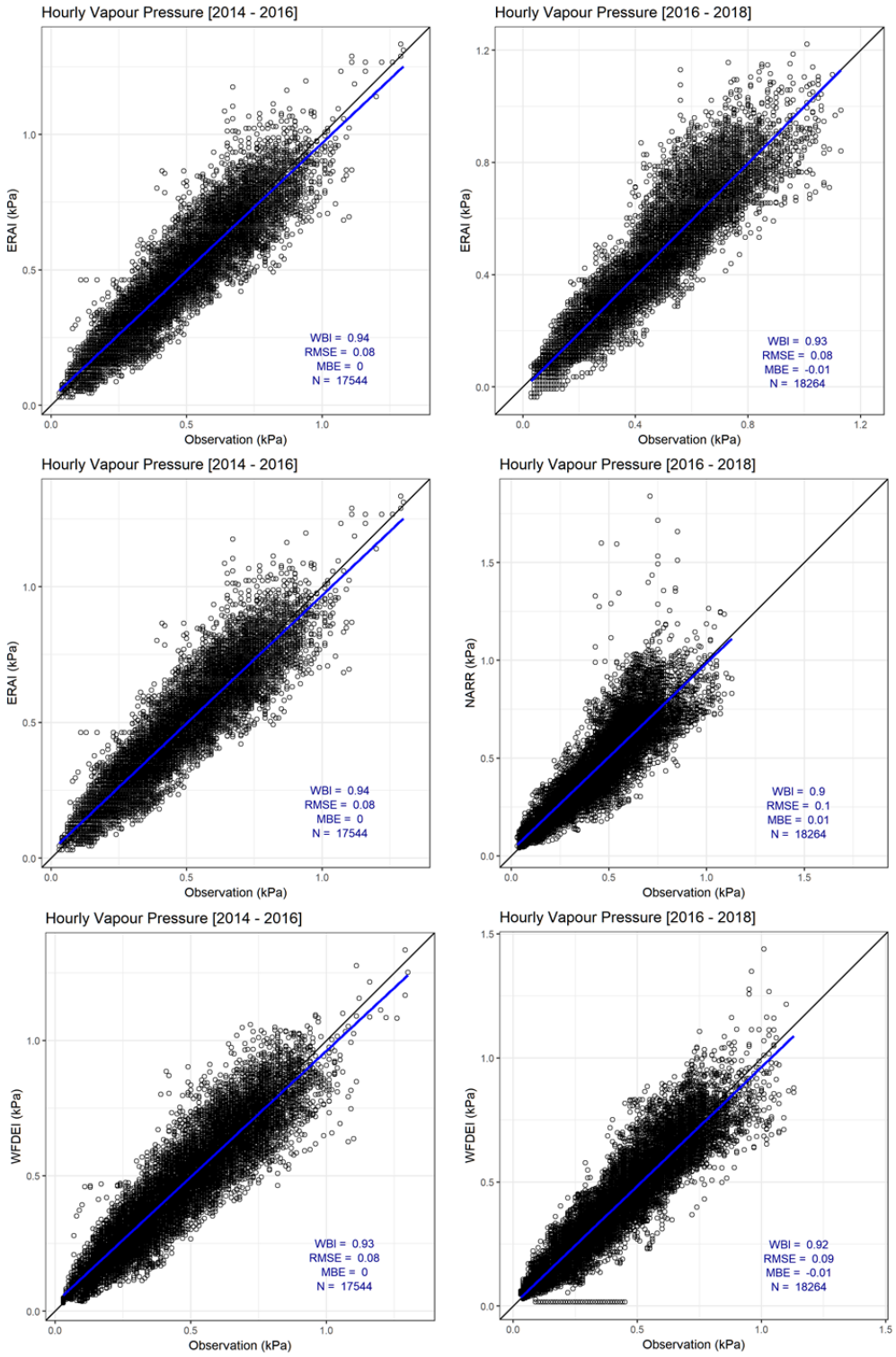

Figure B.4: Comparison of hourly vapour pressure from the reanalysis datasets with observation at Athabasca Moraine station [left is for calibration, and right is for validation]

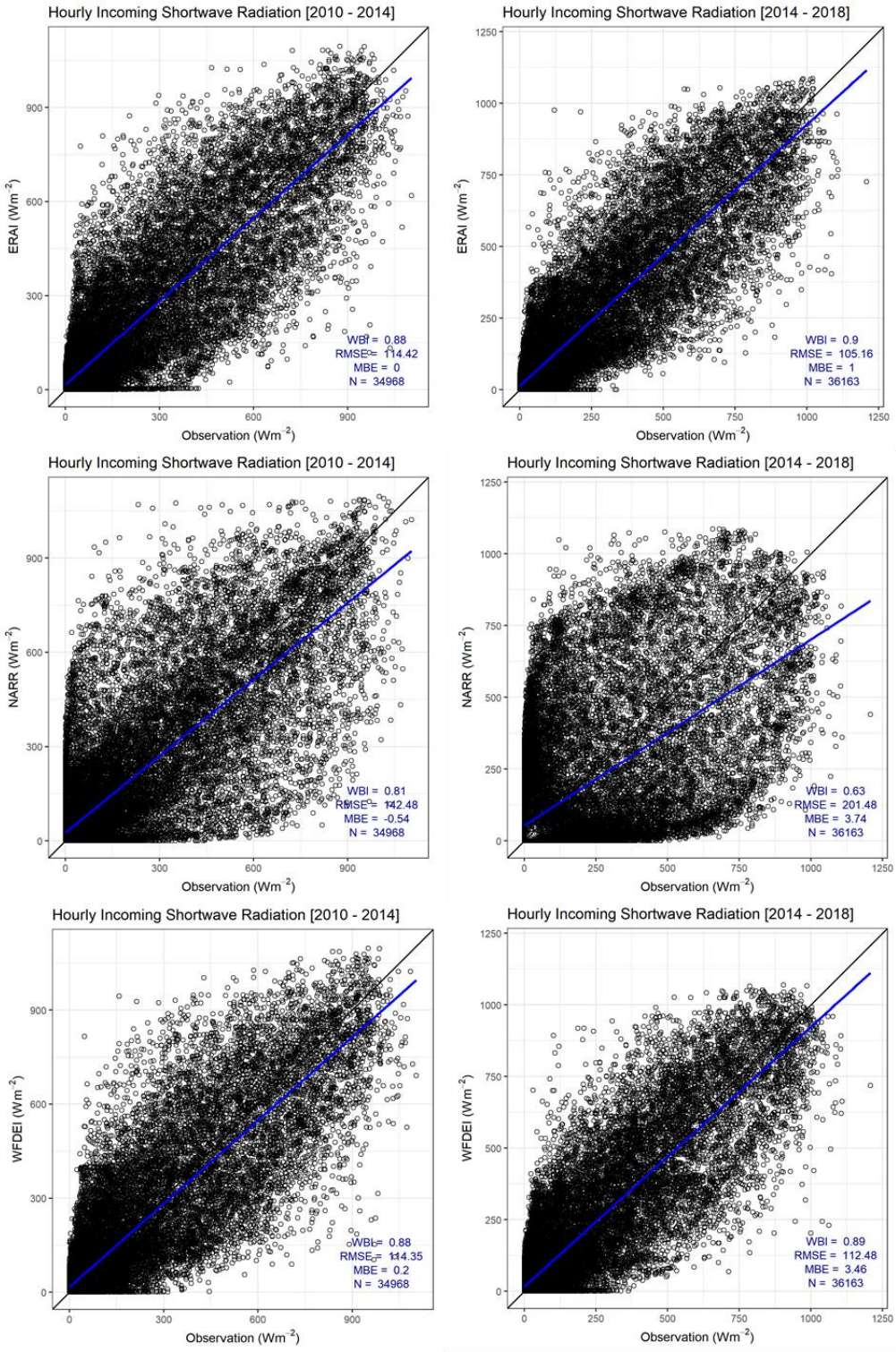

Figure B.5: Comparison of hourly shortwave irradiance from the reanalysis datasets with observation at Peyto Main station [left is for calibration, and right is for validation]

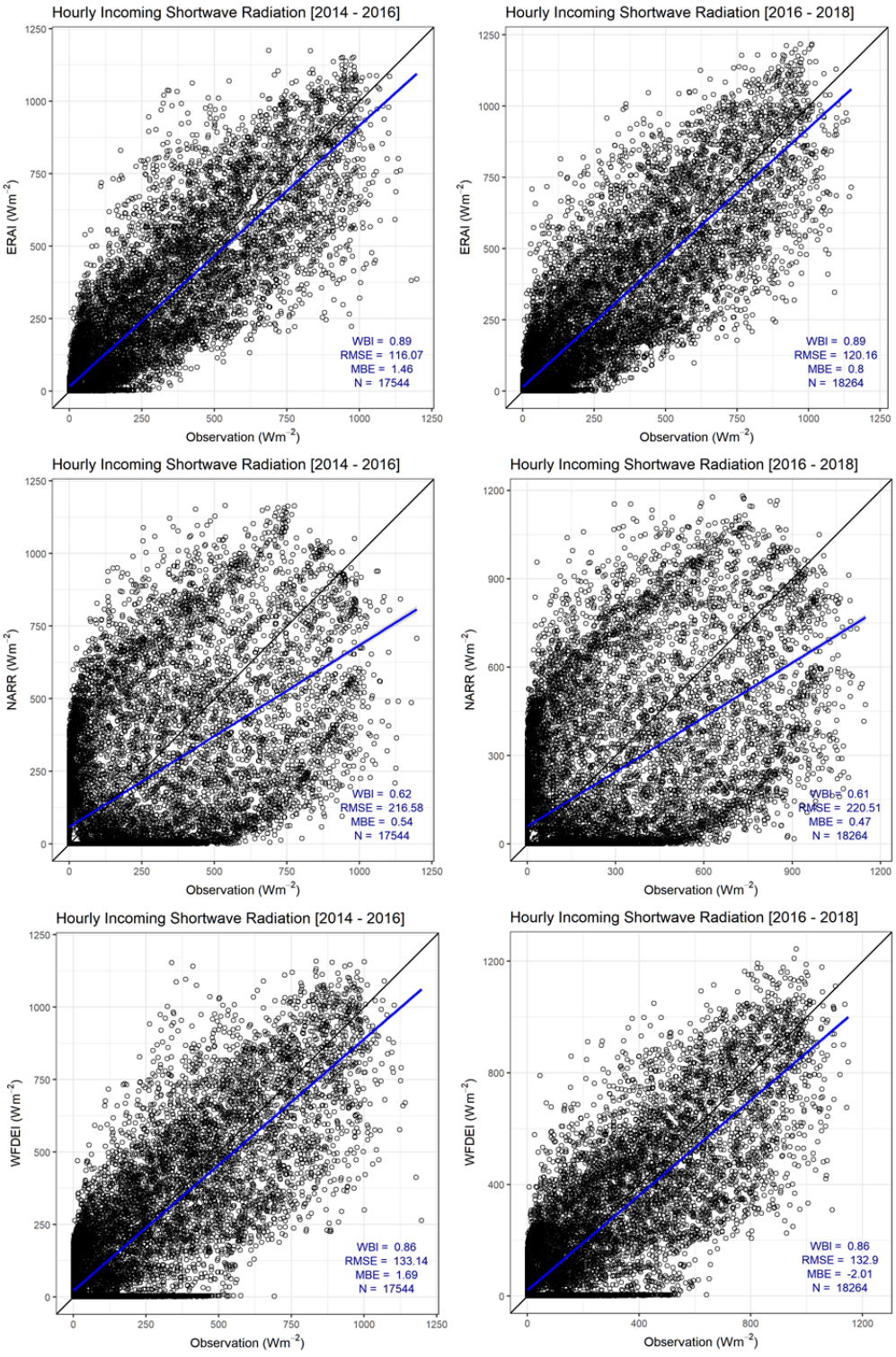

Figure B.6: Comparison of hourly shortwave irradiance from the reanalysis datasets with observation at Athabasca Moraine station [left is for calibration, and right is for validation]

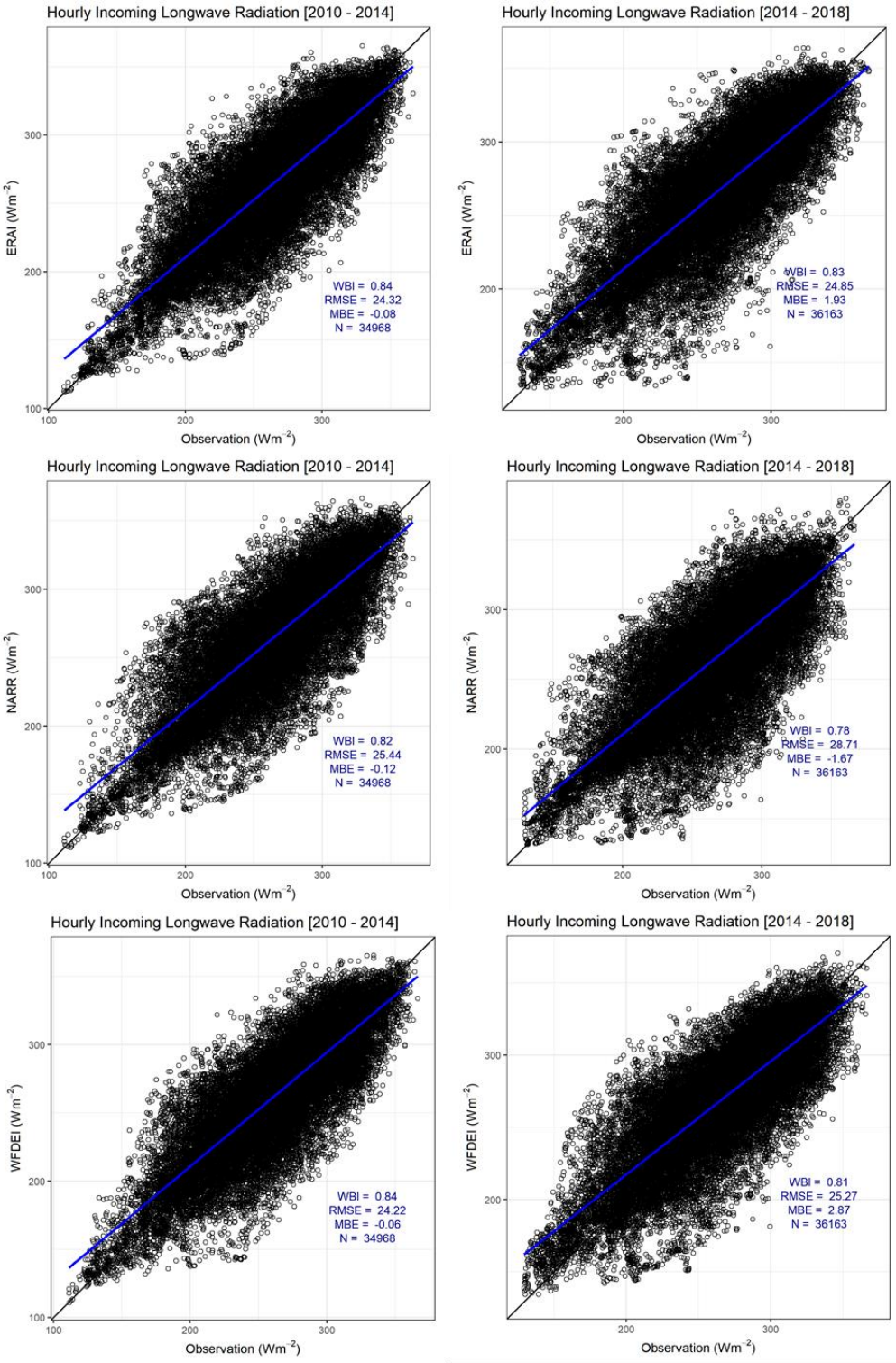

Figure B.7: Comparison of hourly longwave irradiance from the reanalysis datasets with observation at Peyto Main station [left is for calibration, and right is for validation]

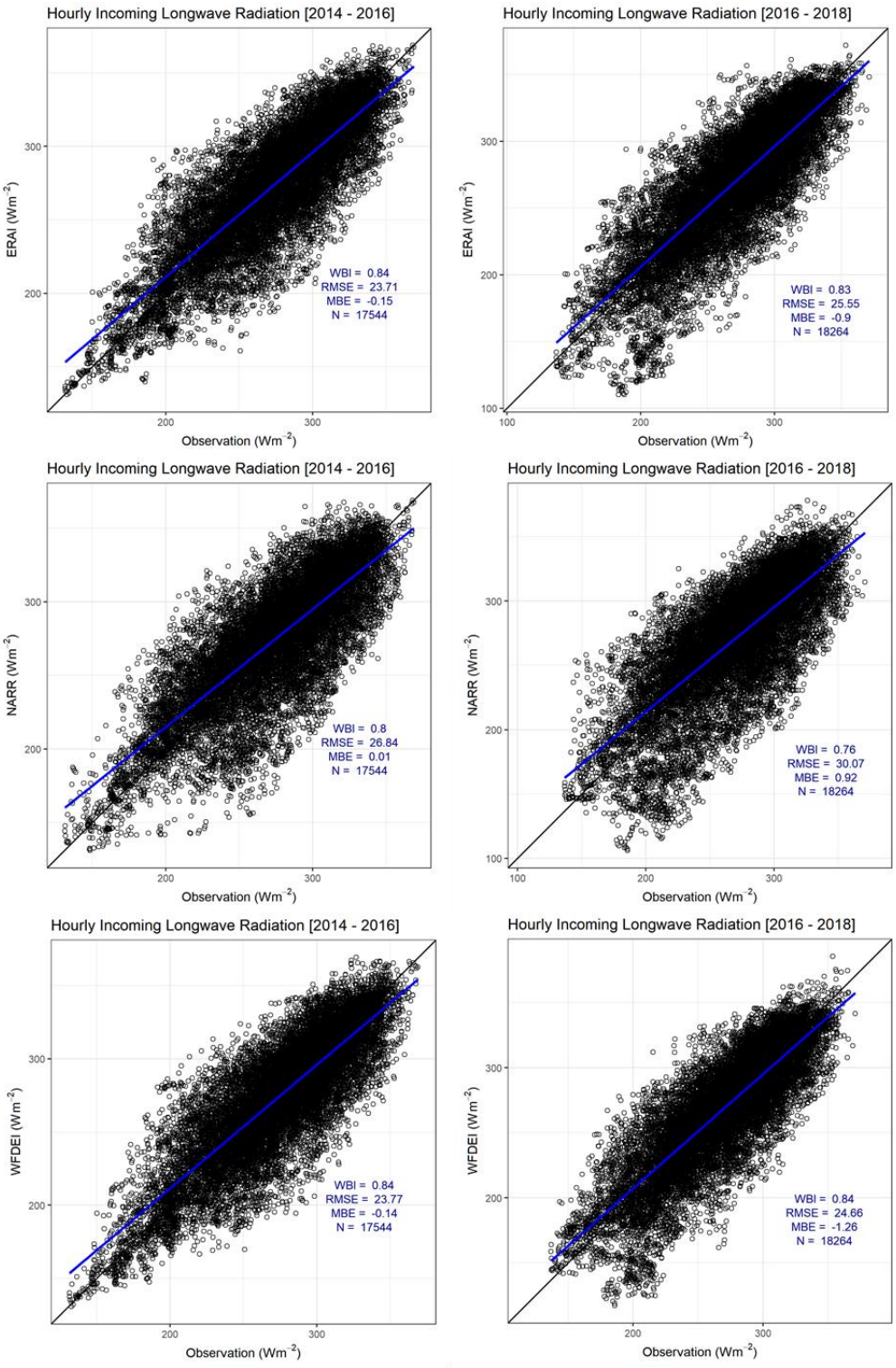

Figure B.8: Comparison of hourly longwave irradiance from the reanalysis datasets with observation at Athabasca Moraine station [left is for calibration, and right is for validation]

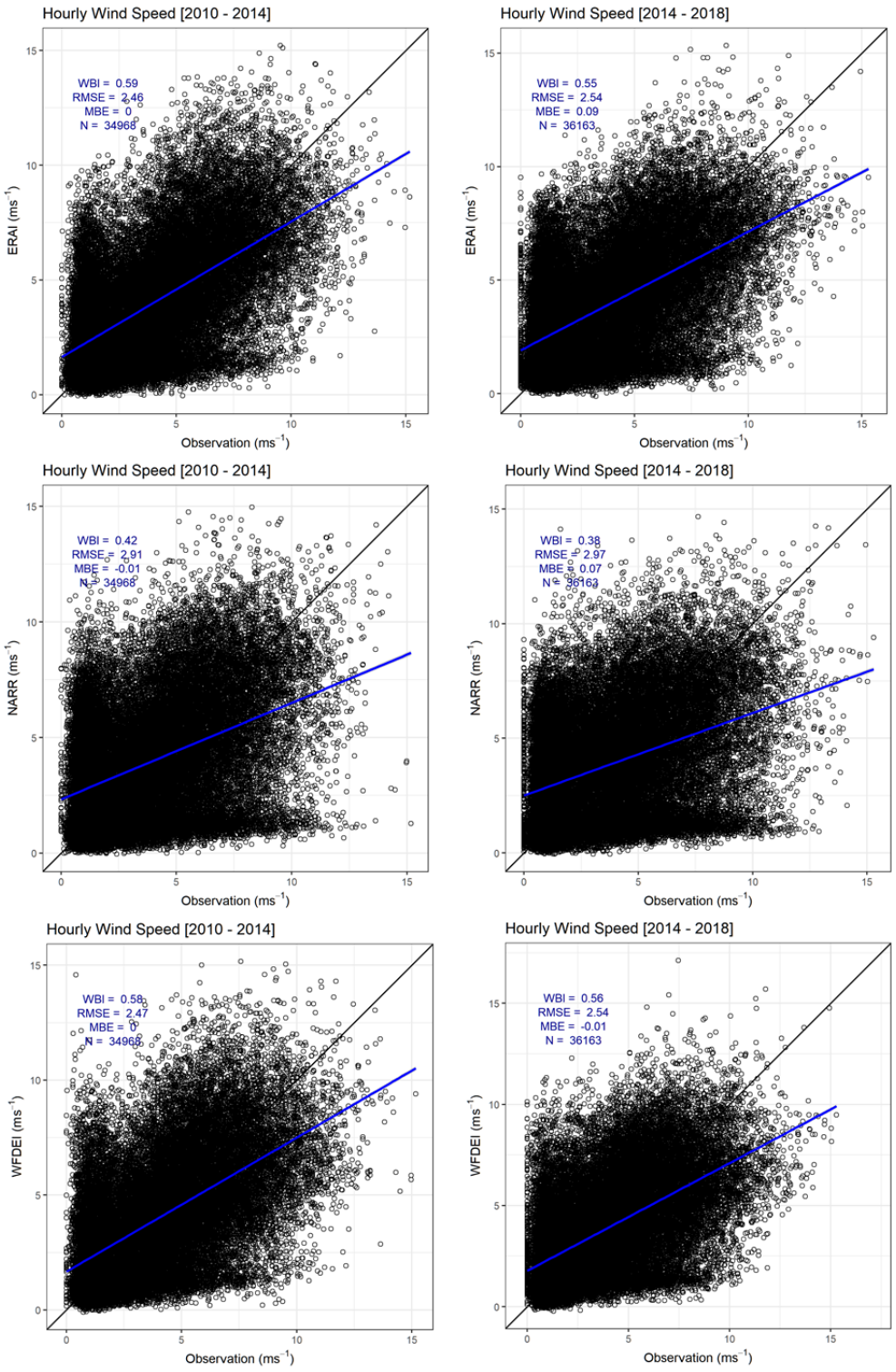

Figure B.9: Comparison of hourly wind speed from the reanalysis datasets with observation at Peyto Main station [left is for calibration, and right is for validation]

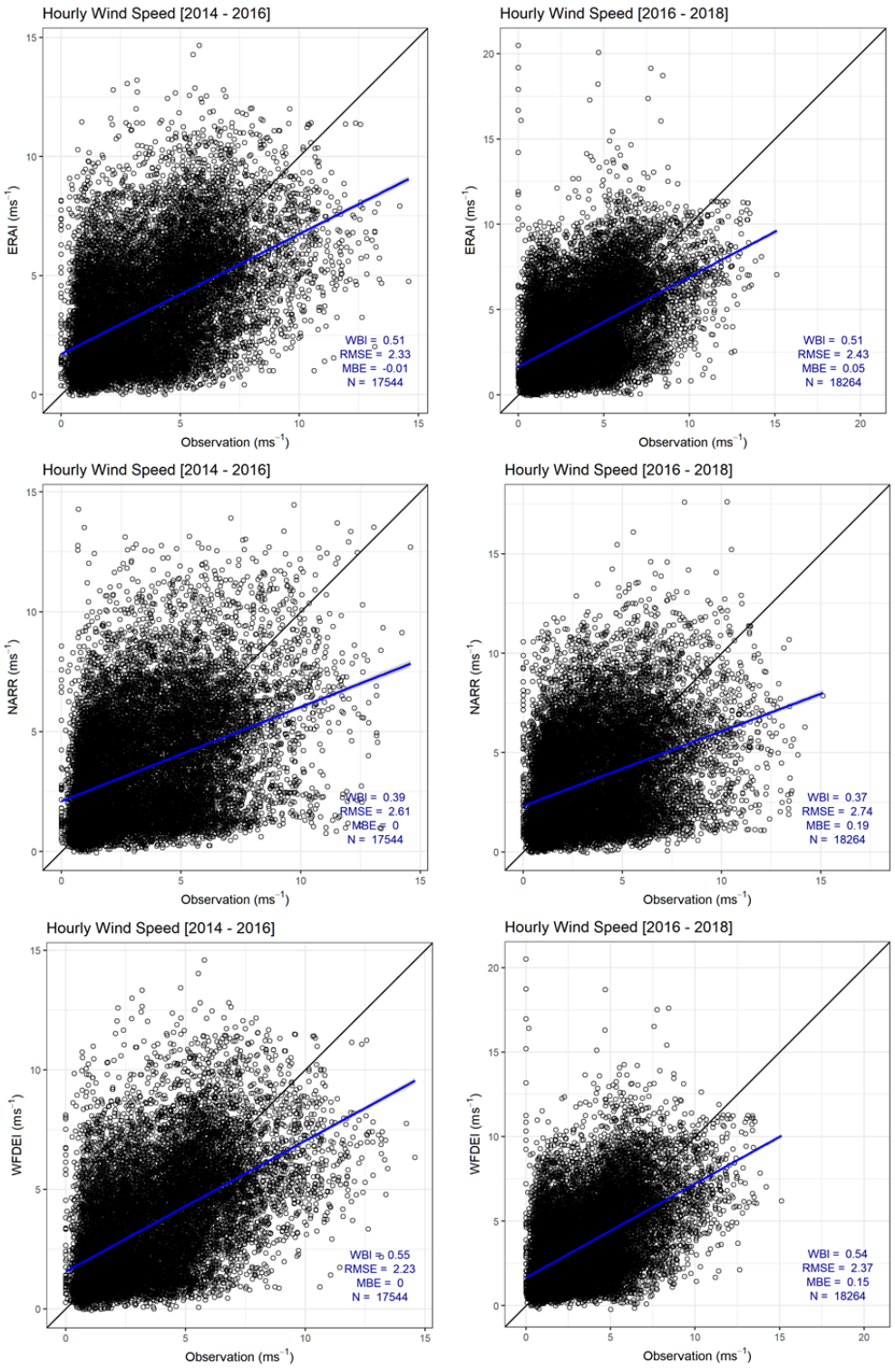

Figure B.10: Comparison of hourly wind speed from the reanalysis datasets with observation at Athabasca Moraine station [left is for calibration, and right is for validation]

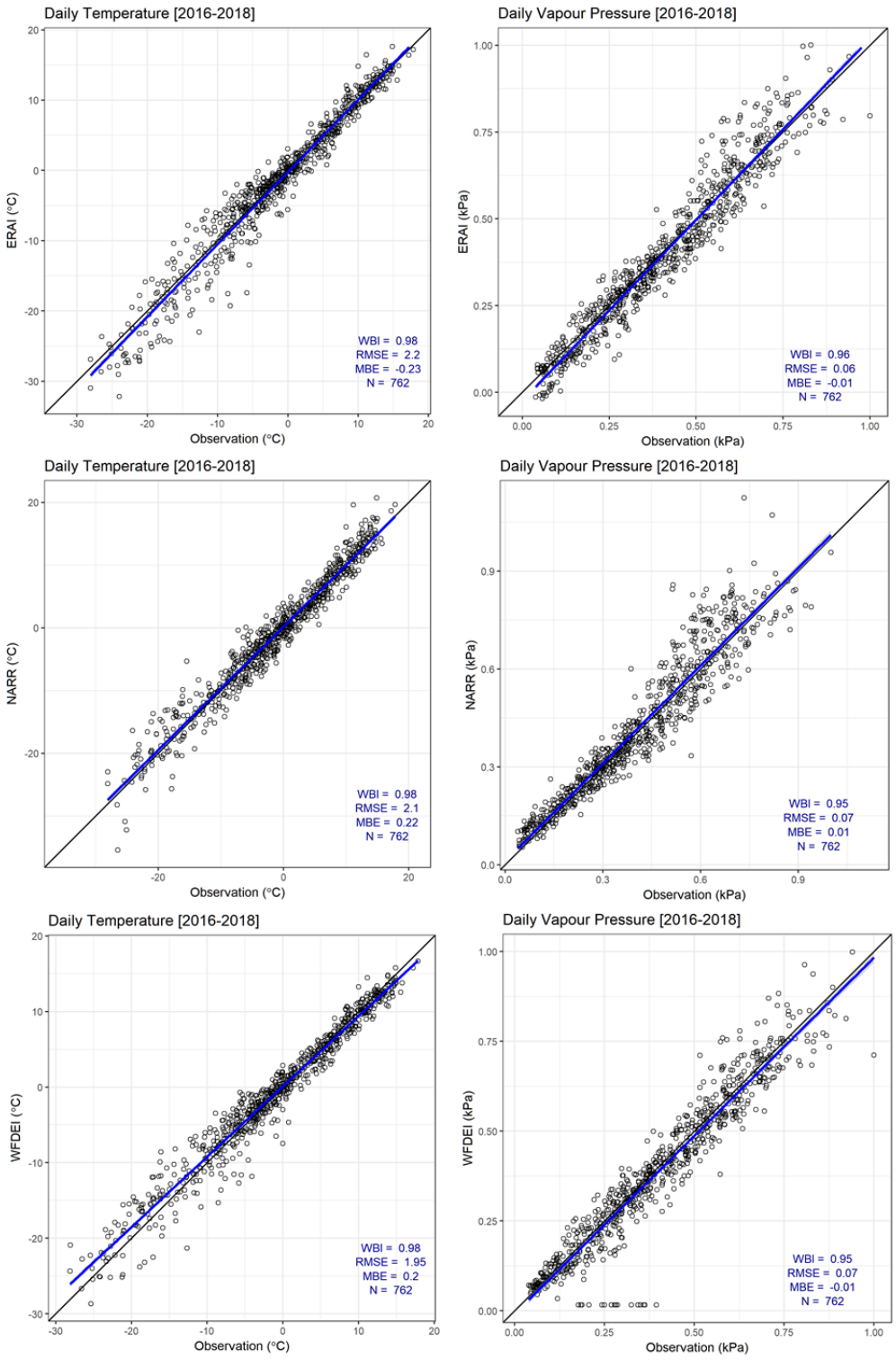

Figure B.11: Comparison of daily mean air temperature (left panel) and daily vapour pressure (right panel) from the reanalysis datasets with observation at Athabasca Moraine station during the validation period

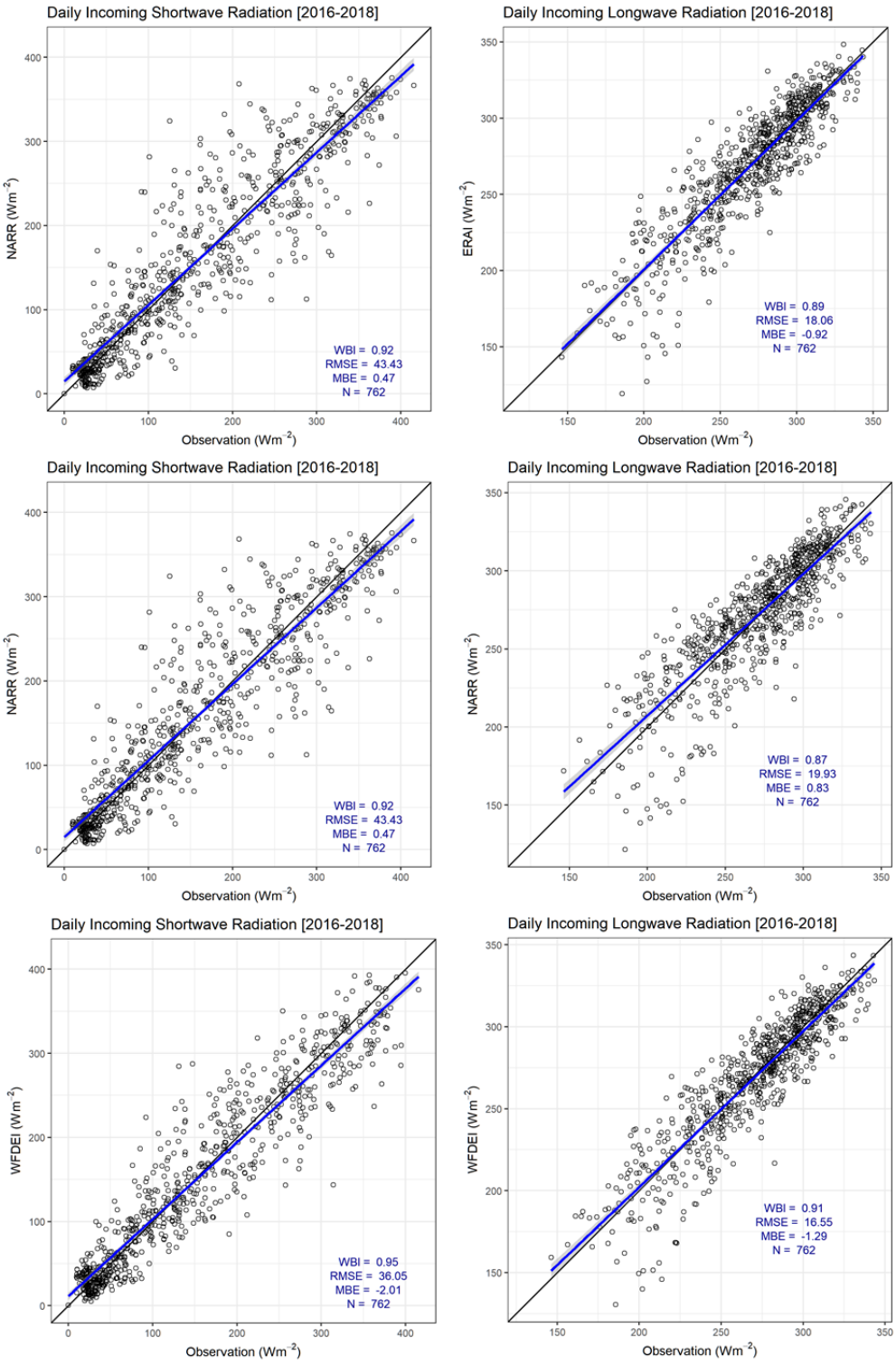

Figure B.12: Comparison of daily mean shortwave irradiance (left panel) and daily mean longwave irradiance (right panel) from the reanalysis datasets with observation at Athabasca Moraine station during the validation period

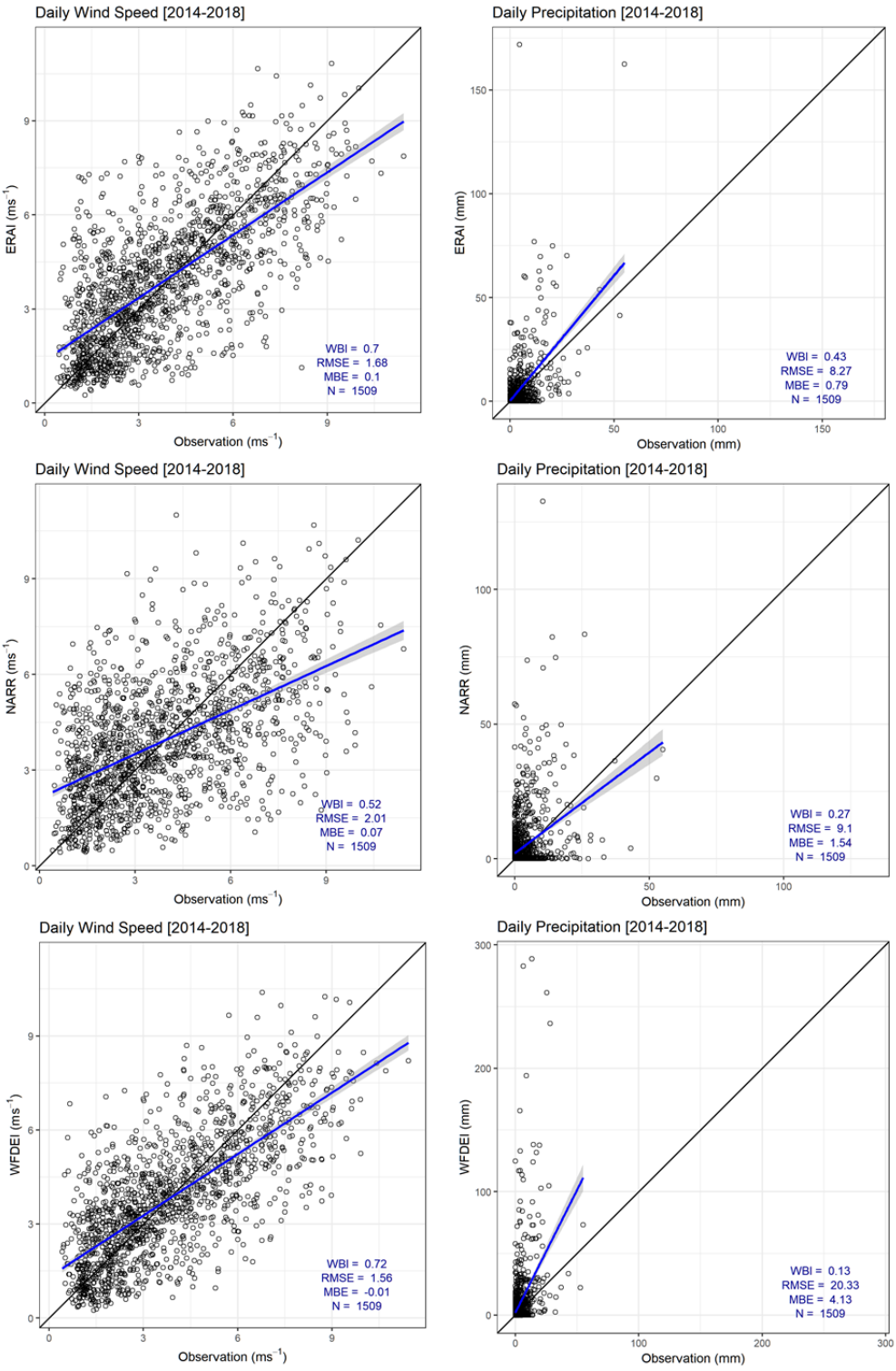

Figure B.13: Comparison of daily mean wind speed (left panel) and daily precipitation (right panel) from the reanalysis datasets with observation at Peyto Main station during the validation period

Appendix C: Scatter plots of tau and QsiD

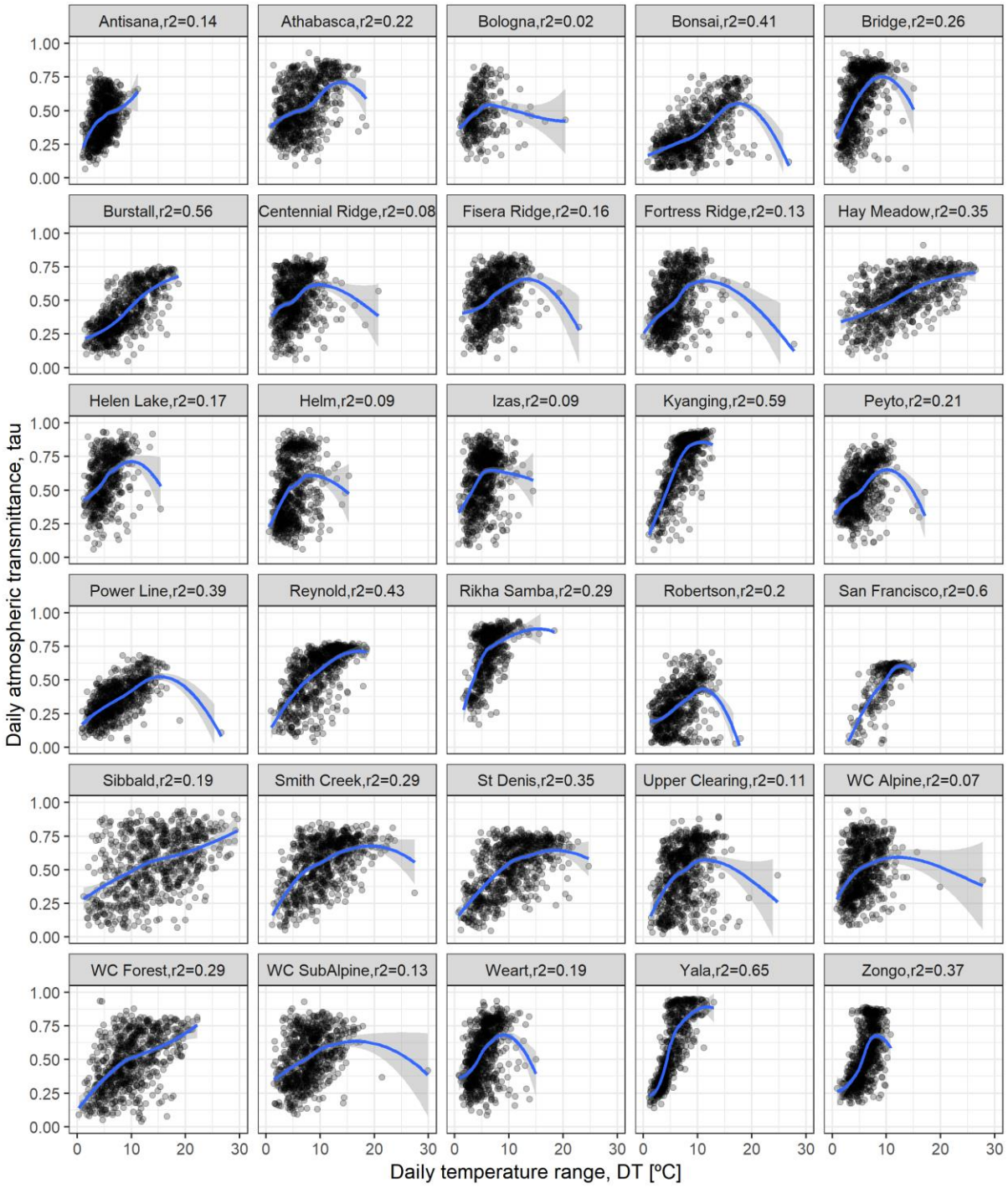

Figure C.1: Scatter plots of daily atmospheric transmittance against daily temperature range. Blue lines are local regression (LOESS, locally weighted scatterplot smoothing)

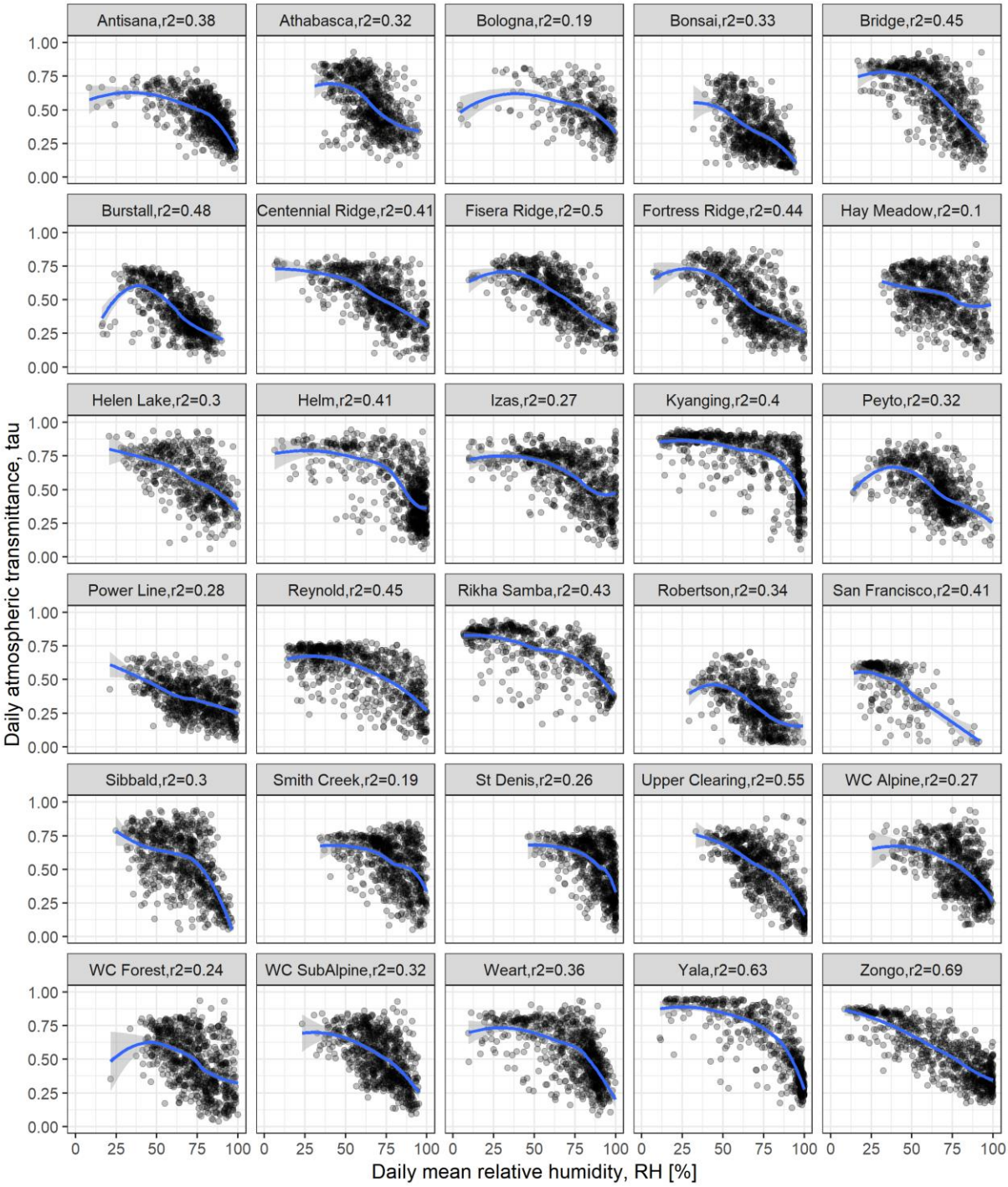

Figure C.2: Scatter plots of daily atmospheric transmittance against daily mean relative humidity.

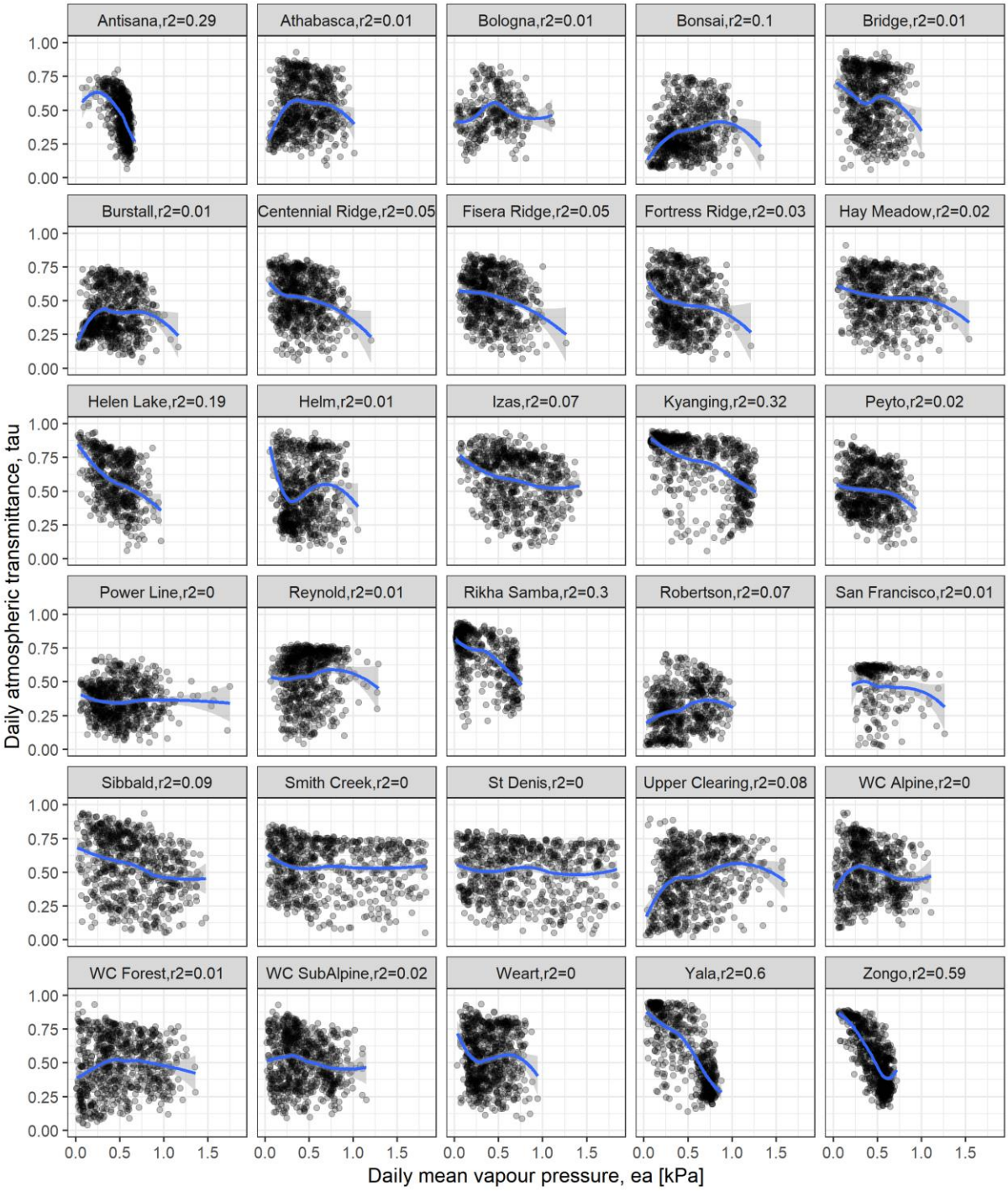

Figure C.3: Scatter plots of daily atmospheric transmittance against daily mean vapour pressure.

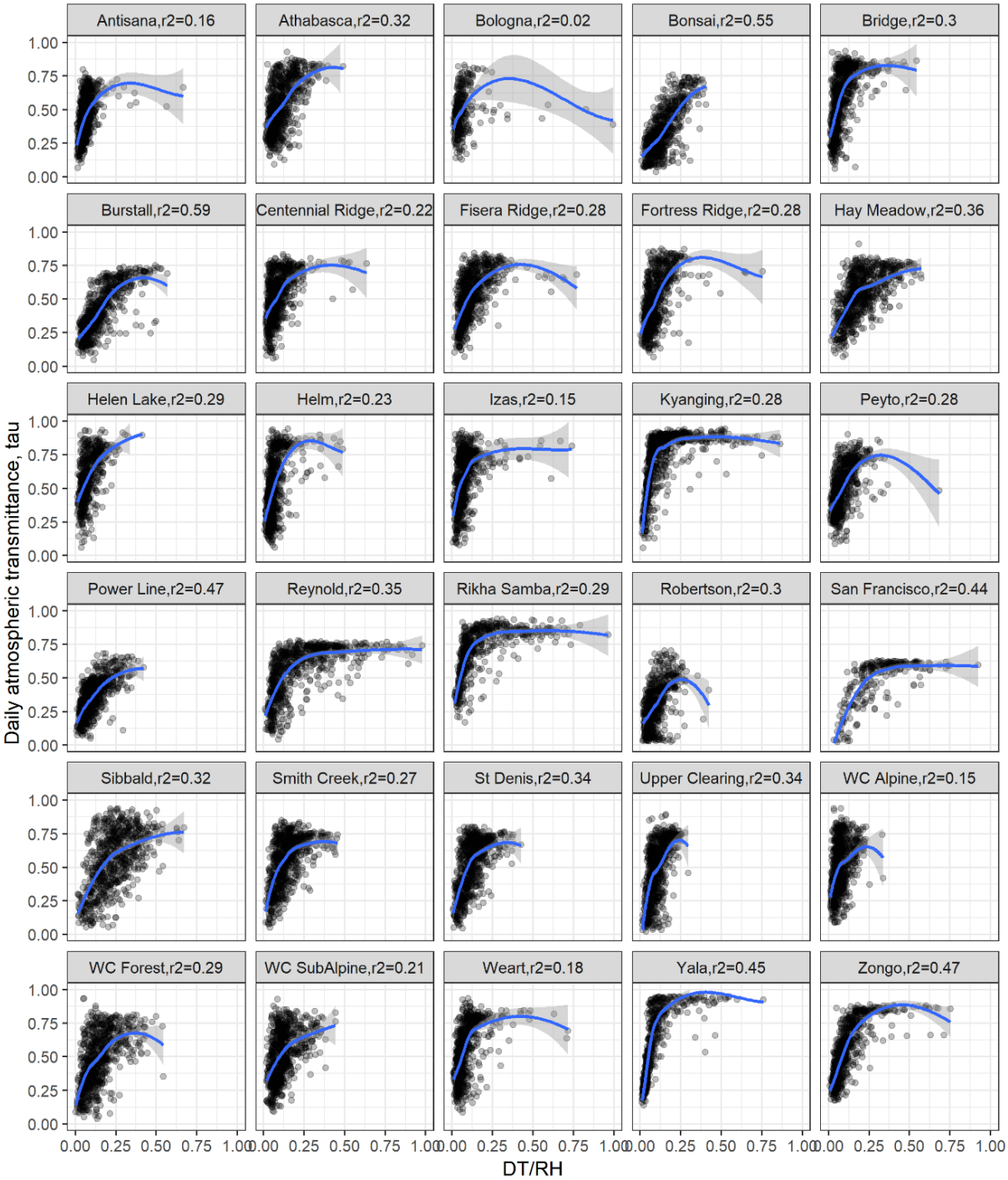

Figure C.4: Scatter plots of daily atmospheric transmittance against ratios of daily temperature range to daily mean relative humidity.

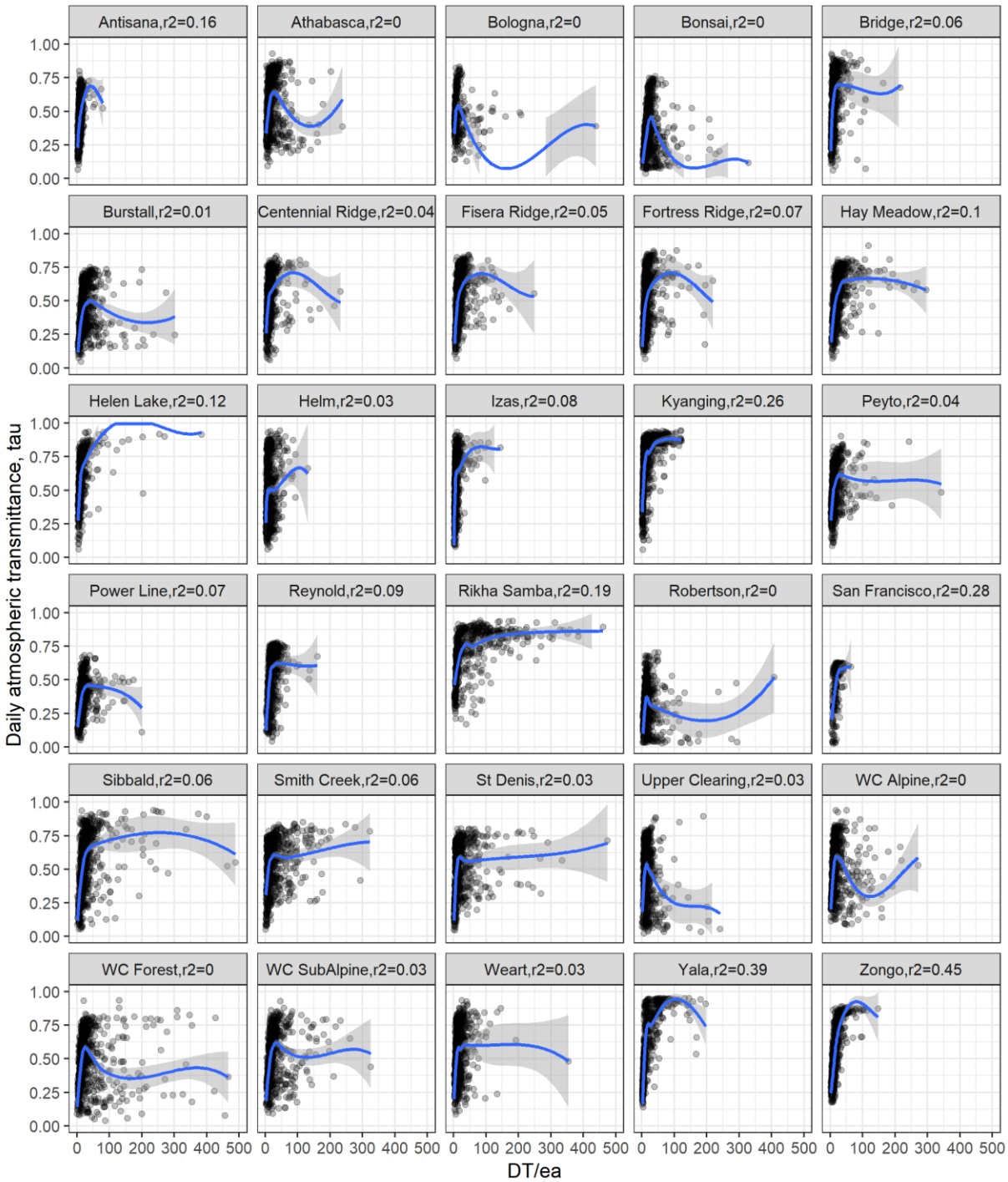

Figure C.5: Scatter plots of daily atmospheric transmittance against ratios of daily temperature range to daily mean vapour pressure.

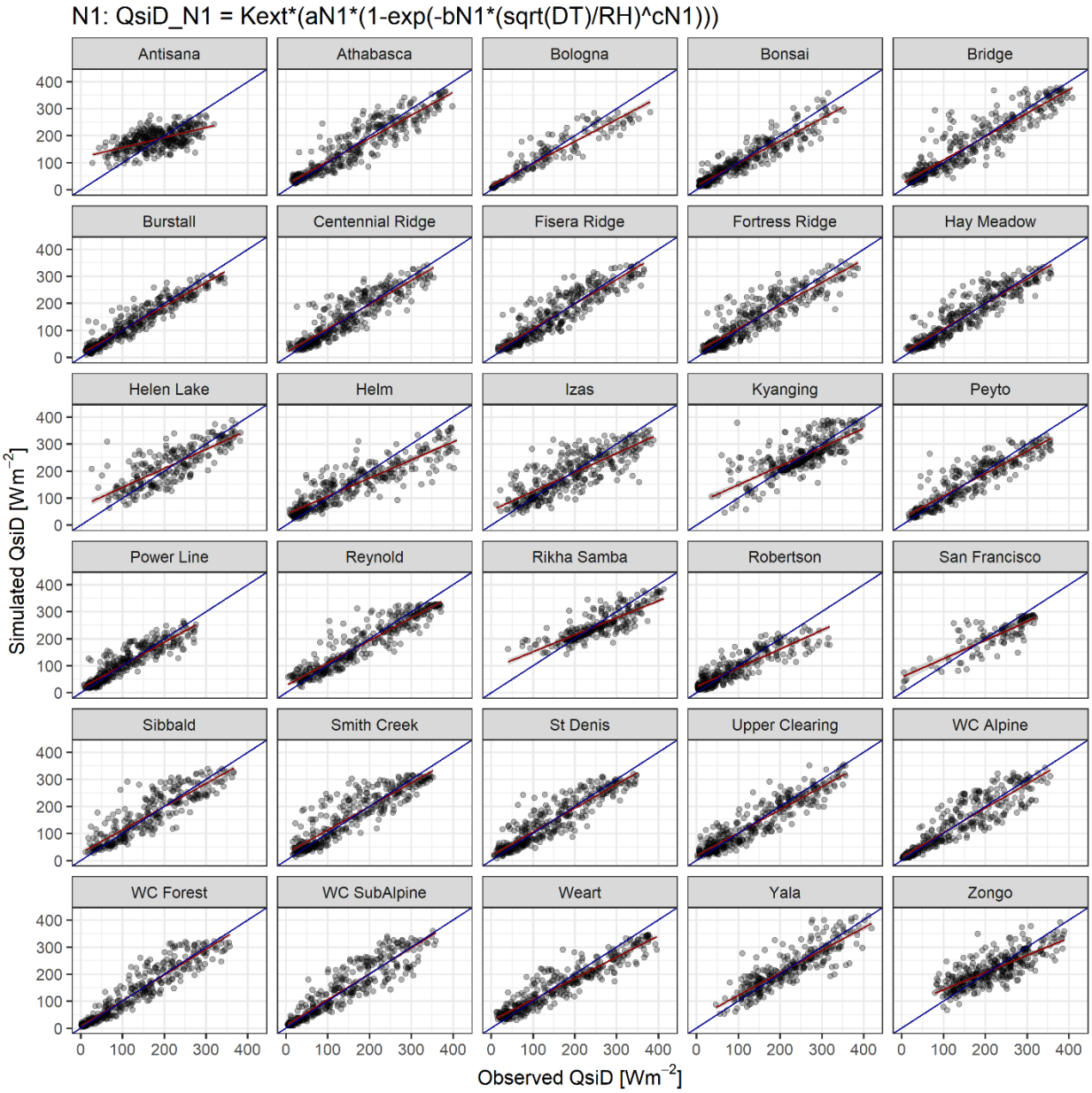

Figure C.6: Scatter plots of daily shortwave irradiance simulated by the model N1 (T/RH) against measured values at the 30 sites. Blue is 1:1 line and red is best fit line.

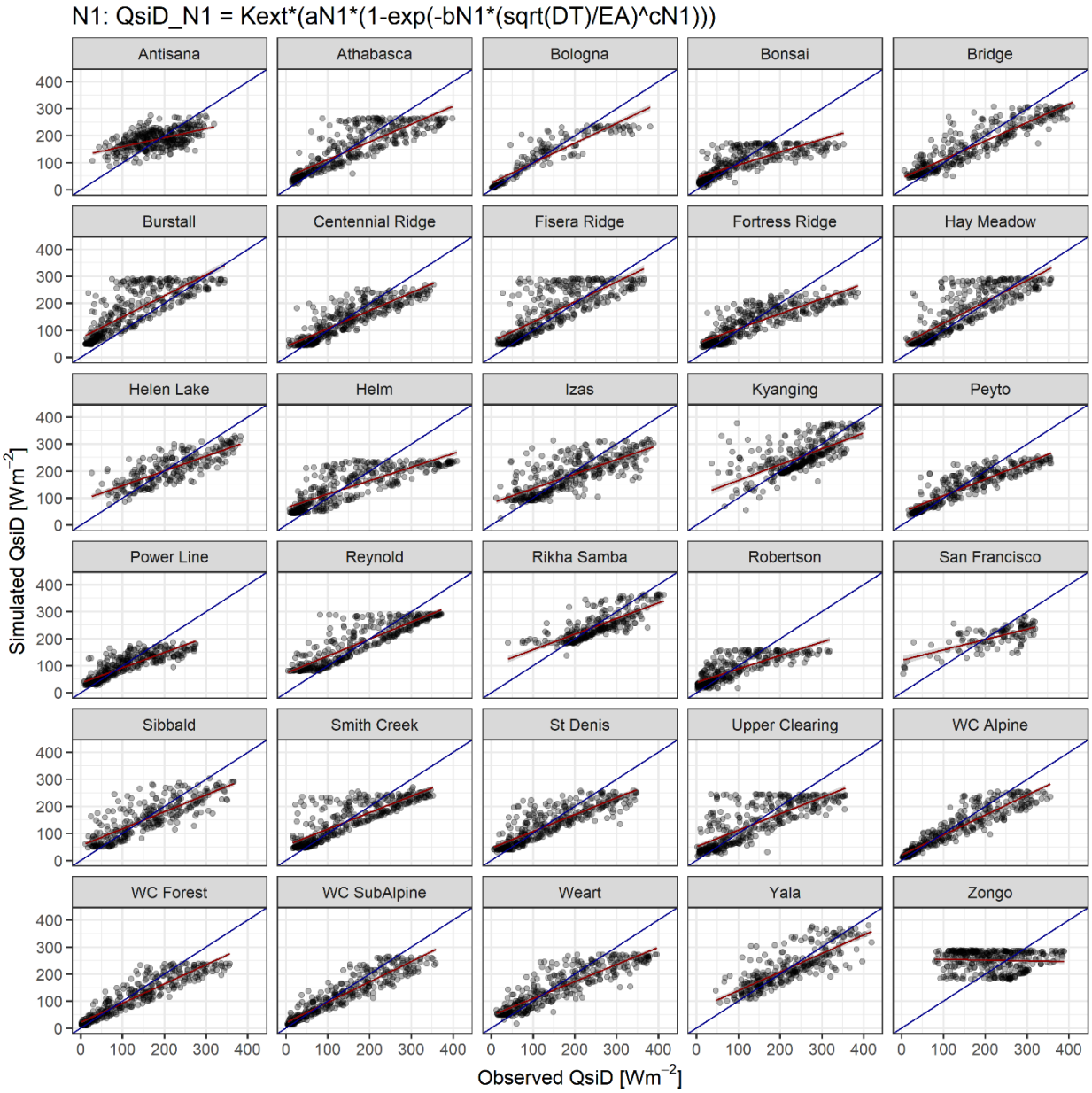

Figure C.7: Scatter plots of daily shortwave irradiance simulated by the model N1 (T/ea) against measured values at the 30 sites. Blue is 1:1 line and red is best fit line.

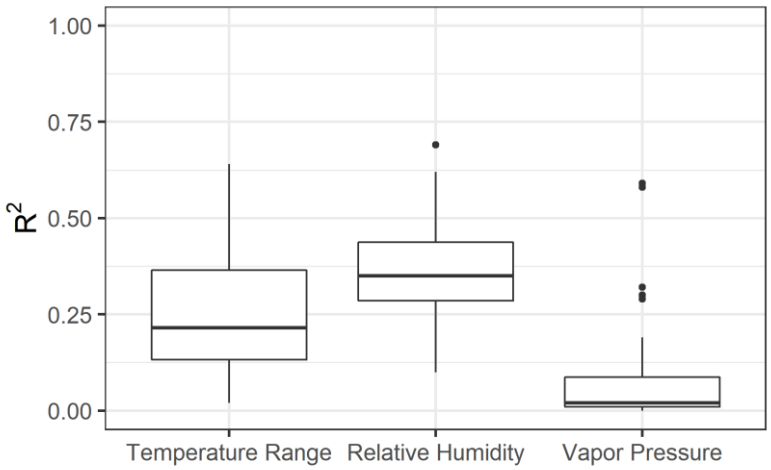

Figure C.8: Boxplot of coefficient of determination between daily atmospheric transmittance and the three variables, temperature range, relative humidity and vapour pressure.

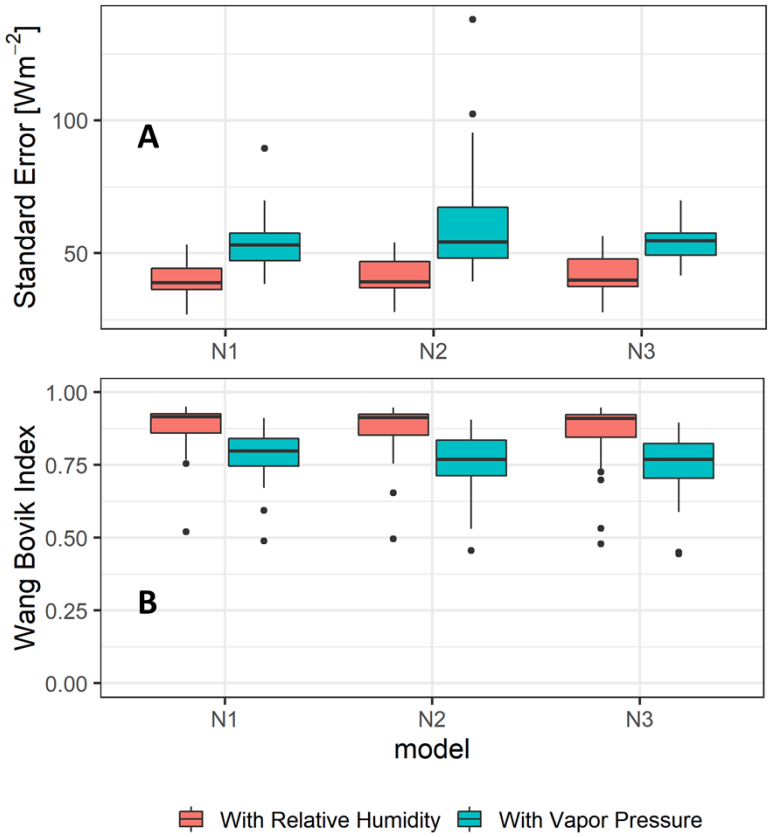

Figure C.9: Boxplots of model performance with relative humidity and with vapour pressure in the three models, N1, N2, and N3. (A) Standard Error of Estimates and (B) Wang Bovik Index.

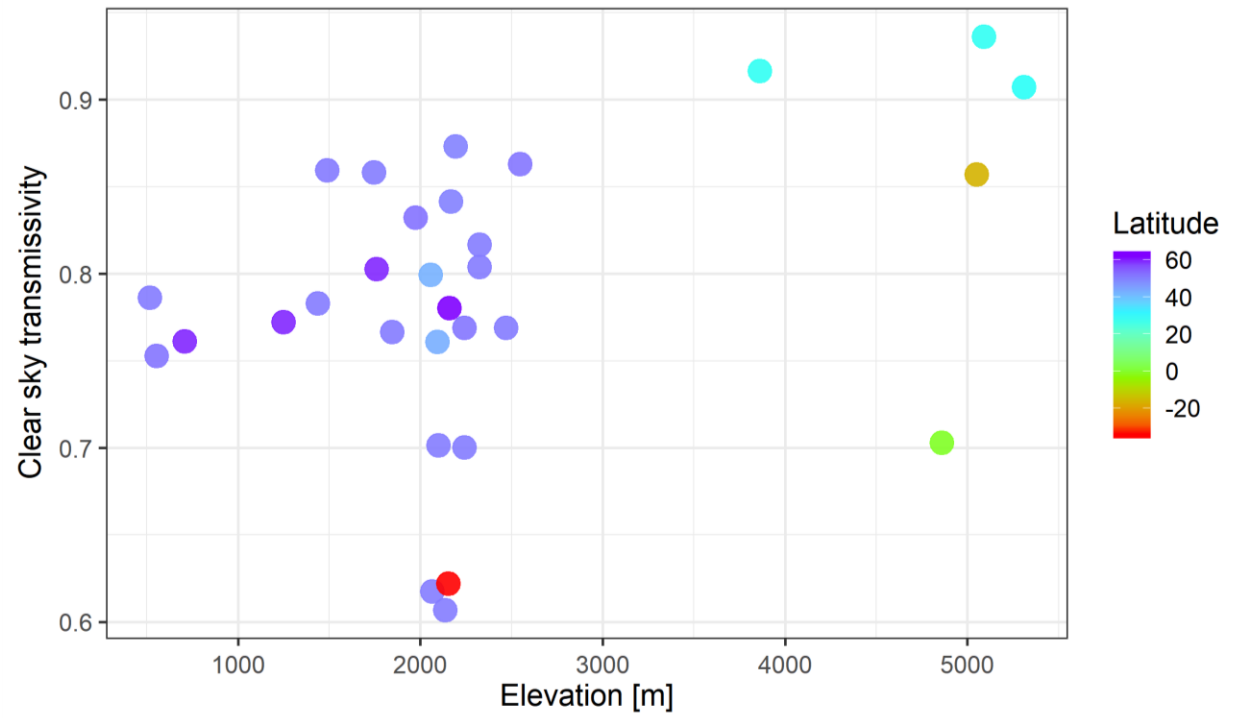

Figure C.10: Clear sky transmissivity

Appendix D: Evaluation of T/RH model performance

Model performance was evaluated based on RMSE. RMSE was calculated based on the comparison against measured data that were not used for model calibration.

Wilcoxon Signed-Rank Test, a non-parametric method, was used at 5% level of significance for two paired datasets using *wilcox.test* function in R. The paired datasets were constituted comparing T/RH models (N1, N2, N3) against T-models (HS, BC, AD) and the reanalysis products (ERAI, WFDEI). The T/RH models were also tested against each other pairwise. N1 was compared with HS, BC, AD, ERAI, WFDEI, N2, and N3; N2 was compared with HS, BC, AD, ERAI, WFDEI, N1, and N3; and N3 was compared with HS, BC, AD, ERAI, WFDEI, N1, and N2. The pair-wise statistical test shows that N1, N2, and N3 are different from each other at AP1 (parameters calibrated at individual sites).

When N1 is compared with N2 and N3 and other models as well as the reanalysis products at 5% level of significance, null hypothesis got rejected and alternative hypothesis got accepted in the AP1 calibration scheme [both cases, with and without τ_{cs}]. Therefore, N1 is the best compared to N2 and N2. While comparing N2 and N3, N2 is significantly better than N3 in the AP1 calibration scheme. However, the differences between N2 and N3 are not significant in the other calibration schemes at 5% level of significance. These conclusions are true with both *in-situ* measured and bias-adjusted reanalysis T and RH. ERAI and WFDEI are better for the high elevation sites [scheme AP3].

Example of hypothesis test:

H0: There is not any difference between Model 1 and Model 2

H1: Model 1 is better than Model 2.

Level of significance: 5%

Table D.1: values of RMSE distribution of 30 sites.

Calibration Scheme	τ_{cs}	Models	p-value (Wilcoxon test): In-situ observation [t, RH]			p-value (Wilcoxon test): bias-adjusted ERAI [t, RH]		
			N1	N2	N3	N1	N2	N3
AP1 (calibration at individual sites)	Without τ_{cs}	HS	0.000	0.000	0.000	0.000	0.000	0.004
		BC	0.000	0.000	0.000	0.000	0.000	0.007
		AD	0.000	0.000	0.000	0.000	0.000	0.001
		ERAI	0.014	0.017	0.033	0.027	0.034	0.043
		WFDEI	0.002	0.002	0.003	0.001	0.003	0.003
		N1	NA	1.000	1.000	NA	0.990	0.998
		N2	0.000	NA	1.000	0.010	NA	0.967
		N3	0.000	0.000	NA	0.002	0.033	NA
	With τ_{cs}	HS	0.000	0.000	0.000	0.000	0.000	0.004
		BC	0.000	0.000	0.000	0.000	0.000	0.007
		AD	0.000	0.000	0.000	0.000	0.000	0.001
		ERAI	0.013	0.018	0.034	0.029	0.036	0.043
		WFDEI	0.001	0.002	0.003	0.001	0.002	0.003
		N1	NA	1.000	1.000	NA	0.995	1.000
		N2	0.000	NA	1.000	0.005	NA	0.971
		N3	0.000	0.000	NA	0.000	0.029	NA
AP2 (global calibration)	Without τ_{cs}	HS	0.000	0.000	0.000	0.000	0.001	0.000
		BC	0.000	0.000	0.000	0.000	0.000	0.000
		AD	0.000	0.000	0.000	0.002	0.001	0.004
		ERAI	0.924	0.935	0.953	0.997	0.999	0.997
		WFDEI	0.755	0.748	0.815	0.955	0.959	0.964
		N1	NA	0.337	0.962	NA	0.633	0.927
		N2	0.663	NA	0.924	0.367	NA	0.577
		N3	0.038	0.076	NA	0.074	0.423	NA
	With τ_{cs}	HS	0.000	0.000	0.000	0.000	0.001	0.000
		BC	0.000	0.000	0.000	0.000	0.000	0.000
		AD	0.000	0.000	0.000	0.004	0.001	0.011
		ERAI	0.233	0.226	0.383	0.700	0.663	0.767
		WFDEI	0.053	0.055	0.114	0.286	0.272	0.329
		N1	NA	0.352	0.994	NA	0.601	0.989
		N2	0.648	NA	0.993	0.399	NA	0.860
		N3	0.006	0.007	NA	0.012	0.140	NA
AP3 (calibration on high-elevation sites only)	Without τ_{cs}	HS	0.112	0.173	0.343	0.112	0.112	0.446
		BC	0.112	0.250	0.343	0.112	0.112	0.446
		AD	0.040	0.069	0.173	0.112	0.112	0.554
		ERAI	0.022	0.022	0.022	0.022	0.022	0.112
		WFDEI	0.022	0.022	0.022	0.022	0.040	0.112
		N1	NA	0.888	0.931	NA	0.750	0.978
		N2	0.112	NA	0.960	0.250	NA	0.978
		N3	0.069	0.040	NA	0.022	0.022	NA
	With τ_{cs}	HS	0.040	0.069	0.343	0.040	0.040	0.657
		BC	0.040	0.069	0.343	0.069	0.069	0.657

Calibration Scheme	τ_{cs}	Models	p-value (Wilcoxon test): In-situ observation [t, RH]			p-value (Wilcoxon test): bias-adjusted ERAI [t, RH]		
			N1	N2	N3	N1	N2	N3
		AD	0.040	0.040	0.173	0.040	0.040	0.657
		ERAI	0.022	0.022	0.022	0.022	0.022	0.040
		WFDEI	0.022	0.022	0.022	0.022	0.022	0.069
		N1	NA	0.888	0.978	NA	0.554	0.978
		N2	0.112	NA	0.978	0.446	NA	0.978
		N3	0.022	0.022	NA	0.022	0.022	NA

Note: Red numbers are p-values greater than 0.05, i.e. null hypothesis could not be rejected. N1, N2, and N3 are compared to seven other models and tested whether N1, N2, and N3 estimate better daily shortwave irradiance than the others. N1 is compared with HS, BC, AD, ERAI, WFDEI, N2, and N3; N2 is compared with HS, BC, AD, ERAI, WFDEI, N1, and N3; and N3 is compared with HS, BC, AD, ERAI, WFDEI, N1, and N2.

Appendix E: Variables and instruments of AWS in the study basins

Table E.1: Instrumentation and range of parameters measured at AWS in the study basins.

Variable	Instrument	Units	Height above ground		
			Athabasca Moraine	Athabasca Ice	Peyto Main
Air temperature	Rotronic HC2-S3 Temperature and Humidity Probe	degree C	2.8 m	1.89 m	4.37 m
Relative humidity		%			
Snow depth	SR50A Sonic Ranger	m	2.3 m	0.58 m	2.95 m
Wind speed	RM Young 05103-10 Wind Monitor 05103AP-10	m/s	3.35 m	1.54 m	5.23 m
Wind direction		degrees			
Incoming SW radiation	Kipp & Zonen CNR4 Net Radiometer	W/m^2	2.19 m	1.59 m	3.79 m
Outgoing SW radiation					
Incoming LW radiation					
Outgoing LW radiation					
Barometric pressure	Vaisala CS106	mbar	In logger box		
Snow temperature	Omega Type E Thermocouple	degree C	20 & 150 cm	20, 60, 100, 140 & 180 cm	20 & 150 cm
Volumetric water content	Campbell Scientific CS650	%	1 – 11 cm below surface	NA	1 – 11 cm below surface
Electroconductivity		ds/m			
Soil temperature		degree C			
Soil heat flux	HFP01	W/m^2	2 cm below surface	NA	2 cm below surface
Rainfall	TB4 tipping bucket rain gauge	mm	~ 0.5 m	NA	3.15 m
Precipitation	Ott Pluvio	mm	268 cm	NA	Not measured

Table E.2: Period and logging frequency of AWS in the study basins.

Station name	**Latitude**	**Longitude**	**Elevation**	**Data period**	**Data logging frequency**
Peyto Main	51.50934	-123.44202	2237 m	July 2013 – Oct 2019	15 mins
Athabasca Moraine	52.21536	-117.22636	1966 m	Sept 2014 – Nov2018	15 mins
Athabasca Ice	52.19167	-117.24167	2177 m	Sept 2014 – Oct 2018	15 mins

Appendix F: Changes in climate and water fluxes

Table F.1: Changes in precipitation in annual, seasonal and monthly time periods [Scheme S1]

Seasons	Athabasca				Peyto			
	p-value Wilcox test	p-value t-test	Mean 1 (mm)	Mean 2 (mm)	p-value Wilcox test	p-value t-test	Mean 1 (mm)	Mean 2 (mm)
Annual	0.912	0.683	611.4	626.6	0.143	0.121	697.0	768.7
Winter	0.043	0.037	254.5	205.0	0.436	0.223	272.2	237.0
Spring	0.089	0.191	115.0	128.1	0.064	0.057	152.4	182.1
Summer	0.052	0.020	132.9	171.4	0.009	0.006	146.2	196.4
Fall	0.481	0.468	109.0	122.1	0.218	0.260	126.2	153.2
January	0.123	0.056	92.9	58.2	0.089	0.060	94.6	60.7
February	0.821	0.882	32.5	31.5	1.000	0.613	48.8	43.4
March	0.436	0.313	40.1	45.1	0.165	0.069	61.2	77.2
April	0.496	0.356	34.6	39.6	0.280	0.259	40.7	48.3
May	0.436	0.571	40.4	43.5	0.393	0.420	50.6	56.5
June	0.043	0.095	47.1	61.0	0.029	0.076	61.9	80.0
July	0.054	0.055	39.0	55.0	0.089	0.064	45.1	63.6
August	0.353	0.319	46.7	55.4	0.123	0.103	39.2	52.8
September	0.280	0.227	48.0	63.6	0.315	0.288	66.2	85.5
October	0.739	0.814	60.9	58.5	0.529	0.497	60.0	67.7
November	0.579	0.462	53.9	58.8	0.063	0.067	73.7	93.7
December	0.082	0.086	75.3	56.5	0.035	0.032	55.1	39.3

Table F.2: Changes daily maximum temperature in annual, seasonal and monthly periods [Scheme S1]

Seasons	Athabasca				Peyto			
	p-value Wilcox test	p-value t-test	Mean 1 (°C)	Mean 2 (°C)	p-value Wilcox test	p-value t-test	Mean 1 (°C)	Mean 2 (°C)
Annual	0.002	0.002	2.1	3.1	0.000	0.000	1.3	2.8
Winter	0.009	0.009	-7.2	-5.3	0.001	0.001	-0.2	1.7
Spring	0.052	0.044	1.5	2.6	0.043	0.016	11	12.1
Summer	0.796	0.979	12.3	12.3	0.315	0.358	5.3	5.9
Fall	0.436	0.529	5.9	6.3	0.007	0.005	-6.8	-5
January	0.000	0.001	-10.1	-5.0	0.000	0.000	-9.4	-4.6
February	0.579	0.668	-6.0	-5.4	0.579	0.740	-5.9	-5.5
March	0.075	0.023	-3.9	-1.9	0.015	0.008	-5.0	-2.7
April	0.063	0.054	0.7	2.2	0.003	0.002	-1.1	1.2
May	0.684	0.878	7.5	7.4	0.165	0.110	5.4	6.5
June	0.631	0.546	10.3	9.9	0.393	0.405	8.7	9.2
July	0.739	0.723	13.3	13.5	0.015	0.012	12.0	13.4
August	0.631	0.771	13.1	13.3	0.123	0.070	12.2	13.4
September	0.912	0.986	8.9	8.9	0.853	0.809	8.5	8.8
October	0.218	0.230	3.0	3.7	0.105	0.157	2.2	3.1
November	0.105	0.081	-4.2	-2.6	0.029	0.032	-4.3	-2.5
December	1.000	0.870	-8.4	-8.2	0.912	0.980	-7.6	-7.6

Table F.3: Changes daily minimum temperature in annual, seasonal and monthly periods [Scheme S1]

Seasons	Athabasca				Peyto			
	p-value Wilcox test	p-value t-test	Mean 1 (°C)	Mean 2 (°C)	p-value Wilcox test	p-value t-test	Mean 1 (°C)	Mean 2 (°C)
Annual	0.190	0.081	-4.5	-4.0	0.000	0.001	-4.9	-3.8
Winter	0.971	0.671	-12.3	-12	0.853	0.673	-11.2	-10.9
Spring	0.089	0.077	-5.7	-4.9	0.001	0.001	-7.0	-5.5
Summer	0.043	0.023	4.5	5.2	0.000	0.000	3.7	5.0
Fall	0.247	0.384	-1.1	-0.7	0.009	0.008	-2.0	-0.6
January	0.007	0.012	-15.0	-11.4	0.001	0.003	-13.3	-9.8
February	0.796	0.517	-12.1	-13.1	0.739	0.382	-11.5	-12.8
March	0.684	0.490	-9.8	-9.2	0.089	0.067	-10.8	-9.3
April	0.029	0.018	-6.9	-5.3	0.015	0.008	-7.9	-6.2
May	1.000	0.699	-0.5	-0.3	0.004	0.004	-2.4	-1.0
June	0.853	0.734	2.9	3.1	0.739	0.516	1.9	2.2
July	0.043	0.023	5.4	6.4	0.000	0.000	4.3	6.2
August	0.019	0.020	5.1	6.1	0.000	0.000	4.8	6.6
September	0.280	0.169	0.7	1.6	0.190	0.182	0.8	1.6
October	0.853	0.937	-2.9	-2.9	0.004	0.004	-4.7	-2.8
November	0.631	0.807	-9.2	-9.4	0.739	0.985	-8.5	-8.5
December	0.280	0.393	-12.7	-13.9	0.190	0.251	-11.4	-12.7

Table F.4: Changes daily mean temperature in annual, seasonal and monthly periods [Scheme S1]

Seasons	Athabasca				Peyto			
	p-value Wilcox test	p-value t-test	Mean 1 (°C)	Mean 2 (°C)	p-value Wilcox test	p-value t-test	Mean 1 (°C)	Mean 2 (°C)
Annual	0.105	0.089	-1.1	-0.6	0.001	0.001	-1.6	-0.6
Winter	0.481	0.336	-9.7	-9	0.529	0.342	-8.9	-8.4
Spring	0.165	0.119	-2	-1.2	0.003	0.003	-3.4	-2
Summer	0.393	0.392	8.7	9	0.003	0.002	7.6	8.7
Fall	0.529	0.799	2.4	2.6	0.280	0.230	1.7	2.4
January	0.004	0.006	-12.5	-8.6	0.000	0.001	-11.3	-7.6
February	0.912	0.704	-9.1	-9.7	0.796	0.537	-8.7	-9.6
March	0.353	0.234	-6.8	-5.8	0.075	0.058	-7.9	-6.3
April	0.063	0.054	-2.9	-1.6	0.007	0.007	-4.3	-2.6
May	0.579	0.943	3.8	3.8	0.105	0.044	1.8	3.0
June	0.912	0.754	7.0	6.8	0.436	0.507	5.7	6.0
July	0.190	0.214	9.7	10.3	0.002	0.001	8.4	10.1
August	0.631	0.373	9.3	9.8	0.019	0.010	8.6	10.1
September	0.739	0.727	4.8	5.1	0.631	0.727	4.7	5.0
October	0.853	0.991	0.1	0.1	0.052	0.089	-1.2	-0.2
November	0.853	0.870	-6.5	-6.4	0.971	0.632	-6.2	-5.8
December	0.436	0.499	-10.4	-11.2	0.247	0.285	-9.4	-10.5

Table F.5: Results of student's t-test for changes in annual mean values of water fluxes.

Schemes	Fluxes	Athabasca			Peyto		
		p-value	Mean 1 (mm)	Mean 2 (mm)	p-value	Mean 1 (mm)	Mean 2 (mm)
S1	Snow	0.443	911	866	0.121	1135	919
	Rain	0.001	175	262	0.304	310	362
	Snowmelt	0.223	687	723	0.309	1105	974
	Firnmelt	0.652	275	307	0.806	163	146
	Icemelt	0.537	532	501	0.000	265	667
	Runoff	0.578	1320	1365	0.005	1581	1888
S2	Snow	0.892	911	901	0.591	1135	1060
	Rain	0.983	175	175	0.923	310	313
	Snowmelt	0.432	687	661	0.683	1105	1056
	Firnmelt	0.930	275	267	0.095	163	39
	Icemelt	0.245	532	470	0.225	265	364
	Runoff	0.279	1320	1236	0.499	1581	1524
S3	Snow	0.546	911	876	0.292	1135	986
	Rain	0.001	175	262	0.326	310	360
	Snowmelt	0.827	687	669	0.613	1105	1041
	Firnmelt	0.587	275	314	0.015	163	414
	Icemelt	0.460	532	571	0.003	265	537
	Runoff	0.125	1320	1452	0.000	1581	2069
S4	Snow	0.545	901	866	0.287	1060	919
	Rain	0.001	175	262	0.340	313	362
	Snowmelt	0.035	661	723	0.527	1056	974
	Firnmelt	0.581	267	307	0.008	39	146
	Icemelt	0.454	470	501	0.006	364	667
	Runoff	0.101	1236	1365	0.001	1524	1888
S5	Snow	0.785	876	866	0.606	986	919
	Rain	0.986	262	262	0.974	360	362
	Snowmelt	0.504	669	723	0.621	1041	974
	Firnmelt	0.908	314	307	0.003	414	146
	Icemelt	0.111	571	501	0.192	537	667
	Runoff	0.295	1452	1365	0.124	2069	1888

Note: Red numbers are significant at 95% confidence level. The comparisons were made as per the schemes defined in Table 5-2.

Table F.6: Results of paired student's t-test and Wilcox test for changes in monthly values of water fluxes.

Schemes	Fluxes	Athabasca		Peyto	
		p-value t-test	p-value Wilcox test	p-value t-test	p-value Wilcox test
S1	Snow	0.424	0.986	0.028	0.018
	Rain	0.000	0.000	0.141	0.000
	Snowmelt	0.525	0.109	0.303	0.922
	Firnmelt	0.540	0.181	0.741	0.552
	Icemelt	0.437	0.859	0.000	0.000
	Runoff	0.500	0.059	0.000	0.000
S2	Snow	0.000	0.000	0.000	0.000
	Rain	0.003	0.000	0.100	0.000
	Snowmelt	0.000	0.000	0.028	0.262
	Firnmelt	0.029	0.027	0.001	0.000
	Icemelt	0.000	0.000	0.000	0.000
	Runoff	0.000	0.000	0.023	0.057
S3	Snow	0.538	0.839	0.138	0.113
	Rain	0.000	0.000	0.162	0.001
	Snowmelt	0.312	0.097	0.604	0.897
	Firnmelt	0.460	0.125	0.003	0.002
	Icemelt	0.336	0.072	0.000	0.000
	Runoff	0.061	0.003	0.000	0.000
S4	Snow	0.531	0.851	0.135	0.113
	Rain	0.000	0.000	0.170	0.001
	Snowmelt	0.265	0.013	0.496	0.613
	Firnmelt	0.453	0.160	0.002	0.000
	Icemelt	0.346	0.078	0.000	0.000
	Runoff	0.048	0.004	0.000	0.000
S5	Snow	0.000	0.000	0.000	0.000
	Rain	0.234	0.000	0.511	0.000
	Snowmelt	0.000	0.003	0.006	0.288
	Firnmelt	0.035	0.062	0.000	0.000
	Icemelt	0.000	0.000	0.000	0.000
	Runoff	0.000	0.000	0.000	0.018

Note: Red numbers are significant at 95% confidence level. The comparisons were made as per the schemes defined in Table 5-2.

Table F.7: Results of Student's t-test and Wilcox test for changes in glacier mass balances.

Schemes	Mass Balance	Athabasca				Peyto			
		p-value Wilcox test	p-value t-test	Mean 1 (mm)	Mean 2 (mm)	p-value Wilcox test	p-value t-test	Mean 1 (mm)	Mean 2 (mm)
S1	**Winter**	0.029	0.019	474	417	0.007	0.009	586	324
	Summer	0.796	0.740	-1176	-1133	0.123	0.149	-857	-1056
	Annual	0.579	0.910	-701	-716	0.029	0.019	-271	-733
S2	**Winter**	0.280	0.233	474	447	0.043	0.059	586	401
	Summer	0.247	0.522	-1176	-1083	0.123	0.249	-857	-709
	Annual	0.315	0.663	-701	-636	0.739	0.830	-271	-308
S3	**Winter**	0.353	0.219	474	444	0.315	0.278	586	474
	Summer	0.481	0.686	-1176	-1229	0.011	0.010	-857	-1306
	Annual	0.529	0.534	-701	-785	0.023	0.016	-271	-832
S4	**Winter**	0.247	0.180	447	417	0.315	0.266	401	324
	Summer	0.481	0.683	-1083	-1133	0.007	0.008	-709	-1056
	Annual	0.529	0.519	-636	-716	0.023	0.014	-308	-733
S5	**Winter**	0.218	0.245	444	417	0.089	0.075	474	324
	Summer	0.218	0.374	-1229	-1133	0.105	0.114	-1306	-1056
	Annual	0.436	0.506	-785	-716	0.481	0.625	-832	-733

Note: Red numbers are significant at 95% confidence level. The comparisons were made as per the schemes defined in Table 5-2.